AVERTISSEMENT

Ce document est le fruit d'un long travail approuvé par le jury de soutenance et mis à disposition de l'ensemble de la communauté universitaire élargie.

Il est soumis à la propriété intellectuelle de l'auteur. Ceci implique une obligation de citation et de référencement lors de l'utilisation de ce document.

D'autre part, toute contrefaçon, plagiat, reproduction illicite encourt une poursuite pénale.

Contact : ddoc-theses-contact@univ-lorraine.fr

LIENS

Code de la Propriété Intellectuelle. articles L 122. 4
Code de la Propriété Intellectuelle. articles L 335.2- L 335.10
http://www.cfcopies.com/V2/leg/leg_droi.php
http://www.culture.gouv.fr/culture/infos-pratiques/droits/protection.htm

Université de Lorraine

École doctorale

Centre de Recherches Pétrographiques et Géochimiques

Thèse de doctorat présentée et soutenue publiquement pour l'obtention du titre

de Docteur de l'Université de Lorraine (Spécialité: Géosciences)

par Antonio Caracausi

Noble gases as geochemical tracers of Earth's dynamic and evolution

Les gaz rares comme traceurs géochimiques de la dynamique et de l'évolution de la Terre

Soutenance publique le 17 Décembre 2019 au CRPG devant le jury composé de Mesdames et Messieurs.

Directeur de thèse:

Pr. Bernard Marty, Université de Lorraine, Centre de Recherches Pétrographiques et Géochimiques (Nancy, France)

Rapporteurs:

Dr. Patrick Allard, Institut de Physique du Globe de Paris (France)

Pr. Pierpaolo Zuddas, Sorbonne Université (France)

Examinateurs:

Dr. Raphaël Pik, Centre National de la recherche Scientifique, Centre de Recherches Pétrographiques et Géochimiques (Nancy, France)

Dr. Evelyn Füri, Centre National de la recherche Scientifique, Centre de Recherches Pétrographiques et Géochimiques (Nancy, France)

Pr. Giada Iacono Marziano, Institut des Sciences de la Terre d'Orléan, CNRS - Université d'Orléans- BRGM (Orléans, France)

Centre de Recherches Pétrographiques et Géochimiques, 15 rue Notre-Dame des Pauvres, 54500 Vandoeuvre-lès-Nancy, France

Tables of Contents

Remerciements

L'opportunité de remercier est toujours un moment important, car elle nous place devant un travail et toutes les personnes qui ont en quelque sorte contribuées à sa réalisation. C'est un moment d'observation intérieure des souvenirs de toutes les étapes du travail qui se sont alternées au cours de la réalisation du projet, de leur intimité, mais aussi une façon de penser au tout début, donc à ceux qui ont permis de commencer cette aventure. Un projet doctoral est certes une période de croissance scientifique mais aussi humaine et son développement, ainsi que sa finalisation, nous mettent nécessairement devant des problèmes scientifiques mais aussi devant des aventures humaines. C'est ce que j'ai vécu et je me dois de remercier tous ceux qui ont contribué à mon voyage. Ici, je ne pourrai pas écrire en détails sur tout le monde, mais je garderai jalousement les anecdotes et les souvenirs.

La première personne que je souhaite remercier est le professeur Bernard Marty pour sa présence constante et intense dans mon parcours humain et scientifique. J'ai commencé ma carrière d'étudiant il y a quelques années et les travaux du professeur Marty ont été, depuis lors, des piliers pour les étudiants en géochimie et en cosmo-géochimie. Au cours de ma carrière scientifique, j'ai suivi ces travaux et de nombreuses idées en sont nées, que j'ai eu l'occasion de développer par la suite. Récemment, je me suis retrouvé avec le privilège de travailler avec lui et je chérirai pour les années à venir les précieux souvenirs rassemblés dans les différents lieux de notre planète que les gaz rares nous ont conduits à explorer, à la recherche de nouvelles signatures isotopiques, ou pour présenter les résultats des études réalisées. Mon souhait et mon engagement sont maintenant de faire vivre ces enseignements reçu et d'essayer de les transmettre aux étudiants et aux chercheurs que je rencontrerai dans la suite de ma carière.

Je tiens à remercier le formidable groupe de travail qui collabore avec le professeur Marty et que j'ai eu le plaisir de rencontrer dans le laboratoire des gaz rares du CRPG, où nous avons partagé de nombreuses expériences: Guillaume Avice, Micheal Broadly; David Bekaert, Evelyn Fury, Laurent Zimmerman.

Parmi les remerciements, il y en a un spécial qui va à Pete Burnard, un grand ami et homme de science. Il est à l'origine de cette aventure, étant la personne avec qui j'ai commencé à collaborer avec le CRPG et qui a fortement marqué mes activités scientifiques. Il nous manque, mais est toujours présent dans nos pensées et nos actions.

Je remercie aussi tout particulièrement Bouchaib Tibari pour son amitié, sa présence précieuse et son expertise au cours de nombreuses journées de travail en laboratoire.

Certes, la vie professionnelle a changé après mon expérience au sein du CRPG et j'ai moi-même changé en tant que personne. Merci à tout le personnel du CRPG qui, avec chaleur et courtoisie, a fait en sorte que je me sente accueilli dans une grande famille.

Après les remerciements et pour parler de la continuité de ces collaborations à l'avenir, je remercie Raphael Pik pour l'occasion qu'il m'offre de continuer à collaborer à des activités qui sont en partie enracinées dans ce projet doctoral, et j'espère que celles-ci seront fructueuses à l'avenir, en écrivant de nouvelles pages de bonne science.

Finalement, je remercie mes collègues d'INGV auprès de qui j'ai été formé scientifiquement depuis le début de ma carrière, rêvant et travaillant avec des volcans actifs en Italie et dernièrement également pour l'étude des tremblements de terre (défi titanesque). Dans ce contexte, je ne peux manquer de mentionner également le professeur Nuccio de l'Université de Palerme, qui m'a choisi comme étudiant, m'a initié dans le monde de la géochimie, de la recherche et du monde universitaire.

Merci à mes parents, à mes amis qui me soutiennent, m'attendent avec patience et m'écoutent. Merci à la professeure Leslie-Anne Foulon qui a essayé de m'apprendre le français (je suis son pire élève).

Introduction

Since the Earth was born as a planet 4.5Ga ago it has continuously evolved undergoing a transformation into its present form. This evolution occurred in its interior producing the three main domains (from the inner outward): core, mantle and crust. Of course, this evolution also had a significant impact on the surface of the planet and this process is still ongoing as well documented by the plate tectonics and other activities such as volcanic and seismic activity. Over and above this, the atmosphere that envelops the Earth and its composition has also evolved over time.

Investigating the different stages of the evolution of the Earth are crucial subjects of the Earth sciences and this is challenged by the various disciplines (e.g., cosmochemistry, geochemistry, geophysics, palaeontology) and how to piece together this complex puzzle.

The history of Earth is in itself an intriguing topic but it is also at its core if we want to fully understand how our planet works. In fact, recognizing what is happening in the modern Earth is furnishing new crucial elements to mitigate the natural risks such as volcanic eruption, earthquakes, global warming, etc. Hence, the Earth's history provides knowledge and the tools to forecast the fate of our planet and its pleasant and long-running habitability. Even so, at this time, it is unthinkable to predict natural disasters (e.g., the frequency of major earthquakes) by simply studying the past, however a meticulous reconstruction of the past can contribute to theoretical studies of the natural forces that govern the processes at the Earth's surface and in its interior (e.g., earthquakes preparatory phases; magma degassing and eruption). Combining the reconstruction of the past, observations and study of the main forces that drive the natural processes and theory behind them is the best way to extrapolate the understanding into the future and confidently challenge the forecasting of natural processes that impact our sustainability on Earth over future generations.

Nowadays noble gases geochemistry is a broad and versatile field of the geochemistry ("latu sensu") and this group of elements is largely used in cosmo-geochemistry, Earth and oceanic science, climate and environmental studies (e.g., Mamyrin and Tolstikhin, 1983; Ozima Podosek, 2002; Porcelli et al., 2002; Burnard, 2013). Therefore the noble gas are recognized as being powerful tracers of Earth's accretion and evolution and they are applied to investigate the evolution of natural processes at the Earth's surface such as the volcanic eruptions (e.g., Caracausi et al., 2003; Rizzo et al., 2006; Sano et al., 2015; Paonita et al. 2016). Considering the disastrous nature of these processes the noble gases are also considered crucial tools in term of forecasting. However, it is well recognized that this application is a powerful and innovative tool but still in its infancy given it is still a significant challenge to be able to measure at high frequency the isotopic ratios of the noble gases in the field.

Overall the noble elements have two main geochemical characteristics:

1) They are chemically inert. This does not mean that they do not react at all. In fact, their interactions are weak (Van der Walls type), so much weaker than those of other elements in usual chemical reactions. It follows that their interactions are less complicated to be resolved restricting the possible processes that control their chemistry in the natural systems. 2) The noble gases are scarce in nature, so they are also called rare gases. These characteristics are common to these elements (He, Ne, Ar, Kr and Xe) making them a group with similar behaviour in the natural processes because their parameters vary smoothly from the light (e.g. He) to the heavier (e.g., Xe) noble gases.

In principle the recent continuous improvement of analytical instrumentation and the associated procedures have led the noble gases to be exceptional geochemical tracers in investigating the Earth mantle, its differentiation, heterogeneity (e.g., Mid Oceanic Ridge mantle reservoirs, Oceanic Islands Basalts mantle reservoirs, Sub Continental Lithospheric Mantle reservoirs, Plume-type mantle reservoirs), evolution over time and how processes,

for instance the subduction that moves shallow materials into the deep interior, contribute to its heterogeneity and in the recycling of atmosphere-derived fluids into the mantle.
It is worthy of note that only 50 years ago it was recognized that the solid Earth is still degassing primordial volatiles into the atmosphere that have been trapped in this planet since its formation. This discovery was based on the excess of 3He in deep oceanic water that were sampled at various locations in the Pacific Ocean (Clarke et al., 1969). Successively this excess has been also recognized in other locations confirming the existence of this process; the excess in 3He in oceanic waters has a well-defined vertical and horizontal distribution that undoubtedly indicates that the outgassing of primordial volatiles does not occur diffusively from the sea bottom but is localized in defined regions that coincide with active tectonics and the divergent plate boundaries where mantle constituents reach the surface (e.g., Craig et al., 1975; Lupton and Craig, 1981). Of course this discovery has had great relevance in the Earth science community given it is proof that the primordial volatiles are stored in the Earth's interior and that they are continuously released in correspondence of the plates boundaries where the new crust is being produced. It is interesting to note that the excess in 3He are systematically higher in the Pacific Ocean than in the Atlantic Ocean and this difference is partially due to the more rapid flushing of the Atlantic waters. Therefore, at the same time the noble gases furnish evidence of the deep Earth dynamic but they also find a significant application in oceanography tracing movement and mixing of different water masses (e.g., Ozima and Podosek, 2002; Stanley and Jenkins, 2013). It is also intriguing to note that the difference of the primordial He excess in the two oceans is simply related to the weaker source in the Atlantic Ocean as would be expected by the lower rate of crust formation in the Atlantic than in the Pacific ocean.
Successively it has been recognized that the outgassing of mantle-derived volatiles extensively occurs in continental volcanic regions. Furthermore, an excess of primordial He has also been identified in fluids (free gases and dissolved into the groundwater) that circulate in active tectonic regions far from any evidence of volcanism (e.g., Mamyrin and Tolstikhin, 1984; O'Nions and Oxburgh, 1986 and 1988; Ozima and Podosek, 2002), so deep faults in active tectonic regions are able to transfer mantle volatiles directly from the mantle, or from magmatic intrusions that are stored, into the crust. This discovery has opened new perspectives in the study of natural degassing and the associated natural hazards because a high degassing of mantle-derived volatiles (e.g., CO2, which can produce a variety of health effects) that also occur in non volcanic regions or linked to volcanoes whose last eruption occurred long time ago (e.g., hundreds or thousands of years). Furthermore, these pioneering noble gas investigations (e.g., Mamyrin and Tolstikhin, 1984; Ozima and Podosek, 2002 and reference therein) drove subsequent geochemical investigations that recognized how an intense degassing of deep-sourced volatiles occur in active tectonic region and it has an active rule in the preparatory phases of disastrous earthquakes (e.g., Italiano et al., 2000; Chiarabba and Chiodini, 2013; Tamburello et al., 2018; Di Luccio et al., 2018).
Of course the use of He, the lightest noble gas, furnished milestones in the study of the Earth dynamic tracing the road of almost fifty years of geochemical investigations in Earth sciences, however successive investigations based on both the light and the heavier noble gases (e.g., Xe) (e.g.,) are producing new fundamental constrains in the study of the Earth history and the origin and evolution of its volatiles (e.g., Marty, 1989; Ballentine et al., 2005; Gonnermann and Mukhophadhyahy 2008; Holland et al., 2009; Mukhophadhyahy, 2012; Marty and Zimmermann, 2012; Parai et al., 2019; Broadley et al., 2020; Labidi et al., 2020).
In principle, convection of the terrestrial mantle controls the present-day solid Earth–atmosphere dynamics, but it has been recognized that mantle volatiles retain the memory of the history of terrestrial degassing. Hence, due to their inert nature, their low abundances and the presence of several different radiochronometers in their isotope systematics, the

noble gases help in the understanding of mantle dynamics, heterogeneity and differentiation with respect to the atmosphere (e.g., Ozima and Podosek, 2002).
Each noble gas has a non-radiogenic and stable isotope that is indicated as "primordial" and also a radiogenic isotope that is continuously produced over time by natural reaction. Thus a combination of the two isotopes undergoes predictable variation over time and result powerful geo-chronometers to investigate the Earth history and date the main process that occurred during the planet evolution.
The noble gases are lost from the mantle reservoirs by degassing and/or together with mantle-derived magmas that move towards the surface. In this scenario only the radiogenic noble gases isotopes grow over time because of the decay of lithophile parent isotopes. As a consequence the mantle reservoirs and the derived products (e.g. up-raised batchs of magmas), which experience large extent of partial melting and degassing, reveal higher ratios of the radiogenic isotopes than the primordial ones compared to the reservoirs that were less reworked by natural processes. Therefore, the noble gases are in low abundances in such reservoirs, so they results more sensitive to the occurring of successive degassing and addition of successively produced isotopes by radiogenic, nucleogenic and fissiogenic processes. In detail, the Isotopes of He, Ne, Ar and Xe are produced by diverse set of short lived (129I and 244Pu) and long lived (235U, 238U and 232Th), so these isotopes are sensitive to processes that occur at different timescales.
Furthermore, neon and xenon deserve particular attention because their isotope systematics can be related to specific processes during terrestrial accretion (e.g., Ozima and Podosek, 2002; Honda et al., 1991; Marty, 1989; Mukhopadhyahy, 2012; Avice and Marty, 2014). The source of primordial Ne in the mantle is most likely solar wind in origin, probably from surface irradiation of accreting particles (Trieloff et al., 2002; Ballentine et al., 2005) or from dissolution of a solar-like atmosphere in magma oceans (e.g., Yokochi and Marty, 2004). In contrast, the origin of the primordial heavy noble gases is less clear, and might not be solar (Holland et al., 2009; Ott, 2014).
Recent heavy noble gas measurements of ocean island basalts (OIB) and mid-ocean-ridge basalts (MORB) strongly support differences in elemental abundances and isotopic ratios between MORB and plume sources (OIB-related) (e.g., Graham, 2002; Ballentine et al., 2005; Mukhopadhyahy, 2012; Parai et al., 2012; Peto et al., 2013; Parai and Mukhopadhyahy, 2015). These investigations show that: 1) “regassing” of the mantle by recycling of atmospheric-derived noble gases (Ar and Xe) has occurred (Holland and Ballentine, 2006; Sumino et al., 2010; Kendrick et al., 2013); and 2) recycled atmospheric Xe dominates the Xe budget of MORB and mantle plume sources, even of those that have primitive He and Ne isotopic compositions (Parai and Mukhopadhyahy, 2015). However, Xe isotope systematics show that plume-derived volatiles are not simply the result of mixing between MORB-type xenon and atmospheric Xe (Mukhopadhyahy, 2012). Instead the differences between MORB and plume-type Xe must result from ancient heterogeneity, which dates from at most a few tens to hundred Ma after accretion of the Earth.
In this scenario, the use of the heavy Xe isotopes is very intriguing because both 129Xe and 136Xe were produced in the early Earth by decay of extinct radiochronometers, 129I (half life = 15.7 Myr) producing 129Xe, and 244Pu (half life = 80 Myr) producing 131-136Xe, while extant 238U also produces 131-136Xe but with slightly different ratios compared to 244Pu. Thus, the U-Xe system evolves over the entire Earth history, while the I-Xe and Pu-Xe systems only reflect the first 100 Myr and 500 Myr, respectively. Hence, 244Pu-Xe and 129I-Xe excesses in natural samples can be used to calculate an I-Pu “closure age” of volatile loss from the mantle (24, 25; supplementary materials); this essentially reflects a differentiation age where Xe was separated from its parent radio-isotopes (129I, 244Pu and 238U).

The present-day fissiogenic Xe spectrum (131,132,134,136Xe) in the mantle is a mixture between four end-members: (a) the atmosphere (Atm); (b) a primordial component (AVCC-Xe); (c) fissiogenicXe produced from 244 Pu (PuXe); and (d) fissiogenic Xe derived from238U (UXe). 244Pu and 238U each produce fissiogenic Xe isotopes in characteristic proportions, which are different from those of atmospheric or chondritic (AVCC) Xe. The measurements of the Xe isotopes in mantle derived gases that are low concentration in air contribute to solve the four components that are constrains to date the evolution of the Earth mantle and make inferences to reconstruct those processes that controlled this evolution (e.g., regassing of the mantle due to the subduction).

The radiogenic and fissiogenic Xe components have been shown to be different in MORB and plume derived volatiles, with lower Pu-Xe/(Pu-Xe+U-Xe) but higher I-Xe/Pu-Xe in MORB type volatiles (Parai and Mukhopadhyay, 2015). There is considerable variation in the 129Xe/136Xe ratio in the mantle and this heterogeneity implies that a) there are variations in the composition of the parent elements (Pu, I and U) and/or their closure ages and b) the different mantle sources have remained isolated since at least 4.45 Ga [refs]. It is possible to define fields for “MORB-type” and “plume-derived” Xe based on their 129Xe/136Xe vs130Xe/136Xe ratios, with plume-derived Xe characterized by higher 129Xe/136Xe ratios for a given 130Xe/136Xe ratio. It is important to note, however, that considerable heterogeneity is present within each field (“MORB-type” or “plume-derived”) and that there is a range in129Xe/136Xe in each mantle source.

Recent geochemical investigations (Broadley et al., 2020; Labidi et al., 2020) highlighted that notwithstanding the power of Xe isotopes for investigating the mantle heterogeneity, however combining all together the noble gases (abundances and isotopic ratios) they result in more powerful tracers to figure out the origin of volatiles on Earth and the processes that contribute to originate the nowadays mantle geochemistry. Hence, grouping the geochemistry of He, Ne, Ar, Kr and Xe provides a particularly rich record of mantle processing history and must be used to investigate the dichotomy of the Earth mantle.

The emerging picture is that the recent high precision measurements of the abundances and isotopes of different noble gases in the same sample are very powerful tools, however these measurements still require long procedure of gas purification and analysis hence these applications are mainly for specialists. If it is true that these new measurements have made it possible to take new steps towards the knowledge of the Earth and it allowed the scientists to make comparisons between chemical compostion of Earth and those of meteorites and other planets, however it is to point out that the samples to be studied are rare (few in number), difficult to discover and scattered in different parts of the world. Therefore, it occurs that the conditions to define this use of noble gases as a pioneering one even though it has been providing avant-garde results in the sciences (e.g., origin of volatiles stored into the mantle and in the atmosphere; origin of the mantle heterogeneity; the rule of processes such as convection and/or subduction in producing and preserving the mantle heterogeneity).

In applying the noble gases to the study of the mantle geochemistry and dynamics, the main condition for having suitable samples is that it has a low air contamination and considering that Ar is one of the main air component a good indication is that the isotopic ratio of Ar in the natural gases is higher than that in atmosphere (40Ar/36ArAIR=298.6). Atmospheric contamination of natural gases is always critical for non-radiogenic noble gases (e.g., 36Ar) and can overprint the original composition. This is less of a problem for 40Ar because this isotope is more abundant in the mantle than primordial 36Ar relative to the atmosphere (40Ar/36Ar = 298.6 in air; ≥ 10,000-40,000 in the mantle). In fact 40Ar is a radiogenic isotope that is continuously produced by 40K, it progressively increases in the interior of the planet. It is possible to assume 40Ar/36Ar of 40,000 and 10,000 for convective mantle and mantle deep plume-type sources respectively (e.g., Graham, 2002; Mukhopadhyay, 2012) and this

discrepance of the 40Ar/36Ar isotope ratio in the two mantle reservoirs is also an evidence of the mantle heterogeneity.
Furthermore, in order to challenge the isotopic measurements of different noble gases in the same sample it is essential that the amount of gas to be analyzed is enough to carry out the different measurements. To reach this goal there are two main types of samples: 1) fluid inclusions volcanic products (e.g., minerals, glasses) and 2) free gases from natural emissions such as volcanic fumaroles, bubbling gases, mofettes etc. Fluid inclusions are trapped at depth, so they trapped deep fluids that theoretically should contain gases that have a low contaminated by air. However, high atmospheric contaminations can also occur in the fluid inclusions and these are not only produced in the natural systems (e.g., volcanic plumbing system) but air entrapment occurs either during samples recovery and/or during samples preparations in the laboratory (e.g., Ballentine and Barfod, 2000).
In addition there are a few of sites in the world where the emitted natural gases have a low air contamination (e.g., Yellowstone, USA; Eifel, Germany; Etna, Italy) to be analized for all the noble gases isotopes. These sites are in active or quiescent volcanic systems. However, CO2-rich wells in gas fields intercept natural traps that alsoo contain a low atmospheric component and the high pressure of the gas in the trap prevents any air contamination during the gas up-rise toward the surface or during the sampling procedures. All this evidence highlights the rare nature of mantle-derived gases to investigate the Earth's mantle.
It is therefore clear that the geochemistry of noble gases is a sector that lends itself well to the study of the dynamics and evolution of the Earth on a wide scale of time and space. However, they also find a large applicability in following the dynamics of the Earth interior that manifest them self through some natural processes that have repercussions on everyday life. In fact, the measure of the abundance and isotopes of noble gases emitted in active volcanic systems allow us to figure out the processes of magmatic degassing and to reconstruct the evolution of the magmatic bodies during the transfer from the mantle sources to the volcanic plumbing systems before eruptions (e.g., Caracausi et al., 2003; Paonita et al.2012 and 2016; Sano and Fisher, 2013; Sano et al., 2015). The arrival of deep magma can be detected by means of increases in the He isotope ratio (3He/4He) measured in fluids that degas from volcanoes (e.g., Sano and Fischer, 2013). This is possible because the ascending primitive magmas outgas volatiles having 3He/4He ratios that are higher than those of fluids from more-evolved melts and/or crust. In the recent case of the Mount Ontake eruption in Japan (Sano et al., 2015), this tracer was the only one capable of providing clues about increasing activity over a timescale of years. Before the 2015 Eruption of Mt Ontake volcano there were no precursor signals such as seismicity and edifice inflation and the 3He significant enrichment over ten years (June 2003 to November 2014), have been a the only recognized precursor of the eruption that took place in 2014.
In volcanic systems the He-Ne-Ar-CO2-N2 systematic in magmatic gases allow also to figure out the paths of magma degassing (closed-open system degassing) and the possible volatiles mixing during their ascent towards the surface because of their different solubility in melts so they have a different release from magma, firstly the less soluble (e.g. Ar<Ne<He, solubility in melts). These remarks allow us to trace the magma up lift in the volcanic plumbing system and furnish constrains to reconstruct the possible structure of the plumbing system such as sill-like reservoirs and vertical structures where different batches of magma (e.g. more or less degassed) can mix each other or with the ascending volatiles (e.g., Paonita et al., 2012).
Recently Paonita et al., (2016) discussed a 12-year time series of 3He/4He ratio in volcanic gases from Mount Etna volcano (Italy), the biggest and most eruptive volcano in Europe, clearly showing that the main eruptive phases are preceded by increases of 3He/4He making this tracer a key precursor for monitoring volcanic activity. The raised characteristic

strongly linked to pressurization at depth beneath the volcano, due to deep magma influx. A pioneering model relates the changes in 3He/4He to the time-dependent outflow of volatiles from a magmatic chamber subjected to evolution of its internal pressure due to magma injection. At Mount Etna, the model made it possible to estimate key parameters in the volcanic surveillance such as the rate of magma input and volume change in deep chamber preceding eruptions in near-real time, and to compare them with geodetic estimations. This represents an unprecedented use of 3He/4He to obtain quantitative information on the physics of magmatic systems. Volcanoes showing changes of 3He/4He ratio in discharged gases due to unrest episodes are widespread in the world, thus this application envisage extensive future applications of our approach. Furthermore, He isotope monitoring at Mt Etna also suggested that the volcano plumbing system is extraordinary large and the main regional tectonic discontinuities work as a network of pathways in transferring mama derived fluids at regional scale (Caracausi et al., 2003). So it can be ascertained that it extends at least 40 km SW from the volcano's boundary along the NE-SW regional fault, where it discharges about 200 tons/day of gas, containing helium with mantle-type isotopic composition. The synchronous variations of 3He/4He isotopic ratios in gas sampled at sites located 60 kilometers apart and in fumaroles of the volcano have allowed to detect pulses of ascending magma in the plumbing system, thus providing a powerful tool for eruption forecasting (Caracausi et al., 2003; Rizzo et al., 2006; Martelli et al., 2008).

It is worthy of note that geochemical monitoring is used in the surveillance of active volcanic system and it has been ascertained the importance of He and the other gas nobles in reconstruct the dynamic of magma transfer through the volcanic plumbing system on long and short period and the evolution of natural processes which last expression is the volcanic eruption. Moreover, those short period phenomenons are also violent and they can generate risks to the society. Thus, it is a fundamental issue to improve our understanding of those events, across the development of predictive tools. However, volcanoes are generally far from facilities equipped with the right material to measure in a short time the chemistry of the natural fluids, and as such, noble gases are sampled and analyzed on long-term periods rarely lower than two-three weeks, so they can be used to investigate process that occur in a long time scale. For instance they cannot be used to investigate explosive volcanoes that are characterized by a high rate of explosions for month or day (e.g., Stromboli volcano, Italy). In summary the noble gases also furnish evidences of the up-rise of fresh and low-degassed magma in active volcanic systems but they are still unable to solve the high frequency volcanic explosions, so the new efforts of the scientific community is focused in developing new instrumentation that can contribute to fill this gap and challenge the understanding of how an explosive volcano works. This is crucial for the volcanic surveillance and the good quality of life of people that live in cities along the flanks or close to active volcanoes.

Here, it has been briefly shown that by combining abundances and isotopic ratios of different noble gases it is possible explore the history of the Earth and the processes that governed the geochemistry of the mantle and its products, therefore the processes that are active on a large scale.

At the same time the use of the individual noble gases also furnish crucial constraints to investigate the natural processes on a regional or local scale and to solve the dynamics and evolution of the Earth in its shallower layers. For instance, that is the case of He, which use permits us to recognize the presence of magma at depth in 1) quiescent volcanoes, where the last eruption occurred hundreds to thousands of years ago (Caracausi et al., 2009) and 2) in absence of volcanic evidence at the surface (e.g., Ballentine et al., 2002, Italiano et al., 2000) or an active degassing in continental regions of mantle-derived volatiles through lithospheric tectonic discontinuities (e.g., Caracausi et al., 2005; Burnard et al., 2013). In fact, He is characterized by two isotopes, 3He that in natural fluids is mainly primordial and

sourced from the mantle and 4He, that in contrast is continuously produced by the radiogenic decay of U and Th (e.g., Mamyrin and Tolstikhin, 1984; Ozima and Podosek, 2002). 3He is much less abundant than 4He, consequently, the 3He/4He ratios in natural fluids (e.g., trapped in minerals and outgassing at the Earth surface) varies in a range of orders of magnitude with values >10-5 in volatiles sourced from the mantle and close to 10-8 in continental region where He is dominated by 4He produced in the crust (e.g., O'Nions and Oxburgh, 1988). Furthermore, the 3He/4He ratio in atmosphere is 1.39 x 10-6 (Ra). It is worthy of note that the presence of primordial 3He in the mantle indicates that the Earth is still degassing volatiles that were trapped since the time of the planet accretion (~4.5Ga ago). This high difference of the He isotopic signature in crustal derived fluids (<0.02-0.05Ra) and mantle derived fluids (8Ra ±1, MORB mantle reservoir; 6.1Ra±0.9 Sub Continental Lithospheric Mantle source) allow 1) to recognize the presence of a small contribution of a mantle derived component in absence of any other evidence and 2) to compute the contribution of each component.

Therefore, the use of the He isotopes contributes to our ability to recognize volcanic systems where a refill of new magma occurred in the plumbing system after long time since the last eruption (e.g., thousands of years). Of course this evidence contributes to the help evaluate the hazardous nature of some areas because there is still an intense degassing of deep fluids (e.g., CO2) that are dangerous for humans. In fact even if the presence of magma at depth does not necessarily imply the occurrence of an eruption, nevertheless magma-derived fluids escaping toward the surface can accumulate in crustal traps and their over pressure are able to produce gas burst (e.g., Chivas et al., 1987). Furthermore, these fluids can also be stored in volcanic lakes and their progressive accumulation into the water can cause limnic eruptions sometimes being catastrophic events as for the tragedies of Lake Monoum and Lake Nyos, August 15th 1984 and August 21st 1986 respectively. During the above mentioned events, huge amounts of CO2 were expelled, causing loss of human life and thereby turning a volcanic lake into a killer (i.e., Kerr, 1986; Kling, 1987; Sano et al., 1990). An investigation of the He isotopic signature in two volcanic lakes at Mt Vulture volcano (Italy), which last eruption occurred 140ky ago, highlighted that it has a magmatic origin and the 3He/4He isotope ratios overlap those measured in minerals of the maar ejecta of the last eruption (Caracausi et al., 2009). In spite of the fact that the amount of dissolved gases in the water is less than that found in Lake Nyos (Cameroon), this result was the first indication that these crater lakes could be highly hazardous sites as supported by successive studies (e.g., Caracausi et al., 2013), even if they are located in a volcanic region currently considered inactive.

Since some geochemical investigations (e.g., Kennedy et al., 1997; Italiano et al., 2000; Caracausi et al., 2005; Caracausi and Paternoster, 2015) highlighted that faults emanate mantle-derived He, its isotopic composition in fault-related fluids has been used to trace the fault behaviour in active tectonic regions and this has contributed to the discovery that the mantle-derived fluids can have an active rule in the preparatory phases of the earthquakes. The tectonic discontinuities can work as a network of pathways (as high permeability passages) that cross the mantle-crust boundary, the ductile crust and the upper fragile crust through which volatiles move from the Earth interior to the atmosphere. The He isotopes are in turn tracers of these mantle derived fluids at the Earth's surface due to two main conditions: firstly, the mantle retains isotopically distinct primordial He and, secondly, He concentrations in shallower sourced fluids are extremely low and the resulting He isotopic ratio is higher enough (>0.1Ra; Ballentine et al., 2002) to clearly show a mantle derived component. As a result, trace inputs of He from the deep Earth can be identified at the surface, and the source of this He (mantle or crust) can be solved by using the He isotopes. The sources of mantle He in those regions can be associated to magmatism at depth (storage of magma at the mantle-crust boundary or into the crust) or to mantle-derived

gases, generally CO2-rich, that are accumulated for long time into the crust (Ballentine et al., 2001). He isotopes in turn give important constraints to the geodynamic and tectonic evolution of the study area and combined with geophysical data can also contribute to solve the mantle-crust tectonic at regional scale and to produce 2D and 3D models of the shallow lithosphere (e.g., Zhao et al., 2002; Klemperer et al., 2013; Crossey et al., 2016). As a consequence in seismically active regions He can furnish critical constraints to investigate the preparatory phases of an earthquakes because mantle He moving towards the surface can mix with that produced in the crust by U and Th over time, which release is function of the field of stress of the rocks. Therefore, once again He is a tracer of the Earth dynamic and it's evolution (here at local scale). More in details, degassing of He produced in the crust occurs under different conditions, and it mainly consists of two stages that act on different scales: (1) the release of volatiles from the mineral/rocks and (2) their transport toward the surface (Ballentine and Burnard, 2002). Experimental studies and theoretical calculations have highlighted that noble gases (e.g., He and Ar) produced in the crust can be effectively released under compression and the related dilatancy (Scholz et al., 1973; Honda et al., 1982). Furthermore, the flux of noble gases produced in the crust is also controlled by the fracturing of rock (Torgersen and O'Donnell, 1991). Scholz et al. (1973) highlighted that the release of volatiles from rock can be explained using a dilatancy model, which represented the first indication of the role of dilatancy in triggering earthquakes. Honda et al. (1982) subsequently highlighted that the amount of rare gases degassed from compressed rock is proportional to the degree of dilatancy, probably due to the creation of newly exposed surfaces by microcracking, which allows atoms of rare gases residing in the vicinity of the fresh surface to escape. Dilatant fractures in normal fault zones are widely recognized as the transfer of He through the crust, from the production site to the near-surface system, needs a driving force. This can take the form of concentration and pressure gradients that result in diffusion and advective fluid flow, respectively. Helium remains in trace amounts in the pore fluids, and its movement is strongly dependent on the behavior of the fluids occupying the pore spaces (Ballentine and Burnard, 2002). Hence, the transfer of fluids within the pore space can carry the crustal He away from the site of production.

A geochemical study carried out in Southern Italy that is one of the most worldwide seismically active regions showed extraordinarily high outputs of crustal derived 4He that cannot be solely due to the whole-rock production rate and a long-lasting diffusion degassing through the crust of the produced 4He. This study explored the relationship between the volume of fractured rock and the related release of Helium. The results support that crustal degassing can be controlled by tectonic processes resulting in seismic events. The high seismicity in this section of the Apennines provides the conditions necessary for a massive release of Helium that has accumulated in the rock structure over a long time period of time. Hence it has been identified that the assessed high crustal 4He output can be attributed to an intense fracturing of a calculable volume of rock, which gives new constraints on the volume of rock involved in high-magnitude earthquakes in the region.

This short dissertation introduces the use of the noble gases as geochemical tracers of the Earth dynamic and evolution and here I have tried to emphasize how these volatiles (amounts and isotopes) are able to trace processes at different scales. Their use contributes to recognition of the different stages of the Earth's history and the main processes that contributed to its evolution (macro-scale issues). This has contributed to a better understanding of the planet and its ability to sustain life for the future. The noble gases also contribute to our understanding as to the processes that can influence our existence such as volcanic eruptions and / or major earthquakes (micro-scale issues) contributing to a quality of life in the regions of the world susceptible to these significant processes. In summation the use of the noble gases as geochemical tracers of Earth dynamic and its evolution have a direct link with life on our planet.

In this project of doctorate I challenged new macro (e.g., mantle heterogeneity and continental mantle geochemistry) and micro-scale issues (e.g., earth degassing and earthquakes; oil maturity and magma degassing) with the purpose to make a little advance in science that can be useful to the scientific community

References

Avice, G., and B. Marty (2014). The iodine–plutonium–xenon age of the Moon–Earth system revisited. Phil. Trans. R. Soc., A 372, 20130260.

Ballentine C.J. and D.N. Barfod (2000). The origin of air-like noble gases in MORB and OIB. Earth Planet. Sci. Lett., 180, 39-48.

Ballentine, C. J., M. Schoell, D. Coleman and B. A. Cain (2001). 300-Myr-old magmatic CO_2 in natural gas reservoirs of the west Texas Permian basin. Nature 409, 327–331, https://doi.org/10.1038/35053046.

Ballentine, C. J., and P. G. Burnard (2002). Production, release, and transport of noble gases in the continental crust. Rev. Mineral. Geochem., 47, 481–538.

Ballentine, C. J., R. Burgess, and B. Marty (2002). Tracing fluid origin, transport, and interaction in the crust. Rev. Mineral. Geochem., 47, 539–614.

Ballentine, C.J., B. Marty, B. Sherwood Lollar and M. Cassidy (2005). Neon isotopes constrain convection and volatile origin in the Earth's mantle. Nature, 433, 33-38.

Broadley, M.K., Barry, P.H., Bekaert, D.V., Byrne, D.J., Caracausi, A., Ballentine, C.J. and B. Marty (2020). Identification of chondritic. Proc. Natl. Acad. Sci. U.S.A. doi/10.1073/pnas.2003907117

Burnard P., S. Bourlange, P. Henry P., l. Geli, M.D. Tryon, B. Natal'in, A.M.C. Sengor, M.S. Ozeren and M.N. Cagatay (2012). Constraints on fluid origins and migration velocities along the Marmara Main Fault (Sea of Marmara, Turkey) using helium isotopes. Earth Planet. Sci. Lett., 341–344, 68–78

Burnard, P. (2013), The Noble Gases as Geochemical Tracers, edited by P. Burnard, pp. 177–223, Springer, Berlin.

Caracausi, A., R. Favara, S. Giammanco, F. Italiano, Paonita, G. Pecoraino, A. Rizzo and P.M. Nuccio (2003). Mount Etna: Geochemical signals of magma ascent and unusually extensive plumbing system. Geophys. Res. Lett. 30, 1057. doi:10.1029/2002gl015463

Caracausi, A., R. Favara, F. Italiano, P.M. Nuccio, A. Paonita A. and A. Rizzo (2005). Active geodynamics of the central mediterranean sea: tensional tectonic evidences in western sicily from mantle-derived Helium. Geophys. Res. Lett., vol. 32, L04312, doi:10.1029/2004GL021608;

Caracausi, A., P.M Nuccio, R. Favara, M. Nicolosi and M. Paternoster (2009). Gas hazard assessment at the Monticchio crater lakes of mt. Vulture, a volcano in southern Italy. Terra Nova 21, 83-87, doi:10.11111/1365-3121.200800858;

Caracausi, A., M. Nicolosi, M.P Nuccio, R. Favara, M. Paternoster and A. Rosciglione (2013). Geochemical insight on the unique case of different structure and dynamic of two adjacent maar lakes, Mt. vulture Volcano (Southern Italy). Geochemistry, Geophysics, Geosystems, vol. 14, N.5, doi:10.1002/ggge.2011

Caracausi, A. and M. Paternoster (2015). Radiogenic helium degassing and rock fracturing: a case study of the southern Apennines active tectonic region, J. Geophys.,

Res.- Solid Earth, doi: 10.1002/2014JB011462;

Chiarabba, C., and G. Chiodini (2013). Continental delamination and mantle dynamics drive topography, extension and fluid discharge in the Apennines. Geology, 41(6), 715–718. https://doi.org/10.1130/G33992.1

Chivas, A. R., I. Barnes, W.C. Evans, J. E. Lupton and J. O. Stone (1987). Liquid carbon dioxide of magmatic origin and its role in volcanic eruptions. Nature, 326, 587 589.

Clarke , W.B, M.A. Beg and H. Craig (1969). Excess ^{3}He in the sea: Evidence for terrestrial primordial helium. Earth Planet. Sci. Lett, 6, 213-20.

Craig, H., W.B Clarke ,and M.A. Beg (1975). Excess ^{3}He in deep water on the East Pacific Rise. Earth Planet. Sci. Lett, 26, 125-32.

Crossey, L.J., K. E. Karlstrom, B. Schmandta, R.R.Crow, D.R.Colman, B. Cron, C.D. Takacs-Vesbach, C. N. Dahm, D. E. Northup, D.R. Hilton, J.W. Ricketts, A.R.Lowry (2015). Continental smokers couple mantle degassing and distinctive microbiology within continents. Earth Planet. Sci. Lett, 435, 22–30.

Di Luccio, F., G. Chiodini, S. Caliro, C. Cardellini, V. Convertito, A.N. Pino, C. Tolomei and G. Ventura (2018). Seismic signature of active intrusions in mountain chains. Sci. Adv. 2018; 4: e1701825;

Gonnermann H. M. and S. Mukhopadhyay (2007). Non-equilibrium degassing and a primordial source for helium in ocean-island volcanism, Nature, Vol 449| 25 October 2007| doi:10.1038/nature06240

Holland, G. and C. J. Ballentine, (2006). Seawater subduction controls the heavy noble gases composition of the mantle. Nature 441/1, 186-191.

Holland, G., Cassidy M. and C.J. Ballentine (2009). Meteorite Kr in the Earth's mantle suggests a late accretionary source for the atmosphere. Science 326, 1522-1525.

Honda, M., K. Kurita, Y. Hamano, and M. Ozima (1982), Experimental studies of He and Ar degassing during rock fracturing. Earth Planet. Sci. Lett., 59, 429–436.

Honda, M., I. McDougall, D.B. Patterson, A. Doulgeris and D.A. Clague (1991). Possible solar noble-gas component in Hawaiian basalts. Nature 349, 149-151.

Kendrick, M. A., M. Honda, T. Pettke, M. Scambelluri, D. Phillips and A. Giuliani, (2013). Subduction zone fluxes of halogens and noble gases in seafloor and forearc serpentinites. Earth Planet. Sci. Lett. 365, 86-96.

Kennedy, B.M., Y.K. Kharaka, W.C. Evans, A. Ellwood, D.J. De Paolo, J.J. Thordsen, G. Ambats, and R.H. Mariner (1997). Mantle fluids in the San Andreas fault system,
California. Science 278, 1278–1281.

Kerr, R. A. (1986). Nyos, the Killer Lake, May Be Coming Back. Science, 233, 1257-1258.ù

Klemperer, S.L., B.M. Kennedy, S.R., Sastry Y. Makovsky , T. Harinarayana, M. L. Leech (2013). Mantle fluids in the Karakoram fault: Helium isotope evidence. Earth Planet. Sci. Lett., 66, 59–70.

Kling, G. W. (1987). Seasonal Mixing and catastrophic Degassing in Tropical Lakes, Cameroon, West Africa. Nature, 237, 1022-1024.

Kunz,J., T. Staudacher and C. J. Allègre (1988), Plutonium-fission xenon found in Earth’s mantle. Science 280, 877–880.

Graham D.W. (2002). Noble gases Isotope Geochemistry of Mid-Ocean Ridge and Oceanic Island Basalts: Characterisation of the mantle source reservoirs. Rev. Mineral. Geochem., 47,247-305.

Italiano, F., M. Martelli, G. Martinelli, and P. M. Nuccio (2000). Geochemical evidence of melt intrusions along lithospheric faults of the southern Apennines, Italy: Geodynamic and seismogenic implications. J. Geophys. Res., 105, 13,569–13,578, doi:10.1029/2000JB900047.

Italiano, F., M. M. Martelli, G. Martinelli, P. M. Nuccio, and M. Paternoster (2001). Significance of earthquake-related anomalies in fluids of Val D’Agri (southern Italy), Terra Nova, 13, 249–257.

Labidi, J., P.H. Barry, D. V. Bekaert, M.W. Broadley, B. Marty, T. Giunta, O. Warr, B. Sherwood Lollar, T.P Fischer, G. Avice, A. Caracausi, C.J. Ballentine, S.A. Halldórsson, A. Stefánsson, M.D. Kurz, I.E. Kohl, E.D. Young (2020). Hydrothermal 15N15N abundances constrain the origins of mantle nitrogen. Nature 580, 367–371. doi:10.1038/s41586-020-2173-4.

Lupton, J.E. and Craig H. (1981). A major helium-3 source at 15°S on the East Pacific Rise. Science, 214, 13-18.

Mamyrin, B.A. and I.N. Tolstikhin (1984). Helium isotopes in nature, Developments in Geochemistry, 3, Elsevier, W.S., Advisory Editor, 1-274.

Martelli, M., A. Caracausi, A. Paonita and A. Rizzo (2008). Geochemical variations of air-free crater fumaroles at Mt Etna (Italy): new inferences for forecasts of shallow volcanic activity. Geophys. Res. Lett., 35, L21302, doi: 10.102972008GL035118;

Marty, B. (1989). Neon and xenon isotopes in MORB: implications for the Earth–atmosphere evolution. Earth Planet. Sci. Lett., 94, 45–56.

Marty, B. and L. Zimmermann (1999). Volatiles (He, C, N, Ar) in mid-ocean ridge basalts: Assesment of shallow-level fractionation and characterization of source composition. Geochim. Cosmochim. Acta 63, 3619–3633.

Mukhopadhyay, S. (2012). Early differentiation and volatile accretion recorded in deep-mantle neon and xenon. Nature 486, 101-106 (2012).

Mukhopadhyay, S. and R. Parai (2019). Noble Gases: A Record of Earth's Evolution and Mantle Dynamics. Annu. Rev. Earth Planet. Sci. 47, 389–419. doi:10.1146/annurev-earth-053018-060238

O'Nions, R. K., and E. R. Oxburgh (1986). Helium volatile fluxes and the development of continental crust, Earth Planet. Sci. Lett., 90, 331–347.

O'Nions, R. K., and E. R. Oxburgh, (1988). Helium, volatile fluxes and the development of continental crust. Earth Planetary Science Letters, 90(3), 331–347. https://doi.org/10.1016/0012-821X(88)90134-3.

Ott, U. (2014). Planetary and pre-solar noble gases in meteorites. Chem. Erde 77, 519-544.

Oxburgh, E. R., R. K., O'Nions and R. I. Hill, (1986). Helium isotopes in sedimentary basins. Nature, 324, 18–25.

Ozima, M., and F. A. Podosek (2002). Noble Gas Geochemistry, 286 pp., Cambridge Univ. Press, Cambridge, U. K.

Paonita, A., A. Carasausi, M. Martelli and A.L. Rizzo (2012). Geochemical evidence for mixing between fluids exolved at different depths in the magmatic system of Mt Etna (Italy). Geochim. Cosmochim. Acta, 84, 380-394;

Paonita, A., A. Caracausi, M. Martelli and A.L. Rizzo (2016). Time variations of He isotopes in volcanic gases quantify pre-eruptive refill and pressure buildup in magma reservoirs: The case of Mount Etna, Geology. DOI: 10.1130/G37807.1;

Parai, R., S. Mukhopadhyay and J. J. Standish (2012). Heterogeneous upper mantle Ne, Ar and Xe isotopic compositions and a possible Dupal noble gas signature recorded in basalts from the Southwest Indian Ridge. Earth Planet. Sci. Lett. 359-360, 227-239.

Parai, R., and S. Mukhopadhyay (2015). The evolution of MORB and plume mantle volatile budgets: Constraints from fission Xe isotopes in Southwest Indian Ridge basalts. Geochem., Geophys. Geosyst. doi: 10.1002/2014GC005566.

Pepin, R.O. and D. Porcelli (2002). Origin of noble gases in the Terrestrial Planets. Rev. Mineral. Geochem., 47, 191–246.

Peto, M. K., S. Mukhopadhyay and K.A. Kelley (2013). Heterogeneities from the first 100 million years recorded in deep mantle noble gases from the Northern Lau Back-arc Basin. Earth Planet. Sci. Lett. 369–370, 13–23

Porcelli, D. and C. J. Ballentine (2002). Models for distribution of terrestrial noble gases and evolution of the atmosphere. Rev. Mineral. Geochem. 47, 411–480.

Porcelli D., C.J., Ballentine and R. Wieler (2002). Noble gases in Gewochemistry and Cosmochemistry, Reviews in Mineralogy & Geochemistry vol.47.14-844.

Rizzo A., A. Caracausi, R. Favara, M. Martelli, P.M. Nuccio, A. Paonita, M. Paternoter, A. Rosciglione (2006). New insights into magma dynamics during last two eruptions of Monte Etna as inferred by geochemical monitoring from 2002 to 2005. Geochemistry, Geophysics, Geosystems, 7, 6, doi: 10.1029/2005GC001175

Sano, Y., M. Kusakabe, J. Hirabayashi, Y. Nojiri, H. Shinohara, T. Njine and G. Tanyileke (1990). Helium and carbon fluxes in lake Nyos, Cameroon: constrain on next gas burst, Earth Planet. Sci. Lett., 99, 303-314.

Sano, Y., T. Kagoshima, N. Takahata, Y. Nishio, E. Roulleau, D.L. Pinti and T.P. Fisher (2015). Ten-year helium anomaly prior to the 2014 Mt Ontake eruption. Scientific reports, Nature, doi: 10.1038/srep13069.

Scholz, C. H., L. R. Sykes, and Y. P. Aggarwal (1973), Earthquake prediction: A physical basis. Science, 181, 803–810.

Stanley, R.H.R. and W.J. Jenkins (2013). Noble gases as Environmental Tracers in Sediment Porewaters and Stalagmite Fluid innclusions, In Noble gases as Geochemical Tracers, Pete Burnard Editor, Springer, 123-154.

Sumino, H., R. Burgess, T. Mizukami, S. R. Wallis, G. Holland, and C. J. Ballentine (2010). Seawater-derived noble gases and halogens preserved in exhumed mantle wedge peridotite. Earth Planet. Sci. Lett. 294, 163-172.

Tamburello, G., S. Pondrelli, G. Chiodini and D. Rouwet (2018). Global-scale control of extensional tectonics on CO_2 earth degassing. Nature Communications, DOI: 10.1038/s41467-018-07087-z

Torgersen, T., and W. B. Clarke (1985), Heliumaccumulation in groundwater: I. An evaluation of sources and the continental flux of crustal 4He in the Great Artesian Basin, Australia. Geochim. Cosmochim. Acta, 49, 1211–1218, doi:10.1016/0016-7037(85)90011-0.

Torgersen, T., and J. O'Donnell (1991). The degassing flux from the solid Earth: Release by fracturing. Geophys. Res. Lett., 18, 951–954, doi:10.1029/91GL00915.

Trieloff M. , J. Kunz and C. J. Allègre (2002). Noble gas systematics of the Réunion mantle plume source and the origin of primordial noble gases in Earth's mantle. Earth Planet. Sci. Lett. 200, 297–313.

Yokochi, R. and B. Marty (2004). A determination of neon isotopic composition of the deep mantle. Earth Planet. Sci. Lett. 225, 77-88.

Zhao, D., O.P. Mishra and R. Sanda (2002). Influence of fluids and magma on earthquakes: seismological evidence, Physics of the Earth and Planetary Interiors, 249–249.

Resumé

Le dégazage des fluides du manteau dans les régions continentales se produit principalement dans les régions volcaniques et sismiques. Ces fluides sont utilisés pour comprendre l'évolution du manteau terrestre, l'origine du volcanisme, les processus sismogéniques, le rôle des discontinuités tectoniques dans le transfert des fluides à travers la croûte, etc. Dans ce cadre, les gaz nobles représentent des outils puissants en sciences de la Terre et des planètes, et de par leur géochimie particulière couvrent un domaine plus vaste et plus polyvalent que presque tous les autres domaines de la géochimie. Ils sont utilisés dans la cosmochimie, les sciences de la Terre, les sciences océaniques, la géodynamique et la tectonique active, les études du climat et les sciences de l'environnement.

Dans mon projet, j'ai utilisé les gaz rares pour étudier les processus naturels dans différents contextes géodynamiques (c'est-à-dire la subduction, la collision continentale, le rifting).

Les résultats de mon projet peuvent être résumés en cinq thèmes principaux :

1) Aperçu de l'histoire du dégazage du manteau terrestre à partir de l'analyse haute précision des gaz rares du gaz magmatique.

L'origine de la province volcanique d'Europe centrale (CEVP) est restée énigmatique compte tenu du potentiel d'une source de type OIB de contribuer au volcanisme intraplaque dans la région de l'Eifel. Dans cette contribution, nous montrons que la source du manteau située sous l'Eifel et, par extension, le CEVP, possède une signature géochimique similaire au réservoir du manteau supérieur échantillonné au niveau des dorsales océaniques. Bien que nos résultats réfutent une origine identique aux OIB issue d'un panache profond pour le volcanisme de l'Eifel, la systématique de Ne et Xe, nous indique des contributions provenant de multiples réservoirs ayant des historiques de dégazage différents, provenant de différentes profondeurs dans le manteau sous le CEVP.

2) Systématique des gaz nobles et des isotopes du carbone sur le volcan Ciomadul, apparemment inactif (Europe centrale et orientale, Roumanie): données probantes sur le dégazage volcanique.

Ici, j'ai étudié les émissions de gaz du volcan Ciomadul, un volcan longtemps dormant d'Europe centrale et orientale. Les compositions isotopiques du carbone et de l'hélium fournissent des preuves d'un composant magmatique important, mis en évidence dans la zone ou le flux de CO_2 du sol est le plus élevé. Les évidences géochimiques concordent avec les observations géophysiques et pétrologiques selon lesquelles une intrusion de magma en cours de dégazage pourrait encore exister sous Ciomadul, bien que la dernière éruption volcanique soit survenue il y a des milliers d'années

3) Fluides dérivés du manteau dans le bassin sédimentaire de Java oriental, Indonésie.

Je rapporte ici les résultats d'un levé géochimique des gaz effectué dans la partie sud du bassin sédimentaire de Java Est. Plusieurs champs d'hydrocarbures (HC) et des sites d'infiltration de surface adjacents sont situés près du volcan Arjuno-Welirang et autour du

site d'éruption de Lusi. Les échantillons prélevés dans les champs de HC et dans les suintements de surface révèlent des espèces de C remarquablement différentes. Cependant, en accord avec la géochimie de He, tous ces fluides ont une signature claire du manteau comparable à celle des fluides émis aux fumerolles de Lusi et Arjuno-Welirang. Ces résultats permettent de mettre en évidence le système de failles qui contrôlent la migration des fluides dérivés du manteau sur une vaste région du bassin sédimentaire abritant les champs de HC et qui relie le HC au volcan Arjuno-Welirang.

4) Dégazage des volatils du manteau dans un régime tectonique de compression hors du volcanisme: rôle de la délamination continentale.

Ce travail démontre que le dégazage des volatils du manteau peut également se produire dans un régime géodynamique en compression (centre de la Méditerranée). Ici, les isotopes permettent de résoudre les différents contributions entre la croûte et le manteau et mettent en évidence la présence de magmas dérivés du manteau sans aucune trace de volcanisme à la surface. Les données géologiques et géophysiques confirment la présence d'un coin de manteau chaud au-dessous de la zone caractérisée par le dégazage des éléments volatils du manteau à la surface. Ce coin de manteau dans un système de collision est dû à des processus de délamination bien connus pour produire du magmatisme à grande échelle.

5) Dégazage continental de l'hélium en milieu tectonique actif (nord de l'Italie): rôle de la sismicité.

Cette étude démontre que dans les régions tectoniquement actives, le dégazage de ^{4}He issu de la croûte terrestre peut se produire de manière épisodique et être alimenté par des processus sismogéniques sous forme advective. En effet, dans la zone étudiée, le flux de ^{4}He traversant la croûte vers l'atmosphère est supérieur à celui dû à un dégazage diffusif à l'état d'équilibre et cet excès peut être contrôlé par la sismicité locale. Compte tenu du lien reconnu entre déformation / fracturation de la roche et dégazage de l’He, la surveillance du flux d’He dans les régions sismiquement actives peut potentiellement apporter la preuve d’une modification du champ de contrainte due à la tectonique active, constituant un paramètre clé pour une meilleure connaissance des processus sismogéniques.

Abstract

Outgassing of mantle fluids in continental regions mainly occur in volcanic region and seismic regions. These fluids are used for understanding the evolution of the Earth mantle, the origin of volcanism, the seismo-genetic processes, the role of the tectonic discontinuities in the transfer of fluids through the crust, etc.. In this scenario, the noble gases are powerful tools in Earth and Planetary sciences, in fact its geochemistry also is a broader and more versatile field than almost any other area of geochemistry. It pervades cosmochemistry, Earth sciences, oceanic sciences, geodynamic and active tectonic, climate studies and environmental sciences.

In my project, I used the noble gases to investigate natural processes in different geodynamical contexts (i.e., subduction, continental collision, rifting).

The results of my project can be summarized in five main themes:

1) Insights into the degassing history of Earth's mantle from high precision noble gas analysis of magmatic gas.
The origin of the Central Europe Volcanic Province (CEVP) has remained enigmatic given the potential for an OIB-like source to contribute to intraplate volcanism in the Eifel region. In this contribution, we show that the mantle source beneath Eifel, and by extension the CEVP, has a geochemical signature akin to the upper mantle reservoir sampled at mid ocean ridges. Although our results refute a deep plume OIB-like origin for volcanism in Eifel, Ne and Xe systematics, therefore point toward contributions from multiple reservoirs with different degassing histories, originating from different depths in the mantle beneath the CEVP.

2) *Noble Gas and Carbon Isotope Systematics at the Seemingly Inactive Ciomadul Volcano*

(Eastern-Central Europe, Romania): Evidence for Volcanic Degassing.

Here, I investigated gas emissions at the Ciomadul volcano, a long-dormant volcano in Eastern-Central Europe and the carbon and He isotopic compositions provide evidences for a significant magmatic component, which major contribution occurs in the area of the highest CO_2 flux from soil.

The geochemical evidences are consistent with geophysical and petrologic that a degassing magmatic intrusion could still exist beneath Ciomadul, notwithstanding the last volcanic eruption occurred thousands of years ago.

3) *Mantle-Derived Fluids in the East Java Sedimentary Basin, Indonesia.*

I report the results of a gas geochemistry survey conducted in the southern part of the East Java sedimentary basin. Here several Hydrocarbon (HC) fields and adjacent surface seepage sites are located near the Arjuno-Welirang volcano and around the Lusi eruption site. The samples collected from the HC fields and from surface seepages reveal remarkably different of the C-species. However, all these fluids have a clear mantle-derived He signature that is comparable to that in the fluids emitted at the Lusi and Arjuno-Welirang fumaroles. These results allow to recognize the system of faults that control the migration of mantle-derived fluids over a larger region of the sedimentary basin hosting the HC fields and connect the HC to the Arjuno-Welirang volcano.

4) *Outgassing of Mantle Volatils in Compressional Tectonic Regime Away From Volcanism: The Role of Continental Delamination.*

This work demonstrates that outgassing of mantle volatils can also occur in a compressional geodynamic regime (central Mediterranean). Here He isotopes contribute to solve the mantle-crust

tectonics and highlight the occurrence of mantle-derived magmas without any evidences of volcanism on the surface. The geological and geophysical data support the presence of a hot mantle wedge below the area characterized by the outgassing of mantle volatils at the surface. This mantle wedge in a collisional system is due to delamination processes that is well recognized to produce magmatism at a large scale.

5) *Continental degassing of helium in an active tectonic setting (northern Italy): the role of seismicity.*

This study demonstrates that in tectonically active regions, the crustal ^{4}He degassing can episodically occur and powered as an advective process by seismo-genetic processes. In fact, in the studied area the ^{4}He flux trough the crust towards the atmosphere is higher than that due to a steady-state diffusive degassing and this excess can be due to the local seismicity. Considering the recognized link between rock deformation/fracturation and He degassing, the monitoring of the He flux in seismically active regions can potentially provide evidences of a modification of the field of stress due to the active tectonics, being a key parameter for a better knowledge of the seismo-genetic processes.

Résumé étendu

1) Nouveaux aperçus de l'histoire du dégazage du manteau terrestre à partir de l'analyse de haute précision des gaz rares du gaz magmatique

La composition isotopique des gaz rares du manteau peut fournir des informations uniques sur l'origine et l'évolution des éléments volatils de la Terre. Les isotopes du xénon combinent des signatures primordiales avec des contributions venant de radionucléides éteints et existants, offrant ainsi le potentiel de donner des contraintes à la fois sur la nature du ou des précurseurs planétaires de la Terre et sur le calendrier de leurs contributions. Cependant, il est difficile de mesurer la composition isotopique du Xe des échantillons dérivés du manteau avec une précision suffisante en raison (i) de la présence importante d'un composant atmosphérique de type moderne dans le manteau et (ii) de la contribution/contamination atmosphérique peu profonde et post-éruptive. Les échantillons dérivés du manteau ne présentent donc que de faibles écarts par rapport à la composition atmosphérique actuelle, ce qui complique l'identification et la déconvolution des signaux de Xe dérivés du manteau.

Les gaz riches en CO_2 dérivés du manteau constituent des ressources particulièrement puissantes pour l'étude des gaz rares dérivés du manteau, car les grandes quantités d'échantillons disponibles permettent des mesures de haute précision (Ballentine et al., 2001 and 2005 ;Holland et al., 2009; Caffee et al., 1999). Nous rapportons ici les mesures isotopiques du xénon dans les gaz d'un puits riche en CO_2 (Victoriaquelle) dans la région volcanique de l'Eifel (Allemagne). Les données géophysiques et géochimiques suggèrent que le volcanisme de l'Eifel, qui s'est déroulé de 700 ka à 11 ka, était lié au rifting continental et à la remontée du manteau à grande échelle sous la plaque (Hoernle et al., 1995; Goes et al., 1999; Buikin et al., 1999). Le puits de Victoriaquelle, au sud-ouest de la région de l'Eifel, émet des gaz dominés par le CO_2 (de 99,6% à 99,8%) avec des rapports isotopiques de He de 4,2 à 4,5 Ra (où Ra est la signature isotopique de l'hélium de l'atmosphère terrestre) et $^{40}Ar/^{36}Ar$ jusqu'à 2690 (Brauer et al., 2013 ; Caracausi et al., 2015), ce qui correspond à de faibles niveaux de contamination atmosphérique et à des émissions volatils provenant principalement du manteau.

Nous utilisons ici la méthode d'échantillonnage de Giggenbach pour concentrer les gaz nobles magmatiques de la région volcanique de l'Eifel (Allemagne) dans des bouteilles en verre afin de réaliser des analyses de haute précision des isotopes de Ne, Ar et Xe. Les trois échantillons prélevés dans les puits de Victoriaquelle et Schwefelquelle (Eifel du Sud-Est) montrent des contributions variables de la contamination atmosphérique, l'échantillon le moins contaminé atteignant un rapport $^{40}Ar/^{36}Ar \sim 8\,300$. Nos données indiquent que le manteau situé sous la zone volcanique de l'Eifel et, par extension, sous la province volcanique d'Europe centrale, ressemble au réservoir convectif du manteau supérieur avec peu de preuves d'une contribution d'une source panache profond de type OIB. Sa signature géochimique est similaire (par exemple, dans la composition isotopique de Ne, $^{40}Ar/^{36}Ar$, $^{129}Xe/^{130}Xe$ et $^{129}Xe/^{136}Xe$) à la source du manteau de ce qu'on appelle les « poping rocks » (censées représenter au mieux le manteau supérieur), avec une source supplémentaire de Xe dérivé de ^{238}U et de $^{3}He/^{4}He$ faible que nous attribuons à l'influence d'un composant ancien subduit (HIMU). Une dichotomie existe entre les principales sources d'isotopes de xénon fissiogéniques mesurées dans des roches à gonfler et dans le gaz d'Eifel, qui semblent être principalement dérivées de ^{244}Pu et de ^{238}U, respectivement. Selon leurs rapports respectifs de Xe dérivé de ^{244}Pu-^{238}U, les sources mantellqiues pour le volcanisme Eifel et pour les popping rocks auraient subi un dégazage important et limité, respectivement. À cet égard, le Pu–Xe/(Pu + U)–Xe élevé peut ne plus être considéré comme révélateur d'une origine profonde du manteau, ce qui appelle une redéfinition des différences géochimiques entre les sources de panache et de MORB, avec la possibilité que

les signatures dans la Terre solide puissent être distribuées de manière plus hétérogène qu'on ne le pensait auparavant.

2) *Dégazage magmatique de volcans inactifs et quiescents : systématique des gaz nobles et des isotopes de carbone sur le volcan Ciomadul, apparemment inactif (Europe centrale et orientale, Roumanie).*

La manière dont le CO_2 et les autres gaz volatils du manteau sont extraits est cruciale pour comprendre l'évolution de la composition de l'atmosphère au cours des temps géologiques, de la vie sur Terre et des changements climatiques. Les émissions de CO_2 de la Terre restent peu contraintes, ce qui nuit à notre compréhension du cycle géologique du carbone (Burton et al., 2013).

Bien entendu, les éléments volatils du manteau (par exemple, CO_2) sont principalement extraites de la Terre dans l'atmosphère par le biais du volcanisme aérien et sous-marin. Des études récentes ont montré que le dégazage des éléments volatils du manteau se produit également à partir de systèmes volcaniques inactifs / au repos, soulignant la nécessité de réévaluer les risques naturels dans ces zones. Un nouveau défi des sciences de la Terre consiste à reconnaître le dégazage des volatils dérivés du manteau de volcans au repos de façon à pouvoir quantifier précisément le flux de éléments volatils dérivés du manteau (par exemple, le CO_2). Ceci est fondamental pour comprendre des problèmes aussi divers que les relations entre le dégazage du magma et l'activité volcanique, la pression de gaz et les risques posés par l'éruption des lacs volcaniques ainsi que la réactivation possible des systèmes volcaniques.

Il est largement admis (Burton et al., 2013) qu'il est difficile de comparer des volcans situés dans des zones géographiques distinctes présentant des caractéristiques volcanologiques et des modes de dégazage différents (par exemple, tailles, panache, fumerolles, sols, systèmes géothermiques), en particulier compte tenu des grandes différences entre les volcans encore actifs, en sommeil et éteints, et aussi puisque les émissions de CO2 vont progressivement diminuer avec le temps après la dernière éruption jusqu'à ce qu'un nouveau magma soit fourni au système volcanique.

Toutefois, des études récentes (Caracausi et al., 2015, par exemple) ont montré qu'il existait une relation entre le bilan de CO_2 et le flux total de CO_2 normalisé en fonction de la taille du volcan, des volcans du monde par rapport au temps écoulé depuis leurs dernières éruptions. Une relation de loi de puissance est proposée pour le bilan de CO_2 total et le flux de CO_2 total normalisé en fonction de la taille, respectivement. Cette relation confirme que le dégazage actif de éléments volatils provenant de corps magmatiques froids ou d'intrusions magmatiques solidifiées se produit très longtemps après la dernière activité volcanique et que la variation des éléments volatils libérées au fil du temps est régulée par une relation bien définie.

Même si le flux de CO_2 diminue avec le temps, un tel paramètre normalisé en fonction de la taille, permet de suivre les variations pendant les périodes d'activité (Caracausi et al., 2015), ainsi que de comparer certaines caractéristiques (par exemple l'intensité des émissions et le système d'alimentation) des volcans de différentes tailles et / ou des extensions de la surface de dégazage. Par contre, ce type de paramètre - contrairement à un paramètre lié au budget - peut être fortement modifié (croissant ou décroissant) par d'autres processus modifiant la répartition du dégazage à la surface du volcan (effondrement, ouverture de nouvelles fractures et changements dans le débit des eaux souterraines) qui ne sont pas liés à la capacité du magma à libérer du CO_2.

Alors que la plupart des études précédentes utilisaient la production totale lors de comparaisons (Burton et al., 2013; Shinohara, 2013), les réflexions ci-dessus mettent en évidence l'extrême complexité de ces types d'études. Malheureusement, chacune des

stratégies de comparaison présente à la fois des avantages et des inconvénients, rendant leur choix difficile.
La relation identifiée constitue un outil important pour mieux évaluer l'état d'activité d'un volcan dont la dernière activité volcanique s'est produite il y a assez longtemps pour qu'il soit considéré comme « au repos » ou même « éteint ». En fait, si la production totale de CO_2 et / ou le flux de CO_2 normalisé est supérieur à celui attendu d'après la relation que nous avons identifiée, cela pourrait indiquer la possibilité d'un nouvel apport et d'une réactivation de magma, qui ont tous deux des implications cruciales pour la surveillance des volcans et / ou la protection civile. De plus, nous considérons que des études analogues pourraient améliorer notre compréhension de l'évolution du dégazage de la Terre, à la fois globalement et dans différents cadres géodynamiques.
Ciomadul est le plus jeune volcan de la région des Carpates et de Pannonie, en Europe centrale et orientale, où la dernière éruption a eu lieu 30 ka. Sa chronologie d'éruption est ponctuée par de longues périodes de repos(jusqu'à > 100 kyr) séparant les phases actives; par conséquent, la longue dormance depuis la dernière éruption (30 ka) n'indique pas sans ambiguïté une inactivité. Savoir si du magma réside dans la croûte est fondamental pour évaluer la nature et l'activité du volcan.
Ce volcan est considéré comme étant inactif, cependant, les preuves combinées à partir de données pétrologiques et magnétotelluriques, ainsi que des études de tomographie sismique, suggèrent l'existence d'une bouillie cristalline subvolcanique à teneur variable en liquide magmatique. La région volcanique se caractérise par un débit de sortie de gaz CO_2 élevé, avec un minimum de 8,7 x 10^3 t/an. Nous avons étudié 31 émissions de gaz à Ciomadul afin de déterminer l'origine des éléments volatils. Les compositions $\delta^{13}C_{CO2}$ et $^3He/^4He$ suggèrent le dégazage d'un composant important de fluides dérivés du manteau. La signature isotopique de He dans les fluides gazeux (jusqu'à 3,10 Ra) est inférieure aux valeurs des xénolites de péridotite du champ volcanique de basalte alcalin voisin (R/Ra 5,95 Ra ± 0,01), qui sont représentatives d'un manteau continental lithosphérique et significativement inférieures aux valeurs de MORB. Compte tenu des caractéristiques chimiques de la dacite de Ciomadul, y compris la composition en éléments traces et en isotopes du Sr–Nd et O, une contamination de la croûte supérieure est moins probable, alors que les magmas primaires auraient pu être dérivés d'une source de manteau enrichi. Les faibles rapports isotopiques de He pourraient indiquer une lithosphère du manteau fortement métasomatisée. Cela pourrait être dû à l'infiltration de fluides liés à la subduction et à la croissance post-métasomatique d'He radiogénique. Les fluides métasomatiques sont supposés contenir du carbonate sous-saturé, ce qui entraîne une composition isotopique du carbone plus lourde ($\delta^{13}C_{CO2}$ se situe dans la plage de -1,4 ‰ à -4,6‰) et une augmentation du rapport $CO_2/^3He$. Cette étude montre la contribution magmatique aux gaz émis, bien que le volcan Ciomadul soit classé volcan volcanique en sommeil.
L'intégration de ces résultats à la modélisation (Laumonier et al., 2019_EPSL) et aux observations géophysiques indique qu'une quantité importante de liquide magmatique siliceux riche en eau (au minimum 15%) doit encore être présente dans la croûte supérieure située sous le volcan, ce qui implique qu'il est probable que le réservoir ait été maintenu dans des conditions suffisamment chaudes pour préserver des domaines importants à l'état quasi-éruptible. Cela attire l'attention sur les volcans dormants depuis longtemps et remet en question la définition des volcans potentiellement actifs, dormants et éteints (Szakács, 1994), étant donné que leurs systèmes de plomberie peuvent être comparables à ceux des volcans actifs.

3) Fluides dérivés du manteau dans les bassins sédimentaires: le cas de Java oriental, Indonésie

Les rejets de gaz carbonés de la Terre sont généralement classés en deux grands domaines géologiques distincts: (a) les systèmes liés aux volcans, libérant des gaz riches en dioxyde de carbone (CO_2), généralement produits par le thermométamorphisme des calcaires ou le dégazage du manteau via les magmas et (b) les bassins sédimentaires à basse température, libérant principalement du méthane biotique (CH_4) et d'autres hydrocarbures, produits par la dégradation microbienne ou thermogénique de matières organiques, de pétrole ou de charbon dans des roches sédimentaires. Il existe de nombreux ouvrages sur la géochimie et la géologie de tels processus de dégazage, qui ont des implications considérables pour l'environnement, les aléas géographiques, les changements climatiques globaux et l'exploration des ressources énergétiques (par exemple, des études de cas et des analyses pertinentes sont rapportés par Kerrick, 2001; Etiope et Klusman, 2002; Mörner et Etiope, 2002; Chiodini et al., 2004; Burton et al., 2013). Dans de nombreux cas, cependant, les domaines volcaniques et sédimentaires peuvent se chevaucher partiellement, ce qui conduit à des systèmes géologiques hybrides avec des mélanges de gaz inorganiques et biotiques. Dans ce scénario, il existe des systèmes hybrides appelés systèmes géothermiques hébergés par des sédiments (SHGS) ou systèmes hydrothermaux hébergés par des sédiments (SHHS). Ces systèmes font référence à des bassins sédimentaires perturbés par des intrusions magmatiques ou impliqués dans des systèmes de plomberie volcanique et caractérisés par des fluides géothermiques riches en CO_2 et du CH_4 biotique (microbien ou thermogénique), provenant de sédiments riches en matières organiques. Les concentrations de CO_2 inorganique dépassent généralement 50% en volume. Les concentrations de CH_4 (et d'alcanes plus lourds, tels que l'éthane et le propane) sont généralement plus élevées (environ> 1 à 2% en volume) que celles présentes dans les fluides volcaniques et géothermiques purs (généralement de l'ordre de ppbv ou ppmv; Capaccioni et al., 2004; Etiope et al., 2007; Fiebig et al., 2015). Les SHGS sont courants, en tant que paléo-systèmes, dans les grandes provinces ignées comme celles d'Afrique du Sud, de Sibérie et de l'Atlantique Nord (Svensen et al., 2004; Svensen et al., 2007a, 2007; Svensen et al., 2009a, b). Les SHGS actifs sont reconnus dans la zone de Rift du bassin de Guaymas (Golfe de Californie; Berndt et al., 2016), dans le champ géothermique de la mer de Salton en Californie (par exemple, Mazzini et al., 2011), à Java, en Indonésie (éruption de Lusi; Mazzini et al., 2012), dans le delta du Tibre, à Fiumicino, en Italie centrale (Ciotoli et al., 2016) et dans le bassin de Songliao en Chine (Shuai et al., 2018). Leurs manifestations de surface, telles que les volcans de boue ou les piscines bouillonnantes, peuvent être similaires aux manifestations de gaz sédimentaires purs (suintements d'hydrocarbures), et peuvent donc être confondues avec elles, telles que les volcans de boue (Mazzini et Etiope, 2017), ou simplement manifestations géothermiques/volcaniques (p. ex. mofettes, mares bouillonnantes, geysers vaseux). La distinction entre SHGS, systèmes sédimentaires purs et complexes géothermiques-volcaniques n'est pas seulement un problème de sémantique. L'attribution de SHGS implique en effet la reconnaissance de processus géologiques et géochimiques spécifiques pouvant avoir des implications particulières pour l'exploration pétrolière et les études du changement climatique mondial. Les SHGS, en fait, (1) peuvent conduire à la production d'hydrocarbures résultant de la maturité thermique accrue des roches mères sédimentaires; (2) peuvent être d'importantes sources naturelles d'émissions de gaz à effet de serre (CO_2 et CH_4) dans l'atmosphère, 3) sont des facteurs potentiels des changements climatiques passés (Svensen et al., 2004). Néanmoins, il manque des études systématiques sur la caractérisation active des SHGS et leur répartition mondiale.

Des éruptions de gaz et de boue sont soudainement apparues le 29 mai 2006 le long de la faille de Watukosek au nord-est de Java, en Indonésie. En quelques semaines, plusieurs villages ont été submergés par la boue bouillante. Le site d'éruption le plus important

s'appelait Lusi. À ce jour (novembre 2011), Lusi est toujours active et une zone d'environ 7 km^2 est couverte par la brèche de boue éclatée.
Les mécanismes responsables de cette éruption dévastatrice restent méconnus. Bien qu'il y ait un consensus sur l'origine de la boue, la source d'eau est incertaine, l'origine du gaz est inconnue et le déclencheur de l'éruption est toujours en discussion. Afin de faire la lumière sur ces inconnues, nous avons acquis une vaste gamme de données de composition moléculaire et isotopique du gaz échantillonné dans plusieurs évents de Lusi, dans les volcans de boue environnants, dans le champ de gaz naturel le plus proche (Wunut) et dans les évents hydrothermaux au complexe volcanique voisin dans la période 2006-2011.
Les fluides en ébullition dans la zone du cratère sont apparemment dominés par du CO_2, tandis que des fluides plus froids, porteurs de CH_4 et porteurs de C_2– C_3, sont identifiés sur plusieurs sites autour de la zone du cratère. Les diagrammes génétiques des gaz, les diagrammes de maturité et la modélisation de la génération de gaz suggèrent que les hydrocarbures sont thermogéniques ($\delta^{13}C_1$ à -35‰; $\delta^{13}C_2$ à -20‰), dérivant du kérogène marin.
Le CO_2 libéré par le cratère et les suintements environnants est également thermogénique ($\delta^{13}C$ de -15‰ à -24‰) en relation avec la décarboxylation du kérogène ou l'oxydation thermique au CH_4 dans les roches profondes, bien que trois évents situés juste à l'extérieur du cratère aient montré une signature inorganique apparente (−7,5 ‰<δ13C<−0,5‰) associé à l'hélium manteau (R/Ra jusqu'à 6,5). Des températures d'équilibre élevées CO_2-CH_4 (200–400°C) sont typiques d'hydrocarbures ou de matières organiques altérés thermiquement. Les données suggèrent principalement des sources organiques thermiquement altérées pour les gaz en éruption, plus profondes que la boue et l'eau (schistes de Kalibeng supérieurs). Ces résultats sont compatibles avec un scénario d'intrusions magmatiques profondes (> 4000 m) et de fluides hydrothermaux responsables de la chaleur accrue qui modifie les roches mères et / ou les réservoirs de gaz.
Le bassin sédimentaire d’arrière-arc tertiaire à Java Est (Indonésie) abrite une grande variété de structures de remonté et de champs d'hydrocarbures. Certains de ces derniers (Wunut, Tanggulangin, Carat, Watudakon) sont situés à quelques kilomètres du complexe volcanique Arjuno-Welirang et de Lusi, le plus grand système hydrothermal actif sur terre hébergé par des sédiments. Afin d'étudier les interactions entre les paramètres volcaniques et sédimentaires, nous avons effectué un échantillonnage de gaz sur ces quatre champs pétrolifères peu profonds (200 à 1000 m de profondeur). Les champs autour de Lusi sont dominés par le gaz thermogénique qui a été altéré lors des processus de biodégradation. Les rapports isotopiques de l'hélium ($^3He/^4He$) sont aussi élevés que 6,7 Ra, ce qui est remarquablement similaire à ceux mesurés aux fumerolles du complexe volcanique adjacent (R = 7,3 Ra) et au site de Lusi (jusqu'à 6,5 Ra). Cela met en évidence le dégazage généralisé des fluides dérivés du manteau dans le bassin sédimentaire. Bien que ces deux systèmes partagent la même source d’hélium provenant du manteau, leurs hydrocarbures ont deux antécédents génétiques différents : le gaz d'hydrocarbure de Lusi a été généré plus récemment et est moins fractionné de façon moléculaire et isotopique, tandis que le gaz piégé dans les réservoirs est plus ancien et plus altéré. Contrairement à Lusi, les champs d'hydrocarbures contiennent de petites quantités de CO_2 résultant des processus de biodégradation. Le système de faille de Watukosek, provenant du complexe volcanique Arjuno-Welirang et s’étendant vers le nord-est de Java, coupe Lusi et les champs d’hydrocarbures. Ce réseau de failles contrôle la migration des fluides dérivés du manteau dans le bassin sédimentaire, alimentant la ventilation ciblée sur le site de Lusi et favorisant la migration plus lente et généralisée dans les réservoirs.

4) Dégazage et compression tectoniques, volatils dérivés du manteau: la région centrale de la Méditerranée

Dans les régions continentales, les signatures dérivées du manteau sont souvent masquées par des processus concurrents (tels que la production de 4He radiogénique dans la croûte riche en U-Th) et par de fortes concentrations de ces éléments volatils dans la croûte (par exemple, Caracausi et al., 2005). Néanmoins, comprendre comment dégazer les volatils du manteau dans les régions continentales, où l'activité volcanique n'est pas présente à la surface, reste un défi majeur, étant donné qu'en l'absence de magma, le manteau ne perd pas facilement ses volatils (Watson et Brenan, 1987). Le transfert de éléments volatils du manteau dans la croûte et successivement extraites vers l'atmosphère est le plus efficace en cas de fusion partielle, car les éléments volatils ont une affinité pour la phase liquide. Le dégazage des volatils du manteau fournit donc des preuves solides d'un manteau au-dessus de son solidus même en cas d'absence de volcanisme de surface. On peut en déduire que la tectonique de la croûte et du manteau peut générer les conditions adéquates pour la fusion et les migrations successives des liquides magmatiques vers la surface.

En outre, dans les systèmes liés à la subduction, les fluides de déshydratation peuvent également transférer des fluides dérivés du manteau à la surface, même en l'absence de fusion du coin du manteau (par exemple, Sano and Fisher, 2013). Dans ce cas, un dégazage en surface du He dérivé du manteau n'est pas couplé à des preuves géophysiques de fusion en profondeur.

La géodynamique de la Méditerranée centrale est caractérisée par l'intéraction de la plaque européenne avec la plaque africaine. À l'intérieur de ce bassin, la géologie de la mer Tyrrhénienne méridionale, de la Sicile occidentale et du canal de Sicile est encore mal connue, même si elle revêt une certaine importance pour la compréhension de l'évolution de l'ensemble de la région. Au cours des 25 derniers millions d'années, la géodynamique de la Méditerranée occidentale a été contrôlée par la migration vers l'est de la chaîne des Apenins et des bassins d'arrière arc associés, donnant lieu à différents processus tectoniques, comme en témoignent également les études paléomagnétiques et magnétiques, les études de susceptibilité et les mesures GPS récentes. La Sicile occidentale est un secteur du prisme d'accrétion des Apennins et des Maghrébides, situé entre deux zones touchées par la tectonique en extension, à savoir le bassin de la mer Tyrrhénienne au nord et le canal de Sicile au sud.

Certains systèmes thermiques ont été reconnus en Sicile occidentale et les études précédentes sur ces systèmes portaient principalement sur la géochimie et la circulation des fluides (Favara et al., 2001, et références y figurant). Elles n'ont pas utilisé la géochimie en tant qu'outil possible pour mieux comprendre les processus tectoniques et géodynamiques à l'œuvre dans la région. À cet égard, l'hélium est un puissant outil géochimique, car sa composition isotopique semble être corrélée à la tectonique.

En fait, la distribution de l'hélium dérivé du manteau dans les continents caractérise les zones en extension ou régions avec ajouts contemporains de basalte (O'Nions et Oxburgh, 1988; Ballentine et Burnard, 2002). À l'inverse, de l'hélium radiogénique produit dans la croûte, et son mélange avec l'hélium atmosphérique, marque des zones continentales stables et / ou des marges continentales et des prismes d'accrétion, à travers lesquels les champs de contraintes qui déforment les roches peuvent extraire les eaux concentrées en éléments chimiques et en gaz accumulés dans la croûte. À leur tour, ces fluides sont acheminés par des discontinuités et des failles (Dickens et Kennedy, 2000), atteignant ainsi la surface. Cependant, comme le flux d'hélium radiogénique est lié à l'abondance d'éléments générateurs de chaleur dans la croûte, il est possible, en utilisant la systématique thermique de l'hélium, de distinguer le composant de flux de radioactivité crustale de la chaleur du manteau transmise de manière conductrice par la croûte (O'Nions et Oxburgh, 1983), alors que les excès d'hélium dans le manteau et de la chaleur indiquent

une addition de magma au-dessous ou dans la croûte (Torgersen, 1993). Par conséquent, la large gamme de rapports isotopiques de l'hélium affichée par les systèmes géothermiques situés dans la croûte continentale reflète les contributions variables de ces différents composants de la chaleur. L'évaluation des rapports isotopiques de l'hélium et des données thermiques pourrait donc apporter des contraintes à la tectonique des zones continentales (Torgersen, 1993; Ballentine et Burnard, 2002).
Dans cette étude, je discute de la présence de chaleur et de éléments volatils (c.-à-d. Hélium et CO_2) provenant du manteau, qui alimentent les systèmes hydrothermaux dans une marge sismique entre deux plaques convergentes (africaine et européenne) sans aucun signe de volcanisme. Les isotopes d'hélium (He) indiquent clairement un composant dérivé du manteau dans les éléments volatils dégazés. Les flux d'He estimés dérivés du manteau sont jusqu'à deux ou trois ordres de grandeur supérieurs à ceux d'une zone continentale stable. De tels flux d'He élevés ne peuvent pas être liés à une diffusion de longue durée, ce qui implique un transport plus efficace (c'est-à-dire, un transport advectif à travers des défauts). Les données couplées à la relation chaleur - He suggèrent la présence d'un dégazage actif d'intrusions magmatiques dans cette zone de collision continentale. Les données géophysiques indiquent la présence d'un coin chaud de manteau à l'aplom du dégazage des éléments volatils mantelliques et d'un système de failles découpant la croûte continentale jusqu'au coin de manteau chaud. Nous discutons ici du coin chaud de manteau et des éventuelles intrusions magmatiques associées en tant que source des gaz volatils dérivés du manteau sortant dans la région. J'ai également évalué la production de CO_2 dérivé du manteau des bassins hydrothermaux étudiés. La possible apparition de magma en profondeur ainsi que la géométrie du coin déformé de manière thick-skin indiquent sans ambiguïté des processus de délamination liés à la subduction continentale. Par conséquent, nous montrons que les processus de délamination peuvent réellement produire du magma en profondeur sans évidences de volcanisme à la surface. Enfin, j'ai également étudié les systèmes de failles qui fonctionnent comme un réseau de voies et soutiennent activement le transfert advectif des fluides du manteau vers la surface.
Il s'agit d'un cas rare de dégazage actif de fluides provenant du manteau dans une région caractérisée par une collision continentale. Ces preuves géochimiques soutiennent la présence de corps magmatiques en profondeur et un flux advectif de éléments volatils et de chaleur à travers la croûte. Les données géophysiques corroborent les preuves géochimiques démontrant la présence d'une partie du manteau chaud entre deux couches de croûte terrestre en correspondance des éléments volatils mantelliques à la surface. La géologie, couplée à la géophysique, montre la présence de discontinuités tectoniques amincissant la croûte jusqu'au manteau, formant un réseau de voies à travers lesquelles les fluides du manteau remontent à la surface.

5) Dégazage continental de l'hélium en milieu tectonique actif (nord de l'Italie): rôle de la sismicité.
L'hélium est reconnu comme un traceur puissant dans divers domaines, dont l'hydrologie des eaux souterraines, l'exploration d'hydrocarbures, les processus du manteau et le dégazage de magma (Burnard, 2013). La fusion et la libération de éléments volatils via les magma sont des processus efficaces pour dégazer le manteau. Le dégazage de He produit dans la croûte se manifeste dans des conditions différentes. Il se compose principalement de deux étapes qui agissent à différentes échelles: (1) la libération des éléments volatils des minéraux / roches et (2) leur transport vers la surface (Ballentine et Burnard 2002).
Il existe une grande variabilité dans le flux de 4He dégazant de la croûte continentale (Torgersen, 2010). En outre, la quantité de He accumulée dans les roches de la croûte et la rapidité avec laquelle l'hélium peut être purgé n'ont pas encore été pleinement explorées (Torgersen, 2010; Lowenstern et al., 2014). Bien qu'il soit très mobile, il ne peut pas

s'échapper de manière importante sans un réseau de voies permettant un écoulement de fluide advectif dans la croûte, et il reste piégé dans les roches de très faible perméabilité. Ces caractéristiques signifient que ^{4}He peut résider dans des régions tectoniquement stables, ce qui lui permet de s'accumuler sur de très longues périodes et d'être potentiellement utilisé comme un outil de datation des eaux souterraines (par exemple, Torgersen, 1980; Zhou et Ballentine, 2006). En outre, il existe des preuves sérieuses que le transport vertical à grande échelle de fluides dans la croûte continentale est probablement à la fois advectif et épisodique (par exemple Hu et al., 2009).
Des études expérimentales et des calculs théoriques ont montré que les gaz rares (He et Ar, par exemple) produits dans la croûte peuvent être libérés efficacement par compression et dilatance associée (Scholz et al., 1973; Honda et al., 1982). De plus, le flux de gaz rares produits dans la croûte est également contrôlé par la fracturation des roches (Torgersen et O'Donnell, 1991). Scholz et al. (1973) ont souligné que la libération de éléments volatils de la roche peut être expliquée à l'aide d'un modèle de dilatance, qui constitue la première indication du rôle de la dilatance dans le déclenchement des séismes. Honda et al. (1982) ont ensuite souligné que la quantité de gaz rares dégazés à partir de roche comprimée était proportionnelle au degré de dilatance, probablement en raison de la création de surfaces nouvellement exposées par microfissuration, ce qui permettait aux atomes de gaz rares résidant à proximité de la surface fraîche de s'échapper.
Les fractures dilatantes dans les zones de failles normales sont largement reconnues comme des voies de circulation des fluides dans la croûte, mais la structure de ces réseaux de fractures, leur connectivité et leur évolution temporelle est mal comprise (Holland et al., 2011). Le transfert de He à travers la croûte terrestre, du site de production aux systèmes proches de la surface, nécessite une force motrice. Cela peut prendre la forme de gradients de concentration et de pression entraînant respectivement une diffusion et un écoulement de fluide advectif. L'hélium reste à l'état de traces dans les fluides des pores et son mouvement dépend fortement du comportement des fluides occupant les espaces des pores (Ballentine et Burnard, 2002). Par conséquent, le transfert de fluides dans l'espace des pores peut extraire l'He crustal du site de production.
J'ai étudié les gaz provenant de volcans de boue, de mofettes sèches, de sources et de puits dans une région de tectonique active et de forte sismicité dans le sud des Apennins (Italie), où les tremblements de terre sont désastreux depuis de nombreuses années (MS = 6,9) en 1980. Les fluides consistent en un mélange de éléments volatils dérivées du manteau et de la croûte, avec une contribution faible de l' atmosphère, identifiées par les mesures de signature des isotopes He et du rapport He/Ne. Une année de surveillance mensuelle des concentrations de He et des isotopes de He n'a révélé aucune modification saisonnière ni variations induites par une faible sismicité. Il y a des rendements extraordinairement élevés de ^{4}He produits dans la croûte terrestre (jusqu'à $2{,}5\times10^{28}$ atomes par an^{-1}). Ces rendements ne peuvent pas être uniquement dus au taux de production de la roche et à un dégazage prolongé par diffusion à travers la croûte. Mon étude a exploré la relation entre le volume de roche fracturée et la libération associée de He. Les résultats montrent que le dégazage dans la croûte peut être contrôlé par des événements tectoniques lors des tremblements de terre. La forte sismicité dans ce secteur des Apennins crée les conditions nécessaires à une libération massive de He accumulée dans la roche sur une longue période. Mon travail a révélé que la production de 4He peut être attribuée à la fracturation intense d'un volume de roche calculable, ce qui crée de nouvelles contraintes sur le volume de roche impliqué dans les séismes de magnitude élevée dans la région.
En outre, afin d'étudier la variabilité du dégazage de l'hélium dans les régions continentales, de ses émissions de roches et de son émission dans l'atmosphère, j'ai également étudié le dégazage de éléments volatils dans une région sismiquement active du centre de l'Italie (Mw_{MAX}= 6) à Nirano-Regnano. Les gaz émis dans la zone d'étude sont dominés par le CH_4

et constituent le vecteur du transfert de l'hélium (He) à travers la croûte terrestre. Les isotopes du carbone et du He indiquent sans équivoque que les fluides dérivés de la croûte terrestre dominent ces systèmes. Une reconstruction tridimensionnelle à haute résolution des réservoirs de gaz alimentant les émissions de gaz observées à la surface nous permet d'estimer la quantité d'He stockée dans les réservoirs naturels. Notre étude a démontré que la production in situ de ^{4}He dans la croûte et une diffusion durable à travers la croûte ne sont pas les processus principaux qui régissent le dégazage de He dans la région. De plus, nous avons démontré que la micro-fracturation due au champ de contrainte qui génère la sismicité locale augmente la libération de He des roches et peut maintenir l'excès de He dans les réservoirs naturels en ce qui concerne le dégazage diffusif à l'état d'équilibre. Ces résultats prouvent que 1) le transport des éléments volatils à travers la croûte peut être épisodique en fonction de la déformation de la roche et de la sismicité et 2) Il peut être utilisé pour mettre en évidence les modifications du champ de contraintes induites par les séismes.

Références

Burnard p., (2013), Noble Gases as Geochemical Tracers, Springer,1-391, Pete Burnard editor.

Ballentine, C. J. & Burnard, P. G. Production, Release and Transport of Noble Gases in the Continental Crust. *Rev. Miner. Geochem.* **47**, 481–538, DOI: 10.2138/rmg.2002.47.12 (2002).

Bräuer, K., Kämpf, H., Niedermann, S. & Strauch, G. Indications for the existence of different magmatic reservoirs beneath the Eifel area (Germany): a multi-isotope (C, N, He, Ne, Ar) approach. Chem. Geol. 356, 193–208 (2013).

Berndt, C., Sarkar, S., Geilert, S., Schmidt, M., Liebetrau, V., Kipfer, R., Scholz, F., Doll, M., Muff, S., Karstens, J., Planke, S., Petersen, S., Böttner, C., Chi, W.C., Moser, M., Behrendt, R., Fiskal, A., Lever, M.A., Su, C.C., Buikin, A. et al. Noble gas isotopes suggest deep mantle plume source of late Cenozoic mafic alkaline volcanism in Europe. Earth Planet. Sci. Lett. 230, 143–162 (2005).

Burton, M.R., Sawyer, G.M., Granieri, D., 2013. Deep carbon emissions from volca-noes. Rev. Mineral. Geochem.75, 323–354.

Capaccioni, B., Taran, Y., Tassi, F., Vaselli, O., Mangani, G., Macias, J.L., 2004. Source conditions and degradation processes of light hydrocarbons in volcanic gases: an example from El Chichon volcano (Chiapas State, Mexico). Chem. Geol., 206, 81-96.

Caracausi A., Favara R., Italiano F., Nuccio P.M., Paonita A., Rizzo A. (2005) - Active geodynamics of the central mediterranean sea: tensional tectonic evidences in western sicily from mantle-derived Helium. Geophys. Res. Lett., vol. 32, L04312, doi:10.1029/2004GL021608;

Caracausi, A., Avice, G., Burnard, P.G., Füri, E., Marty, B., 2016. Chondritic xenon in the Earth's mantle. Nature533 (7601), 82.

Caracausi, A., Paternoster, M., & Nuccio, P. M. (2015). Mantle CO2 degassing at Mt. Vulture volcano (Italy): Relationship between CO2 outgassing of volcanoes and the time of their last eruption. Earth and Planetary Science Letters, 411, 268–280. https://doi.org/10.1016/j. epsl.2014.11.049

Chiodini, G., Cardellini, C., Amato, A., Boschi, E., Caliro, S., Frondini, F., Ventura, G., 2004. Carbon dioxide Earth degassing and seismogenesis in central and southern Italy. Geophys. Res. Lett., 31, doi.org/10.1029/2004GL019480.

Ciotoli, G., Etiope, G. Marra, F., Florindo, F., Giraudi C., Ruggiero, L., 2016. Tiber delta CO2-CH4 degassing: A possible hybrid, tectonically active Sediment-Hosted Geothermal System near Rome, J. Geophys. Res. Solid Earth, 121, doi:10.1002/2015JB012557.

Dickens, G. R., and B. M. Kennedy (2000), Noble gases in methane hydrate from Blake Ridge, Proc. Ocean Drill. Program Sci. Results, 164,165– 170.

Etiope, G., Klusman, R., 2002. Geologic emissions of methane to the atmosphere. Chemosphere 49, 777-789.

Etiope, G., Fridriksson, T., Italiano, F., Winiwarter, W., Theloke, J., 2007. Natural emissions of methane from geothermal and volcanic sources in Europe. Journal of Volcanology and Geothermal Research, 165, 76–86.

Fiebig, J., Hofmann, S., Tassi, F., D'Alessandro, W., Vaselli, O., Woodland, A.B., 2015. Isotopic patterns of hydrothermal hydrocarbons emitted from Mediterranean volcanoes. Chemical Geology, 396, 152-163.

Hoernle, K., Zhang, Y. S. & Graham, D. Seismic and geochemical evidence for large-scale mantle upwelling beneath the eastern Atlantic and western and central Europe. Nature 374, 34–39 (1995).

Honda, M., K. Kurita, Y. Hamano, and M. Ozima (1982), Experimental studies of He and Ar degassing during rock fracturing, Earth Planet. Sci.
Lett., 59, 429–436.

Hu, R.-Z., P. G. Burnard, X. W. Bi, M.-F. Zhou, J.-T. Peng, W.-C. Su, and J.-H. Zhao (2009), Mantle-derived gaseous components in ore-forming fluids of the Xianshan uranium deposit, Jiangxi province, China: Evidence from He, Ar, and C isotopes, Chem. Geol., 266, 86–95, doi:10.1016/j.chemgeo.2008.07.017.
Goes, S., Spakman, W. & Bijwaard, H. A lower mantle source for central European volcanism. Science 286, 1928–1931 (1999).
Kerrick, D.M., 2001. Present and past non-anthropogenic CO2 degassing from the solid earth. Rev Geophys 39, 4, 565-585.
Laumonier, M., Karaka, O., Bachmann, O., Gaillard, F., Lukács, R., Seghedi, I., Menand, T., Harangi, S., (2019), Evidence for a persistent magma reservoir with large melt content beneath an apparently extinct volcano, Earth and Planetary Science Letters, https://doi.org/10.1016/j.epsl.2019.06.004.
Lowenstern, J. B., W. C. Evans, D. Bergfeld, and A. G. Hunt (2014), Prodigious degassing of a billion years of accumulated radiogenic helium at Yellowstone, Nature, 506, 355–358, doi:10.1038/nature12992.
Mazzini, A., Svensen, H., Etiope, G., Onderdonk, N., Banks, D. 2011. Fluid origin, gas fluxes and plumbing system in the sediment-hosted Salton Sea Geothermal System (California, USA), J. Volcanol. Geotherm. Res., 205, 76-83.
Mazzini, A., Etiope, G., Svensen, H., 2012. A new hydrothermal scenario for the 2006 Lusi eruption, Indonesia. Insights from gas geochemistry. Earth and Planetary Science Letters, 317–318, 305–318.
Mazzini, A., Etiope, G., 2017. Mud volcanism: An updated review. Earth Science Reviews, 168, 81-112.
Mörner, N.A., Etiope, G., 2002. Carbon degassing from the lithosphere, Global Planet. Change, 33, 185-203.
O'Nions, R. K., and E. R. Oxburgh (1983), Heat and helium in the Earth, Nature, 306, 429– 431.
O'Nions, R. K., and E. R. Oxburgh (1988), Helium, volatile fluxes and the development of continental crust, Earth Planet. Sci. Lett., 90, 331– 347.
Sano Y. And Fisher T., (2013) The Analysis and Interpretation of the noble gases in modern hydrothermal systems, 249-317, In Noble Gases as Geochemical Tracers, Springer,1-391, Pete Burnard editor.
Scholz, C. H., L. R. Sykes, and Y. P. Aggarwal (1973), Earthquake prediction: A physical basis, Science, 181, 803–810.
Shinohara, H., 2013. Volatile flux from subduction zone volcanoes: insights from a detailed evaluation of the fluxes from volcanoes in Japan. J. Volcanol. Geotherm. Res.268, 46–63.
Shuai, Y., Etiope, G., Zhang, S., Douglas, P.M.J., Huang, L., Eiler, J.M., 2018. Methane clumped isotopes in the Songliao Basin (China): New insights into abiotic vs. biotic hydrocarbon formation. Earth and Planetary Science Letters, 482, 213-221.
Svensen, H., Planke, S., Malthe-Sørenssen, A., Jamtveit, B., Myklebust, R., Eidem, T. R., Rey, S.S., 2004. Release of methane from a volcanic basin as a mechanism for initial Eocene global warming. Nature, 429, 542-545.
Svensen, H., Karlsen, D.A., Sturz, A., Backer-Owe, K., Banks, D.A., Planke, S., 2007. Processes controlling water and hydrocarbon composition in seeps from the Salton Sea geothermal system, California, USA, Geology, 35, 85-88.
Svensen, H., Planke, S., Chevallier, L., Malthe-Sørenssen, A., Corfu, F., Jamtveit, B., 2007. Hydrothermal venting of greenhouse gases triggering Early Jurassic global warming. Earth Planet. Sci. Lett., 256, 554-566.
Svensen, H., Planke, S., Polozov, A.G., Schmidbauer, N., Corfu, F., Podladchikov, Y.Y., Jamtveit, B., 2009. Siberian gas venting and the end- Permian environmental crisis. Earth
Planet. Sci. Lett., 277, 490–500.
Svensen, H., Hammer, Ø., Mazzini, A., Onderdonk, N., Polteau, S., Planke, S., Podladchikov, Y.Y., 2009. Dynamics of hydrothermal seeps from the Salton Sea geothermal ystem (California, USA) constrained by temperature monitoring and time series analysis. J. Geoph. Res., 114, doi.org/10.1029/2008JB006247.
Szakács, A., 1994. Redefining active volcanoes: a discussion. Bull. Volcanol.56, 321–325.
Torgersen, T. (1980), Controls on pore fluid concentration of ^{4}He and ^{222}Rn and the calculation of 4He/222Rn ages, J. Geochem. Explor., 13, 57–75, doi:10.1016/0375-6742(80)90021-7.
Torgersen, T., and J. O'Donnell (1991), The degassing flux from the solid Earth: Release by fracturing, Geophys. Res. Lett., 18, 951–954, doi:10.1029/91GL00915.
Torgersen, T. (1993). ^{3}He fluxes in extensional basins: Limits on the role of magmatism in extensional basins. Journal Geophysical Research, 98(B9), 16,257–16,269. https://doi.org/10.1029/93JB00891
Torgersen, T. Continental degassing flux of 4He and its variability. *Geochem. Geophys. Geosystems* **11**, 1–15, DOI: 10.1029/2009GC002930 (2010).
Watson, E. B., & Brenan, J. M. (1987). Fluids in the lithosphere 1: Experimentally-determined wetting characteristics of CO2-H2O fluids and their implications for fluids transport, host-rock physical properties, and fluid inclusion formation. Earth Planetary Science Letters, 85(4), 497–515. https://doi.org/10.1016/0012-821X(87)90144-0
Zhou, Z., and C. J. Ballentine (2006), 4He dating of groundwater associated with hydrocarbon reservoirs, Chem. Geol., 226, 309–327, doi:10.1016/j.chemgeo.2005.09.030.

Results

1) *Novel insights into the degassing history of Earth's mantle from high precision noble gas analysis of magmatic gas*

Le cycle des éléments volatils (H, C, N, halogènes et gaz rares) entre la surface de la Terre et son intérieur silicaté joue un rôle crucial dans le contrôle de l'évolution de l'atmosphère et des océans, ainsi que de la rhéologie et de la dynamique du manteau. La découverte du krypton primordial (Holland et al., 2009, gisement de gaz Bravo Dome au Nouveau-Mexique, États-Unis) et du xénon (Caracausi et al., 2016, zone volcanique de l'Eifel, Allemagne; Péron et Moreira, 2018, roches éclatantes) dans le manteau d'origine chondritique, a permis des avancées majeures dans notre compréhension de l'histoire de l'accrétion de la Terre. Bien qu'aucune donnée de Kr ou de Xe provenant de sources dérivées du manteau suggère une contribution solaire dans le manteau, le néon et vraisemblablement l'hélium, dans le manteau profond ont des signatures isotopiques similaires à celles du soleil, ce qui suggère que ces gaz ont été piégés tôt lors de l'accrétion terrestre, avant la dissipation de la nebuleuse solaire (Yokochi et Marty, 2004; Williams et Mukhopadhyay, 2019). Cependant, la signature isotopique de Ne du manteau supérieur a été supposée provenir de Ne implanté par le vent solaire dans des matériaux chondritiques (Ballentine et al., 2005), ce qui indique que la Terre pourrait avoir accumulé des volatils de multiples origines et réservoirs. L'accrétion hétérogène peut également être évidente pour les isotopes de H, avec à la fois une origine solaire (Hallis et al., 2015) et / ou chondritique (Loewen et al., 2019). La présence de gaz rares solaires - et non lourds - dans le manteau peut être liée à la solubilité plus élevée de He et de Ne dans les liquides silicatés et / ou à leur épuisement en éléments dans les chondrites par rapport aux gaz rares lourds (Tucker et al., 2012).). Le krypton, le xénon et probablement l'argon dans le manteau ont été vraisemblablement amenés avec des éléments volatils majeurs tels que l'azote par un astéroïde avant la «fermeture» du manteau (c'est-à-dire moins de 100 Myr après le début de la formation du système solaire - Caracausi et al., 2016). L'évolution ultérieure de l'inventaire des gaz rares lourds du manteau a été dominée par le recyclage de l'atmosphère par subduction (Holland et Ballentine, 2006), ainsi que par le dégazage dans l'atmosphère et les productions radiogéniques dans le manteau (Allègre et al., 1983; Marty, 1989; Ozima et Podosek, 2002; Mukhopadhyay et Parai, 2019).

Étant donné le recyclage prolongé et étendu des gaz atmosphériques dans la Terre solide, l'inventaire actuel de Xe dans le manteau est largement dominé (80 à 90%) par une atmosphère moderne recyclée (Holland et Ballentine, 2006; Parai et Mukhopadhyay, 2018). Les différences dans les signatures chimiques entre les basaltes de dorsale océaniques (MORB) provenant d'échantillons convectifs du manteau supérieur et de volcan intra-plaque, y compris les basaltes d'îles océaniques (OIB), qui puisent dans le manteau profond, ont été utilisées pour affirmer que le manteau est géochimiquement hétérogène , les sources du manteau MORB et OIB connaissant différents antécédents de dégazage (Kellogg et Wasserburg, 1990). En particulier, le manteau MORB est caractérisé par un $^{3}He/^{4}He$ élevé (8 ± 2 Ra, où Ra = 1,39 × 10^{-6}, le rapport $^{3}He/^{4}He$ de l'air), $^{20}Ne/^{22}Ne$ (~12,5) et $^{21}Ne/^{22}Ne$. (≥ 0,065), ainsi que des ratios élevés $^{40}Ar/^{36}Ar$ (jusqu'à 40 000) par rapport à l'air (Sarda et al., 1985; Burnard et al., 1997; Graham, 2002; Moreira et al., 1998; Péron et Moreira, 2018). Nous pensons que la source de manteau OIB a connu un mélange direct limité avec la source de manteau convectif de type MORB et un transfert de volatils vers celle-ci (Mukhopadhyay, 2012). En conséquence, la source de manteau OIB a préservé les restes des éléments volatils primordiaux (gaz piégés dans la nébuleuse solaire, par exemple) isolés depuis l'accrétion de la Terre (Craig et Lupton, 1976; Allègre et al., 1983; Honda et al., 1993; Mukhopadhyay , 2012; Williams et Mukhopadhyay, 2019), qui ne sont

pas observés ou sont moins répandus dans le réservoir mantellique de type MORB. Bien que les OIB puissent être classés en différentes catégories en fonction de leur composition chimique - sources de type HIMU («high μ»; μ = $^{238}U/^{204}Pb$, Pettke et al., 2018), deux variétés de manteaux enrichis (EM 1 et EM 2; Zindler et Hart, 1986) et FOZO (Zone focale, définie pour la première fois par Hart et al., 1992), nous appelons simplement OIB le réservoir de manteau profond en grande partie non dégazé, caractérisé par le panache islandais, avec de forts $^{3}He/^{4}He$ (jusqu'à 50 Ra, où Ra est le $^{3}He/^{4}He$ atmosphérique: 1,39 × 10^{-6}, Stuart et al., 2003) et $^{20}Ne/^{22}Ne$ (> 12,5; Yokochi et Marty, 2004; Péron et al., 2016; Mukhopadhyay, 2012; Williams et Mukhopadhyay, 2019).

Le xénon possède neuf isotopes, qui constituent un puissant outil de discrimination entre les sources de manteau MORB et OIB. Les ^{129}Xe et $^{131–136}Xe$ radiogéniques ont été produits au début de l'histoire de la Terre par désintégration β de 129I éteinte ($T_{1/2}$=15,7 Ma) et par fission spontanée de ^{244}Pu éteinte ($T_{1/2}$=80,0 Myr), respectivement (Porcelli et Ballentine, 2002). Ces nucléides radioactifs éteints fournissent un horodatage pour la formation et l'évolution ultérieure de différents réservoirs du manteau (Mukhopadhyay, 2012). De plus, la fission spontanée de ^{238}U existant ($T_{1/2}$ = 4,48 Gyr) produit en continu $^{131−136}Xe$. Les isotopes fissiogéniques de Xe sont produits dans des proportions différentes par ^{244}Pu et ^{238}U, permettant ainsi la déconvolution des isotopes de Xe dérivés de Pu et de U. Un réservoir qui est resté fermé aux pertes volatils au cours de l'histoire de la Terre devrait produire 97% des isotopes de fission Xe à partir de ^{244}Pu (Azbel et Tolstikhin, 1993). Comme les épisodes de dégazage après l'extinction de ^{244}Pu conduiront à une réduction progressive du Xe dérivé du (Pu/U), ce rapport peut être utilisé pour contraindre l'historique de dégazage de différentes sources de manteau (par exemple, Allègre et al., 1983; Kunz et al., 1998; Moreira et al., 1998; Caffee et al., 1999; Mukhopadhyay, 2012; Tucker et al., 2012; Petö et al., 2013; Parai et Mukhopadhyay, 2015).

Les modèles de manteau à l'état d'équilibre ont longtemps requis 129Xe et des gaz nobles primordiaux tels que ^{3}He, ^{22}Ne et ^{36}Ar dans le manteau supérieur appauvri en volatils à dériver d'un manteau inférieur primitif riche en volatils via l'entrée de panache (Porcelli et Wasserburg, 1995). Cependant, les différences de I/Xe (comme on le voit dans $^{129}Xe/^{130}Xe$, où ^{129}Xe est le produit de la désintégration du ^{129}I éteint) entre les sources du manteau MORB et OIB indiquent que la différenciation de ces deux réservoirs a eu lieu pendant l'existence du ^{129}I. (80 Myr) et a résisté à l'homogénéisation depuis, malgré l'impact de la Lune et les 3 Gyr de subduction (Mukhopadhyay, 2012; Parai et Mukhopadhyay, 2015). Cela implique que les panaches n'ont pas pu fournir le Xe et tous les volatils primordiaux à la source MORB. En combinaison avec la production de $^{131–136}Xe$ de la fission de ^{244}Pu (demi-vie = 80 Myr), les âges de fermeture I – Pu – Xe des différents réservoirs du manteau ont été calculés selon des ratios de ^{129*} Xe / 136 Xe, où 136 ∗ Xe représente les produits de désintégration du 244Pu éteint (Allègre et al., 1983; Marty, 1989; Mukhopadhyay, 2012; Caracausi et al., 2016). Étant donné que l'129I a une demi-vie plus courte que celle du ^{244}Pu, les domaines mantelliques avec un ^{129}Xe /^{136}Xe plus élevé auraient dû être fermés plus tôt à la perte volatile, en supposant que les deux réservoirs aient démarré avec le même rapport I/Pu. Dans ce cas, les valeurs ^{129}Xe /^{136}Xe inférieures dans les échantillons d'OIB (Mukhopadhyay, 2012) par rapport à ceux des MORB (Parai et Mukhopadhyay, 2015) suggèrent que le manteau supérieur a été fermé à la perte volatile plus tôt que le manteau profond OIB source, ce qui est peu probable. Il a donc été suggéré que le manteau inférieur avait un rapport I / Pu inférieur à celui du manteau supérieur.

En effet, pour que le manteau supérieur ait un âge de fermeture plus court que celui du manteau inférieur, il faudrait que le manteau source des MORB ait un rapport I / Pu initial 3,5 fois supérieur à celui du manteau inférieur (par exemple, Caracausi et al., 2016). Ces différences d'I / Pu entre les sources de manteaux MORB et OIB pourraient être dues à plusieurs processus, notamment (i) l'ajout ultérieur de matériaux chondritiques riches en

volatils I/Pu au manteau supérieur (Caracausi et al., 2016; Mukhopadhyay , 2012), (ii) la séquestration de I du manteau inférieur dans le noyau (Jackson et al., 2018) et / ou (iii) le dégazage rapide des éléments volatils du manteau à la surface (Clay et al., 2017).
Étant donné que le Xe dans les échantillons dérivés du manteau est dominé par le Xe atmosphérique moderne, il peut être difficile d'identifier et de déconvoluer les signatures de Xe dérivées du manteau. Les verres basaltiques sous-marins (Moreira et al., 1998) et les gaz de puits (Holland et al., 2009) constituent des échantillons convaincants pour fournir des informations sur la composition des éléments volatils dérivées du manteau. Cependant, les gaz de puits peuvent également apporter une contribution significative aux composants de la lithosphère, et les verres basaltiques ont une faible abondance en gaz rares, ce qui entrave les mesures isotopiques des gaz rares de haute précision des isotopes les moins abondants. Afin de contourner cette difficulté, les gaz volcaniques riches en CO_2 (c'est-à-dire les gaz libérés en profondeur par leur magma hôte avant de remonter à la surface) sont analysés, car ils transportent également des gaz rares dérivés du manteau (Moreira et al., 2018; Caracausi et al., 2016). Les gaz libres de la région de l'Eifel (Allemagne) et du Massif Central (France) montrent des contributions importantes du manteau dans les gaz nobles légers et lourds, offrant ainsi une opportunité d'enquêter sur l'histoire instable du manteau (Caracausi et al., 2016; Moreira et al., 2018).
L'origine de la province volcanique d'Europe centrale (CEVP), qui englobe les régions du Massif Central et de l'Eifel, est révélée par des plumes de manteau ascendant et par la fonte du manteau supérieur, qui pourraient être des moteurs possibles du volcanisme en Europe (par exemple, Buikin et al., 2005; Bräuer et al., 2013; Caracausi et al., 2016; Moreira et al., 2018). Le volcanisme en Eifel est actuellement en sommeil, mais pas éteint (éruption la plus récente 11 ka, Schmincke, 2007). Les volatils qui s'échappent du centre de dégazage de l'Eifel Est sont caractérisés par des flux de CO^2 élevés (> 99% en volume), avec des rapports $^3He/^4He$ élevés (jusqu'à 5,6 Ra) et $\delta^{13}C$ dans la plage de MORB (moyenne - 4,6 ± 0,6), indiquant une origine volcanique des gaz de l'Eifel (Bräuer et al., 2013). Selon les abondances relatives de N_2 magmatique, He et Ar, les puits de Victoriaquelle et de Schwefelquelle (Eifel du Sud-Est) montrent la plus grande contribution de gaz dérivés des réservoirs magmatiques dans la région de l'Eifel (Bräuer et al., 2013). Leurs valeurs $\delta^{15}N$ sont proches de la plage de MORB, la composition en isotopes de Ne étant également cohérente avec une signature du manteau supérieur (Bräuer et al., 2013). De même, la signature chimique du gaz de Lignat (Massif Central, France) ressemble au manteau source MORB, nécessitant peu ou pas de contribution d'un panache mantellique (Moreira et al., 2018). Cependant, les images tomographiques montrent la présence d'une structure à faible vitesse jusqu'à 2 000 km de profondeur, représentant une remontée profonde du manteau sous l'Europe centrale, qui pourrait alimenter de plus petits panaches du manteau supérieur exprimés dans la région de l'Eifel (Goes et al., 1999; Ritter, 1999, 2007; Weber et al., 2007). Récemment, il a été démontré que les mesures de haute précision de Xe isotope du puits de Victoriaquelle étaient compatibles avec une origine de panache de manteau profond non dégazé (Caracausi et al., 2016). La source de volcanisme dans la CEVP reste donc énigmatique.
Dans cette contribution, nous nous concentrons sur la détermination de l'origine du volcanisme dans la CEVP en effectuant des analyses de haute précision des isotopes Ne, Ar et Xe pour trois échantillons de gaz libres prélevés avec des bouteilles de Giggenbach des puits de Victoriaquelle et de Schwefelquelle. En comparant la signature géochimique du manteau sous la CEVP avec celles des réservoirs MORB et OIB, nous fournissons de nouvelles informations sur l'origine de la CEVP et sur la relation entre les manteaux supérieur et inférieur en termes d'historique de dégazage et d'hétérogénéité actuelle.
L'origine du CEVP est restée énigmatique compte tenu du potentiel d'une source de type OIB de contribuer au volcanisme intraplaque dans la région de l'Eifel. Dans cette

contribution, nous montrons que la source du manteau située sous l'Eifel et, par extension, le CEVP, possède une signature géochimique similaire au réservoir du manteau supérieur échantillonné au niveau des dorsales océaniques. La détermination précise des rapports $^{244}Pu/^{238}U$ dans des échantillons dérivés du manteau a été couramment utilisée pour traiter les états de dégazage des réservoirs de manteau correspondants. Selon leur Pu–Xe /(Pu + U)–Xe, les sources du volcanisme de l'Eifel et les poping rocks auraient toutefois connu un dégazage important et limité, respectivement. Le réservoir MORB semble donc présenter des rapports variables Pu–Xe/(Pu+U)–Xe, ce qui indique que la présence de deux réservoirs mantelliques (MORB et OIB) ne peut plus être pleinement justifiée par les seules différences de Pu–Xe/(Pu+U)–Xe. Les différences entre les sources MORB et OIB ne résideraient donc que dans la présence de Ne d'origine solaire, de $^{20}Ne/^{21}$NeE supérieurs et de $^{3}He/^{4}He$ supérieurs dans les OIB, ainsi que des $^{40}Ar/^{36}Ar$ et I/Xe plus élevés dans les MORB par rapport aux OIB. Il est intéressant de noter que, pour tenir compte à la fois de la forte $^{129}Xe/^{136}Xe$ par rapport au DMM et de la fission dérivée de Pu à U Xe dans la source Eifel, un réservoir de type MORB non dégazé peut être nécessaire, avec une source de type HIMU pour expliquer les faibles $^{3}He/^{4}He$ renconré dans les gaz d’Eifel. Bien que nos résultats réfutent une origine de type OIB ressemblant à un panache profond pour le volcanisme dans les systèmes systématiques d'Eifel, la systématique de Ne et Xe nous indique des contributions de multiples réservoirs ayant des histoires de dégazage différents, provenant de différentes profondeurs dans le manteau sous le CEVP.

Earth and Planetary Science Letters 525 (2019) 115766

Contents lists available at ScienceDirect

Earth and Planetary Science Letters

www.elsevier.com/locate/epsl

Novel insights into the degassing history of Earth's mantle from high precision noble gas analysis of magmatic gas

David V. Bekaert [a,*], Michael W. Broadley [a], Antonio Caracausi [b], Bernard Marty [a]

[a] Centre de Recherches Pétrographiques et Géochimiques, UMR 7358 CNRS – Université de Lorraine, 15 rue Notre Dame des Pauvres, BP 20, 54501 Vandoeuvre-lès-Nancy, France
[b] Instituto Nazionale di Geofisica e Vulcanologia, Sezione di Palermo, 90146 Palermo, Italy

ARTICLE INFO

Article history:
Received 14 March 2019
Received in revised form 2 August 2019
Accepted 8 August 2019
Available online 22 August 2019
Editor: F. Moynier

Keywords:
noble gas
MORB
Eifel
mantle
xenon
volatiles

ABSTRACT

The noble gas isotope composition of the mantle can provide unique insights into the origin and evolution of volatile elements on Earth. Xenon isotopes combine primordial signatures with contributions from extinct and extant radionuclides, therefore offering the potential to set constraints on both the nature of Earth's planetary precursor(s) and the timing of their contributions. However, measuring the Xe isotope composition of mantle-derived samples to sufficiently high-precision has proven difficult due to (i) large occurrence of a modern-like atmospheric component in the mantle, and (ii) contribution from shallow and post-eruptive atmospheric contamination. Mantle-derived samples therefore exhibit only small deviations from the modern atmospheric composition, making the identification and deconvolution of mantle-derived Xe signals challenging. Here, we use the Giggenbach sampling method to concentrate magmatic noble gases from the Eifel volcanic area (Germany) into glass bottles in order to conduct high-precision analyses of Ne, Ar and Xe isotopes. The three samples collected from Victoriaquelle and Schwefelquelle wells (South East Eifel) show variable contributions from atmospheric contamination, with the least contaminated sample reaching $^{40}Ar/^{36}Ar$ ~8,300. Our data indicate that the mantle beneath the Eifel volcanic area, and by extension the Central European Volcanic Province, resembles the convective upper mantle reservoir with limited evidence for an OIB-like deep plume source contribution. It has a geochemical signature that is similar (e.g. in Ne isotopic composition, $^{40}Ar/^{36}Ar$, $^{129}Xe/^{130}Xe$ and $^{129}Xe/^{136}Xe$) to the mantle source of the so-called popping rocks (thought to best represent the upper mantle), with an additional source of ^{238}U-derived Xe and low $^{3}He/^{4}He$ that we attribute to the influence of an ancient subducted component (HIMU). A dichotomy exists between the main sources of fissiogenic xenon isotopes measured in popping rocks and Eifel gas, which appear to be mainly derived from ^{244}Pu and ^{238}U, respectively. According to their respective ratios of ^{244}Pu- to ^{238}U-derived Xe, the mantle sources for Eifel volcanism and popping rocks would have experienced extensive and limited degassing, respectively. In this regard, high Pu–Xe/(Pu+U)–Xe may no longer be considered as being indicative of a mantle deep origin, therefore calling for the geochemical differences between plume and MORB sources to be redefined, with the possibility that volatile signatures within the solid Earth may be more heterogeneously distributed than previously thought.

© 2019 The Author(s). Published by Elsevier B.V. This is an open access article under the CC BY-NC-ND license (http://creativecommons.org/licenses/by-nc-nd/4.0/).

1. Introduction

The cycling of volatile elements (i.e., H, C, N, halogens and noble gases) between Earth's surface and its silicate interior plays a crucial role in controlling the evolution of the atmosphere and oceans, as well as the rheology and dynamics of the mantle. The discovery that primordial krypton (Holland et al., 2009, Bravo Dome gas field in New Mexico, United States) and xenon (Caracausi et al., 2016, Eifel volcanic area, Germany; Péron and Moreira, 2018, popping rocks) components in the mantle are of chondritic origin allowed major advances in our understanding of Earth's accretion history to be made. Although no Kr or Xe data from mantle-derived sources points toward a solar contribution in the mantle, neon, and presumably helium, in the deep mantle have solar-like isotopic signatures, suggesting that these gases were trapped early during terrestrial accretion, before dissipation of the solar nebula (Yokochi and Marty, 2004; Williams and Mukhopadhyay, 2019). However, the Ne isotopic signature of the upper mantle has been purported to originate from solar wind-implanted Ne within chon-

* Corresponding author.
E-mail address: dbekaert@crpg.cnrs-nancy.fr (D.V. Bekaert).

https://doi.org/10.1016/j.epsl.2019.115766
0012-821X/© 2019 The Author(s). Published by Elsevier B.V. This is an open access article under the CC BY-NC-ND license (http://creativecommons.org/licenses/by-nc-nd/4.0/).

dritic materials (Ballentine et al., 2005), indicating the Earth may have accreted volatiles from multiple reservoirs. Heterogeneous accretion may also be evident for H isotopes, with both a solar (Hallis et al., 2015) and/or chondritic (Loewen et al., 2019) origin being argued for. The presence of light – and not heavy – solar noble gases in the mantle may be related to the higher solubility of He and Ne in silicate melts and/or to their elemental depletion in chondrites relative to heavy noble gases (Tucker et al., 2012). Krypton, xenon and likely argon in the mantle were presumably delivered together with major volatiles such as nitrogen by asteroidal material before mantle 'closure' (i.e., within <100 Myr after the start of Solar System formation – Caracausi et al., 2016). Subsequent evolution of the mantle heavy noble gas inventory was dominated by atmosphere recycling via subduction (Holland and Ballentine, 2006) as well as degassing to the atmosphere and radiogenic productions within the mantle (Allègre et al., 1983; Marty, 1989; Ozima and Podosek, 2002; Mukhopadhyay and Parai, 2019).

Given the protracted and extensive recycling of atmospheric gases into the solid Earth, the present-day inventory of Xe in the mantle is largely dominated (80–90%) by recycled modern atmosphere (Holland and Ballentine, 2006; Parai and Mukhopadhyay, 2018). Differences in chemical signatures between mid-ocean ridge basalts (MORB) originating from the convecting upper mantle and intraplate volcanic samples, including ocean island basalts (OIB) which tap in to the deep mantle, has been used to argue that the mantle is geochemically heterogeneous, with the MORB and OIB mantle sources experiencing different degassing histories (Kellogg and Wasserburg, 1990). In particular, the MORB mantle is characterised by elevated $^{3}He/^{4}He$ (8 ± 2 Ra, where Ra $= 1.39 \times 10^{-6}$, the $^{3}He/^{4}He$ ratio of air), $^{20}Ne/^{22}Ne$ ($\sim$12.5) and $^{21}Ne/^{22}Ne$ ($\geq$0.065), as well as high $^{40}Ar/^{36}Ar$ (up to 40,000) ratios, relative to air (Sarda et al., 1985; Burnard et al., 1997; Graham, 2002; Moreira et al., 1998; Péron and Moreira, 2018). The OIB mantle source is thought to have experienced limited direct mixing with, and volatile transfer to, the convecting MORB mantle source (Mukhopadhyay, 2012). As a consequence, the OIB mantle source has preserved remnants of primordial volatiles (e.g., gases trapped from the solar nebula) isolated since Earth's accretion (Craig and Lupton, 1976; Allègre et al., 1983; Honda et al., 1993; Mukhopadhyay, 2012; Williams and Mukhopadhyay, 2019), which are not witnessed, or are less prevalent, within the MORB mantle reservoir. Although OIBs can be classified into different categories depending on their chemical composition – HIMU type sources ("high-μ"; $\mu = {}^{238}U/{}^{204}Pb$, Pettke et al., 2018), two varieties of enriched mantle (EM 1 and EM 2; Zindler and Hart, 1986) and FOZO (Focal Zone, first defined by Hart et al., 1992) –, we simply refer to OIB as the largely undegassed deep mantle reservoir typified by the Iceland plume, which is characterised by high $^{3}He/^{4}He$ (up to 50 Ra, where Ra is the atmospheric $^{3}He/^{4}He$: 1.39×10^{-6}, Stuart et al., 2003) and $^{20}Ne/^{22}Ne$ (>12.5; Yokochi and Marty, 2004; Péron et al., 2016; Mukhopadhyay, 2012; Williams and Mukhopadhyay, 2019).

Xenon has nine isotopes, which constitute a powerful tool for discriminating between MORB and OIB mantle sources. Radiogenic ^{129}Xe and $^{131-136}Xe$ were produced early in Earth's history by β-decay of extinct ^{129}I ($T_{1/2} = 15.7$ Ma) and spontaneous fission of extinct ^{244}Pu ($T_{1/2} = 80.0$ Myr), respectively (Porcelli and Ballentine, 2002). These extinct radioactive nuclides provide a timestamp for the formation and subsequent evolution of different mantle reservoirs (Mukhopadhyay, 2012). In addition, spontaneous fission of extant ^{238}U ($T_{1/2} = 4.468$ Gyr) continuously produces $^{131-136}Xe$. The fissiogenic Xe isotopes are produced in different proportions by ^{244}Pu and ^{238}U, allowing the Pu- and U-derived Xe to be deconvolved. A reservoir that has remained closed to volatile loss over Earth's history should have 97% of the fission Xe isotopes being produced from ^{244}Pu (Azbel and Tolstikhin, 1993). As episodes of degassing after the extinction of ^{244}Pu will lead to progressively lower (Pu/U)-derived Xe, this ratio can be used to constrain the degassing history of different mantle sources, (e.g., Allègre et al., 1983; Kunz et al., 1998; Moreira et al., 1998; Caffee et al., 1999; Mukhopadhyay, 2012; Tucker et al., 2012; Petö et al., 2013; Parai and Mukhopadhyay, 2015).

Steady-state mantle models have long required ^{129}Xe and primordial noble gases such as ^{3}He, ^{22}Ne and ^{36}Ar in the volatile-depleted upper mantle to be derived from a primitive volatile-rich lower mantle via plume input (Porcelli and Wasserburg, 1995). However, differences in I/Xe (as seen in the $^{129}Xe^{*}/^{130}Xe$, where $^{129*}Xe$ is the decay product of extinct ^{129}I) between the MORB and OIB mantle sources indicate that the differentiation of these two reservoirs occurred during the existence of ^{129}I (80 Myr) and has resisted homogenisation ever since despite the Moon forming impact and 3 Gyr of subduction (Mukhopadhyay, 2012; Parai and Mukhopadhyay, 2015). This implies that plumes could not have supplied Xe, and all of the primordial volatiles, to the MORB source. Combined with the production of $^{131-136}Xe$ from the fission of extinct ^{244}Pu (half-life = 80 Myr), I–Pu–Xe closure ages for the different mantle reservoirs have been calculated through $^{129*}Xe/^{136*}Xe$ ratios, where $^{136*}Xe$ is the decay products of extinct ^{244}Pu (Allègre et al., 1983; Marty, 1989; Mukhopadhyay, 2012; Caracausi et al., 2016). Given that ^{129}I has a shorter half-life than ^{244}Pu, mantle domains with a higher $^{129*}Xe/^{136*}Xe$ should have become closed to volatile loss earlier, assuming that both reservoirs started with the same I/Pu ratio. In this case, the lower $^{129*}Xe/^{136*}Xe$ in OIB samples (Mukhopadhyay, 2012) compared to MORB (Parai and Mukhopadhyay, 2015) would suggest that the upper mantle became closed to volatile loss earlier than the deep OIB mantle source, which is unlikely. It has therefore been suggested that the lower mantle had a lower I/Pu ratio than the upper mantle. Indeed, for the upper mantle to have a younger closure age than the lower mantle would require the upper MORB source mantle to have had an initial I/Pu ratio 3.5 times higher than that of the lower mantle (e.g., Caracausi et al., 2016). Such differences in I/Pu between the MORB and OIB mantle sources could have resulted from several processes, including (i) later addition of volatile-rich, high I/Pu chondritic material to the upper mantle (Caracausi et al., 2016; Mukhopadhyay, 2012), (ii) sequestration of I from the lower mantle into the core (Jackson et al., 2018), and/or (iii) rapid degassing of mantle volatiles to the surface (Clay et al., 2017).

Given that Xe in mantle-derived samples is dominated by modern atmospheric Xe, identifying and deconvoluting the mantle-derived Xe signatures can be challenging. Submarine basaltic glasses (Moreira et al., 1998) and well gases (Holland et al., 2009) constitute compelling samples to provide insights into the composition of mantle-derived volatiles. However, well gases may also have a significant contribution from lithospheric components, and basaltic glasses have low noble gas abundances, hampering high precision noble gas isotopic measurements of the least abundant isotopes. In order to circumvent this difficulty, volcanic CO_2-rich free gases (i.e., gases that have been released from their host magma at depth before travelling to the surface) are analysed, as they also carry mantle-derived noble gases (Moreira et al., 2018; Caracausi et al., 2016). Free gases in the Eifel region (Germany) and Massif Central (France) show significant mantle contributions in light and heavy noble gases, therefore providing an opportunity to investigate the mantle's volatile history (Caracausi et al., 2016; Moreira et al., 2018).

The origin of the Central European Volcanic Province (CEVP), which includes the Massif Central and the Eifel regions, is debated with both upwelling mantle plumes and melting of upper mantle material being advocated as possible drivers of volcan-

ism under Europe (e.g., Buikin et al., 2005; Bräuer et al., 2013; Caracausi et al., 2016; Moreira et al., 2018). The volcanism in Eifel is presently dormant, but not extinct (youngest eruption ~11 ka, Schmincke, 2007). Volatiles escaping from East Eifel degassing centre are characterised by high CO_2 fluxes (>99 vol.%), with high $^3He/^4He$ ratios (up to 5.6 Ra) and $\delta^{13}C$ values within the MORB range (average -4.6 ± 0.6‰), pointing to a mantle-derived origin of Eifel volcanic gases (Bräuer et al., 2013). According to the relative abundances of magmatic N_2, He and Ar, the Victoriaquelle and Schwefelquelle wells (South East Eifel) show the highest contribution of mantle-derived gas in the Eifel region (Bräuer et al., 2013). Their $\delta^{15}N$ values are close to the MORB range, with Ne isotope compositions also being consistent with an upper mantle signature (Bräuer et al., 2013). Likewise, the chemical signature of the Lignat gas (Massif Central, France) resembles the MORB source mantle, requiring little to no plume contribution (Moreira et al., 2018). Yet, tomographic images show evidence for a low-velocity structure at depth down to 2,000 km, representing deep mantle upwelling under central Europe, which may feed smaller upper-mantle plumes expressed in the Eifel region (Goes et al., 1999; Ritter, 2007; Weber et al., 2007). Recently, high precision Xe isotope measurements from the Victoriaquelle Well were shown to be consistent with a deep undegassed mantle plume origin (Caracausi et al., 2016). The source of volcanism in the CEVP therefore remains enigmatic.

In this contribution, we focus on determining the origin of the volcanism in the CEVP by carrying out high-precision analyses of Ne, Ar and Xe isotopes for three free gas samples collected with Giggenbach bottles from the Victoriaquelle and Schwefelquelle wells. By comparing the geochemical signature of the mantle beneath the CEVP with those of the MORB and OIB reservoirs, we provide novel insights regarding the origin of the CEVP, and relationship between the upper and lower mantle in terms of degassing histories and present-day heterogeneities.

2. Samples and methods

2.1. Sampling and gas preparation

Noble gas isotopic compositions were determined in samples of volcanic free gas collected from the Victoriaquelle and Schwefelquelle wells in the Eifel volcanic district (Germany). These two locations are close to the village of Heckenmünster, south of the inferred plume centre, near the city of Gerolstein (Bräuer et al., 2013). The springs are at a distance of approximately 100 m from each other and are both characterised by high gas/water ratios. In order to optimize magmatic noble gas concentration into sampling volumes, we used 200 cm^3 pre-evacuated (10^{-3} Pa) glass flasks equipped with double Teflon stopcocks and filled with 50–80 cm^3 of 7N NaOH solution (Giggenbach and Goguel, 1989). The solution absorbs reactive gases (water vapour, CO_2, SO_2, H_2S, HCl, HF), allowing the build up of a large partial pressure of non-reactive gases (N_2, H_2, O_2, CO, hydrocarbons and noble gases) in the headspace volume. Once in the laboratory, collected volcanic gases were rapidly transferred by volume equilibration into 500 cm^3 steel tanks for storage. This procedure of gas sampling vastly increases the amount of gas available for analysis, whilst also increasing the efficiency of purification of the samples in the laboratory since H_2O and CO_2 have been largely removed from the pristine gas.

The samples analysed in this study were collected during two sampling sessions at Victoriaquelle and Schwefelquelle wells. In May 2018, Giggenbach bottles labelled E2 and E3 were collected from Schwefelquelle and Victoriaquelle wells, respectively. In September 2018, only the Victoriaquelle well could be sampled following the Giggenbach method (sample E4 in the present study) as the water level at Schwefelquelle well was too low to form a seal for noble gas sampling. Two steel tanks (Schw-t and Vict-t) from a previous sampling trip in 2015 were also analysed for their Ne and Ar isotope composition. In this case, purification was carried out using the same purification line as Caracausi et al. (2016) and gases were then analysed using the same procedure as detailed here below. All samples were analysed for their Ne, Ar and Xe isotope compositions using the Helix MC *Plus* (Thermofisher Scientific) noble gas mass spectrometer at the Centre de Recherches Pétrographiques et Géochimiques (CRPG) noble gas analytical facility, following the analytical procedures described in Supplementary Information. Neon, argon and xenon blank contributions were measured before running the samples and found to be insignificant (<1%). Therefore, blank corrections were not applied to the abundances or isotope ratios reported here. Standard runs were analysed before and during each analytical session. The three samples collected in Giggenbach bottles and analysed in this study are referred to as E2, E3 and E4. These were analysed using a different purification line than used by Caracausi et al. (2016). Finally, we report He isotope measurements for samples collected in 2015 from Schwefelquelle and Victoriaquelle wells, and analysed at the Instituto Nazionale di Geofisica e Vulcanologia in Palermo.

2.2. Extrapolating mantle signatures

The Monte Carlo linear least square code adapted from Parai and Mukhopadhyay (2015) was used to compute best fit mixings of ^{132}Xe from initial mantle, modern atmosphere (recycled into the mantle and acting as a contaminant during sampling), ^{238}U-fission Xe and ^{244}Pu–Xe, with $^{128-136}Xe$ isotopes being taken into account (Supplementary Information). Also, air contamination of the pristine mantle component generates hyperbolic trends in $^{20}Ne/^{22}Ne$–$^{40}Ar/^{36}Ar$ and $^{40}Ar/^{36}Ar$–$^{129}Xe/^{130}Xe$ spaces (e.g., Mukhopadhyay, 2012; Fig. S1). Best-fit hyperbola reflecting two-component mixing between air and mantle are determined using total least-squares hyperbolic fits, therefore allowing the mantle source $^{40}Ar/^{36}Ar$ and $^{129}Xe/^{130}Xe$ ratios to be extrapolated. First, the $^{40}Ar/^{36}Ar$ of the mantle source is calculated by extrapolation to a mantle $^{20}Ne/^{22}Ne$ value (12.5, 13.22 or 13.8, depending on the Ne isotope composition of the source; Fig. S1, Table S1). The curvature of the two-component mixing hyperbolic array is parameterized as $k = (^{36}Ar/^{22}Ne)_{mantle}/(^{36}Ar/^{22}Ne)_{atm}$. We use a grid search to find the combination of k and mantle $^{40}Ar/^{36}Ar$ that minimizes the χ^2 cost function:

$$\chi^2 = \sum_{i=1}^{N} \frac{1}{N^2} * \left[\left(\frac{\text{x\_meas} - \text{x\_fit}}{\sigma_{\text{x\_meas}}} \right)^2 + \left(\frac{\text{y\_meas} - \text{y\_fit}}{\sigma_{\text{y\_meas}}} \right)^2 \right]$$

where (x_meas $\pm$ σ_{x_meas}, y_meas $\pm$ σ_{y_meas}) are the N observed data points for a given sample and (x_fit, y_fit) are the closest points to the data along a candidate hyperbola. The error associated with the extrapolated $^{40}Ar/^{36}Ar$ of the mantle is calculated using the method described by Parai and Mukhopadhyay (2015), with the 1 sigma confidence interval (68.3%) being defined where the fit degrades by a fixed amount $\chi^2 \leq \chi^2$ min + 2.30 (for a 2 parameter fit; e.g., Press et al., 1992). In the $^{129}Xe/^{130}Xe$–$^{40}Ar/^{36}Ar$ space ($k = (^{130}Xe/^{36}Ar)_{mantle}/(^{130}Xe/^{36}Ar)_{atm}$), the mantle source $^{129}Xe/^{130}Xe$ is then computed by extrapolation to the mantle $^{40}Ar/^{36}Ar$. The final error associated with the mantle source $^{129}Xe/^{130}Xe$ takes into account propagation of the mantle $^{40}Ar/^{36}Ar$ uncertainty. Note that $^{36}Ar/^{22}Ne$ and $^{130}Xe/^{36}Ar$ values for the mantle source (which define the k parameters) were freely varied between 4–12 and 2.0–4.3 $\times$ 10^{-4}, respectively, in order to span the full range of possibilities from MORB- to OIB-like elemental compositions (Graham, 2002).

The code was tested on published data for different types of mantle sources. Results are reported in Fig. S1 and Table S1.

3. Results

3.1. Helium, neon and argon

Helium isotopic ratios measured in the present study (4.1–4.2 Ra; Table S2) for the Schwefelquelle and Victoriaquelle wells are in excellent agreement with those reported by Bräuer et al., 2013 (4.2–4.5 Ra). The $^{20}Ne/^{22}Ne$ of samples E2, E3 and E4 range from 10.3 to 11.2 (Table S3), which is higher than the maximum previously found $^{20}Ne/^{22}Ne$ for Eifel free gas (10.6; Bräuer et al., 2013), but still lower than the maximum value from stepwise crushing of mantle xenoliths (11.88; Buikin et al., 2005). Samples E2-E4 plot on the mixing line between air and the MORB end-member (Fig. 1). The two samples collected using steel tanks and analysed for their Ne isotope composition (Schw-t and Vict-t) plot along the same mantle-atmosphere mixing line as samples from Giggenbach bottles (Fig. 1). Argon isotope compositions of samples E2, E3 and E4 show increasing contributions of air contamination ($^{40}Ar/^{36}Ar$ of 8,287 ± 140, 4,040 ± 69 and 1,974 ± 45, respectively), with $^{38}Ar/^{36}Ar$ being consistently within error of the atmospheric ratio (Table S4). These $^{40}Ar/^{36}Ar$ ratios are higher than reported by Caracausi et al., 2016 for E1 ($^{40}Ar/^{36}Ar$ = 1,780; Fig. 2), indicating higher mantle contributions. The maximum $^{40}Ar/^{36}Ar$ reported here (~8,300) is the highest value yet measured for Eifel free gas.

3.2. Xenon

The Xe isotopic spectra of samples E2-E4 show excesses in radiogenic $^{129}Xe^*$ and fissiogenic $^{131-136}Xe$ relative to modern atmosphere (Fig. 2; Table S5-S6) supporting the presence of a mantle-derived component in Eifel free gases. These excesses are correlated (Fig. 3), indicating they have a common origin, and are higher than those reported for sample E1 (Caracausi et al., 2016, Fig. 2), in agreement with the lower contributions of air contamination seen for Ar isotopes. The $^{129}Xe/^{136}Xe$ of the Eifel magmatic gas appears similar to that of the source of popping rocks (Péron and Moreira, 2018; Fig. 3a). Fission spectra for Xe isotopes in E2-E4 indicate a dominant contribution from ^{238}U-derived Xe, with limited contribution from ^{244}Pu-derived Xe (Fig. 3b). In contrast, the source of popping rocks is dominated by ^{244}Pu-derived Xe (Péron and Moreira, 2018; Fig. 3).

3.3. Composition of the mantle beneath Eifel

A least-square hyperbolic fit through Eifel data (see section 2.2) yields a $^{40}Ar/^{36}Ar$ of $39,400^{+2900}_{-15200}$ (Fig. S1) and a $^{129}Xe/^{130}Xe$ of $7.84^{+0.09}_{-0.45}$ for a mantle source $^{20}Ne/^{22}Ne$ of 12.5 (Fig. 4). Extrapolating the $^{20}Ne/^{22}Ne$ to 13.8 would yield a mantle source $^{40}Ar/^{36}Ar$ of $64,800^{+4900}_{-30,700}$ (Fig. S2), which would not significantly change our conclusions. Results of linear least squares determinations of initial, recycled atmospheric, Pu- and U-fissiogenic Xe components for Eifel (Caracausi et al., 2016; This study), popping rocks (Péron and Moreira, 2018) and Lignat (Moreira et al., 2018) samples are reported in Table 1. These indicate that E2 (which is the Eifel gas least contaminated by air, $^{40}Ar/^{36}Ar$ ~8,300) is best accounted for by mixing $93.3^{+1.2}_{-1.2}$% modern air with $5.2^{+1.1}_{-1.1}$% AVCC, $1.1^{+0.1}_{-0.2}$% U-derived Xe and $0.4^{+0.3}_{-0.2}$% Pu-derived Xe. The $I-^{129}Xe/Pu-^{136}Xe$ and $Pu-^{136}Xe/(Pu+U)-^{136}Xe$ for the source of Eifel gas are $13.8^{+25.4}_{-5.3}$ and $0.21^{+0.13}_{-0.14}$, respectively). Importantly, linear least squares determinations of initial, recycled atmospheric, Pu- and U-fissiogenic Xe components in the Eifel gas (sample E2, this study) give consistent outcomes if ^{128}Xe is taken or not into account (Table 1).

4. Discussion

4.1. Origin of the Central European Volcanic Province

In neon three-isotope space (Fig. 1), Eifel samples reflect a two component mixing between air and the MORB source, requiring negligible if any contribution from an OIB-like source. This is consistent with Ne data reported by Bräuer et al. (2013) for the Schwefelquelle and Victoriaquelle wells, interpreted to reflect a mixture of atmospheric and MORB-like Ne, that had been additionally affected by mass dependent fractionation (MDF, Fig. 1). These results are at odds with Ne isotope data on ultramafic xenoliths from the Eifel region by Buikin et al. (2005), which were interpreted to suggest the presence of hot spot-type, OIB-like noble gases in the Eifel region. However, the authors acknowledge that contributions from variably fractionated atmosphere-derived contaminants and variably fractionated mantle-derived noble gases are involved in individual Eifel xenoliths, and consider only one sample (DW1) to define a reliable hyperbola fit in the $^{40}Ar/^{36}Ar$ versus $^{20}Ne/^{22}Ne$ space. Our data, which do not show evidence for significant MDF, as also seen in the consistently atmospheric $^{38}Ar/^{36}Ar$ ratios (Table S4), confirm that Ne isotopes in the Eifel gas exclude a significant deep mantle plume contribution of the Iceland, Reunion, or Kerguelen type for Ne (Fig. 1). Extrapolating the $^{21}Ne/^{22}Ne$ of the Eifel gas source to a $^{20}Ne/^{22}Ne$ of 12.5 by error weighted least squares linear regression through the Eifel data points yields a range of values that is distinct from popping rocks and "HIMU-like MORBs" (Tucker et al., 2012), but which overlaps with the range of depleted MORBs (DMM, Fig. 5). Although analysing more Eifel samples with varying $^{20}Ne/^{22}Ne$ will ultimately help better constraining the $^{21}Ne/^{22}Ne$ of the Eifel source, this suggests potential contribution from a degassed MORB-like mantle source.

The $^{40}Ar/^{36}Ar$ of the source constrained by Ne isotopes ($39,400^{+2900}_{-15200}$, Fig. 4) is similar to that estimated for the more radiogenic MORB ($^{40}Ar/^{36}Ar$ up to 40,000; Graham, 2002), and not OIB ($^{40}Ar/^{36}Ar$ ~5,000 to ~10,000; Colin et al., 2015; Mukhopadhyay, 2012), reservoir. Likewise, the $^{129}Xe/^{130}Xe$ of the Eifel source ($7.84^{+0.09}_{-0.45}$) is characteristic for the MORB reservoir (7.44–7.83; Moreira et al., 1998; Tucker et al., 2012), but distinct from OIB (6.98 ± 0.07; Mukhopadhyay, 2012). The highest $^{129}Xe/^{130}Xe$ measured in the Eifel samples (6.94 for sample E2) is similar to the value of the OIB source as defined by the Iceland plume composition (6.98 ± 0.07; Mukhopadhyay, 2012). For the Xe isotope composition of Eifel magmatic gas to have a plume origin would require that sample E2 is 100% mantle-derived gas, which is not possible. This suggests that an OIB-like mantle plume origin for volcanism the Eifel area, and by extension volcanism in the Central European Volcanic Province (CEVP), is unlikely. Taken together, Ne, Ar and Xe systematics indicate that the source of magmatic gas in Eifel is similar to the MORB source mantle. The potential increase in mantle-derived gas contribution in Eifel over the last years, as seen in the increasing $^{40}Ar/^{36}Ar$ from 2005 (Bräuer et al., 2013; Caracausi et al., 2016) to 2018 (this study), could be related to a rise in the flux of magmatic volatiles beneath the Eifel region. However, the different sampling methods used in both studies (steel tanks versus Giggenbach bottles, respectively) may preclude firm comparison of the two results.

4.2. Degassing history of mantle reservoirs

Based on Xe isotope measurements in the Victoriaquelle well gas, Caracausi et al. (2016) concluded for the origin of Eifel magmatism to be related to a deep mantle plume. This result was primarily based on a significant ^{244}Pu-derived Xe contribution, and computed $Pu-Xe/(Pu+U)-Xe$ and $^{129}Xe_I/^{136}Xe_{Pu}$ ratios that

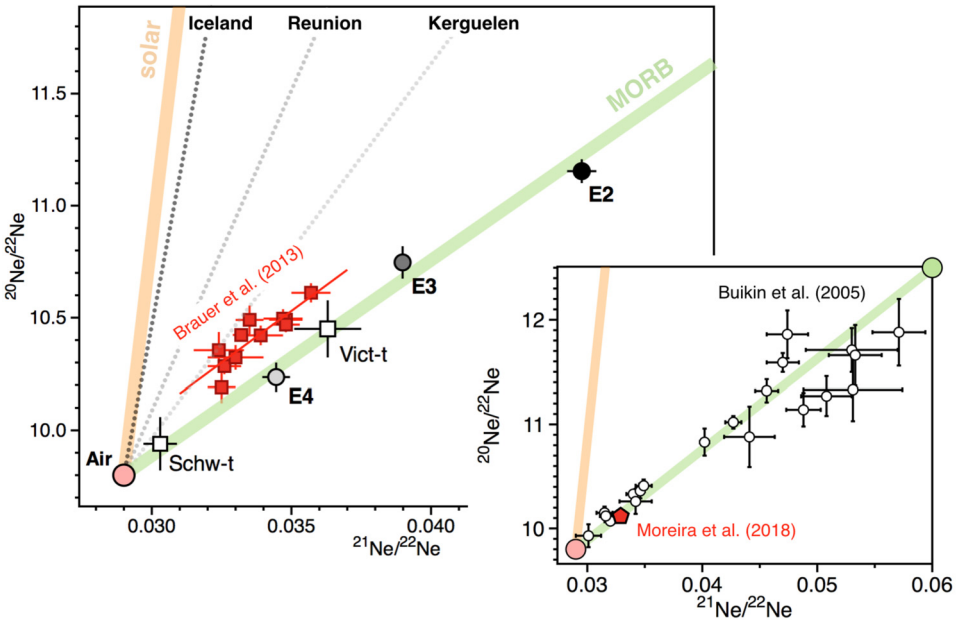

Fig. 1. Neon three-isotope plot displaying the three Eifel samples (E2, E3 and E4), air, solar and MORB, together with different OIB endmembers. Two samples of Eifel gas from steel tanks were also analysed for their Ne isotope compositions (white squares Schw-t and Vict-t). Eifel samples define a mixing line between Air and MORB compositions, requiring no contribution from a plume-like source. Data reported by Bräuer et al. (2013) for Victoriaquelle and Schwefelquelle wells, Moreira et al. (2018) for the Lignat thermal spring (Massif Central, France) and Buikin et al. (2005) for ultramafic xenoliths from the Eifel Quaternary volcanic field "Dreiser Weiher", are shown for comparison. Error bars indicate $\pm 1\sigma$. Air composition is from Ozima and Podosek (2002).

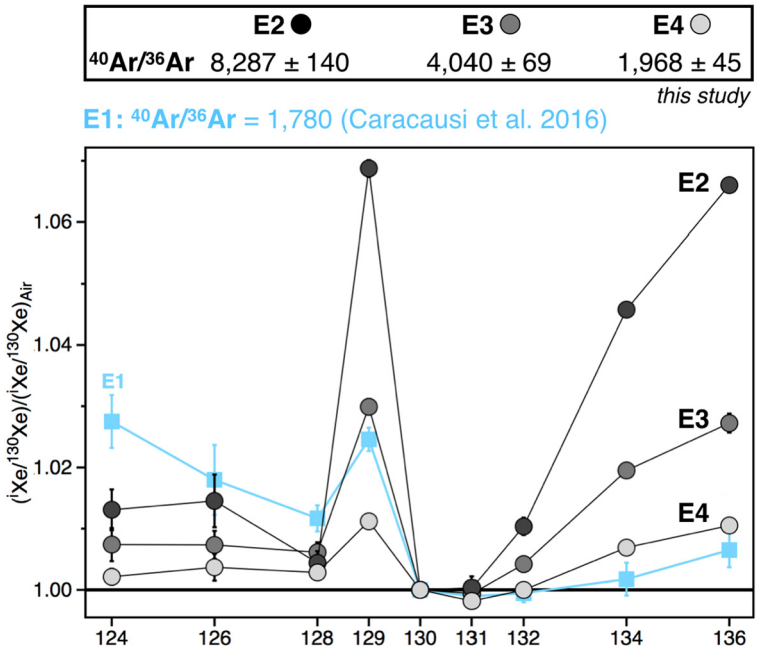

Fig. 2. Argon and xenon isotope composition of the three Eifel samples (E2, E3 and E4) analysed in this study. Xenon isotopic composition of E2, E3 and E4 are normalised to air and to ^{130}Xe, and compared to the xenon isotope composition reported by Caracausi et al. (2016) for the Eifel source (E1). Although E1 shows a greater enrichment in the light isotopes, E2-E4 show greater excesses in radiogenic ^{129}Xe and fissiongenic $^{131-136}Xe$, indicating greater contributions from mantle-derived components. This suggests that E1 might have been partially fractionated in favour of the light isotopes during purification and/or analysis. Error bars indicate $\pm 1\sigma$. Air composition is from Ozima and Podosek (2002).

overlap those from the Icelandic and Rochembeau rift plumes (Parai and Mukhopadhyay, 2015). From linear least squares fitting calculations, our data indicate a predominant contribution from ^{238}U-derived Xe, as well as "MORB-like" Pu–Xe/(Pu+U)–Xe and $^{129}Xe_I/^{136}Xe_{Pu}$ ratios (Table 1), regardless if ^{128}Xe is taken in to account or not. However, these outcomes are associated with much larger uncertainties when ^{128}Xe is not taken into account (Table 1). Henceforth, we only consider the results using ^{128}Xe for sample E2. Importantly, determining the initial, recycled atmospheric, Pu- and U-fissiogenic Xe components in the Eifel gas as measured by Caracausi et al. (2016) gives more contrasted outcomes depending on whether ^{128}Xe is taken into account (Table 1). If ^{128}Xe is taken into account, the data are best accounted for by mixing $91.4^{+0.8}_{-0.8}$% air, $8.2^{+0.8}_{-0.7}$% AVCC and $0.3^{+0.1}_{-0}$% ^{244}Pu-derived Xe with negligible contribution from ^{238}U-derived Xe. In this case, $^{129}Xe_I/^{136}Xe_{Pu}$ and Pu–Xe/(Pu+U)–Xe ($5.8^{+1}_{-0.8}$ and $0.96^{+0}_{-0.01}$, re-

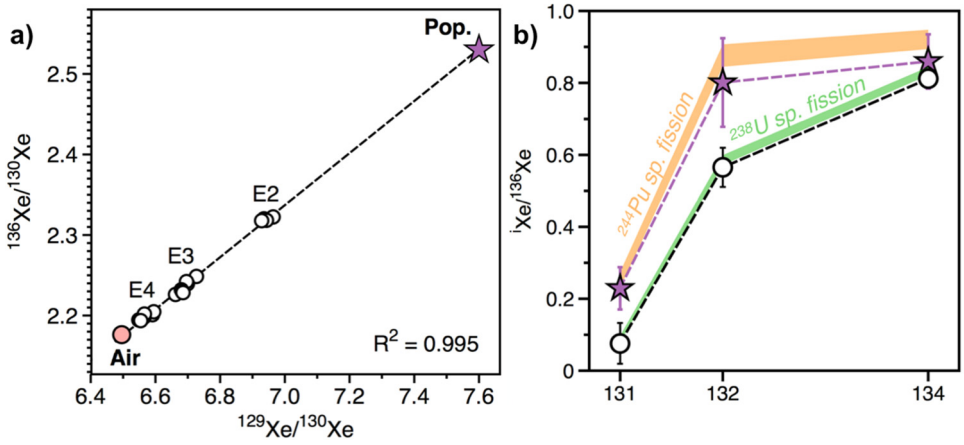

Fig. 3. a) $^{129}Xe/^{130}Xe$ vs. $^{136}Xe/^{130}Xe$ diagram showing air (in pink), Eifel samples (white circles) and popping rock 2πD43 (purple star, Péron and Moreira, 2018). b) Fission spectra of E2 (white circles) and popping rock 2πD43 (purple star, Péron and Moreira, 2018) compared with the fission spectra for fission of ^{238}U (green area) and ^{244}Pu (orange area). Irrespective of their degassing histories, the mantle sources of Eifel gas and popping rocks have therefore preserved similar $^{129}Xe/^{136}Xe$, although the main fissiongenic sources of ^{136}Xe excess are different (^{244}Pu for popping rocks and ^{238}U for the Eifel gas). Air composition is from Ozima and Podosek (2002). (For interpretation of the colours in the figure(s), the reader is referred to the web version of this article.)

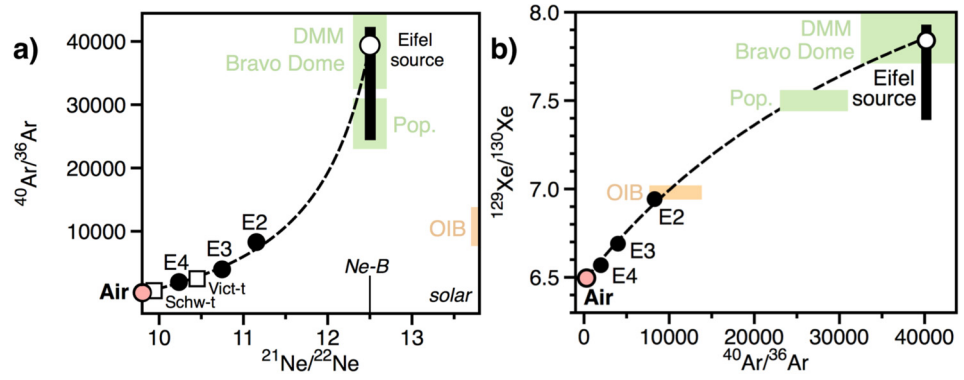

Fig. 4. Ne–Ar (a) and Ar–Xe (b) correlations for the Eifel gas. The data reflect mixing between a mantle component and post-eruptive atmospheric contamination. A least-squares hyperbolic fit through the data yields a $^{40}Ar/^{36}Ar$ ratio of $39,400^{+2900}_{-15200}$ (Fig. S1) and a $^{129}Xe/^{130}Xe$ of $7.84^{+0.09}_{-0.45}$, for a MORB-like $^{20}Ne/^{22}Ne$ ratio of 12.5. DMM, Bravo Dome, popping rocks and OIB compositions are from Tucker et al. (2012). Air compositions are from Ozima and Podosek (2002).

Table 1
Outcomes of Monte Carlo linear least square simulations adapted from Parai and Mukhopadhyay (2015). We tested the code on SWIR-E and SWIR-W samples reported by Parai and Mukhopadhyay (2015; in italics) to ensure similar results were obtained. The code was then run for popping rocks (Péron and Moreira, 2018), Lignat (Moreira et al., 2018), Eifel E1 (with and without ^{128}Xe being taken into account; Caracausi et al., 2016) and Eifel E2 (this study). The ranges of values for OIB and MORB as compiled by Caracausi et al. (2016) are also given for comparison.

Sample	I–$^{129}Xe/Pu–^{136}Xe$	Pu/(Pu+U)–^{136}Xe	%Mantle contribution	%Pu	%U
SWIR-E	$8.8^{+20.3}_{-3.6}$	$0.31^{+0.20}_{-0.21}$	$7.8^{+4.2}_{-4.1}$	$1.0^{+0.7}_{-0.7}$	$1.4^{+0.4}_{-0.3}$
Parai+15	$8.3^{+14.6}_{-3.2}$	$0.32^{+0.19}_{-0.20}$	$8.3^{+4.1}_{-3.9}$	$1.1^{+0.6}_{-0.7}$	$1.4^{+0.4}_{-0.4}$
SWIR-W	$10.3^{+27.3}_{-4.4}$	$0.28^{+0.20}_{-0.20}$	$11^{+6.7}_{-6.4}$	$1.5^{+1.1}_{-1.1}$	$2.5^{+0.6}_{-0.6}$
Parai+15	$10.8^{+40.3}_{-4.8}$	$0.27^{+0.20}_{-0.21}$	$11^{+6.9}_{-6.3}$	$1.4^{+1.2}_{-1.1}$	$2.5^{+0.7}_{-0.6}$
Popping rock	$3.6^{+8.5}_{-1.2}$	$0.99^{+0.01}_{-0.78}$	$0^{+23.7}_{-0}$	$3.3^{+1.7}_{-2.3}$	$0^{+2.5}_{-0}$
Lignat	$2.8^{+0.2}_{-0.3}$	$0.94^{+0}_{-0.01}$	$0^{+0.9}_{-0}$	$0.2^{+0.1}_{-0}$	0^{+0}_{-0}
Eifel E1 (+128)	$5.8^{+1}_{-0.8}$	$0.96^{+0}_{-0.01}$	$8.2^{+0.8}_{-0.7}$	$0.3^{+0.1}_{-0}$	0^{+0}_{-0}
Eifel E1 (−128)	$213.5^{+7.1}_{-7.2}$	$0.05^{+0.01}_{-0.01}$	$2.8^{+1.1}_{-1.1}$	0^{+0}_{-0}	$0.1^{+0.1}_{-0}$
Eifel E2 (+128)	$13.8^{+25.4}_{-5.3}$	$0.21^{+0.13}_{-0.14}$	$5.2^{+1.1}_{-1.1}$	$0.4^{+0.3}_{-0.2}$	$1.1^{+0.1}_{-0.2}$
Eifel E2 (−128)	$600.1^{+8.2}_{-583.5}$	$0.01^{+0.18}_{-0.01}$	$2.7^{+1.7}_{-1.1}$	$0^{+0.4}_{-0}$	$1.3^{+0}_{-0.2}$
OIB range	2.3–4	0.72–1			
MORB range	5–50	0.05–0.5			

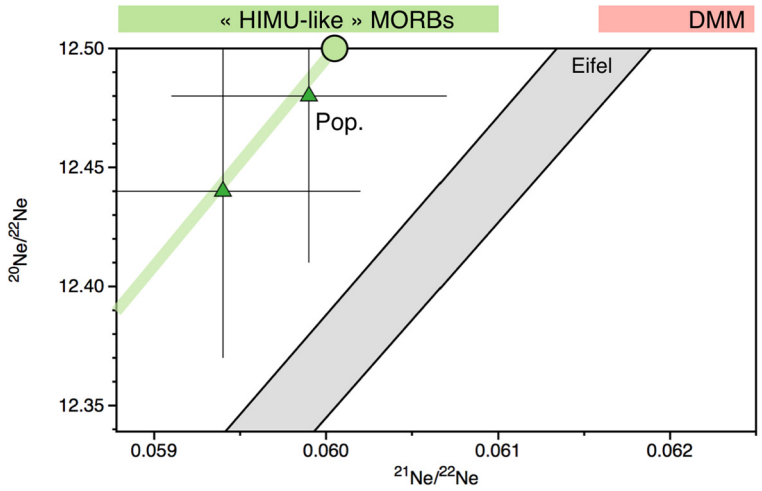

Fig. 5. Neon three-isotope plot displaying the extrapolated $^{21}Ne/^{22}Ne$ for a range of MORB and DMM samples (values extrapolated to $^{21}Ne/^{22}Ne = 12.5$; Tucker et al., 2012). Note that, according to Xe isotopes (Fig. 7), HIMU-type MORBs are referred to as MORBs. Also shown as green triangles are the two upper points for popping rocks (Pop., Moreira et al., 1998). Error weighted least squares linear regression through the Eifel data points gives an error envelope that is represented as a grey area. The extrapolated $^{21}Ne/^{22}Ne$ for the Eifel source appears to be distinct from the MORB range as sampled by popping rocks but overlaps with the field of the DMM.

spectively; Table 1) are consistent with the classical view of OIB-like signatures. However, if ^{128}Xe is excluded, the data are best accounted for by mixing $97^{+1.2}_{-1.1}$% air, $2.8^{+1.1}_{-1.1}$% AVCC and $0.1^{+0.1}_{-0}$% ^{238}U-derived Xe with negligible contribution from ^{244}Pu-derived Xe. In this case, $^{129}Xe_I/^{136}Xe_{Pu}$ and Pu–Xe/(Pu+U)–Xe ($213.5^{+7.1}_{-7.2}$ and $0.05^{+0.01}_{-0.01}$, respectively; Table 1) are in better agreement with the classical view of MORB-like signatures.

Importantly, Xe isotope spectra of samples E2-E4 show greater contributions of mantle-derived gas compared to sample E1 (Fig. 2; Caracausi et al., 2016). Yet, the light isotope excess reported by Caracausi et al. (2016) is greater than observed in the present study, indicating that data reported for sample E1 have been fractionated in favour of the light isotopes, as recently suggested by Moreira et al. (2018). Data points corresponding to repeated measurements of a single sample from Caracausi et al. (2016) appear to plot along MDF lines (Fig. 8 and Fig. S3), suggesting that isotope fractionation occurred during gas analysis rather than during sampling. Analytical issues might have occurred during sample preparation, especially during purification. In the present paper, gases were collected using Giggenbach bottles, therefore removing reactive gases and allowing the build up of a large partial pressure of noble gases. This procedure of gas sampling vastly improved the efficiency of purification of the samples for analysis. In addition, samples were purified using a different purification line than Caracausi et al. (2016). Taking together these considerations, we conclude that the dataset reported in the present study is more appropriate to constrain the source of volcanism in the Eifel region.

Taken together, our result show the mantle reservoir sampled by the Eifel volcanism to have a geochemical signature ($^{40}Ar/^{36}Ar$, $^{129}Xe/^{136}Xe$, Ne isotope composition; Fig. 1 and 4) that is similar to the convective upper mantle, with low Pu–Xe/(Pu+U)–Xe. Despite large error bars at the 1-sigma level, heavy Xe excesses measured in popping rocks, thought to best represent the upper mantle, appear to be dominated by ^{244}Pu-derived Xe (Péron and Moreira, 2018). We calculate the I-Xe/Pu-Xe and Pu–Xe/(Pu+U)–Xe of the popping rock source to be $3.6^{+8.5}_{-1.2}$ and $0.99^{+0.01}_{-0.78}$, respectively (Table 1). According to the Pu–Xe/(Pu+U)–Xe, the MORB sources for Eifel volcanism and popping rocks would therefore have experienced extensive and limited degassing, respectively, whilst both sampling the convective mantle. Likewise, the source of the Lignat thermal spring (Massif Central, France) analysed by Moreira et al. (2018) is best accounted for by an I–Xe/Pu–Xe of $2.8^{+0.2}_{-0.3}$ and a Pu–Xe/(Pu+U)–Xe of $0.94^{+0}_{-0.01}$ (Table 1). These values for popping rock and Lignat fall within the range of OIB (2.3–4 and 0.72–1, respectively) but are distinct from what has been commonly considered as the MORB range (5–50 and 0.05–0.5, respectively; Caracausi et al., 2016). The atmospheric contribution required to explain the Lignat data is extremely high ($99.7^{+0.01}_{-0.9}$% air, Table 1). Nonetheless, the fissiogenic isotope ratios for the Lignat gas require a $0.2^{+0.1}_{-0}$% contribution of Pu-derived Xe with no contribution of U-derived Xe. If truly representative of the mantle source then this would suggest that variable Pu–Xe/(Pu+U)–Xe might co-exist within the CEVP source(s), with fissiogenic Xe isotope being derived from both ^{244}Pu (Lignat gas, Moreira et al., 2018) and ^{238}U (Eifel gas, this study). However, drawing definite conclusion from Lignat gas is difficult given the large amount of atmospheric contamination, with only two of the four fissiogenic isotopes (^{134}Xe and ^{136}Xe) being in excess of air. Also note that the mean mantle contribution computed for popping rocks and Lignat gas (Table 1) are 0%, despite respective $^{129}Xe/^{130}Xe$ being in excess of air, which requires positive mantle contributions. A statistical bias during deconvolution of atmosphere- and mantle-derived signatures for these samples might be introduced during translation of ^{130}Xe-normalised ratios, as provided in the corresponding studies, into ^{132}Xe-normalised ratios, causing significant correlated errors in the ^{132}Xe-normalised ratios used for the calculations (Supplementary Information). As shown in Fig. 8b, Lignat gas data points might also show some extent of mass dependent fractionation, therefore causing a potential bias in the determination of its Pu–Xe/(Pu+U)–Xe.

The $^{3}He/^{4}He$ ratios, the slopes of mantle-air mixing lines in the Ne three isotope plot (Fig. 1) and the Pu–Xe/(Pu+U)–Xe are interpreted as reflecting the extent of degassing experienced by a given mantle reservoir. As depicted on Fig. 6, the OIB-like mantle sources akin to Iceland (Mukhopadhyay, 2012) and Rochambeau (Petö et al., 2013) exhibit high $^{3}He/^{4}He$ and $^{20}Ne/^{21}Ne_E$ ratios (where $^{20}Ne/^{21}Ne_E$ reflects the slope of mantle-air mixing lines in the Ne three isotope plot) that are not seen in samples deriving from the convective mantle. Although OIB-like mantle sources show consistently high Pu–Xe/(Pu+U)–Xe, it appears that samples from the convective upper mantle span the whole range of Pu–Xe/(Pu+U)–Xe values (Fig. 6) implying that fissiogenic Xe excesses in mantle-derived samples may not relate solely to different states of degassing and cannot therefore yield any strong indication regarding the source of volcanism (MORB or OIB). In other

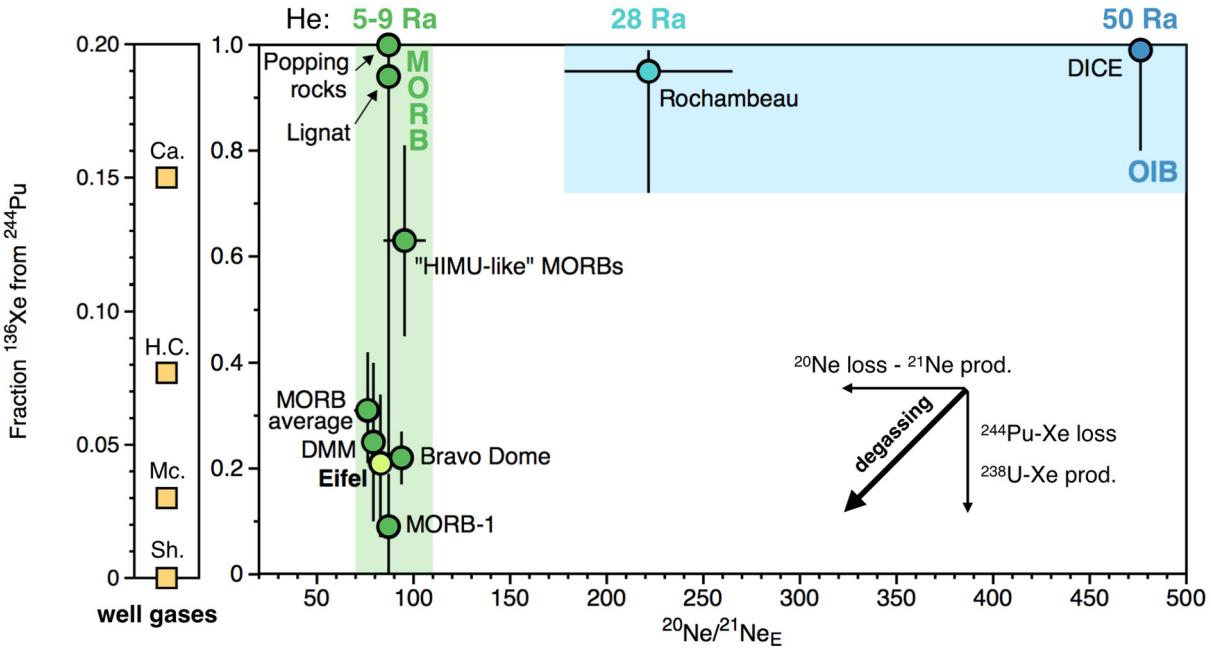

Fig. 6. Fractions of ^{136}Xe derived from ^{244}Pu vs. slopes of air-mantle mixing lines in Ne three-isotope space (^{20}Ne/^{21}Ne$_E$). Two OIB-like samples, Rochambeau (Petö et al., 2013) and DICE (Mukhopadhyay, 2012), are represented. Popping rocks are computed from data by (Péron and Moreira, 2018). MORB-1 is computed by Mukhopadhyay (2012) from popping rock data by Kunz et al. (1998). "Himu-like" MORBs and DMM are from Tucker et al. (2012). The error-weighted MORB average composition computed by Parai and Mukhopadhyay (2015) is also shown. Also represented are well gases data. The Bravo Dome mantle composition is from Holland and Ballentine (2006) and computation by Parai and Mukhopadhyay (2015). Other well gas data (Ca.: Caroline, Australia; H.C.: Harding County; Mc.: McElmo Dome; Sh.: Sheep Mountain; orange squares) are from Caffee et al. (1999), for which the Ne isotope composition of the mantle source is not known. Eifel (this study) is shown in light green. Differences in ^{130}Xe/^{22}Ne between highly degassed (MORB) and less degassed (e.g., Iceland or Rochambeau) mantle components (Williams and Mukhopadhyay, 2019) appear to be too small to account for hyperbolic mixing trends allowing to span a large range of Pu/(Pu+U)–Xe for a single 20/21$_E$.

words, high Pu–Xe/(Pu+U)–Xe may no longer be considered as being indicative of a deep undegassed origin for the sampled mantle sources. Likewise, whilst the ^{129}Xe$_I$/^{136}Xe$_{Pu}$ of Eifel gas ($13.8^{+25.4}_{-5.3}$) overlaps with the range MORB range (5-50), the ^{129}Xe$_I$/^{136}Xe$_{Pu}$ of popping rocks and Lignat ($3.6^{+8.5}_{-1.2}$ and $2.8^{+0.2}_{-0.3}$, respectively) are in better agreement with the OIB range (2.3-4; Table 1, Fig. S4). This indicates that, although MORB and OIB reservoirs can be discriminated from their differences in I/Xe (Fig. 4), they may no longer be distinguished on the basis of their ^{129}Xe$_I$/^{136}Xe$_{Pu}$ relationship.

The isotopic composition of atmospheric Xe evolved throughout the Archean via mass-dependent fractionation up until 2.5 Gyr ago, starting from a precursor (titled U-Xe) exhibiting deficits in ^{134}Xe and ^{136}Xe (Avice et al., 2018). Early recycling of atmospheric xenon with an isotopic composition intermediate between U-Xe and modern atmospheric Xe would render precise deconvolution of the chondritic, atmospheric, fissiogenic and radiogenic contributions to the mantle Xe array difficult (Péron and Moreira, 2018). It would also complicate the identification of primordial sources (solar, chondritic) of Xe in the mantle. Heavy noble gases (Kr, Xe) in the upper mantle carry signatures that are distinct from solar (as defined by Meshik et al., 2014), but similar to chondrites (Holland et al., 2009; Caracausi et al., 2016; Péron and Moreira, 2018). However, no unambiguous, high precision heavy noble gas data allowing chondritic and solar sources to be discriminated have been reported so far for the deep, undegassed mantle sampled by OIB-like plumes.

4.3. Noble gas reservoirs in the mantle

In a ^{129}Xe/^{130}Xe vs. ^{136}Xe/^{130}Xe diagram, OIB- and MORB-air mixing lines have distinct slopes, with the OIB line being slightly steeper due to lower ^{129}Xe/^{136}Xe for the MORB source (Fig. 7; Tucker et al., 2012). From the ^{129}Xe/^{130}Xe of the Iceland plume source (6.98±0.07; Mukhopadhyay, 2012), we calculate the corresponding ^{136}Xe/^{130}Xe (Fig. 7) and plot the composition of the Iceland source in Fig. 8. According to this diagram, higher ^{129}Xe/^{136}Xe in OIB relative to MORB cannot be related solely to recycling of atmospheric Xe or by adding fissiogenic ^{136}Xe to MORB Xe (Mukhopadhyay, 2012). Interestingly, the source of popping rocks (Péron and Moreira, 2018) and Eifel samples (this study) plot along a single line passing through the MORB mantle as previously defined by the popping rock 2πD43 mean composition (see compilation by Moreira et al., 2018). Irrespective of their degassing histories, the mantle sources of Eifel gas and popping rocks have preserved similar ^{129}Xe/^{136}Xe, although their main sources of fissiogenic Xe appear to be different (^{244}Pu for popping rocks and ^{238}U for the Eifel gas; Fig. 3).

The limited contribution from ^{244}Pu-derived Xe in Eifel gas (Fig. 3b) relative to popping rocks suggests either that (i) ^{244}Pu-derived Xe has been degassed early and therefore lost from the mantle reservoir, or that (ii) enhanced production of ^{238}U-derived Xe has overprinted the budget of fission-derived Xe isotopes. Given that the half-life of ^{129}I ($T_{1/2}$ = 15.7 Ma) is shorter than that of ^{244}Pu ($T_{1/2}$ = 80 Ma), ^{129}I would have been extinct before ^{244}Pu and so complete degassing of ^{244}Pu-derived Xe would also imply extensive degassing of ^{129}I-derived Xe, which is at odds with the preservation of radiogenic ^{129}Xe in the Eifel mantle source. Regarding the second hypothesis, a high contribution of ^{238}U-derived Xe in the Eifel magmatic gas could have several origins, including an HIMU-type source influence, or an additional input of radiogenic crustal derived noble gases as seen in well gases (Holland and Ballentine, 2006). Noble gas systematics in Eifel xenoliths are for example compatible with the addition of crustal material to a MORB-source signature (Dunai and Baur, 1995). However, from Ne isotopes, we see no evidence for extraneous crustal ^{21}Ne (Fig. 1). Concerning Xe isotopes, the composition of continental well gases deviates from the MORB and OIB trend toward lower ^{129}Xe/^{136}Xe because of crustal inputs of ^{238}U-derived ^{136}Xe and limited ex-

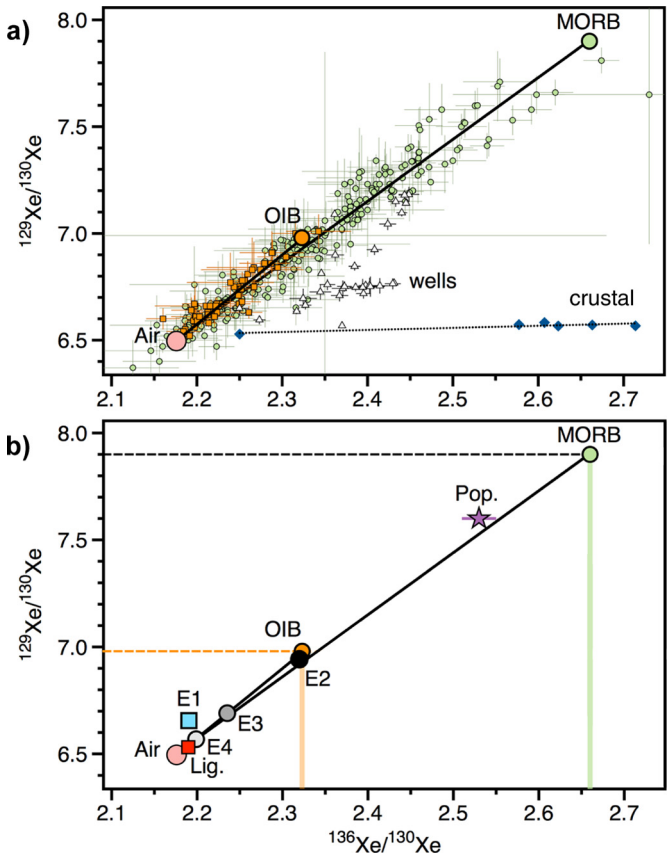

Fig. 7. $^{129}Xe/^{130}Xe$ vs. $^{136}Xe/^{130}Xe$ diagrams showing (a) air (Ozima and Podosek, 2002; pink circles), OIB (Iceland plume, DICE Mukhopadhyay, 2012; orange squares), MORBs (Kunz et al., 1998; Tucker et al., 2012; Parai and Mukhopadhyay, 2015; green circles), CO_2 well gases and thermal springs (diamonds; Caffee et al., 1999; Holland and Ballentine, 2006), as well as crustal fluids (blue diamonds; Holland et al., 2013). On panel (b), we also report the Lignat sample (Lig., red square; Moreira et al., 2018), popping rocks (Pop., purple star; Péron and Moreira, 2018), as well as the Eifel sample by Caracausi et al. (2016) (E1, blue square) and this study (grey circles). The known $^{129}Xe/^{130}Xe$ of OIB and MORB mantle sources (Mukhopadhyay, 2012) are used to determine the corresponding $^{136}Xe/^{130}Xe$.

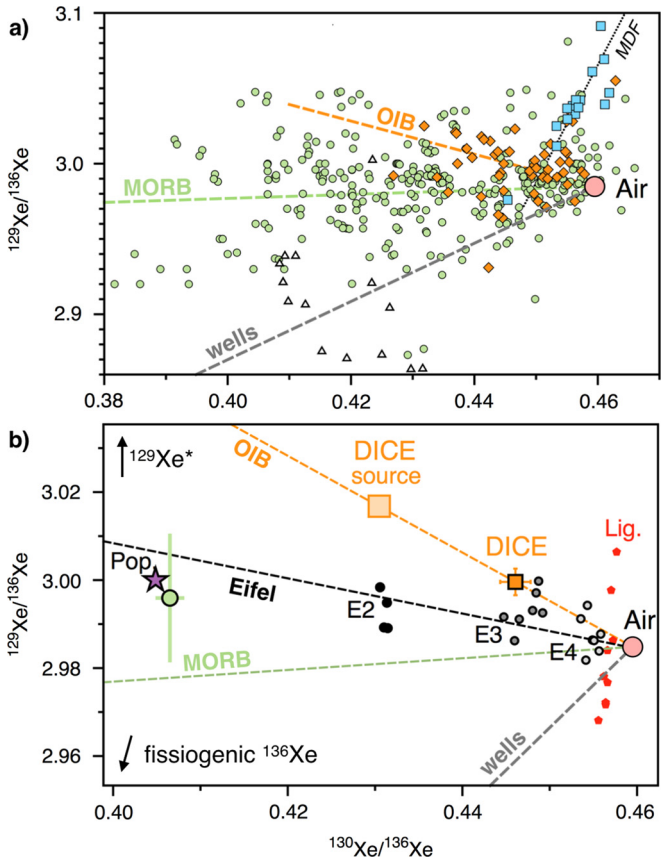

Fig. 8. $^{129}Xe/^{136}Xe$ vs. $^{130}Xe/^{136}Xe$ diagram showing (a) air (pink circle, Ozima and Podosek, 2002), OIB (Iceland plume, DICE Mukhopadhyay, 2012; orange diamonds), MORBs (green circles; Kunz et al., 1998; Tucker et al., 2012; Parai and Mukhopadhyay, 2015), CO_2 well gases (triangles; Caffee et al., 1999; Holland and Ballentine, 2006) and E1 sample from Eifel (blue squares, Caracausi et al., 2016). Fitting the respective datasets through atmosphere produces the wells, MORB and OIB lines. Mass dependent fractionation line is also represented as MDF. On panel (b), we report the wells, MORB and OIB lines along with E2, E3 and E4 Eifel samples (black, grey and white circles, respectively; this study) and Lignat measurements (red pentagons, labelled Lig.; Moreira et al., 2018). Popping rock sample (Pop., purple star) is from Péron and Moreira (2018). The green point is the average MORB composition compiled by Moreira et al. (2018). The OIB line defined by Iceland samples is distinct from that defined by MORB samples, with a lower $^{129}Xe/^{136}Xe$. Such differences cannot be related solely through recycling atmospheric Xe or by adding fissiogenic ^{136}Xe to MORB Xe (Mukhopadhyay, 2012). Given that the MORB reservoir has a higher I/Xe ratio, higher $^{129}Xe/^{136}Xe$ in OIB can only be accounted for by lower (Pu-U)/Xe in the OIB source. Irrespective of their degassing histories, the mantle sources of Eifel gas and popping rocks appear to have preserved similar $^{129}Xe/^{136}Xe$, although the main fissiogenic sources of ^{136}Xe excess are different (^{244}Pu for popping rocks and ^{238}U for the Eifel gas).

cesses of mantle-derived $^{129}Xe^*$ (Figs. 7–8). Such deviations are not observed for the Eifel gas, which plots exactly on the mantle-air mixing line in $^{129}Xe/^{130}Xe$-$^{136}Xe/^{130}Xe$ space (Fig. 7). Although we cannot rule out the potential for small crustal inputs, these data seem to exclude a significant crustal contribution in the Eifel gas. Likewise, relative abundances of the non-reactive components reported by Bräuer et al. (2013) together with the isotope signatures of the stable isotopes, especially of the major magmatic volatile CO_2, do not indicate any crustal contribution in the Victoriaquelle and Schwefelquelle wells, but seem to be characteristic for a MORB-like reservoir. Similarly, the low $^3He/^4He$ and high $^{40}Ar/^{36}Ar$ ratios in the Eifel region (Victoriaquelle and Schwefelquelle gases) have been suggested to be the result of magma ageing resulting in the continuous radioactive decay of U, Th and ^{40}K within the magmatic reservoir (Bräuer et al., 2013). However, once again this process cannot account for the observed excesses in ^{238}U-derived Xe given that these correlate with mantle-derived $^{129}Xe^*$ (Fig. 3) indicating that the low $^3He/^4He$, high $^{40}Ar/^{36}Ar$ and ^{238}U-derived Xe excesses all have a similar mantle origin.

Subduction recycling of altered oceanic crust with associated transport of U to the mantle over the last 2 billion years can make a significant contribution to U recycling into the mantle, potentially even dominating the total net U-addition to the post-Archean convecting mantle (Pettke et al., 2018). Portions of the mantle thought to derive from melting of these ancient sections of oceanic crust, referred to as HIMU, could have been significantly enriched in ^{238}U through this process. These are defined by He isotope ratios from 4.5 Ra to 12.8 Ra and Ne isotopic signatures that extend from the MORB range to compositions less nucleogenic than MORBs (Parai et al., 2009; Day and Hilton, 2011). Noble gases in mantle xenoliths from various European Cenozoic volcanic provinces depict mixtures between DMM-EM-HIMU end-members within the European sub-continental mantle source (e.g., Dunai and Baur, 1995). A HIMU-like source contribution in Eifel free gas samples could notably account for both the low $^3He/^4He$ (~4–5*Ra; Bräuer et al., 2013) and high contribution from ^{238}U fission derived Xe. The $^3He/^4He$ values of ultramafic xenoliths from the Eifel Quaternary volcanic field "Dreiser Weiher" (5.97 ± 0.49 Ra; Buikin et al., 2005) are in good agreement with the intrinsic signature of the subcontinental lithospheric mantle (SCLM; 6±1 Ra) although the authors acknowledge that there is also an obvious similarity to oceanic HIMU islands (Buikin et al., 2005). However, for the ^{238}U-derived

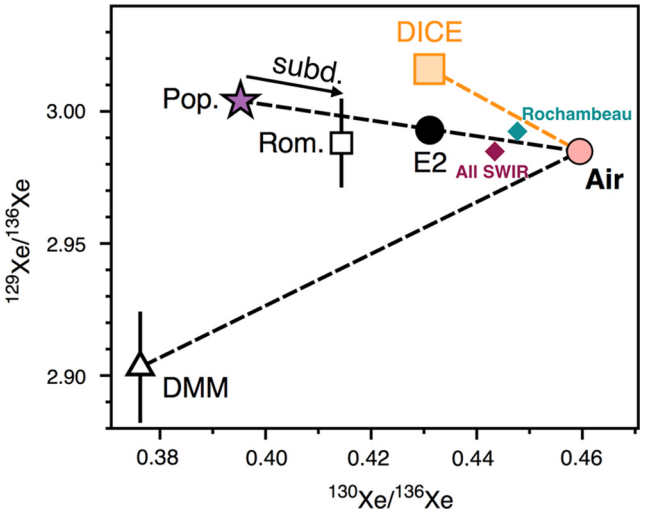

Fig. 9. $^{129}Xe/^{136}Xe$ vs. $^{130}Xe/^{136}Xe$ diagram showing air (Ozima and Podosek, 2002), mantle source compositions of OIB (DICE, Mukhopadhyay, 2012), popping rocks (Pop.; Péron and Moreira, 2018), the DMM (Tucker et al., 2012) and HIMU-type MORB from the north of the Romanche fracture zone (Rom.; Tucker et al., 2012). Also displayed are the error-weighted average compositions of the Rochambeau Rift (Pető et al., 2013) and SWIR Orthogonal Supersegment (Parai and Mukhopadhyay, 2015). The source of the HIMU-type MORB in the Romanche fracture zone is explained by addition of subducted air to the mantle source of popping rocks. The composition of Eifel sample E2 ($^{40}Ar/^{36}Ar \sim 8300$) also appears to plot on the MORB-air mixing line, which is at odds with the budget of fission-derived Xe isotopes being dominated by ^{238}U-derived Xe for Eifel, and by ^{244}Pu-derived Xe for popping rocks. A possibility is that the Eifel composition reflects a mixture between a HIMU-type source and a less degassed MORB reservoir, causing the resulting signature to fortuitously plot close to the popping rocks-air mixing line.

Xe in Eifel gas and $^{129}Xe^*$ to both have a HIMU-like origin would imply that transport of subducted crust in the mantle occurred at a time where ^{129}I was still extant, i.e. within 80 Myr after the start of Solar System formation, which is unlikely (Parai and Mukhopadhyay, 2018). The average time commonly postulated for ageing of a HIMU-type source component is 1.9 Ga (Pettke et al., 2018). We therefore conclude that at least two mantle sources, one of which being of HIMU-type and the other being little degassed, may be required to account for the geochemical signature of the Eifel gas.

Xenon isotopic measurements from equatorial Mid-Atlantic Ridge basalts previously indicated the mantle sources of DMMs, popping rocks and HIMU-influenced MORBs to have distinct $^{129}Xe/^{136}Xe$ (Tucker et al., 2012). The mantle source of North Mid-Atlantic Ridge samples (popping rock and HIMU-influenced MORBs) appears to have a $^{129}Xe/^{136}Xe$ that is intermediate between the DMM (low $^{129}Xe/^{136}Xe$) and OIB (high $^{129}Xe/^{136}Xe$) (Fig. 9). The lower $^{129}Xe/^{136}Xe$ of the DMM is consistent with a more degassed source than the mantle source of Mid-Atlantic Ridge samples. The high proportion of Pu-derived Xe in Romanche fracture zone samples (63^{+18}_{-18}%; labelled "HIMU-like MORB" in Tucker et al., 2012) was interpreted as requiring contribution from a less degassed mantle component to dominate over the ^{238}U-produced fission Xe in the recycled crust. More degassed sources will indeed have lower concentrations of primordial Xe isotopes, $^{129}Xe^*$ and Pu-derived Xe, such that adding ^{136}Xe from ^{238}U fission will produce lower $^{129}Xe/^{136}Xe$. Any addition of HIMU-like material to an OIB-like component would therefore lower the mantle source $^{129}Xe/^{136}Xe$ from high values akin to the Icelandic plume, toward MORB-like values. However, the recently determined Xe isotope composition of popping rocks (compilation from Moreira et al., 2018; Péron and Moreira, 2018) is different from that used by Tucker et al. (2012) to define the MORB end-member. This newly determined Xe isotope composition of the popping rock mantle source, representative of the convective mantle, has high Pu–Xe/(Pu+U)–Xe (99^{+1}_{-78}%, Table 1) and $^{129}Xe/^{136}Xe$ (similar to that of previously defined HIMU-influenced MORB mantle source at the Romanche fracture zone, Tucker et al., 2012; Fig. 9). HIMU-influenced MORBs defined by Tucker et al. (2012) might therefore represent the same MORB source as that of popping rocks, with a higher contribution from the atmospheric component (Fig. 9). The overlapping Pu–Xe/(Pu+U)–Xe of 99^{+1}_{-78}% for popping rocks (Péron and Moreira, 2018) and 63^{+18}_{-18}% for HIMU-influenced MORBs (Tucker et al., 2012) suggests that contribution of a deep undegassed source to the HIMU mantle defined by Tucker et al. (2012) may no longer be required.

As witnessed by its high $^{40}Ar/^{36}Ar$ and ^{238}U-derived Xe contribution, the Eifel gas has a large radiogenic contribution. However, the observation that the mantle sources of popping rocks and Eifel appear to have similar $^{129}Xe/^{136}Xe$ ratios indicates that the Eifel gas cannot be solely related to the DMM. To account for both the high $^{129}Xe/^{136}Xe$ relative to the DMM (Fig. 9) and low Pu- to U-derived fission Xe of the Eifel source may require contributions from both an undegassed reservoir with high $^{129}Xe/^{136}Xe$, and a highly degassed HIMU component primarily containing fissiogenic Xe continuously produced from the spontaneous decay of ^{238}U throughout its residence in the mantle. The undegassed reservoir with high $^{129}Xe/^{136}Xe$ is required to have a high I/Xe to account for the MORB-like $^{129}Xe/^{130}Xe$ of the Eifel mantle source (Fig. 4), and could not therefore correspond to a deep OIB-like reservoir akin to the Icelandic plume. Such a reservoir may have originated from a similar mantle source to that of MORB (popping rock and HIMU-like MORB) but with an even lower degree of degassing. The existence of this undegassed MORB reservoir remains to be proven although it is not inconceivable that sections of the mantle have remained less degassed than those currently expressed at mid ocean ridges. Addition of recycled, subduction-related material to such an undegassed source could have lowered the $^{129}Xe/^{136}Xe$ of the Eifel mantle source to produce intermediate $^{129}Xe/^{136}Xe$ values akin to that of the MORB mantle source. A promising avenue of investigation to further improve the deconvolution of mantle-derived signatures and better determine the $^{244}Pu/^{238}U$ of mantle reservoirs would be to better constrain the Xe fission spectrum of ^{244}Pu. Also note that the distribution of Pu in the early mantle is poorly constrained and often assumed to be similar to that of U. However, the potential for U and Pu to have been heterogeneously distributed in the early mantle, and for variations in the Pu- to U-derived fission Xe to not only be related to differences in degassing states, remains to be explored.

5. Conclusion

The origin of the CEVP has remained enigmatic given the potential for an OIB-like source to contribute to intraplate volcanism in the Eifel region. In this contribution, we show that the mantle source beneath Eifel, and by extension the CEVP, has a geochemical signature akin to the upper mantle reservoir sampled at mid ocean ridges. Accurate determination of $^{244}Pu/^{238}U$ ratios in mantle-derived samples has been commonly used to address the degassing states of corresponding mantle reservoirs. According to their Pu–Xe/(Pu+U)–Xe, the sources for Eifel volcanism and popping rocks would however have experienced extensive and limited degassing, respectively. The MORB reservoir therefore appears to exhibit variable Pu–Xe/(Pu+U)–Xe ratios which indicates that the presence of two mantle reservoirs (MORB and OIB) cannot be fully substantiated anymore solely by differences in Pu–Xe/(Pu+U)–Xe ratio. Differences between MORB and OIB sources would therefore only reside in the occurrence of solar-derived Ne, higher $^{20}Ne/^{21}Ne_E$ and higher $^{3}He/^{4}He$ in OIB, as well as higher $^{40}Ar/^{36}Ar$ and I/Xe in MORB relative to OIB. Interestingly, to account for both the high $^{129}Xe/^{136}Xe$ relative to the DMM and low Pu- to

U-derived fission Xe in the Eifel source may require contributions from both an undegassed MORB-like reservoir, with high $^{129}Xe/^{136}Xe$, and a deep HIMU-like mantle source also accounting for the low $^{3}He/^{4}He$ seen in Eifel gas. Although our results refute a deep plume OIB-like origin for volcanism in Eifel, Ne and Xe systematics therefore point toward contributions from multiple reservoirs with different degassing histories, originating from different depths in the mantle beneath the CEVP.

Author contributions

B.M, D.V.B, and M.W.B developed the Giggenbach sampling/storage method for noble gases. D.V.B, M.W.B, and B.M collected the samples. D.V.B. and M.W.B. did the noble gas analyses, discussed the results and their interpretations, and wrote the manuscript. B.M. and A.C. discussed the results and their interpretations, and contributed to writing the manuscript.

Data and materials availability

All data needed to evaluate the conclusions in the paper are present in the paper and/or the Supplementary Materials. Additional data related to this paper may be requested from the authors.

Competing interests

The authors declare that they have no competing interests.

Acknowledgements

We gratefully thank Rita Parai for providing us with the MATLAB code developed by Parai and Mukhopadhyay (2015). Sujoy Mukhopadhyay is thanked for his fruitful insights into how to improve our manuscript. We also thank Manuel Moreira for his review, and for having initiated this study by triggering insightful discussions about the origin of volcanism beneath Central Europe. This study was supported by the European Research Council (grant PHOTONIS 695618 to B.M.). This is CRPG contribution N° 2693.

Appendix A. Supplementary material

Supplementary material related to this article can be found online at https://doi.org/10.1016/j.epsl.2019.115766.

References

Allègre, C.J., Staudacher, T., Sarda, P., Kurz, M., 1983. Constraints on evolution of Earth's mantle from rare gas systematics. Nature 303 (5920), 762.
Avice, G., Marty, B., Burgess, R., Hofmann, A., Philippot, P., Zahnle, K., Zakharov, D., 2018. Evolution of atmospheric xenon and other noble gases inferred from Archean to Paleoproterozoic rocks. Geochim. Cosmochim. Acta 232, 82–100.
Azbel, I.Y., Tolstikhin, I.N., 1993. Accretion and early degassing of the Earth: constraints from Pu–U–I–Xe Isotopic systematics. Meteoritics 28 (5), 609–621.
Ballentine, C.J., Marty, B., Lollar, B.S., Cassidy, M., 2005. Neon isotopes constrain convection and volatile origin in the Earth's mantle. Nature 433 (7021), 33.
Bräuer, K., Kämpf, H., Niedermann, S., Strauch, G., 2013. Indications for the existence of different magmatic reservoirs beneath the Eifel area (Germany): a multi-isotope (C, N, He, Ne, Ar) approach. Chem. Geol. 356, 193–208.
Buikin, A., Trieloff, M., Hopp, J., Althaus, T., Korochantseva, E., Schwarz, W.H., Altherr, R., 2005. Noble gas isotopes suggest deep mantle plume source of late Cenozoic mafic alkaline volcanism in Europe. Earth Planet. Sci. Lett. 230 (1–2), 143–162.
Burnard, P., Graham, D., Turner, G., 1997. Vesicle-specific noble gas analyses of "popping rock": implications for primordial noble gases in Earth. Science 276 (5312), 568–571.
Caffee, M.W., Hudson, G.B., Velsko, C., Huss, G.R., Alexander, E.C., Chivas, A.R., 1999. Primordial noble gases from Earth's mantle: identification of a primitive volatile component. Science 285 (5436), 2115–2118.
Caracausi, A., Avice, G., Burnard, P.G., Füri, E., Marty, B., 2016. Chondritic xenon in the Earth's mantle. Nature 533 (7601), 82.
Clay, P.L., Burgess, R., Busemann, H., Ruzié-Hamilton, L., Joachim, B., Day, J.M., Ballentine, C.J., 2017. Halogens in chondritic meteorites and terrestrial accretion. Nature 551 (7682), 614.
Colin, A., Moreira, M., Gautheron, C., Burnard, P., 2015. Constraints on the noble gas composition of the deep mantle by bubble-by-bubble analysis of a volcanic glass sample from Iceland. Chem. Geol. 417, 173–183.
Craig, H., Lupton, J.E., 1976. Primordial neon, helium, and hydrogen in oceanic basalts. Earth Planet. Sci. Lett. 31 (3), 369–385.
Day, J.M., Hilton, D.R., 2011. Origin of $^{3}He/^{4}He$ ratios in HIMU-type basalts constrained from Canary Island lavas. Earth Planet. Sci. Lett. 305 (1–2), 226–234.
Dunai, T.J., Baur, H., 1995. Helium, neon, and argon systematics of the European subcontinental mantle: implications for its geochemical evolution. Geochim. Cosmochim. Acta 59 (13), 2767–2783.
Giggenbach, W.F., Goguel, R.L., 1989. Collection and Analysis of Geothermal and Volcanic Water and Gas Discharges. Chem. DIV. DSIR REPT. CD 2401, 81 pp.
Goes, S., Spakman, W., Bijwaard, H., 1999. A lower mantle source for central European volcanism. Science 286 (5446), 1928–1931.
Graham, D.W., 2002. Noble gas isotope geochemistry of mid-ocean ridge and ocean island basalts: characterization of mantle source reservoirs. Rev. Mineral. Geochem. 47 (1), 247–317.
Hallis, L.J., Huss, G.R., Nagashima, K., Taylor, G.J., Halldórsson, S.A., Hilton, D.R., Meech, K.J., 2015. Evidence for primordial water in Earth's deep mantle. Science 350 (6262), 795–797.
Hart, S.R., Hauri, E.H., Oschmann, L.A., Whitehead, J.A., 1992. Mantle plumes and entrainment—isotopic evidence. Science 256, 517–520.
Holland, G., Ballentine, C.J., 2006. Seawater subduction controls the heavy noble gas composition of the mantle. Nature 441 (7090), 186.
Holland, G., Cassidy, M., Ballentine, C.J., 2009. Meteorite Kr in Earth's mantle suggests a late accretionary source for the atmosphere. Science 326 (5959), 1522–1525.
Holland, G., Lollar, B.S., Li, L., Lacrampe-Couloume, G., Slater, G.F., Ballentine, C.J., 2013. Deep fracture fluids isolated in the crust since the Precambrian era. Nature 497 (7449), 357.
Honda, M., McDougall, I., Patterson, D.B., Doulgeris, A., Clague, D.A., 1993. Noble gases in submarine pillow basalt glasses from Loihi and Kilauea, Hawaii: a solar component in the Earth. Geochim. Cosmochim. Acta 57 (4), 859–874.
Jackson, C.R., Bennett, N.R., Du, Z., Cottrell, E., Fei, Y., 2018. Early episodes of high-pressure core formation preserved in plume mantle. Nature 553 (7689), 491.
Kellogg, L.H., Wasserburg, G.J., 1990. The role of plumes in mantle helium fluxes. Earth Planet. Sci. Lett. 99 (3), 276–289.
Kunz, J., Staudacher, T., Allegre, C.J., 1998. Plutonium-fission xenon found in Earth's mantle. Science 280 (5365), 877–880.
Loewen, M.W., Graham, D.W., Bindeman, I.N., Lupton, J.E., Garcia, M.O., 2019. Hydrogen isotopes in high $^{3}He/^{4}He$ submarine basalts: primordial vs. recycled water and the veil of mantle enrichment. Earth Planet. Sci. Lett. 508, 62–73.
Marty, B., 1989. Neon and xenon isotopes in MORB: implications for the earth-atmosphere evolution. Earth Planet. Sci. Lett. 94 (1–2), 45–56.
Meshik, A., Hohenberg, C., Pravdivtseva, O., Burnett, D., 2014. Heavy noble gases in solar wind delivered by Genesis mission. Geochim. Cosmochim. Acta 127, 326–347.
Moreira, M., Kunz, J., Allegre, C., 1998. Rare gas systematics in popping rock: isotopic and elemental compositions in the upper mantle. Science 279 (5354), 1178–1181.
Moreira, M., Rouchon, V., Muller, E., Noirez, S., 2018. The xenon isotopic signature of the mantle beneath Massif Central. Geochem. Perspect. Lett. 6, 28–32.
Mukhopadhyay, S., 2012. Early differentiation and volatile accretion recorded in deep-mantle neon and xenon. Nature 486 (7401), 101.
Mukhopadhyay, S., Parai, R., 2019. Noble gases: a record of Earth's evolution and mantle dynamics. Annu. Rev. Earth Planet. Sci. 47, 389–419.
Ozima, M., Podosek, F.A., 2002. Noble Gas Geochemistry. Cambridge University Press, Cambridge.
Parai, R., Mukhopadhyay, S., 2015. The evolution of MORB and plume mantle volatile budgets: constraints from fission Xe isotopes in Southwest Indian Ridge basalts. Geochem. Geophys. Geosyst. 16 (3), 719–735.
Parai, P., Mukhopadhyay, S., Lassiter, J.C., 2009. New constraints on the HIMU mantle from neon and helium isotopic compositions of basalts from the Cook–Austral Islands. Earth Planet. Sci. Lett. 277, 253–261.
Parai, R., Mukhopadhyay, S., 2018. Xenon isotopic constraints on the history of volatile recycling into the mantle. Nature 560 (7717), 223.
Péron, S., Moreira, M., Colin, A., Arbaret, L., Putlitz, B., Kurz, M.D., 2016. Neon isotopic composition of the mantle constrained by single vesicle analyses. Earth Planet. Sci. Lett. 449, 145–154.
Péron, S., Moreira, M., 2018. Onset of volatile recycling into the mantle determined by xenon anomalies. Geochem. Perspect. Lett. 9, 21–25.
Pető, M.K., Mukhopadhyay, S., Kelley, K.A., 2013. Heterogeneities from the first 100 million years recorded in deep mantle noble gases from the Northern Lau Back-arc Basin. Earth Planet. Sci. Lett. 369, 13–23.
Pettke, T., Kodolányi, J., Kamber, B.S., 2018. From ocean to mantle: new evidence for U-cycling with implications for the HIMU source and the secular Pb isotope evolution of Earth's mantle. Lithos 316, 66–76.

Porcelli, D., Ballentine, C.J., 2002. Models for distribution of terrestrial noble gases and evolution of the atmosphere. Rev. Mineral. Geochem. 47 (1), 411–480.
Porcelli, D., Wasserburg, G.J., 1995. Mass transfer of helium, neon, argon, and xenon through a steady-state upper mantle. Geochim. Cosmochim. Acta 59 (23), 4921–4937.
Press, W.H., Teukolsky, S.A., Vetterling, W.T., Flannery, B.P., 1992. Numerical Recipes in C: The Art of Scientific Computing, second edition. Cambridge University Press, New York.
Ritter, J.R.R., 2007. The seismic signature of the Eifel plume. In: Ritter, J.R.R., Christensen, U.R. (Eds.), Mantle Plumes: A Multidisciplinary Approach. Springer-Verlag, Berlin, Heidelberg, pp. 379–404.
Sarda, P., Staudacher, T., Allègre, C.J., 1985. $^{40}Ar/^{36}Ar$ in MORB glasses: constraints on atmosphere and mantle evolution. Earth Planet. Sci. Lett. 72 (4), 357–375.
Schmincke, H.U., 2007. The Quaternary volcanic fields of the east and west Eifel (Germany). In: Mantle Plumes. Springer, Berlin, Heidelberg, pp. 241–322.
Stuart, F.M., Lass-Evans, S., Fitton, J.G., Ellam, R.M., 2003. High $^{3}He/^{4}He$ ratios in picritic basalts from Baffin Island and the role of a mixed reservoir in mantle plumes. Nature 424 (6944), 57.
Tucker, J.M., Mukhopadhyay, S., Schilling, J.G., 2012. The heavy noble gas composition of the depleted MORB mantle (DMM) and its implications for the preservation of heterogeneities in the mantle. Earth Planet. Sci. Lett. 355, 244–254.
Weber, M., Bock, G., Budweg, M., 2007. Upper mantle structure beneath the Eifel from receiver functions. In: Ritter, J.R.R., Christensen, U.R. (Eds.), Mantle Plumes: A Multidisciplinary Approach. Springer-Verlag, Berlin, Heidelberg, pp. 405–415.
Williams, C.D., Mukhopadhyay, S., 2019. Capture of nebular gases during Earth's accretion is preserved in deep-mantle neon. Nature 565 (7737), 78.
Yokochi, R., Marty, B., 2004. A determination of the neon isotopic composition of the deep mantle. Earth Planet. Sci. Lett. 225 (1–2), 77–88.
Zindler, A., Hart, S., 1986. Chemical geodynamics. Annu. Rev. Earth Planet. Sci. 14, 493–571.

Supplementary Materials

Supplementary text.

* Details regarding the purification and analytical procedure of ^{3}He, ^{4}He, and ^{20}Ne analysis at INGV (Palermo, Italy).

** Details regarding the purification and analytical procedure of Ne isotope analysis at CRPG (Nancy, France).

*** Details regarding the purification and analytical procedure of Ar and Xe isotope analysis at CRPG (Nancy, France).

**** Linear least squares determination of initial, recycled atmospheric, Pu- and U-fissiogenic Xe components.

***** Normalizing isotope: an issue with correlated errors?

Supplementary Figures (Fig. S1-S4)

Supplementary Tables (Table S1-S6)

SI references

Supplementary text.

* Details regarding the purification and analytical procedure of ^{3}He, ^{4}He, and ^{20}Ne analysis at INGV (Palermo, Italy).

^{3}He, ^{4}He, and ^{20}Ne analyses performed in the noble gas isotope laboratory of INGV (Istituto Nazionale di Geofisica e Vulcanologia), Sezione di Palermo (Italy), were carried out following an internal protocol reported e.g. in Rizzo et al. (2018). An aliquot of the sample was first expanded in to three distinct stainless-steel preparation lines in order to remove all species in the gas mixture other than noble gases. In detail, each of the three preparation lines is dedicated to a single noble gas species, in our case He, Ne, and Ar, and is equipped with a pipette system connected to a pressure gauge to introduce a known number of moles of gas sample. The purification and separation procedure for helium and neon consists of a first step of purification, during which the gas was exposed for 15-20 min to two Zr-Al GP50 getters, one at room temperature, the other at 400 °C. The gas was subsequently exposed for 20 min to a charcoal trap cooled at 77 °K (liquid nitrogen). During the second step of purification, the gas was exposed for 10 min to one Zr-Al GP50 getter at room temperature and to a charcoal trap cooled at -196 °C (liquid nitrogen). Then, helium and neon remaining in the line were expanded into a cryogenic trap cooled at 10°K and adsorbed for 20 min. Helium was released from the cryogenic trap by increasing its temperature to 40 °K and admitted into a Helix SFT-GVI for the isotopic analysis. Tuning parameters of the source were as follows: trap current 800 □A, source voltage 2.1 V and filament current 2.8 A. This consisted of one block of 80 cycles after automatic peak centring. The $^{3}He/^{4}He$ ratio analytical error was generally below 0.8% (1σ). This corresponds to the quadratic sum of the internal error and external reproducibility determined from the daily analysis of standards. Internal standard was helium purified from air, whose $^{3}He/^{4}He$ reproducibility over 1 year of analysis was <3%. The $^{3}He/^{4}He$ ratio is expressed as R/Ra (being Ra the He isotope ratio of air and equal to $1.39x10^{-6}$) and was corrected for the atmospheric contamination based on the measured $^{4}He/^{20}Ne$ ratio (e.g., Sano and Wakita, 1985) as follows:

$$Rc/Ra = ((R_M/Ra)(He/Ne)_M - (He/Ne)_A)/((He/Ne)_M - (He/Ne)_A)$$

where subscripts M and A refer to measured and atmosphere theoretical values, respectively [$(He/Ne)_A$=0.318]. After helium isotopic analysis started, neon was released from the cryogenic trap by increasing its temperature to 80 K, and introduced into a Helix MC Plus Thermo. Tuning parameters of the source for neon analyses were as follows: trap current 150 μA and source current 418.96 μA. Adjacent to the mass spectrometer's ion source, a charcoal finger at 77 K and a Zr-Al GP50 getter at room temperature were used to minimize the contribution of doubly charged ^{40}Ar and CO_2 to the ^{20}Ne and ^{22}Ne signals, respectively. However, for the set of analysis carried out at INGV-Palermo laboratory, only ^{20}Ne was analysed. The analysis was performed on L2 faraday detector and consisted of one block of 30 cycles after manual peak centring. The high mass resolution of the Helix MC Plus enables the discrimination of the ^{20}Ne peak from $^{40}Ar^{++}$ (Honda et al., 2015). The correct separation of the two peaks was checked at the start and end of analysis by manual scan. However, the $^{40}Ar^{++}$ signal was negligible compared to the signal of ^{20}Ne. The ^{20}Ne analytical error was generally below 0.06% (1σ). This corresponds to the quadratic sum of the internal error and external reproducibility determined from the daily analysis of standards. Internal standard was neon purified from air, and ^{20}Ne reproducibility over 1 year of analysis was <4%. Typical blanks for He and Ne were $<10^{-15}$ and $<10^{-16}$ mol, respectively, being at least two orders of magnitude lower than samples signals. Standards and samples were processed through the same purification line under identical analytical conditions.

**** Details regarding the purification and analytical procedure of Ne isotope analysis at CRPG (Nancy, France).**

An aliquot of the sample was first expanded in to the extraction line with Ar, Kr and Xe being adsorbed onto a charcoal finger at 77 K to separate He and Ne from the heavy noble gases. The separated He and Ne gas was then passed through an in-line Ti-sponge getter heated at 550°C (10 min). The gas was subsequently exposed to two Ti-sponge getters at 550°C and a second charcoal finger at 77 K (10 min). Neon was then trapped onto a He-cooled cryogenic trap at 34 K. After He was pumped from the line, Ne was released from the cryogenic trap by increasing the temperature to 90 K, and purified with a further two Ti-sponge getters, one at 550°C and the other at room temperature (~20°C) for 10 min. Adjacent to the mass spectrometer's ion source, a charcoal finger at 77 K and a Zr-Al getter at room temperature were used to minimize the contribution of doubly charged ^{40}Ar and CO_2 to the ^{20}Ne and ^{22}Ne signals, respectively. The three isotopes of neon were then analysed in peak-jumping mode on the axial (Ax) compact discrete dynode (CDD) detector. Neon isotope analyses consisted of four blocks of fifteen cycles, and manual peak centering was performed at the start of each measurement block. The high mass resolution of the Helix MC *Plus* (m/□m ≈ 1800) enables the discrimination of the ^{20}Ne peak from $^{40}Ar^{++}$ (Honda et al., 2015). The contribution from CO_2^{++} to the ^{22}Ne peak was monitored and corrected for each analysis. The correction for CO_2^{++} to ^{22}Ne was < 3%. Acceleration voltage was 9.9 KV, filament trap current was 280 μA and filament trap voltage was 50 V. Daily standards were analysed for subsequent spectrometer mass discrimination corrections and reproducibility determination. Multiple analyses of each samples was performed in order to increase measurement precision, with standard errors computed as standard deviation/√(n-1), where n is the number of duplicate measurements for a given sample.

***** Details regarding the purification and analytical procedure of Ar and Xe isotope analysis at CRPG (Nancy, France).**

A second aliquot of gas was then admitted to the line for Ar and Xe analysis. First Xenon was condensed on to a quartz tube at 77 K for 20 min in order to concentrate it and reduce the partial pressure of Ar. The trapped gas was then heated to room temperature and purified through an in-line Ti-sponge getter heated at 550°C to remove any active species (10 min), before re-condensing xenon on to a quartz tube held at 77 K for 20 min. The fraction of Ar remaining in the preparation line was then expanded to a series of Ti-sponge getters, three at 550°C and one at room temperature, respectively, for 20 minutes. Argon was finally expanded into the spectrometer (Helix MC Plus, Thermo Fisher@) and analysed in multi-collection mode on faraday (^{40}Ar) and compact dynode multiplier (^{36,38}Ar) collectors. For Ar, acceleration voltage was 9.9 KV, filament trap current was 230 µA and filament trap voltage was 20.45 V. After thorough pumping of the purification line, three dilutions from the glass tube (20 cm^3) held at 77 K to the whole line (1,500 cm^3) in static mode were made in order to decrease the partial pressure of Ar remaining in the cold finger. Xenon was then released at room temperature and purified following the same protocol as for Ar. Xenon was ultimately expanded into the spectrometer and analysed by peak jumping on the axial compact dynode multiplier (AxCDD). For Xe, acceleration voltage was 9.9 KV, filament trap current was 200 µA and filament trap voltage was 33.17 V. Daily standards were analysed for subsequent spectrometer mass discrimination corrections and reproducibility determination. In order to increase measurement precision, multiple analyses of each sample (minimum of four analyses per sample) was performed for Xe isotopes by splitting the purified gas into different aliquots in the line, with standard errors for each samples computed as standard deviation/$\sqrt{}$(n-1), where n is the number of duplicate measurements. Reproducibility (standard deviation / mean) for each isotopic ratio of Xe normalized to ^{130}Xe is given below from the analysis of 25 aliquots of standard:

Isotope	^{124}Xe	^{126}Xe	^{128}Xe	^{129}Xe	^{131}Xe	^{132}Xe	^{134}Xe	^{136}Xe
Reproducibility (%)	0.71	0.72	0.45	0.34	0.20	0.30	0.30	0.36

****** Linear least squares determination of initial, recycled atmospheric, Pu- and U-fissiogenic Xe components.**

We used a Monte Carlo linear least square code adapted from Parai and Mukhopadhyay (2015) to compute the best fit mixing of ^{132}Xe from initial mantle, modern atmosphere (recycled in to the mantle and acting as a contaminant during sampling), ^{238}U-fission Xe and ^{244}Pu-Xe. The initial Xe mantle composition is considered to be chondritic and not solar (Caracausi et al. 2016; Péron and Moreira 2018), and is taken here to be the average carbonaceous chondrite composition (AVCC). Although Xe isotope cannot distinguish the nature of their chondritic precursor in the mantle (Q, an ubiquitous noble gas component found in all classes of primitive meteorites, or AVCC), Kr isotopes in the mantle have been shown to be genetically linked with AVCC and not Q (Holland et al. 2009) and so a common origin for Kr and Xe in the mantle is assumed. Given that substantial full scale recycling of atmospheric Xe into the deep Earth would have become significant only when the atmosphere had reached its present-day isotopic composition (Parai and Mukhopadhyay 2018), the recycled atmosphere component is taken to have a modern-like isotopic composition. Also note that, since ^{128}Xe is the only isotope among $^{128\text{-}136}$Xe (except the normalizing isotope ^{130}Xe) that is not contributed by any radiogenic or fissiongenic production here, we also ran best fit mixing calculations excluding ^{128}Xe. If the ^{128}Xe/^{130}Xe are not affected by any mass dependent fractionation effect, simulations taking ^{128}Xe in to account or not should give similar outcomes.

***** Normalizing isotope: an issue with correlated errors?

Sample	I-^{129}Xe/Pu-^{136}Xe	Pu/(Pu+U)-^{136}Xe	%Mantle contribution	%Pu	%U
Eifel E2 (/132)	$13.8^{+25.4}_{-5.3}$	$0.21^{+0.13}_{-0.14}$	$5.2^{+1.1}_{-1.1}$	$0.4^{+0.3}_{-0.2}$	$1.1^{+0.1}_{-0.2}$
Eifel E2 (/130)	$583.5^{+14.5}_{-578.8}$	$0.01^{+0.56}_{-0.01}$	$5.2^{+6.2}_{-2.0}$	$0^{+1.3}_{-0}$	$1.2^{+0.1}_{-0.6}$

Here above are shown the outcomes of Monte Carlo linear least square simulations adapted from Parai and Mukhopadhyay (2015) for the Eifel 2 sample analysed as part of the study, with the rough data being processed through two different methods. For Eifel E2 (/132), rough data were normalised to ^{132}Xe, before applying spectrometer mass discrimination corrections and error propagation, and computing the mean isotopic composition of E2 aliquots (Table S5). For Eifel E2 (/130), rough data were initially normalised to ^{130}Xe, spectrometer mass discrimination corrections and error propagation were applied, and the mean isotopic composition was computed (Table S6). Then, these ^{130}Xe-normalised ratios were converted into ^{132}Xe -normalised ratios for Monte Carlo simulations. This second case is similar to what had to be done for Lignat and Popping rock samples (Table 1), for which ^{130}Xe-normalised ratios only are provided in the literature, and so post-processing normalization to ^{132}Xe has to be carried out to run Monte Carlo simulations. Outcomes for Eifel E2 (/132) and Eifel E2 (/130) are slightly different, indicating that a statistical bias might be introduced for Monte Carlo simulations using ^{132}Xe-normalised ratios transferred from ^{130}Xe-normalised ratios (Table 1). This statistical bias cannot be further constrained without accessing to ^{132}Xe-normalised raw isotopic ratios.

Supplementary Figures

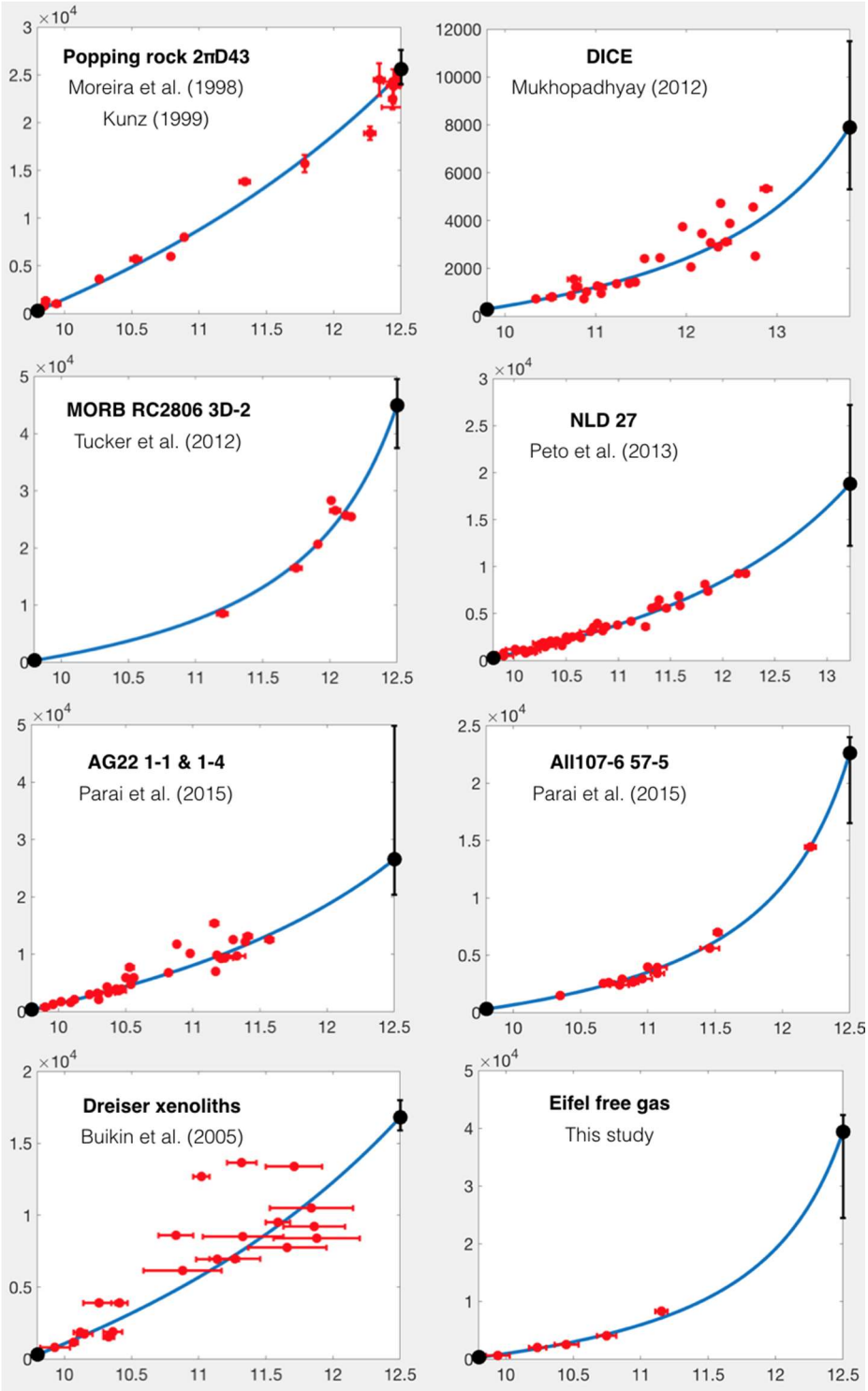

Fig. S1: Extrapolation of mantle source $^{40}Ar/^{36}Ar$ by total least-square hyperbolic fits in $^{20}Ne/^{22}Ne$-$^{40}Ar/^{36}Ar$ spaces. In every panel, the y-axis corresponds to $^{40}Ar/^{36}Ar$ values. Mantle $^{20}Ne/^{22}Ne$ are 12.5 for popping rock 2πD43, MORB RC2806 3D-2, AG22 1-1 & 1-4, All107-6 57-5, Dreiser xenoliths and Eifel free gas. Mantle $^{20}Ne/^{22}Ne$ are higher for OIB-like samples, with 13.22 and 13.8 for NDL 27 and DICE, respectively. Corresponding data are reported in Table S1.

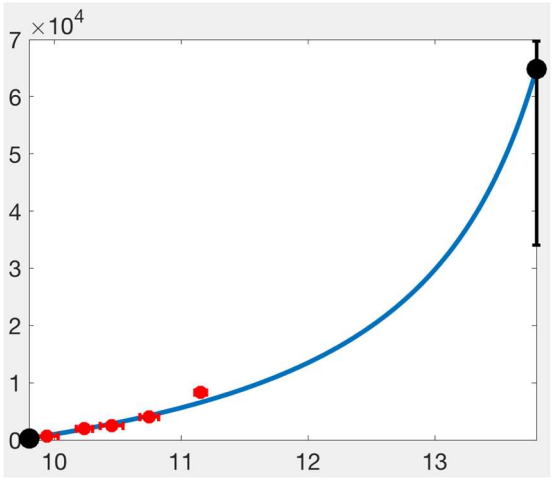

Fig. S2: Extrapolation of mantle source $^{40}Ar/^{36}Ar$ for sample E2 by total least-square hyperbolic fit to a $^{20}Ne/^{22}Ne$ of 13.8.

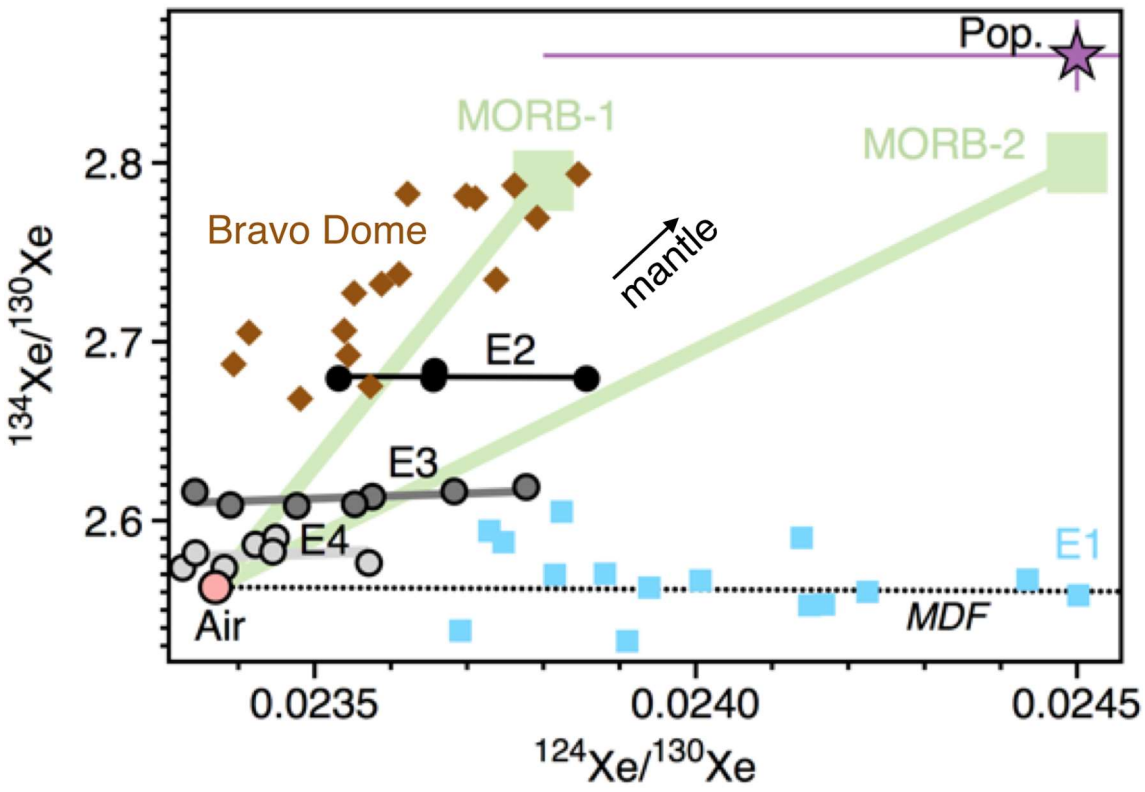

Fig. S3: $^{129}Xe/^{130}Xe$ vs. $^{136}Xe/^{130}Xe$ diagram showing air (pink), Eifel samples (E2-E4, this study; E1, Caracausi et al. 2016), well gases (Bravo Dome, Holland et al. 2009), popping rock 2πD43 (purple star, Péron and Moreira 2018). MORB-1 and MORB-2 are well gases and popping rocks, respectively, from compilation by Moreira et al. (2018). While E2-E4 samples show increasing contribution from mantle-derived gas, E1 data appear to plot along a mass dependent fractionation line.

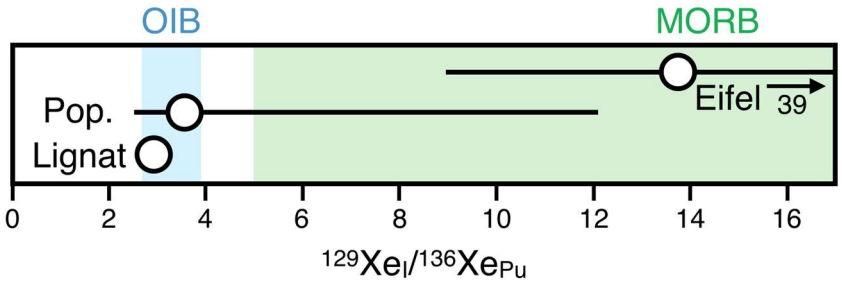

Fig. S4: $^{129}Xe_I/^{136}Xe_{Pu}$ of the mantle source of Eifel (E2, This study), popping rocks (Péron and Moreira, 2018) and Lignat (Moreira et al. 2018), calculated from Monte Carlo linear least square simulations adapted from Parai and Mukhopadhyay (2015). The ranges of values for OIB and MORB as compiled by Caracausi et al. 2016 are also given for comparison.

Supplementary Tables.

Sample	$^{20}Ne/^{22}Ne$ source	$^{40}Ar/^{36}Ar$ source	$^{40}Ar/^{36}Ar$ (This study)
Popping rock 2πD43 Moreira et al. (1998); Kunz (1999)	12.5	25,000	$25{,}600^{+2000}_{-1600}$
DICE Mukhopadhyay (2012)	13.8	10,745± 3,080	7900^{+3600}_{-2600}
MORB RC2806 3D-2 Tucker et al. (2012)	12.5	41,500 ± 9,000	$44{,}900^{+4600}_{-7400}$
NLD 27 Petö et al., 2013	13.22	16,763 ± 1,144	$18{,}800^{+8400}_{-6600}$
AG22 1-1 & 1-4 Parai and Mukhopadhyay (2015)	12.5	$49{,}300^{+6000}_{-4600}$	$26{,}500^{+23{,}300}_{-6200}$
All107-6 57-5 Parai and Mukhopadhyay (2015)	12.5	$23{,}700^{+3400}_{-2400}$	$22{,}600^{+1400}_{-6100}$
Dreiser xenoliths Buikin et al. (2005)	12.5	15,000 ± 1200	$16{,}800^{+1200}_{-900}$
Eifel free gas This study	12.5	-	$39{,}400^{+3000}_{-15200}$

Table S1: Comparison of extrapolated (this study) and published $^{40}Ar/^{36}Ar$ of mantle sources from literature datasets. Corresponding hyperbolic curves are reported in Fig. S1.

Sample	date	R/Ra	error	$^{3}He/^{20}Ne$
Victoriaquelle 1	27/10/15	4.21	0.0438	47.449
Victoriaquelle 2	27/10/15	4.15	0.0387	498.975
Victoriaquelle 3	27/10/15	4.17	0.0397	563.043
Victoriaquelle 4	27/10/15	4.17	0.0376	355.285
Schwefelquelle 1	27/10/15	4.10	0.0356	637.040
Schwefelquelle 2	27/10/15	4.16	0.0364	577.571
Sanwefelquelle 3	27/10/15	4.22	0.0398	353.853
Sanwefelquelle 4	27/10/15	4.13	0.0392	150.752
Schwellquelle 5	27/10/15	4.22	0.0399	126.360

Table S2: Helium isotopic composition and $^{3}He/^{20}Ne$ of the Eifel free magmatic gas measured at INGV (Palermo, Italy).

	$^{21}Ne/^{22}Ne$	±1σ	$^{20}Ne/^{22}Ne$	±1σ
E2: Schwefelquelle (05/18)	0.0464	0.0017	11.2074	0.1469
($5.6x10^{-14}$ mol ^{22}Ne)	0.0442	0.0016	11.0300	0.1160
	0.0455	0.0014	11.1398	0.1047
mean	**0.0454**	**0.0005**	**11.1539**	**0.0533**
E3: Victoriaquelle (05/18)	0.0391	0.0013	10.7094	0.1054
($3.4x10^{-14}$ mol ^{22}Ne)	0.0387	0.0017	10.5869	0.1165
	0.0390	0.0013	10.8250	0.1213
	0.0392	0.0010	10.8655	0.1073
mean	**0.0390**	**0.0001**	**10.7467**	**0.0724**
E4: Victoriaquelle (09/18)	0.0348	0.0012	10.2256	0.1129
($5.5x10^{-14}$ mol ^{22}Ne)	0.0349	0.0015	10.3309	0.1141
	0.0337	0.0014	10.1490	0.1201
mean	**0.0345**	**0.0005**	**10.2352**	**0.0646**
Schw-t	0.0303	0.0006	9.9408	0.1189
Vict-t	0.0363	0.0012	10.4505	0.1275

Table S3: Neon isotopic composition of the Eifel free magmatic gas. Errors for Giggenbach samples are computed as standard deviation/√(n-1), where n is the number of duplicate measurements.

	$^{38}Ar/^{36}Ar$	±1σ	$^{40}Ar/^{36}Ar$	±1σ
E2: Schwefelquelle (05/18) $2.3x10^{-12}$ mol ^{36}Ar	0.1895	0.0009	8287	140
E3: Victoriaquelle (05/18) $5.3x10^{-12}$ mol ^{36}Ar	0.1908	0.0012	4040	70
E4: Victoriaquelle (09/18) $1.5x10^{-11}$ mol ^{36}Ar	0.1876	0.0011	1974	45
Schw-t	0.1876	0.0014	663	14
Vict-t	0.1884	0.0015	2501	51

Table S4: Argon isotopic composition of the Eifel free magmatic gas.

	$^{124}Xe/^{132}Xe$	$^{126}Xe/^{132}Xe$	$^{128}Xe/^{132}Xe$	$^{129}Xe/^{132}Xe$	$^{130}Xe/^{132}Xe$	$^{131}Xe/^{132}Xe$	$^{134}Xe/^{132}Xe$	$^{136}Xe/^{132}Xe$
Schwefelquelle 05/18	0.0036 ± 0.0001	0.0033 ± 0.0001	0.0710 ± 0.0010	1.0395 ± 0.0093	0.1493 ± 0.0015	0.7820 ± 0.0070	0.3999 ± 0.0033	0.3467 ± 0.0033
Sample E2	0.0035 ± 0.0001	0.0033 ± 0.0001	0.0708 ± 0.0007	1.0396 ± 0.0056	0.1499 ± 0.0008	0.7796 ± 0.0065	0.4023 ± 0.0030	0.3478 ± 0.0025
	0.0035 ± 0.0001	0.0033 ± 0.0001	0.0709 ± 0.0009	1.0417 ± 0.0066	0.1500 ± 0.0010	0.7811 ± 0.0053	0.4020 ± 0.0024	0.3478 ± 0.0019
	0.0035 ± 0.0001	0.0033 ± 0.0001	0.0711 ± 0.0008	1.0393 ± 0.0080	0.1500 ± 0.0009	0.7819 ± 0.0052	0.4019 ± 0.0021	0.3477 ± 0.0026
mean	**0.0035 ± 7x10^{-6}**	**0.0033 ± 1x10^{-5}**	**0.0709 ± 0.0001**	**1.0400 ± 0.0006**	**0.1498 ± 0.0002**	**0.7812 ± 0.0006**	**0.4015 ± 0.0006**	**0.3475 ± 0.0003**
Victoriaquelle 05/18	0.0035 ± 0.0001	0.0033 ± 0.0001	0.0711 ± 0.0007	1.0026 ± 0.0049	0.1505 ± 0.0011	0.7809 ± 0.0042	0.3926 ± 0.0023	0.3350 ± 0.0021
Sample E3	0.0036 ± 0.0001	0.0033 ± 0.0001	0.0717 ± 0.0007	1.0091 ± 0.0068	0.1500 ± 0.0017	0.7862 ± 0.0034	0.3928 ± 0.0026	0.3373 ± 0.0032
	0.0036 ± 0.0001	0.0033 ± 0.0001	0.0717 ± 0.0006	1.0120 ± 0.0054	0.1511 ± 0.0015	0.7876 ± 0.0046	0.3948 ± 0.0035	0.3383 ± 0.0022
	0.0036 ± 0.0001	0.0033 ± 0.0001	0.0716 ± 0.0007	1.0071 ± 0.0053	0.1504 ± 0.0012	0.7864 ± 0.0032	0.3935 ± 0.0023	0.3373 ± 0.0019
	0.0035 ± 0.0001	0.0033 ± 0.0001	0.0715 ± 0.0007	1.0093 ± 0.0052	0.1511 ± 0.0011	0.7847 ± 0.0054	0.3941 ± 0.0027	0.3372 ± 0.0024
	0.0035 ± 0.0001	0.0033 ± 0.0001	0.0715 ± 0.0006	1.0071 ± 0.0042	0.1507 ± 0.0011	0.7840 ± 0.0039	0.3942 ± 0.0021	0.3360 ± 0.0020
	0.0036 ± 0.0001	0.0033 ± 0.0001	0.0715 ± 0.0006	1.0115 ± 0.0039	0.1513 ± 0.0009	0.7869 ± 0.0035	0.3948 ± 0.0024	0.3371 ± 0.0017
mean	**0.0035 ± 9x10^{-6}**	**0.0033 ± 5x10^{-6}**	**0.0715 ± 0.0001**	**1.0084 ± 0.0013**	**0.1507 ± 0.0002**	**0.7852 ± 0.0009**	**0.3938 ± 0.0004**	**0.3369 ± 0.0004**
Victoriaquelle 09/18	0.0035 ± 0.0001	0.0033 ± 0.0001	0.0715 ± 0.0006	0.9935 ± 0.0056	0.1507 ± 0.0009	0.7848 ± 0.0039	0.3899 ± 0.0022	0.3318 ± 0.0018
Sample E4	0.0035 ± 0.0001	0.0033 ± 0.0001	0.0716 ± 0.0009	0.9941 ± 0.0059	0.1507 ± 0.0013	0.7860 ± 0.0057	0.3905 ± 0.0037	0.3323 ± 0.0028
	0.0036 ± 0.0001	0.0033 ± 0.0001	0.0718 ± 0.0007	0.9955 ± 0.0045	0.1516 ± 0.0013	0.7893 ± 0.0041	0.3907 ± 0.0023	0.3334 ± 0.0022
	0.0035 ± 0.0001	0.0034 ± 0.0001	0.0715 ± 0.0006	0.9956 ± 0.0038	0.1517 ± 0.0011	0.7882 ± 0.0040	0.3905 ± 0.0033	0.3334 ± 0.0020
	0.0035 ± 0.0001	0.0033 ± 0.0001	0.0717 ± 0.0006	0.9932 ± 0.0051	0.1517 ± 0.0012	0.7903 ± 0.0041	0.3903 ± 0.0022	0.3328 ± 0.0023
	0.0035 ± 0.0001	0.0033 ± 0.0001	0.0714 ± 0.0008	0.9958 ± 0.0065	0.1517 ± 0.0016	0.7888 ± 0.0061	0.3916 ± 0.0027	0.3340 ± 0.0035
	0.0035 ± 0.0001	0.0033 ± 0.0001	0.0715 ± 0.0005	0.9920 ± 0.0054	0.1514 ± 0.0010	0.7859 ± 0.0043	0.3909 ± 0.0018	0.3320 ± 0.0016
mean	**0.0035 ± 6x10^{-6}**	**0.0033 ± 9x10^{-6}**	**0.0716 ± 5x10^{-5}**	**0.9943 ± 0.0006**	**0.1514 ± 0.0002**	**0.7876 ± 0.0008**	**0.3906 ± 0.0002**	**0.3328 ± 0.0003**
Air	**0.0035**	**0.0033**	**0.0714**	**0.9832**	**0.1514**	**0.7890**	**0.3879**	**0.3294**

Table S5: Xenon isotopic composition of the Eifel free magmatic gas, normalised to ^{130}Xe. Uncertainties associated with mean compositions are computed as standard deviation/√(n-1), where n is the number of duplicate measurements. Uncertainties are given at the 1σ level. Air composition (Ozima and Podosek, 2002) is given for comparison.

	$^{124}Xe/^{130}Xe$	$^{126}Xe/^{130}Xe$	$^{128}Xe/^{130}Xe$	$^{129}Xe/^{130}Xe$	$^{131}Xe/^{130}Xe$	$^{132}Xe/^{130}Xe$	$^{134}Xe/^{130}Xe$	$^{136}Xe/^{130}Xe$
Schwefelquelle 05/18	0.0239 ± 0.0010	0.0222 ± 0.0009	0.4755 ± 0.0075	6.9637 ± 0.0799	5.2391 ± 0.0587	6.6994 ± 0.0676	2.6793 ± 0.0300	2.3225 ± 0.0274
Sample E2	0.0237 ± 0.0007	0.0223 ± 0.0008	0.4722 ± 0.0052	6.9352 ± 0.0453	5.2011 ± 0.0468	6.6712 ± 0.0370	2.6836 ± 0.0215	2.3201 ± 0.0188
($9.3x10^{-16}$ mol ^{130}Xe)	0.0235 ± 0.0007	0.0221 ± 0.0005	0.4724 ± 0.0061	6.9429 ± 0.0655	5.2063 ± 0.0454	6.6651 ± 0.0462	2.6794 ± 0.0222	2.3183 ± 0.0212
	0.0237 ± 0.0006	0.0219 ± 0.0009	0.4742 ± 0.0059	6.9281 ± 0.0659	5.2124 ± 0.0445	6.6663 ± 0.0420	2.6791 ± 0.0181	2.3178 ± 0.0226
mean	**0.0237 ± 0.0001**	**0.0221 ± 0.0001**	**0.4736 ± 0.0009**	**6.9425 ± 0.0089**	**5.2147 ± 0.0098**	**6.6755 ± 0.0093**	**2.6804 ± 0.0013**	**2.3197 ± 0.0012**
Victoriaquelle 05/18	0.0234 ± 0.0006	0.0219 ± 0.0005	0.4726 ± 0.0041	6.6622 ± 0.0381	5.1888 ± 0.0397	6.6449 ± 0.0477	2.6087 ± 0.0211	2.2263 ± 0.0170
Sample E3	0.0238 ± 0.0007	0.0222 ± 0.0007	0.4776 ± 0.0060	6.7268 ± 0.0759	5.2407 ± 0.0527	6.6660 ± 0.0766	2.6187 ± 0.0346	2.2485 ± 0.0255
($8.8x10^{-16}$ mol ^{130}Xe)	0.0236 ± 0.0007	0.0219 ± 0.0004	0.4746 ± 0.0053	6.6987 ± 0.0569	5.2136 ± 0.0480	6.6198 ± 0.0637	2.6133 ± 0.0265	2.2395 ± 0.0184
	0.0237 ± 0.0005	0.0220 ± 0.0004	0.4759 ± 0.0064	6.6958 ± 0.0609	5.2286 ± 0.0462	6.6484 ± 0.0530	2.6163 ± 0.0246	2.2422 ± 0.0222
	0.0235 ± 0.0006	0.0219 ± 0.0004	0.4730 ± 0.0056	6.6803 ± 0.0439	5.1938 ± 0.0356	6.6187 ± 0.0498	2.6083 ± 0.0206	2.2319 ± 0.0184
	0.0233 ± 0.0005	0.0219 ± 0.0006	0.4745 ± 0.0051	6.6832 ± 0.0479	5.2026 ± 0.0408	6.6360 ± 0.0502	2.6162 ± 0.0204	2.2299 ± 0.0158
	0.0236 ± 0.0005	0.0219 ± 0.0003	0.4725 ± 0.0051	6.6851 ± 0.0431	5.2006 ± 0.0426	6.6089 ± 0.0394	2.6092 ± 0.0229	2.2285 ± 0.0188
mean	**0.0235 ± 0.0001**	**0.0220 ± $5x10^{-5}$**	**0.4744 ± 0.0008**	**6.6903 ± 0.0082**	**5.2098 ± 0.0077**	**6.6347 ± 0.0082**	**2.6130 ± 0.0017**	**2.2353 ± 0.0034**
Victoriaquelle 09/18	0.0234 ± 0.0006	0.0219 ± 0.0003	0.4746 ± 0.0048	6.5906 ± 0.0453	5.2062 ± 0.0320	6.6338 ± 0.0403	2.5865 ± 0.0200	2.2011 ± 0.0197
Sample E4	0.0234 ± 0.0006	0.0219 ± 0.0009	0.4747 ± 0.0072	6.5949 ± 0.0538	5.2144 ± 0.0460	6.6343 ± 0.0586	2.5905 ± 0.0236	2.2048 ± 0.0207
($2.4x10^{-15}$ mol ^{130}Xe)	0.0236 ± 0.0007	0.0219 ± 0.0006	0.4734 ± 0.0045	6.5651 ± 0.0537	5.2048 ± 0.0405	6.5946 ± 0.0574	2.5763 ± 0.0245	2.1983 ± 0.0225
	0.0234 ± 0.0004	0.0221 ± 0.0006	0.4710 ± 0.0035	6.5620 ± 0.0431	5.1952 ± 0.0329	6.5911 ± 0.0463	2.5736 ± 0.0219	2.1974 ± 0.0164
	0.0233 ± 0.0006	0.0218 ± 0.0005	0.4725 ± 0.0039	6.5485 ± 0.0451	5.2108 ± 0.0317	6.5936 ± 0.0501	2.5736 ± 0.0193	2.1946 ± 0.0184
	0.0233 ± 0.0010	0.0216 ± 0.0009	0.4710 ± 0.0049	6.5658 ± 0.0671	5.2005 ± 0.0528	6.5933 ± 0.0716	2.5818 ± 0.0248	2.2019 ± 0.0259
	0.0234 ± 0.0005	0.0219 ± 0.0005	0.4726 ± 0.0037	6.5544 ± 0.0457	5.1927 ± 0.0379	6.6070 ± 0.0416	2.5826 ± 0.0174	2.1938 ± 0.0162
mean	**0.0234 ± $4x10^{-5}$**	**0.0219 ± 0.0001**	**0.4728 ± 0.0006**	**6.5688 ± 0.0072**	**5.2035 ± 0.0032**	**6.6068 ± 0.0079**	**2.5807 ± 0.0027**	**2.1988 ± 0.0016**
Air	**0.0234**	**0.0218**	**0.4715**	**6.4958**	**5.2127**	**6.6068**	**2.5628**	**2.1763**

Table S6: Xenon isotopic composition of the Eifel free magmatic gas, normalised to ^{130}Xe. Uncertainties associated with mean compositions are computed as standard deviation/√(n-1), where n is the number of duplicate measurements. Uncertainties are given at the 1σ level. Air composition (Ozima and Podosek, 2002) is given for comparison.

Supplementary Information references

Buikin, A., Trieloff, M., Hopp, J., Althaus, T., Korochantseva, E., Schwarz, W. H., & Altherr, R. (2005). Noble gas isotopes suggest deep mantle plume source of late Cenozoic mafic alkaline volcanism in Europe. *Earth and Planetary Science Letters*, *230*(1-2), 143-162.

Caracausi, A., Avice, G., Burnard, P. G., Füri, E., & Marty, B. (2016). Chondritic xenon in the Earth's mantle. *Nature*, *533*(7601), 82.

Holland, G., Cassidy, M., & Ballentine, C. J. (2009). Meteorite Kr in Earth's mantle suggests a late accretionary source for the atmosphere. *Science*, *326*(5959), 1522-1525.

Kunz, J., Staudacher, T., & Allegre, C. J. (1998). Plutonium-fission xenon found in Earth's mantle. *Science*, *280*(5365), 877-880.

Moreira, M., Kunz, J., & Allegre, C. (1998). Rare gas systematics in popping rock: isotopic and elemental compositions in the upper mantle. *Science*, *279*(5354), 1178-1181.

Moreira, M., Rouchon, V., Muller, E., & Noirez, S. (2018). The xenon isotopic signature of the mantle beneath Massif Central. *GPL*, *6*, 28-32.

Mukhopadhyay, S. (2012). Early differentiation and volatile accretion recorded in deep-mantle neon and xenon. *Nature*, *486*(7401), 101.

Parai, R., & Mukhopadhyay, S. (2015). The evolution of MORB and plume mantle volatile budgets: constraints from fission Xe isotopes in Southwest Indian Ridge basalts. *Geochemistry, Geophysics, Geosystems*, *16*(3), 719-735.

Parai, R., & Mukhopadhyay, S. (2018). Xenon isotopic constraints on the history of volatile recycling into the mantle. *Nature*, *560*(7717), 223.

Péron, S., Moreira, M. (2018) Onset of volatile recycling into the mantle determined by xenon anomalies. *Geochem. Persp. Let.* 9, 21–25.

Pető, M. K., Mukhopadhyay, S., & Kelley, K. A. (2013). Heterogeneities from the first 100 million years recorded in deep mantle noble gases from the Northern Lau Back-arc Basin. *Earth and Planetary Science Letters*, *369*, 13-23.

Honda, M., Zhang, X., Phillips, D., Hamilton, D., Deerberg, M., & Schwieters, J. B. (2015). Redetermination of the 21Ne relative abundance of the atmosphere, using a high resolution, multi-collector noble gas mass spectrometer (HELIX-MC Plus). *International Journal of Mass Spectrometry*, *387*, 1-7.

Rizzo, A. L., Pelorosso, B., Coltorti, M., Ntaflos, T., Bonadiman, C., Matusiak-Małek, M., ... & Bergonzoni, G. (2018). Geochemistry of noble gases and CO2 in fluid inclusions from lithospheric mantle beneath Wilcza Góra (Lower Silesia, southwest Poland). *Frontiers in Earth Science*.

252 Sano, Y., & Wakita, H. (1985). Geographical distribution of 3He/4He ratios in Japan:
253 Implications for arc tectonics and incipient magmatism. *Journal of Geophysical Research:*
254 *Solid Earth*, *90*(B10), 8729-8741.
255 Tucker, J. M., Mukhopadhyay, S., & Schilling, J. G. (2012). The heavy noble gas
256 composition of the depleted MORB mantle (DMM) and its implications for the preservation of
257 heterogeneities in the mantle. *Earth and Planetary Science Letters*, *355*, 244-254.

2) *Noble Gas and Carbon Isotope Systematics at the Seemingly Inactive Ciomadul Volcano (Eastern-Central Europe, Romania): Evidence for Volcanic Degassing*

Les émissions de gaz sont souvent associées à des zones volcaniques actives ou en sommeil et à des régions affectées par la tectonique extensive (par exemple, O'Nions et Oxburgh, 1988; Oppenheimer et al., 2014). La surveillance des fluides (compositions chimiques et isotopiques et propriétés physiques) dans les régions volcaniques fournit des informations importantes sur les processus intervenant en profondeur (par exemple, Agusto et al., 2013; Barry et al., 2013, 2014; Caliro et al., 2015; Christopher et al., 2010; Edmonds, 2008; Fischer, 2008; Mazot et al., 2011; Roulleau et al., 2016; Ruzié et al., 2012; Tassi et al., 2010, 2011, 2016, Wei et al. ., 2016). La composition chimique et isotopique des fluides émis dans les volcans actifs est principalement contrôlée par des processus magmatiques, tels que l'injection de nouveau magma dans le système de plomberie ou le dégazage de magma mafique profond dans la croûte inférieure, ou une interaction avec les systèmes hydrothermaux volcaniques (par exemple, Caracausi et al., 2003, 2013; Christopher et al., 2010; Edmonds, 2008; Paonita et al., 2012, 2016; Sano et al., 2015). D'autre part, le changement de composition des fluides peut également être corrélé avec la sismicité à l'échelle régionale (par exemple, Bräuer et al., 2008, 2018; Cardellini et al., 2017; Chiodini et al., 2004; Melián et al., 2012).

La compréhension des facteurs de contrôle des émissions de gaz dans les zones volcaniques actives et dormantes a beaucoup progressé au cours des deux dernières décennies (Aiuppa et al., 2007; Edmonds, 2008; Lee et al., 2016; Moussallam et al., 2018; Oppenheimer et al., 2014); cependant, beaucoup moins d'attention a été accordée aux zones volcaniques apparemment inactives (Roulleau et al., 2015). Ce sont des volcans dont l'éruption s'est déroulée il y a au moins 10 ka et qui, à la surface, ne montrent aucun signe de réveil. Le complexe volcanique de Tatun à Taiwan est un exemple d'un tel système volcanique. Bien que la dernière éruption ait eu lieu il y a 20 ka, les données géophysiques indiquent un stockage magmatique toujours actif. La composition des gaz émis est conforme à cette interprétation, car ils contiennent des composants magmatiques importants (Roulleau et al., 2015). L'importance et le danger potentiel de tels volcans sont illustrés par le cas du volcan Ontake au Japon. Avant l'événement éruptif phréatique de 1979, il n'y avait aucune trace prouvée d'éruptions historiques, voire même holocènes, et par conséquent, il n'y avait aucune étude détaillée ni surveillance sur ce volcan. En 2014, une autre éruption phréatique s'est produite, causant de nombreux décès (Kato et al., 2015) et soulignant la nécessité de mieux comprendre ces volcans longtemps dormants. Sano et al., 2015 ont démontré qu'une surveillance régulière des gaz volcaniques est fondamentale pour comprendre le comportement de ces volcans apparemment inactifs. À cet égard, la détection d'une chambre magmatique contenant une fraction de liquide magmatique pourrait constituer un potentiel de réactivation, même après plusieurs dizaines de milliers d'années de dormance. L'émission de gaz à signatures isotopiques dans la gamme des valeurs magmatiques peut constituer une preuve d'intrusion de magma en profondeur (Bräuer et al., 2008, 2018; Caracausi et al., 2013, 2015; Carapezza et al., 2003, 2012; Carapezza & al. Tarchini, 2007; Farrar et al., 1995; Fischer et al., 2014; Pizzino et al., 2002; Rouwet et al., 2014, 2017; Sano et al., 2015; Sorey et al., 1998), en plus de la reconnaissance des anomalies géophysiques reflétant les poches de liquide en profondeur (Comeau et al., 2015, 2016; Harangi, Novák, et al., 2015).

Ciomadul est le plus jeune volcan de la région des Carpates-Pannoniennes, Europe centrale-orientale, où la dernière éruption a eu lieu il y a 30 ka (Harangi et al., 2010; Harangi, Lukács et al., 2015; Molnár et al., 2019). Ainsi, il est généralement considéré comme un volcan inactif. En dépit de sa longue dormance, des preuves combinées de données pétrologiques et magnétotelluriques (Harangi, Novák et al., 2015; Kiss et al., 2014), ainsi

que de la tomographie sismique (Popa et al., 2012), suggèrent la présence de liquide magmatique sous le volcan.
Cela correspond à un flux thermique élevé local (85–120 mW/m^2) par rapport à la chaîne des Carpates où cette valeur diminue à 40–60 mW/m^2 (Demetrescu et Andreescu, 1994; Horváth et al., 2006), un flux de dioxyde de carbone de 8,7 × 103 t/y (Kis et al., 2017), la présence d'eaux minérales et thermales jusqu'à 78°C (Jánosi, 1980; Rădulescu et al., 1981) et une région géodynamiquement active (Ismail Zadeh et al., 2012; Wenzel et al., 1999). La chronologie des éruptions du champ du dôme de lave de Ciomadul (Molnár et al., 2018) est caractérisée par des périodes de repos prolongées entre les phases actives, dépassant souvent les 100 ka.
Ciomadul présente un certain nombre de sites où une quantité importante de CO_2 est émise (Kis et al., 2017). Althaus et al. (2000), Vaselli et al. (2002), Frunzeti (2013) et Sarbu et al. (2018) ont étudié la composition des gaz collectés à plusieurs endroits et ont conclu qu'ils pourraient indiquer un corps magmatique profond situé sous le volcan. Nous présentons ici une systématique complète de la signature isotopique de l'hélium (ci-après $^3He/^4He$) et de l'isotope carbone (ci-après $\delta^{13}C_{CO2}$) du dégazage volatile de Ciomadul. Elle est basée sur un échantillonnage détaillé de tous les principaux sites connus des émissions de gaz afin de contraindre l'origine des fluides et caractériser la nature d'un volcan apparemment inactif. Dans le cadre de ce projet, 31 émissions de gaz ont été étudiées sur le volcan Ciomadul, un volcan PAMS longtemps dormant en Europe centrale et orientale, afin de déterminer l'origine des éléments volatils émis et les processus susceptibles de modifier leur chimie au cours du transfert réactif de ces fluides vers la surface. Les compositions isotopiques de carbone et d'hélium fournissent la preuve d'un composant magmatique important. Notre étude montre une composante magmatique claire dans les fluides émis et les valeurs les plus élevées correspondent à la zone caractérisée par le flux de CO_2 le plus élevé émis par le sol; les flux élevés peuvent donc être associés à la plus forte contribution de éléments volatils dérivés d'un corps magma.
Les émissions de CO_2 relativement importantes et la composante magmatique importante des gaz sont compatibles avec les modèles géophysiques et pétrologiques (Harangi, Lukács et al., 2015; Harangi, Novák et al., 2015; Popa et al., 2012), pour qui une intrusion magmatique dégazante pourrait encore exister sous Ciomadul. Un corps de magma siliceu en cours de cristallisation depuis longtemps doit être développé dans la croûte peu profonde, tandis qu'une zone d'accumulation de magma mafique est déduite au niveau de la croûte inférieure. Les gaz magmatiques pourraient provenir d'un magma mafique profond et /ou des zones d'accumulation volatils développées dans le corps de bouillie de cristal felsique crustal peu profond. La pétrologie et la géochimie du magma dacitique en éruption impliquent que la contamination de la croûte supérieure ne joue aucun rôle ou qu'elle est subordonnée et que les magmas primaires auraient pu provenir d'une source du manteau contaminée par des fluides liés à la subduction, compatibles avec la composition en isotopes He et C des gaz émis au Volcan Ciomadul.
Ainsi, une source de magma avec une valeur relativement faible en isotope de He (3.10 Ra), similaire à celle proposée pour les systèmes volcaniques du centre de l'Italie, semble être viable sous Ciomadul. Ceci diffère de la valeur de SCLM détectée sur le champ volcanique de Persani (Althaust et al., 1998; cette étude) à proximité ainsi que dans le bassin de Pannonian (Bräuer et al., 2016; Cornides, 1993; Palcsu et al., 2014) et nécessite un manteau lithosphérique modifié, spatialement variable même à petite échelle. La composition isotopique (He et CO_2) des éléments volatils émis implique une interaction des gaz crustaux à des degrés divers, bien que certains d'entre eux puissent atteindre la surface sans modification majeure

Geochemistry, Geophysics, Geosystems

RESEARCH ARTICLE
10.1029/2018GC008153

Special Section:
Carbon degassing through volcanoes and active tectonic regions

Noble Gas and Carbon Isotope Systematics at the Seemingly Inactive Ciomadul Volcano (Eastern-Central Europe, Romania): Evidence for Volcanic Degassing

B. M. Kis[1,2,3], A. Caracausi[4], L. Palcsu[3], C. Baciu[5], A. Ionescu[1,5,6], I. Futó[3], A. Sciarra[7], and Sz. Harangi[1,8]

[1]MTA-ELTE Volcanology Research Group, Budapest, Hungary, [2]Faculty of Biology and Geology, Babes-Bolyai University, Cluj-Napoca, Romania, [3]Isotope Climatology and Environmental Research Centre, Institute for Nuclear Research, Hungarian Academy of Sciences, Debrecen, Hungary, [4]Istituto Nazionale di Geofisica e Vulcanologia, Palermo, Italy, [5]Faculty of Environmental Science and Engineering, Babes-Bolyai University, Cluj-Napoca, Romania, [6]Department of Physics and Geology, University of Perugia, Perugia, Italy, [7]Istituto Nazionale di Geofisica e Vulcanologia, Rome, Italy, [8]Department of Petrology and Geochemistry, Eötvös Loránd University, Budapest, Hungary

Key Points:
- CO_2 emissions at Ciomadul, Eastern-Central Europe, suggest a still-active plumbing system beneath the volcano in spite of long dormancy
- The CO_2 and He isotope compositions provide evidence for significant contribution of magma-derived volatiles, up to 80%
- Isotopic signatures of gases indicate that primary magmas could have derived from a mantle source modified by subduction-related fluids

Correspondence to:
B. M. Kis,
kis.boglarka@ubbcluj.ro

Citation:
Kis, B. M., Caracausi, A., Palcsu, L., Baciu, C., Ionescu, A., Futó, I., et al. (2019). Noble gas and carbon isotope systematics at the seemingly inactive Ciomadul volcano (Eastern-Central Europe, Romania): Evidence for volcanic degassing. *Geochemistry, Geophysics, Geosystems*, *20*. https://doi.org/10.1029/2018GC008153

Received 17 DEC 2018
Accepted 5 MAY 2019
Accepted article online 17 MAY 2019

Abstract Ciomadul is the youngest volcano in the Carpathian-Pannonian Region, Eastern-Central Europe, which last erupted 30 ka. This volcano is considered to be inactive, however, combined evidence from petrologic and magnetotelluric data, as well as seismic tomography studies, suggests the existence of a subvolcanic crystal mush with variable melt content. The volcanic area is characterized by high CO_2 gas output rate, with a minimum of 8.7×10^3 t/year. We investigated 31 gas emissions at Ciomadul to constrain the origin of the volatiles. The $\delta^{13}C$–CO_2 and $^3He/^4He$ compositions suggest the outgassing of a significant component of mantle-derived fluids. The He isotope signature in the outgassing fluids (up to 3.10 R_a) is lower than the values in the peridotite xenoliths of the nearby alkaline basalt volcanic field (R/R_a 5.95 $R_a \pm$ 0.01), which are representative of a continental lithospheric mantle and significantly lower than MORB values. Considering the chemical characteristics of the Ciomadul dacite, including trace element and Sr–Nd and O isotope compositions, an upper crustal contamination is less probable, whereas the primary magmas could have been derived from an enriched mantle source. The low He isotopic ratios could indicate a strongly metasomatized mantle lithosphere. This could be due to infiltration of subduction-related fluids and postmetasomatic ingrowth of radiogenic He. The metasomatic fluids are inferred to have contained subducted carbonate material resulting in a heavier carbon isotope composition ($\delta^{13}C$ is in the range of −1.4‰ to −4.6‰) and an increase of $CO_2/^3He$ ratio. Our study shows the magmatic contribution to the emitted gases.

Plain Language Summary Determining the fluxes and composition of gases in active and dormant volcanoes could help to constrain their origin. Ciomadul is the youngest volcano of the Carpathian-Pannonian Region, Eastern-Central Europe, where the last eruption occurred 30 ka. Its eruption chronology is punctuated by long quiescence periods (even >100 kyr) separating the active phases; therefore, the long dormancy since the last eruption (30 ka) does not unambiguously indicate inactivity. Knowing if melt-bearing magma resides in the crust is fundamental to evaluate the nature of the volcano. Isotopic compositions of helium ($^3He/^4He$) and carbon ($\delta^{13}C_{CO2}$) are important tools for the study of the origin of the gases. We show that the isotope variation of the emitted gases suggests a metasomatized lithospheric mantle origin for the primary magmas. This is consistent with a degassing deep magma body existing beneath Ciomadul, and this long-dormant volcano cannot be considered as extinct.

1. Introduction

Gas emissions are often associated with active or dormant volcanic areas and regions affected by extensional tectonics (e.g., O'Nions & Oxburgh, 1988; Oppenheimer et al., 2014). Monitoring of fluids (chemical and isotopic compositions and physical properties) in volcanic regions provides important information concerning the processes occurring at depth (e.g., Agusto et al., 2013; Barry et al., 2013, 2014; Caliro et al., 2015; Christopher et al., 2010; Edmonds, 2008; Fischer, 2008; Mazot et al., 2011; Roulleau et al., 2016; Ruzié et al., 2012; Tassi et al., 2010, 2011, 2016; Wei et al., 2016). The chemical and isotopic composition of the

©2019. American Geophysical Union. All Rights Reserved.

emitted fluids in active volcanoes is primarily controlled by magmatic processes, such as the injection of new magma into the plumbing system or degassing of deep mafic magma in the lower crust, or interaction with the volcanic hydrothermal systems, among others (e.g., Caracausi et al., 2003, 2013; Christopher et al., 2010; Edmonds, 2008; Paonita et al., 2012, 2016; Sano et al., 2015). Furthermore, compositional change of the fluids may also correlate with the seismicity at regional scale (e.g., Bräuer et al., 2008, 2018; Cardellini et al., 2017; Chiodini et al., 2004; Melián et al., 2012).

There has been major progress in understanding the factors controlling gas emissions in active and dormant volcanic areas during the last two decades (Aiuppa et al., 2007; Edmonds, 2008; Lee et al., 2016; Moussallam et al., 2018; Oppenheimer et al., 2014); however, much less attention has been given to seemingly inactive volcanic areas (Roulleau et al., 2015). These are volcanoes that last erupted more than 10 ka, and at the surface, there are no signs of reawakening. The Tatun volcanic complex in Taiwan is an example of such a volcanic system. Although the last eruption occurred 20 ka, geophysical data indicate a still-active magma storage. The composition of emitted gases is consistent with this interpretation, as they contain significant magmatic components (Roulleau et al., 2015). The importance and the potential hazard of such volcanoes are shown by the case of the Ontake volcano in Japan. There were no proven records of historical and even Holocene eruptions before the phreatic eruptive event in 1979, and therefore, there were no detailed studies and monitoring on this volcano. In 2014, another phreatic eruption occurred, causing serious fatalities (Kato et al., 2015) and pointed to the requirement to better understand such long-dormant volcanoes. Sano et al., 2015 demonstrated that regular monitoring of volcanic gases is fundamental to understand the behavior of these apparently inactive volcanoes. In this regard, detection of a magmatic chamber containing some melt fraction could mean the potential for reactivation even after several tens of kiloyears dormancy. Emission of gases with isotopic signatures in the range of magmatic values can be evidence of magma intrusions at depth (Bräuer et al., 2008, 2018; Caracausi et al., 2013, 2015; Carapezza et al., 2003, 2012; Carapezza & Tarchini, 2007; Farrar et al., 1995; Fischer et al., 2014; Pizzino et al., 2002; Rouwet et al., 2014, 2017; Sano et al., 2015; Sorey et al., 1998), in addition to recognition of geophysical anomalies reflecting melt pockets at depth (Comeau et al., 2015, 2016; Harangi, Novák, et al., 2015).

Ciomadul is the youngest volcano within the Carpathian-Pannonian Region, Eastern-Central Europe, where the last eruption occurred 30 ka (Harangi et al., 2010; Harangi, Lukács, et al., 2015; Molnár et al., 2019). Thus, it is usually considered as an inactive volcano. In spite of its long dormancy, combined evidence from petrologic and magnetotelluric data (Harangi, Novák, et al., 2015; Kiss et al., 2014), as well as seismic tomography (Popa et al., 2012), suggest the presence of a melt-bearing crystal mush beneath the volcano. This is consistent with the local high heat flow (85–120 mW/m^2) compared to the Carpathian Range where this value decreases to 40–60 mW/m^2 (Demetrescu & Andreescu, 1994; Horváth et al., 2006), the high flux of carbon dioxide of 8.7×10^3 t/year (Kis et al., 2017) the presence of mineral and thermal waters up to 78 °C (Jánosi, 1980; Rădulescu et al., 1981) and the geodynamically active region (Ismail-Zadeh et al., 2012; Wenzel et al., 1999). The eruption chronology of the Ciomadul lava dome field (Molnár et al., 2018) is characterized by prolonged quiescence periods between the active phases, often exceeding 100 kyr.

There are a number of sites at Ciomadul, where significant amount of CO_2 gases are emitted (Kis et al., 2017). Althaus et al. (2000), Vaselli et al. (2002), Frunzeti (2013), and Sarbu et al. (2018) studied the composition of gases collected from a few locations and concluded that they could indicate a deep-seated magma body below the volcano. Here we present a comprehensive helium isotope signature (hereafter $^3He/^4He$) and carbon isotope (hereafter $\delta^{13}C_{CO2}$) systematics of the volatile degassing from Ciomadul based on a detailed sampling of all the main known locations of gas emissions to constrain the origin of fluids and to characterize the nature of a seemingly inactive volcano.

2. Geological Setting

2.1. Ciomadul Volcanic Dome Field

Ciomadul volcano is located at the southeastern edge of the Carpathian-Pannonian Region, at the southern end of the Călimani-Gurghiu-Harghita volcanic chain (Szakács et al., 1993; Szakács & Seghedi, 1995; Pécskay et al., 2006; Figure 1). It is part of a postcollisional volcanic belt, which comprises a series of andesitic to dacitic volcanoes, developed parallel with the Carpathian orogeny. The volcanism occurred well after the continent-continent collision between the Tisza-Dacia microplate and the western margin of the

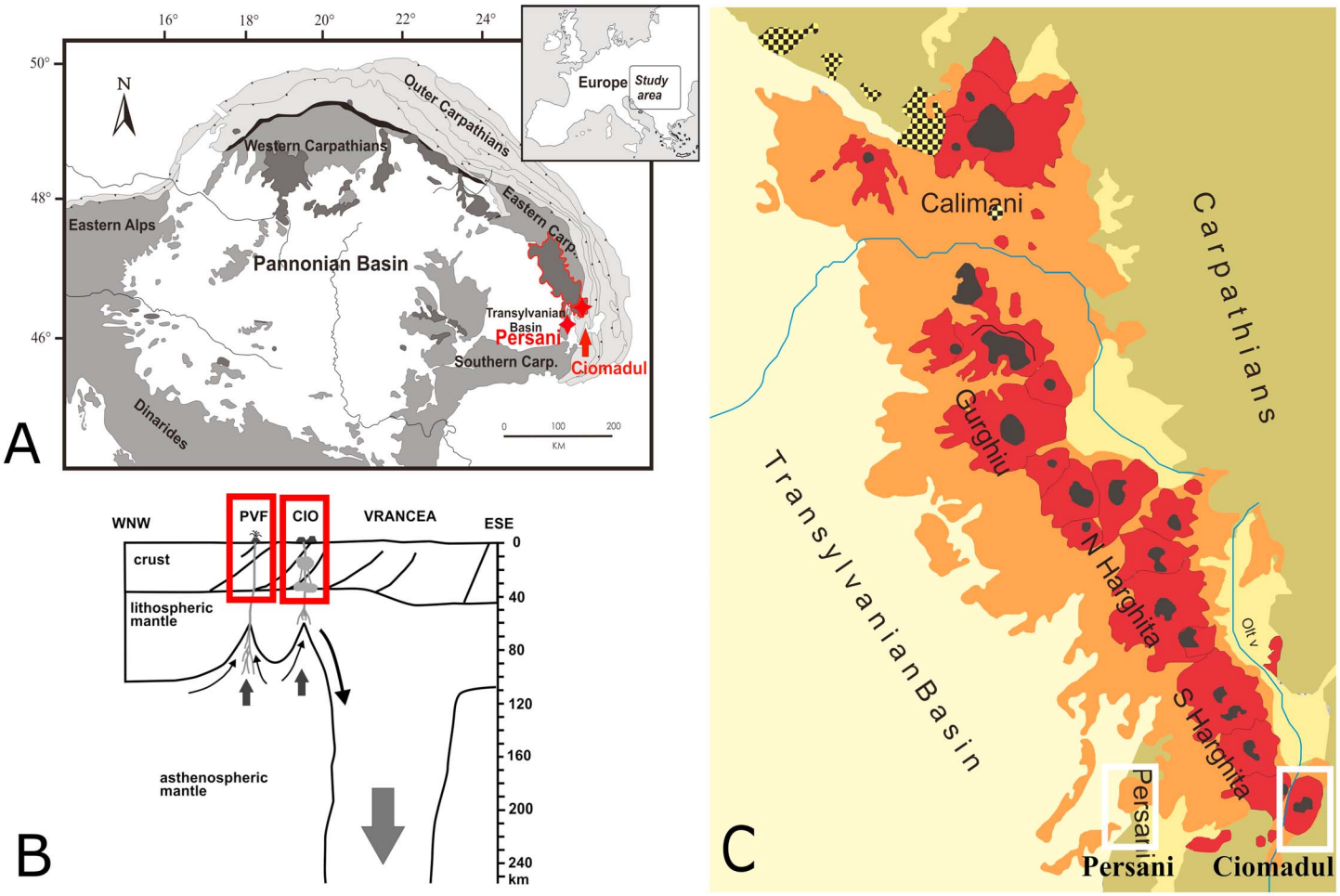

Figure 1. (a) Location of Ciomadul and Persani volcanoes in the southeastern Carpathian area of the Carpathian-Pannonian Region (after Harangi et al., 2013). (b) Geotectonic model of the Persani and Ciomadul volcanic areas. PVF = Persani Volcanic Field; CIO = Ciomadul (after Harangi et al., 2013). (c) Location of Ciomadul and Persani volcanoes in the volcanic range of the Eastern Carpathians (modified after Szakács & Seghedi, 1995).

Eurasian plate (Cloetingh et al., 2004; Csontos et al., 1992; Mațenco et al., 2007; Mațenco & Bertotti, 2000; Seghedi et al., 2004, 2005, 2011). Ciomadul is part of a lava dome field and this central volcanic complex involves 8–14 km^3 of high-K dacitic lavas (Karátson & Timár, 2005; Molnár et al., 2019; Szakács et al., 2015). The volcano developed on the Early Cretaceous clastic flysch sedimentary unit of the Eastern Carpathians that forms several nappes. It consists of binary alternation of sandstones, calcareous sandstones, limestones, and clays/marls from the Sinaia Formation of the Ceahlau nappe and the Bodoc flysch (Băncilă, 1958; Grasu et al., 1996; Ianovici & Rădulescu, 1968; Nicolaescu, 1973). The flysch unit has a thickness up to 2,500 m.

The Ciomadul volcanic complex is made up by amalgamation of several lava domes truncated by two explosion craters called Mohos and Saint Anna (Szakács et al., 2015). This central volcano is surrounded by further isolated lava domes (Baba Laposa, Haramul Mic, Dealul Mare, Büdös-Puturosul and Bálványos; Molnár et al., 2018, Figure 2). Volcanism at the Ciomadul volcanic dome field started around 1 Ma, while the most voluminous Ciomadul volcanic structure has developed over the last approximately 160 kyr (Molnár et al., 2018, 2019). During the first volcanic stage, the intermittent lava dome extrusions were separated by relatively long dormant periods even exceeding 100 kyr. The second volcanic stage was characterized by initial lava dome effusion and then, after approximately 40 kyr of quiescence, a more explosive volcanic activity occurred (from 57 to 30 ka, Harangi et al., 2010; Harangi, Lukács, et al., 2015; Karátson et al., 2016; Molnár et al., 2018, 2019; Moriya et al., 1995, 1996; Vinkler et al., 2007). This stage involved lava-dome collapse events, vulcanian and subplinian to plinian explosive eruptions (Harangi, Lukács,

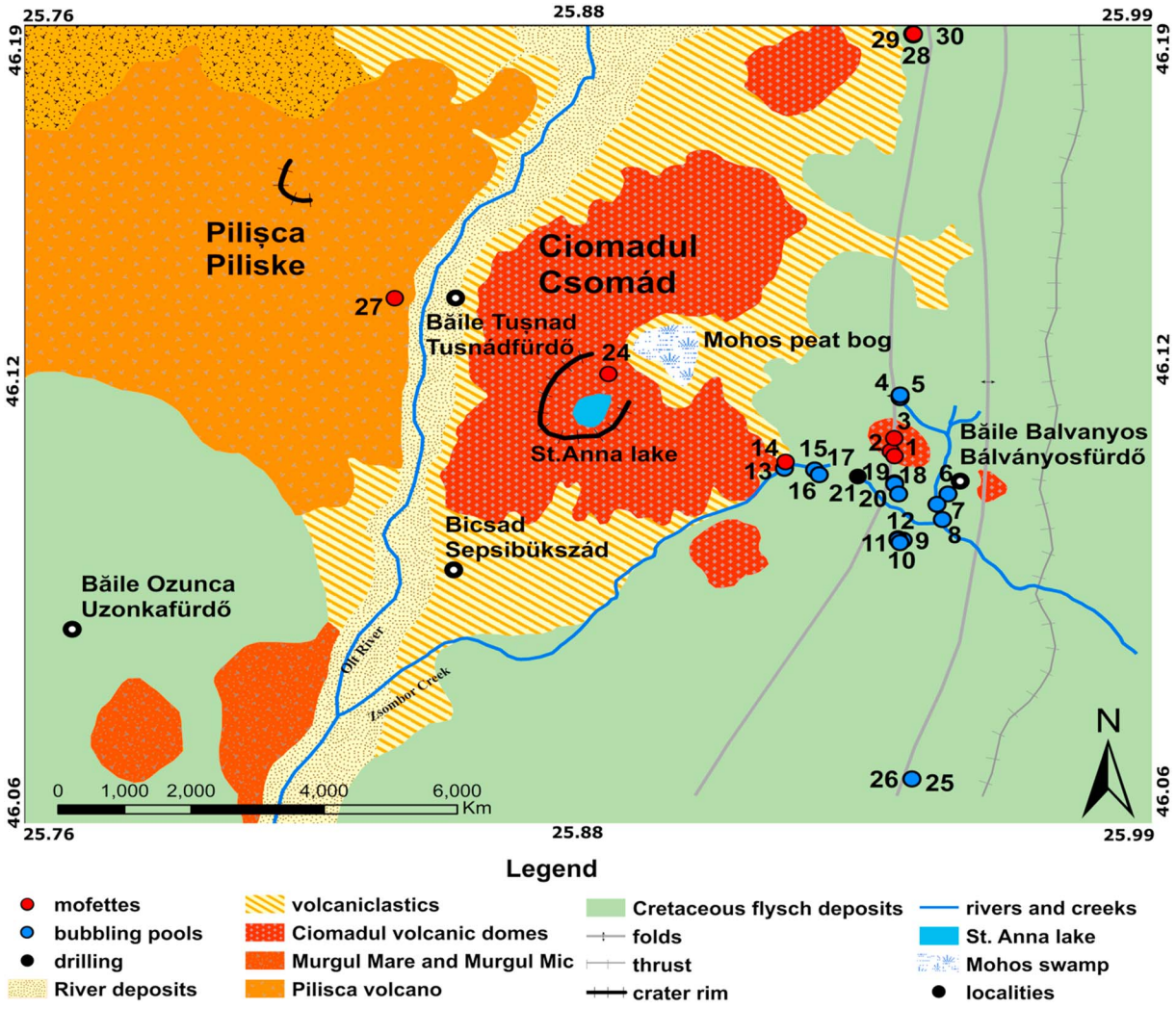

Figure 2. Geological sketch map of the study area. The red, black, and blue dots indicate the type of the sampling points: mofette, drilling, and bubbling pool, respectively. The numbers on the sampling sites are the same as in Table 1. (Geological map is modified after Ianovici & Rădulescu, 1968).

et al., 2015; Karátson et al., 2016; Vinkler et al., 2007). The eruptive products are relatively homogeneous K-rich dacites (Molnár et al., 2018, 2019; Szakács et al., 1993; Szakács & Seghedi, 1987; Vinkler et al., 2007). Petrogenetic and thermobarometric studies on amphiboles as well as combined U-Th/He and U/Th zircon dating suggest the presence of a long-lasting (up to 350 kyr) crystal mush body in the crust. This appears to be mostly at relatively low-temperature just above the solidus (700–750 °C) and is periodically partly remobilized by injections of fresh basaltic magmas that could rapidly trigger volcanic eruptions (Harangi, Lukács, et al., 2015; Harangi, Novák, et al., 2015; Kiss et al., 2014).

The Ciomadul volcano is located near (~50 km) the Vrancea seismic region (Ismail-Zadeh et al., 2012; Wenzel et al., 1999) located at the arc bend between the Eastern and the Southern Carpathians. Frequently occurring earthquakes have deep hypocentres (70–170 km) delineating a narrow, vertical region. This is consistent with a high-velocity seismic anomaly interpreted as a cold lithosphere slab descending slowly into the asthenospheric mantle (Wortel & Spakman, 2000). Further crustal and subcrustal earthquakes ($M < 4$) occur occasionally around the Perșani basalt volcanic field and the Ciomadul volcano (Popa et al., 2012). The seismic tomographic model indicates a vertically extended low-velocity anomaly beneath Ciomadul. This can be interpreted as transcrustal magma storage with an upper melt-dominated magma chamber (Popa et al., 2012). The seismic tomographic model is supported by the result of combined petrologic and magnetotelluric studies that demonstrated the existence of a low-resistivity anomaly and the

depth of 5–20 km beneath the volcanic centers of Ciomadul, inferred to be a melt-bearing crystal mush (Harangi, Novák, et al., 2015). In addition, a deeper low-resistivity anomaly was also detected at a depth of 30–40 km, possibly related to a deeper magma accumulation zone at the crust-mantle boundary.

Another Pleistocene monogenetic basalt volcanic field is approximately 40 km from the Ciomadul, at the southeastern part of the Carpathian-Pannonian Region (Figure 1), at the boundary between the Perşani Mountains and the Transylvanian basin (Downes et al., 1995; Harangi et al., 2013; Seghedi et al., 2016; Seghedi & Szakács, 1994). Basaltic volcanism occurred here between 1.14 Ma and 683 ka (Panaiotu et al., 2004, 2013) and formed several volcanic centers accompanied by maars, scoriacones, and lava flows. The erupted basaltic magma carried significant amount of ultramafic xenoliths from the lithospheric mantle (peridotites and amphibole pyroxenites) revealing the nature of the uppermost mantle of this region (Falus et al., 2008; Vaselli et al., 1995).

2.2. Gas Emissions and Mineral Water Springs at Ciomadul Volcanic Area

Gas emanations in the form of bubbling pools and low-temperature (T ~ 8–10 °C) dry mofettes are characteristic of the Ciomadul volcano. CO_2-bubbling peat bogs can be also found, mainly at the northeastern (Buffogó peat bog) and southern parts of the Puturosul Mountains (Zsombor-Valley, Jánosi et al., 2011). The minimum total CO_2 flux was estimated to be 8.7×10^3 t/year (Kis et al., 2017). The aquifers of this area are represented by CO_2-rich sparkling mineral water, with temperature up to 22.5 °C (Berszán et al., 2009; Italiano et al., 2017; Jánosi et al., 2011).

3. Sampling and Analytical Methods

A total of 31sites were selected for this study, including bubbling pools, dry gas emissions (mofettes), and one drilling (Figure 2 and Table 1). We collected fluids during two field campaigns carried out in the spring and autumn of 2016, respectively. In the first field campaign, gas samples were collected for $\delta^{13}C–CO_2$ and $^3He/^4He$ composition in 1-L evacuated Pyrex glass tubes with a vacuum stopcock, while for chemical composition, gas samples were collected in 150-ml glass tubes with two vacuum stopcocks. Chemical compositions were analyzed at the Istituto Nazionale di Geofisica e Vulcanologia, Rome, Italy, whereas chemical and isotopic composition of water, noble gas compositions (He and Ne) and $\delta^{13}C–CO_2$ of gas samples were measured at the Isotope Climatology and Environmental Research Centre (ICER), Institute for Nuclear Research, Hungarian Academy of Sciences, Debrecen, Hungary. During the second field campaign, the samples were collected in glass and steel samplers equipped with two valves. These samples were analyzed for their elemental composition (He, Ne, Ar, H_2, O_2, N_2, CO, CH_4, and CO_2), $\delta^{13}C$ (CO_2), $^3He/^4He$ ratios, and ^{20}Ne abundances at the Istituto Nazionale di Geofisica e Vulcanologia, Palermo, Italy (INGV-Palermo).

We also separated clinopyroxene mineral grains (>3 g in weight) from one of the lherzolite xenoliths collected at the foot of the Gruiu scoria cone, in the Perșani volcanic field. The noble gas composition of the fluid inclusions was analyzed at INGV-Palermo.

3.1. Chemical and Isotopic Composition of Gases

The chemical composition of the samples from the first campaign was analyzed with a Portable Varian CP4900 Micro Gas Chromatograph (GC). This Micro GC is configured for the analysis of He, Ne, H_2, O_2, and N_2 by means of a molecular sieve 5A (20 m unheated) column and CO_2, CH_4, and H_2S by means of a PoraPlot (PPQ 10 m heated) column. The instrument is equipped with a microthermal conductivity detector responding to the difference in thermal conductivity between the carrier gas (argon) and the sample composition. The detection limit is 1 ppm, operating range is from 1 ppm to 100% level concentrations, and repeatability is <0.5% relative standard deviation in peak area at constant temperature and pressure.

For the analysis of $\delta^{13}C_{CO2}$, carbon dioxide was cryogenically removed from the gas samples by liquid nitrogen and measured by Thermo Finnigan Delta ^{PLUS} XP isotope ratio mass spectrometer. Isotope ratios are given in the standard δ notation in permil (‰) versus VPDB (Vienna Pee Dee Belemnite). Errors for $\delta^{13}C$ are 0.5‰.

Noble gas isotopic ratios ($^3He/^4He$ and $^4He/^{20}Ne$) were measured from each gas sample that was inserted into the preparation line of the VG5400 noble gas mass spectrometer. The argon and the other chemically active gases (N_2, CO_2, etc.) were separated in a cryogenic cold system consisting of two cold traps and

Table 1
List of the Sites Investigated Including Location Names, Geographical Position (Geographical Coordinates in WGS84), Type of Manifestation (Mofetta, Bubbling Pool, and Drilling), Type of Sample (Free Gas), and Field Data (Temperature, pH, and EC Expressed in Microsiemens per Centimeter) Where Available

No.	Site	N	E	Type of manifestation	Sample type	*T* (°C)	pH	EC (μS/cm)
1	Torjai Stinky Cave	46.1198	25.9488	Mofetta	Free gas	nd	nd	nd
2	Timsós Cave	46.1191	25.9495	Mofetta	Free gas	nd	nd	nd
3	Gyilkos Cave	46.1218	25.9494	Mofetta	Free gas	nd	nd	nd
4	Buffogó peat bog pool	46.1279	25.9504	Bubbling pool	Free gas	1	3	472
5	Buffogó peat bog	46.1283	25.9504	Bubbling pool	Free gas	nd	nd	nd
6	Várpad-Ibolya pool	46.1134	25.9600	Bubbling pool	Free gas	7.1	6.46	3,220
7a	Bálványos mofetta	46.1118	25.9579	Bubbling pool	Free gas	9.7	4.99	3,722
7b	Bálványos mofetta	46.1118	25.9579	Bubbling pool	Free gas	9.7	4.99	3,722
8	Bálványos pool	46.1095	25.9590	Bubbling pool	Free gas	5	6.54	9,360
9	Csiszárfürdő-Iker pool white	46.1063	25.9514	Bubbling pool	Free gas	1.2	5.12	741
10	Csiszárfürdő-Hammas pool	46.1065	25.9504	Bubbling pool	Free gas	3.6	5.29	2,040
11	Csiszárfürdő-Timsós pool	46.1063	25.9504	Bubbling pool	Free gas	4.7	5.9	1,274
12	Csiszárfürdő-Csokoládés pool	46.1059	25.9508	Bubbling pool	Free gas	2.7	4.2	837
13	Mikesfürdő-Vallató pool	46.1170	25.9281	Bubbling pool	Free gas	5	6.16	2,300
14	Mikesfürdő-Vallató mofetta	46.1180	25.9283	Mofetta	Free gas	5	2.72	1,620
15	Mikesfürdő-Hammas pool	46.1168	25.9340	Bubbling pool	Free gas	1.9	2.96	968
16	Mikesfürdő-Bükkös pool	46.1161	25.9349	Bubbling pool	Free gas	2.3	3.6	584
17	Apor lányok feredeje-Small pool	46.1150	25.9496	Bubbling pool	Free gas	4.8	1.71	3,620
18	Apor lányok feredeje-spring on fault 2	46.1148	25.9496	Bubbling pool	Free gas	6.9	2.2	7,100
19	Apor lányok feredeje-Szemvíz 4	46.1148	25.9496	Bubbling pool	Free gas	4.2	2.6	2,080
20	Gyógyvizek	46.1133	25.9504	Bubbling pool	Free gas	3.7	1.85	2,780
21	Bálványos Sósmező drilling 1	46.1159	25.9424	Drilling	Free gas	nd	nd	nd
22	Bálványos Sósmező drilling 2	46.1159	25.9424	Drilling	Free gas	nd	nd	nd
23	Bálványos Sósmező drilling 3	46.1159	25.9424	Drilling	Free gas	nd	nd	nd
24	St Anna crater rim	46.1310	25.8936	mofetta	Free gas	nd	nd	nd
25	Jajdon pool	46.0701	25.9538	Bubbling pool	Free gas	4.6	7.3	1,489
26	Jajdon mofetta	46.0699	25.9538	Mofetta	Free gas	nd	nd	nd
27	Băile Tușnad mofetta	46.1421	25.8518	Mofetta	Free gas	nd	nd	nd
28	Lăzărești Nyírfürdő mofetta	46.1831	25.9520	Mofetta	Free gas	nd	nd	nd
29	Lăzărești Nyírfürdő pool	46.1831	25.9518	Bubbling pool	Free gas	6.6	5.96	768
30	Lăzărești Nyírfürdő pool 2	46.1829	25.9519	Bubbling pool	Free gas	nd	nd	nd
31	Ciucsângeorgiu mofetta	46.3363	25.9642	Mofetta	Free gas	nd	nd	nd

Note. EC = electrical conductivity; nd = not determined.

were adsorbed in an empty trap at 25 K. The Ne and He were adsorbed in a charcoal trap at 10 K. He was desorbed at 42 K and neon at 90 K and measured sequentially. The measurement procedure was calibrated with known air aliquots. The analytical uncertainties are 1% for He concentrations and 5% for Ne concentrations and 2.5% for $^3He/^4He$. $^3He/^4He$ ratio is expressed as R/R_a (being R_a the He isotope ratio of air and equal to $1.384 \cdot 10^{-6}$. He isotopic composition was corrected for the atmospheric He contamination (R/R_{ac}) considering the $^4He/^{20}Ne$ ratio; $R/R_{ac} = [R/R_a * (X - 1)]/(X - 1)$, where X is the air-normalized $^4He/^{20}Ne$ ratio taken as 0.318 (Sano & Wakita, 1985).

For the samples of the second analysis campaign, the chemical and isotopic composition of He-Ne and $^{13}C_{CO2}$ was determined in the laboratories of INGV-Palermo.

The concentrations of CO_2, CH_4, O_2, and N_2 were analyzed using an Agilent 7890B gas chromatograph with Ar as carrier and equipped with a 4-m Carbosieve S II and PoraPlot–U columns. A thermal conductivity detector was used to measure the concentrations of He, O_2, N_2, and CO_2 and a flame ionization detector for CO and CH_4. The analytical errors were 10% for He and 5% for O_2, N_2, CO, CH_4, and CO_2. More details on the analytical procedures used during this analysis are given in Liotta and Martelli (2012).

The carbon isotopic composition of CO_2 ($\delta^{13}C_{CO2}$) was determined using a Thermo Delta XP isotope ratio mass spectrometer equipped with a Thermo Scientific™ TRACE™ Ultra GC, and a 30-m Q-plot column (i.e., of 0.32 mm). The resulting $\delta^{13}C_{CO2}$ values are expressed in permil with respect to the international VPDB standard and analytical uncertainties are ±0.15‰. The method for the $\delta^{13}C$ determination of total

dissolved carbon is based on chemical and physical CO_2 stripping (Capasso et al., 2005). Isotopic ratios were measured using a Finnigan Delta Plus Mass Spectrometer. The results are expressed in permil of the international VPDB standard. The standard deviations of the $^{13}C/^{12}C$ ratios are ±0.2‰.

^3He, ^4He, and ^{20}Ne and the $^4He/^{20}Ne$ ratios were determined by separately inserting He and Ne into a split flight tube mass spectrometer (GVI-Helix SFT, for He analysis) and into a multicollector mass spectrometer (Thermo-Helix MC plus, for Ne analysis), after standard purification procedures (Rizzo et al., 2015). The analytical reproducibility was <0.1% for ^4He and ^{20}Ne. However, the estimation of He and Ne concentration agrees within 10% uncertainty respect to GC measurements. In this study, the time from sampling to analysis was lower than 2 weeks and results are fully reliable. The analytical error for He and Ne concentration measurements is generally below 0.3%.

3.2. Noble Gas Isotope Data for the Perşani Clinopyroxene

The chosen xenolith is a fresh spinel lherzolite with about 12% clinopyroxene content. Here we performed new noble gas analyses. The preparation, single-step crushing and analysis of fluid inclusions was the same as described by Correale et al. (2012) and references therein. Helium (^3He and ^4He) isotopes were measured separately by two different split-flight-tube mass spectrometers (Helix SFT-Thermo). The analytical uncertainty of the determination of the TGC (thermal conductivity detector) and the He and Ne abundances was ~10%. Error in the $^3He/^4He$ ratios is reported at the 1σ level.

4. Results

The site, sample names, and geographical locations with their GPS coordinates (WGS84, geographical coordinates), source type (mofettes or bubbling pools), temperature, pH, and electrical conductivity for bubbling pool samples are presented in Table 1, chemical and isotopic composition are listed in Tables 2 and 3. Noble gas isotopic compositions of clinopyroxenes from mantle xenoliths are shown in Table 4.

4.1. Chemical and Isotopic Composition of Gases

The CO_2 concentration in the collected gases ranges from 6.40% to 98.36%. Besides CO_2, H_2S (2.7×10^{-4} to 1.72×10^{-1}%), He (5.91×10^{-5} to 1.66×10^{-2}%), Ne (6.39×10^{-7} to 5.80x10^{-3}%), H_2 (1×10^{-5} to 2.3×10^{-1}%) CO (6×10^{-5} to 5×10^{-4}%), CH_4 (3.5×10^{-2} to 1.69%), N_2 (1.5×10^{-1} to 74.5%), and O_2 (2×10^{-3} to 18.99) are present in the gas samples. The ternary diagram $CO_2/50–N_2–O_2$ (Figure 3) shows a progressive enrichment in N_2 and O_2 of the samples, indicating a variable amount of air.

The $^3He/^4He$ ratios range between 0.77 and 3.10 R_a and the $^4He/^{20}Ne$ ratios from 0.36 to 1,700, which show that some of the collected gases are affected by air contamination (Table 3). The $^3He/^4He$ ratios after corrections for the air contamination (R/R_{ac}) are up to 3.25. The $\delta^{13}C_{CO2}$ ranges between −1.40‰ and −17.2‰ versus VPDB (Table 3).

4.2. Noble Gas Ratios of Fluid Inclusions From Persani Clinopyroxenes

Helium content in the fluid inclusions in clinopyroxenes ranged between 4.06×10^{-12} and 3.81×10^{-12} mol/g and Ne content between 2×10^{-15} and 2.74×10^{-15} mol/g, so the He/Ne ratios ranged between 1,390 and 2,030. The He isotopic signature in fluid inclusions was 5.95 Ra ± 0.01 (Table 4).

5. Discussion

5.1. Crustal Assimilation Versus Mantle Metasomatism

Helium comes from three different sources (mantle, crust, and air), which can be readily distinguished based on their characteristic isotopic ratios (Sano & Wakita, 1985). Helium isotopes are useful tracers for detecting deep fluids and their possible origin (crust, mantle, or atmosphere; Ozima & Podosek, 2002). It has been demonstrated that in the case of quiescent volcanoes, the active degassing of deep volatiles can occur for a long time after the last volcanic activity (Caracausi et al., 2009, 2015; Carapezza & Tarchini, 2007; Tassi et al., 2013).

The last eruption in Ciomadul occurred 30 ka (Harangi et al., 2010; Harangi, Lukács, et al., 2015; Molnár et al., 2019), yet there is an intense CO_2 degassing with a minimum flux of 8.7×10^3 t/year (Kis et al.,

Geochemistry, Geophysics, Geosystems

10.1029/2018GC008153

Table 2
Chemical Composition of the Different Gas Samples, Expressed in Percent

No.	Site	Campaign	Laboratory	H_2S	He	Ne	H_2	CO	CH_4	N_2	O_2	CO_2	Source
1	Torjai Stinky Cave	1st Campaign	Debrecen	nd	6.3×10^{-4}	3.5×10^{-5}	nd	nd	nd	nd	nd	nd	This work
	Torjai Stinky Cave		Rome	5.2×10^{-2}	7.0×10^{-4}	4.0×10^{-4}	2.0×10^{-5}		8.4×10^{-1}	1.6×10^{1}	4.9E+00	78.09	This work
	Torjai Stinky Cave	2nd Campaign	Palermo	1.8×10^{-2}	6.1×10^{-4}	6.4×10^{-7}	nd	5.0×10^{-4}	8.9×10^{-1}	1.2×10^{1}	2.9E+00	82.68	This work
2	Timsós Cave	1st Campaign	Debrecen	nd	6.9×10^{-4}	2.9×10^{-5}	nd	nd	nd	nd	nd	nd	This work
	Timsós Cave		Rome	6.8×10^{-2}	7.0×10^{-4}	3.0×10^{-4}	3.0×10^{-5}		8.4×10^{-1}	1.2×10^{1}	3.8E+00	83.05	This work
	Timsós Cave	2nd Campaign	Palermo	nd	6.3×10^{-4}	4.8×10^{-5}	nd	1.0×10^{-4}	9.3×10^{-1}	2.1E+00	7.3×10^{-2}	95.24	This work
3	Gyilkos Cave	1st Campaign	Debrecen	nd	5.6×10^{-4}	4.0×10^{-4}	nd	nd	nd	nd	nd	nd	This work
	Gyilkos Cave		Rome	nd	6.0×10^{-4}	1.0×10^{-3}	4.0×10^{-5}	nd	1.1×10^{-1}	3.8×10^{1}	9.5E+00	52.54	This work
4	Buffogó peat bog pool	1st Campaign	Debrecen	nd	6.7×10^{-4}	8.8×10^{-7}	nd	nd	nd	nd	nd	64.98	This work
	Buffogó peat bog pool		Rome	nd	8.0×10^{-4}	5.0×10^{-4}	4.0×10^{-5}	nd	9.7×10^{-1}	2.6×10^{1}	7.6E+00	64.98	This work
	Buffogó peat bog pool	2nd Campaign	Palermo	5.0×10^{-4}	7.1×10^{-4}	7.9×10^{-4}	nd	nd	1.3E+00	1.9E+00	1.5×10^{-1}	95.50	This work
5	Buffogó peat bog	1st Campaign	Debrecen	nd	9.4×10^{-4}	2.0×10^{-6}	nd	nd	nd	nd	nd	nd	This work
6	Várpad-Ibolya pool	1st Campaign	Debrecen	nd	5.9×10^{-5}	1.4×10^{-4}	nd	nd	nd	nd	nd	75.97	This work
	Várpad-Ibolya pool		Rome	nd	2.0×10^{-4}	5.0×10^{-4}	2.0×10^{-5}	nd	2.2×10^{-1}	1.8×10^{1}	5.7E+00	75.97	This work
7a	Bálványos mofetta	1st Campaign	Debrecen	nd	8.3×10^{-4}	1.8×10^{-6}	nd	nd	nd	nd	nd	nd	This work
7b	Bálványos mofetta	1st Campaign	Debrecen	nd	4.6×10^{-4}	1.8×10^{-4}	nd	nd	nd	nd	nd	94.87	This work
	Bálványos mofetta		Rome	nd	5.9×10^{-3}	4.1×10^{-3}	3.4×10^{-2}	nd	6.4×10^{-1}	3.7E+00	8.2×10^{-1}	94.87	This work
	Bálványos mofetta	2nd Campaign	Palermo	nd	1.0×10^{-3}	2.5×10^{-4}	1.4×10^{-3}	nd	1.3E+00	2.2×10^{1}	6.1E+00	68.25	This work
8	Bálványos pool	1st Campaign	Debrecen	nd	1.7×10^{-3}	1.7×10^{-4}	nd	nd	nd	nd	nd	63.84	This work
	Bálványos pool		Rome	nd	1.7×10^{-2}	5.8×10^{-3}	2.3×10^{-1}	nd	1.7E+00	2.6×10^{1}	8.4E+00	63.84	This work
9	Csiszárfürdő-Iker pool white	1st Campaign	Debrecen	nd	1.3×10^{-3}	1.0×10^{-5}	nd	nd	nd	nd	nd	nd	This work
	Csiszárfürdő-Iker pool white	2nd Campaign	Palermo	nd	9.5×10^{-4}	1.1×10^{-5}	nd	nd	1.7E+00	1.8E+00	1.7×10^{-1}	94.73	This work
10	Csiszárfürdő-Hammas pool	1st Campaign	Debrecen	nd	1.1×10^{-3}	6.4×10^{-7}	nd	nd	nd	nd	nd	96.72	This work
			Rome	1.1×10^{-1}	1.0×10^{-2}	2.3×10^{-3}	9.0×10^{-4}	nd	1.2E+00	9.8×10^{-1}	3.5×10^{-1}	96.72	this work
	Csiszárfürdő-Hammas pool	2nd Campaign	Palermo	nd	6.9×10^{-4}	5.5×10^{-6}	nd	nd	1.2E+00	8.8×10^{-1}	3.0×10^{-2}	94.81	This work
11	Csiszárfürdő-Timsós pool	1st Campaign	Debrecen	nd	1.1×10^{-3}	1.2×10^{-3}	nd	nd	nd	nd	nd	11.23	This work
	Csiszárfürdő-Timsós pool		Rome	nd	6.0×10^{-4}	1.0×10^{-3}	4.0×10^{-5}	nd	1.7×10^{-1}	7.0×10^{1}	1.9×10^{1}	11.23	This work
12	Csiszárfürdő-Csokoládés pool	1st Campaign	Debrecen	nd	9.4×10^{-4}	7.8×10^{-4}	nd	nd	nd	nd	nd	89.49	This work
	Csiszárfürdő-Csokoládés pool		Rome	1.7×10^{-2}	1.3×10^{-2}	4.6×10^{-3}	2.3×10^{-3}	nd	1.5E+00	7.4	1.6E+00	89.49	This work
	Csiszárfürdő-Csokoládés pool	2nd Campaign	Palermo	nd	8.7×10^{-4}	1.6×10^{-5}	nd	9.0×10^{-5}	1.5E+00	1.5E+00	1.4×10^{-1}	94.51	This work
13	Mikesfürdő-Vallató pool	1st Campaign	Debrecen	nd	4.5×10^{-4}	8.5×10^{-6}	nd	nd	nd	nd	nd	41.34	This work
	Mikesfürdő-Vallató pool		Rome	nd	5.9×10^{-3}	nd	6.0×10^{-4}	nd	5.5E-01	4.6×10^{1}	1.3×10^{1}	41.34	This work
	Mikesfürdő-Vallató pool	2nd Campaign	Palermo	nd	4.3×10^{-4}	1.4×10^{-5}	nd	nd	1.2E+00	1.8E+00	1.8×10^{-1}	93.95	This work
14	Mikesfürdő-Vallató mofetta	1st Campaign	Debrecen	nd	3.0×10^{-4}	4.0×10^{-5}	nd	nd	nd	nd	nd	91.86	This work
			Rome	2.7×10^{-2}	3.0×10^{-4}	2.0×10^{-4}	1.0×10^{-5}	nd	9.6×10^{-1}	5.2E+00	1.9E+00	91.86	This work

Geochemistry, Geophysics, Geosystems

10.1029/2018GC008153

Table 2 *(continued)*

No.	Site	Campaign	Laboratory	H_2S	He	Ne	H_2	CO	CH_4	N_2	O_2	CO_2	Source
	Mikesfürdő-Vallató mofetta												
15	Mikesfürdő-Hammas pool	1st Campaign	Debrecen	nd	7.2×10^{-4}	2.7×10^{-6}	nd	nd	nd	nd	nd	87.67	This work
	Mikesfürdő-Hammas pool		Rome	nd	7.0×10^{-4}	2.0×10^{-4}	4.0×10^{-5}	nd	9.9×10^{-1}	8.5E+00	2.9E+00	87.67	This work
	Mikesfürdő-Hammas pool	2nd Campaign	Palermo	nd	5.9×10^{-4}	7.9×10^{-6}	nd	nd	1.1E+00	1.1E+00	2.0×10^{-3}	94.83	This work
16	Mikesfürdő-Bükkös pool	1st Campaign	Debrecen	nd	8.0×10^{-4}	6.7×10^{-4}	nd	nd	nd	nd	nd	82.58	This work
	Mikesfürdő-Bükkös pool		Rome	nd	7.0×10^{-4}	4.0×10^{-4}	2.0×10^{-5}	nd	9.0×10^{-1}	1.3×10^{1}	4.0E+00	82.58	This work
	Mikesfürdő-Bükkös pool	2nd Campaign	Palermo	nd	7.7×10^{-4}	3.9×10^{-4}	nd	1.0×10^{-4}	1.1E+00	9.9E+00	2.4E+00	84.33	This work
17	Apor lányok feredeje-Small pool	1st Campaign	Debrecen	nd	1.2×10^{-3}	5.0×10^{-6}	nd	nd	nd	nd	nd	58.09	This work
	Apor lányok feredeje-Small pool		Rome	nd	8.0×10^{-4}	7.0×10^{-4}	3.0×10^{-5}	nd	7.7×10^{-1}	3.2×10^{1}	9.4E+00	58.09	This work
17	Apor lányok feredeje-Small pool	2nd Campaign	Palermo	2.7×10^{-4}	8.3×10^{-4}	6.5×10^{-5}	nd	9.0×10^{-5}	1.2E+00	1.1E+00	2.8×10^{-3}	97.15	This work
18	Apor lányok feredeje-spring on fault 2	1st Campaign	Debrecen	nd	7.8×10^{-4}	6.6×10^{-5}	nd	nd	nd	nd	nd	98.36	This work
	Apor lányok feredeje-spring on fault 2		Rome	1.7×10^{-1}	9.7×10^{-3}	2.2×10^{-3}	3.2×10^{-3}	nd	1.2E+00	1.5×10^{-1}	1.2×10^{-1}	98.36	This work
	Apor lányok feredeje-spring on fault 2	2nd Campaign	Palermo	3.5×10^{-4}	6.5×10^{-4}	7.8×10^{-7}	nd	nd	1.2E+00	8.6×10^{-1}	nd	96.38	This work
19	Apor lányok feredeje-Szemvíz 4	1st Campaign	Debrecen	nd	1.2×10^{-3}	2.8×10^{-6}	nd	nd	nd	nd	nd	36.24	This work
	Apor lányok feredeje-Szemvíz 4		Rome	2.0×10^{-2}	7.0×10^{-4}	1.0×10^{-3}	2.0×10^{-4}	nd	4.4×10^{-1}	5.0E+01	1.4×10^{1}	36.24	This work
	Apor lányok feredeje-Szemvíz 4	2nd Campaign	Palermo	nd	nd	nd	nd	6.0×10^{-5}	9.2×10^{-1}	2.0E+01	5.0E+00	74.99	This work
20	Gyógyvizek	1st Campaign	Debrecen	nd	8.1×10^{-4}	1.6×10^{-6}	nd	nd	nd	nd	nd	97.62	This work
	Gyógyvizek		Rome	1.1×10^{-1}	1.1×10^{-2}	2.6×10^{-3}	9.0×10^{-4}	nd	1.3E+00	5.3×10^{-1}	4.9×10^{-1}	97.62	This work
	Gyógyvizek	2nd Campaign	Palermo	nd	7.5×10^{-4}	8.6×10^{-4}	2.0×10^{-3}	1.5×10^{-4}	8.9×10^{-1}	1.4×10^{1}	3.5E+00	78.42	This work
21	Bálványos Sósmező drilling 1	1st Campaign	Debrecen	nd	2.6×10^{-4}	6.4×10^{-4}	nd	nd	nd	nd	nd	79.78	This work
	Bálványos Sósmező drilling 1		Rome	nd	2.0×10^{-4}	5.0×10^{-4}	3.0×10^{-5}	nd	3.5×10^{-2}	1.5×10^{1}	4.9E+00	79.78	This work
22	Bálványos Sósmező drilling 2	1st Campaign	Debrecen	nd	4.4×10^{-4}	5.4×10^{-4}	nd	nd	nd	nd	nd	80.62	This work
	Bálványos Sósmező drilling 2		Rome	nd	2.0×10^{-4}	4.0×10^{-4}	3.0×10^{-5}	nd	8.9×10^{-2}	1.5×10^{1}	4.6E+00	80.62	This work
23	Bálványos Sósmező drilling 3	1st Campaign	Debrecen	nd	6.2×10^{-4}	4.7×10^{-4}	nd	nd	nd	nd	nd	nd	This work
24	St Anna crater rim	1st Campaign	Debrecen	nd	8.2×10^{-4}	1.0×10^{-3}	nd	nd	nd	nd	nd	22.74	This work
	St Anna crater rim		Rome	nd	6.0×10^{-4}	1.0×10^{-3}	4.0×10^{-5}	nd	1.1×10^{-1}	6.1×10^{1}	1.6×10^{1}	22.74	This work
25	Jajdon pool	1st Campaign	Debrecen	nd	1.0×10^{-3}	1.1×10^{-3}	nd	nd	nd	nd	nd	20.50	This work

Geochemistry, Geophysics, Geosystems

10.1029/2018GC008153

Table 2 *(continued)*

No.	Site	Campaign	Laboratory	H_2S	He	Ne	H_2	CO	CH_4	N_2	O_2	CO_2	Source
	Jajdon pool		Rome	4.1×10^{-2}	8.6×10^{-3}	nd	4.0×10^{-4}	nd	4.0×10^{-1}	6.2×10^{1}	1.7×10^{1}	20.50	This work
26	Jajdon mofetta	1st Campaign	Debrecen	nd	5.9×10^{-4}	1.7×10^{-3}	nd	nd	nd	nd	nd	12.11	This work
	Jajdon mofetta		Rome	nd	5.8×10^{-3}	nd	5.0×10^{-4}	nd	1.3×10^{-1}	6.9×10^{1}	1.9×10^{1}	12.11	This work
27	Băile Tușnad mofetta	1st Campaign	Debrecen	nd	4.1×10^{-4}	3.2×10^{-4}	nd	nd	nd	nd	nd	97.97	This work
	Băile Tușnad mofetta		Rome	nd	4.1×10^{-3}	2.7×10^{-3}	7.0×10^{-4}	nd	5.9×10^{-1}	9.2×10^{-1}	5.2×10^{-1}	97.97	This work
28	Lăzărești Nyírfürdő mofetta	1st Campaign	Debrecen	nd	1.3×10^{-4}	2.0×10^{-5}	nd	nd	nd	nd	nd	97.99	This work
	Lăzărești Nyírfürdő mofetta		Rome	8.4×10^{-2}	2.2×10^{-3}	2.4×10^{-3}	2.0×10^{-4}	nd	7.8×10^{-1}	7.1×10^{-1}	4.3×10^{-1}	97.99	This work
29	Lăzărești Nyírfürdő pool	1st Campaign	Debrecen	nd	3.7×10^{-4}	9.7×10^{-4}	nd	nd	nd	nd	nd	93.14	This work
	Lăzărești Nyírfürdő pool		Rome	5.0×10^{-3}	3.7×10^{-3}	4.0×10^{-3}	1.4×10^{-3}	nd	1.3E+00	4.8E+00	7.3×10^{-1}	93.14	This work
	Lăzărești Nyírfürdő pool	2nd Campaign	Palermo	nd	1.1×10^{-4}	2.7×10^{-6}	nd	nd	8.1×10^{-1}	1.7E+00	5.0×10^{-2}	96.71	This work
30	Lăzărești Nyírfürdő pool 2	1st Campaign	Debrecen	nd	1.3×10^{-4}	2.7×10^{-5}	nd	nd	nd	nd	nd	97.66	This work
	Lăzărești Nyírfürdő pool 2		Rome	5.9×10^{-2}	1.9×10^{-3}	2.9×10^{-3}	9.0×10^{-4}	nd	7.9×10^{-1}	8.6×10^{-1}	6.2×10^{-1}	97.66	This work
31	Ciucsângeorgiu mofetta	1st Campaign	Debrecen	nd	5.9×10^{-4}	1.5×10^{-3}	nd	nd	nd	nd	nd	6.40	This work
	Ciucsângeorgiu mofetta		Rome	nd	5.4×10^{-3}	nd	5.0×10^{-4}	nd	6.4×10^{-2}	7.5×10^{1}	1.9×10^{1}	6.40	This work
32	Csiszárfürdő Băile Reci			nd	2.3×10^{-3}	2.3×10^{-3}	nd	nd	8.0×10^{-3}	nd	nd	99.99	Frunzeti, 2013
33	Gyógyvizek Izvoarele Tămăduitoare			nd	3.5×10^{-3}	4.6×10^{-6}	nd	nd	1.3E+00	1.4E+00	nd	97.24	Frunzeti, 2013
34	Apor lányok feredeje			nd	3.5×10^{-3}	1.3×10^{-6}	nd	nd	1.3E+00	1.9E+00	nd	96.76	Frunzeti, 2013
35	Torjai Büdös Cave (Stinky Cave)			nd	2.7×10^{-3}	4.6×10^{-6}	nd	nd	1.2E+00	2.1E+00	nd	96.80	Frunzeti, 2013
36	Mikesfürdő-Hammas			nd	3.3×10^{-3}	5.0×10^{-6}	nd	nd	1.3E+00	1.5E+00	nd	97.17	Frunzeti, 2013
37	Buffogó peat bog			nd	3.7×10^{-3}	1.4×10^{-6}	nd	nd	1.6E+00	1.6E+00	nd	96.80	Frunzeti, 2013
38	Tusnad			nd	5.3×10^{-5}	7.3×10^{-6}	nd	nd	3.0×10^{-3}	4.4E+00	nd	95.70	Frunzeti, 2013
39	Tusnad Nadas			nd	6.0×10^{-6}	nd	3.4×10^{-5}	nd	3.8×10^{-3}	3.2×10^{-1}	1.1×10^{-1}	99.56	Vaselli et al., 2002
40	Lăzărești Nyir			5.0×10^{-3}	7.8×10^{-4}	nd	4.0×10^{-5}	2.2×10^{-5}	3.4E+00	7.4E+00	1.4×10^{-2}	89.11	Vaselli et al., 2002
41	Sf Ana			nd	6.9×10^{-4}	nd	5.0×10^{-6}	7.0×10^{-6}	6.5×10^{-1}	1.6E+00	4.2×10^{-2}	97.69	Vaselli et al., 2002
42	Puturosul			1.2×10^{-2}	4.1×10^{-4}	nd	3.7×10^{-5}	nd	7.8×10^{-1}	9.0×10^{-1}	4.2×10^{-2}	98.26	Vaselli et al., 2002
43	Puturosul Sud			nd	1.4×10^{-3}	nd	9.0×10^{-6}	9.0×10^{-6}	2.4E+00	2.0E+00	3.0×10^{-2}	95.63	Vaselli et al., 2002
44	Bálványos			6.0×10^{-3}	6.3×10^{-4}	nd	1.5×10^{-4}	4.0×10^{-6}	1.1E+00	8.9×10^{-1}	4.4×10^{-2}	97.97	Vaselli et al., 2002
45	Torjai Büdös Cave (Stinky Cave)			nd	1.1×10^{-3}	nd	nd	nd	8.0×10^{-1}	9.7×10^{-1}	6.0×10^{-2}	98.20	Althaus et al., 2000
46	Apor lányok feredeje-Upper pool			nd	1.3×10^{-3}	nd	nd	nd	1.2E+00	1.5E+00	1.8×10^{-1}	97.75	Althaus et al., 2000

Table 2 *(continued)*

No.	Site	Campaign	Laboratory	H_2S	He	Ne	H_2	CO	CH_4	N_2	O_2	CO_2	Source
47	Apor lányok feredeje-Lower pool			nd	1.3×10^{-3}	nd	nd	nd	9.4×10^{-1}	7.3×10^{-1}	2.0×10^{-2}	98.16	Althaus et al., 2000
48	Bi × ad			nd	nd	nd	nd	nd	2.3×10^{-1}	8.9×10^{-1}	2.7×10^{-1}	99.00	Althaus et al., 2000
49	Bi × ad			nd	nd	nd	nd	nd	nd	nd	nd	nd	Althaus et al., 2000
50	Tusnad Nagy			nd	nd	nd	nd	nd	nd	nd	nd	nd	Althaus et al., 2000
51	Balvanyos Carpatii			nd	nd	nd	nd	nd	nd	nd	nd	nd	Althaus et al., 2000
52	Gyógyvízek			nd	nd	nd	nd	nd	nd	nd	nd	nd	Unpublished data
53	Bancu			nd	nd	nd	nd	1.0×10^{-5}	7.0×10^{-1}	2.4E+00	2.0×10^{-1}	95.88	Unpublished data
54	Lazaresti			nd	nd	nd	nd	nd	8.5×10^{-1}	2.0E+00	1.8×10^{-1}	96.4	Unpublished data

Note. nd = not determined.

2017), which is comparable to other dormant volcanic areas such as Panarea (1.72×10^4 t/year) and Roccamonfina (7.48×10^3 t/year) from Italy or Jefferson (7.92×10^3 t/year) from the United States.

In addition, previous investigations (Althaus et al., 2000; Vaselli et al., 2002; Túri et al., 2016) highlighted the outgassing of mantle-derived volatiles at Ciomadul volcano. He isotopic ratios in the fluids collected in this study are up to 3.1 R_a similar to those obtained from previous studies (Figure 4 and Table 3). These values are higher than those obtained from the surrounding areas such as in the Carpathian Foredeep and the Transylvanian Basin where He isotopic ratios are between 0.02 and 0.03 R_a (Baciu et al., 2017; Italiano et al., 2017; Vaselli et al., 2002, Figure 4). These latter values are typical of crustal fluids dominated by ^{4}He produced by decay of U and Th (e.g., Ozima & Podosek, 2002). The higher R_a values measured at Ciomadul could imply a higher contribution of magmatic He. Nevertheless, the 3.1 R_a value is significantly lower than the MORB and subcontinental lithospheric mantle (SCLM) value (Sano & Marty, 1995) requiring addition of radiogenic ^{4}He that decreased the pristine isotopic signature.

The mantle xenoliths of the Perşani volcanic field (approximately 40 km from the Ciomadul area) could provide the He isotopic signature of the lithospheric mantle beneath the region. The He isotopic ratios in fluid inclusions of the Persani clinopyroxenes are 5.95 ± 0.01 (Table 4), and these are lower than those of of previous measurements, from 6.5 to 7.3 R_a, obtained by Althaust et al. (1998) but consistent with the values of the SCLM ($R/R_a = 6.1 \pm 0.9$ R_a, Gautheron & Moreira, 2002). The continental crust ($R/R_a = 0.02$, Ozima & Podosek, 2002) and atmosphere ($R/R_a = 1$) have distinct isotopic values, and ^{4}He/^{20}Ne can be used to infer how mixing between the three possible end members can support the He isotopic signature of the fluids that outgass in the Ciomadul region (Figure 4). Most Ciomadul samples indicate a possible trend between air and a magmatic source, where the He ratio of the magmatic end member (3.1 R_a) is lower than that of the ECLM and the Perşani clinopyroxene. This is also supported by the trend line in the ^{3}He–CO_2–^{4}He ternary diagram (Figure 5), where the Ciomadul samples are along a trend showing variable amounts of CO_2 and R/R_{ac} values between 2 and 3. This trend reflects the dominance of radiogenic He in the fluids outgassing from the Ciomadul volcano. We have now to assess the possible processes that can add the radiogenic He component to the mantle component.

Such a relatively low He isotope ratio of the magma source is not uncommon in volcanic arc settings (e.g., Hilton et al., 1992; Allard et al., 1997; Martelli et al., 2004) and can be due to several processes involving the addition of radiogenically produced ^{4}He, such as magma aging, crustal assimilation, mixing between mantle, and crustal-derived fluids (Kennedy & van Soest, 2006; Torgersen et al., 1995). Unfortunately, there are no undifferentiated mantle-derived mafic rocks in the region of the Ciomadul volcano, so we cannot investigate the He isotope composition of the mantle directly below the volcano. In Ciomadul, only high-K dacitic volcanic products are found (Mason et al., 1996; Molnár et al., 2018, 2019; Vinkler et al., 2007), although occurrence of high-Mg minerals such as olivine and clinopyroxene in the dacites suggest involvement of primitive mafic magmas in the magma evolution of Ciomadul (Kiss et al., 2014; Vinkler et al., 2007).

Magma aging and crustal assimilation are two mechanisms that could account for the addition of the radiogenic He component to the mantle-derived melts. Both these processes have been invoked to explain low He isotopic ratios (<MORB and SCLM) in different volcanic regions, worldwide, such as Aeolian Island, Italy (Mandarano et al., 2016), and Iceland (Condomines et al., 1983). The magma-aging mechanism considers an addition of ^{4}He by radiogenic decay in the magma itself.

Table 3
Isotopic Composition of the Gas Samples

No.	Site	Campaign	Laboratory	R/Ra measured	R/Ra corrected	4He/20Ne	$\delta^{13}C–CO_2$	δ18 O–CO_2	CO_2/3He	Source
1	Torjai Stinky Cave	1st Campaign	Debrecen	2.67	2.69	18.07	−3.24	−6.74	3.29E+10	This work
		2nd Campaign	Palermo	3.01	3.01	955.55	−3.09	nd	3.24E+10	This work
2	Timsós Cave	1st Campaign	Debrecen	2.71	2.73	23.83	−3.36	−6.08	3.17E+10	This work
		2nd Campaign	Palermo	2.90	2.95	13.20	−3.47	nd	3.69E+10	This work
3	Gyilkos Cave	1st Campaign	Debrecen	2.12	2.40	1.40	−3.22	−6.63	nd	This work
4	Buffogó peat bog pool	1st Campaign	Debrecen	2.86	2.86	758.43	−2.70	−9.00	2.45E+10	This work
		2nd Campaign	Palermo	2.27	2.95	0.90	−3.15	nd	3.27E+10	This work
5	Buffogó peat bog	1st Campaign	Debrecen	1.78	1.78	477.09	nd	nd	nd	This work
6	Várpad-Ibolya pool	1st Campaign	Debrecen	1.49	2.43	0.44	−3.13	nd	3.81E+11	This work
7a	Bálványos mofetta	1st Campaign	Debrecen	1.13	1.13	456.45	nd	nd	nd	This work
7b	Bálványos mofetta	1st Campaign	Debrecen	2.06	2.19	2.62	−4.20	nd	6.71E+10	This work
		2nd Campaign	Palermo	2.06	2.15	4.0	−17.20	nd	nd	This work
8	Bálványos pool	1st Campaign	Debrecen	2.14	2.17	9.75	−2.84	nd	1.26E+10	This work
9	Csiszárfürdő-Iker pool white	1st Campaign	Debrecen	2.43	2.44	127.86	−3.06	−7.44	nd	This work
		2nd Campaign	Palermo	2.81	2.82	90.4	nd	nd	2.53E+10	This work
10	Csiszárfürdő-Hammas pool	1st Campaign	Debrecen	1.97	1.97	1695.21	−3.59	−8.40	3.23E+10	This work
10		2nd Campaign	Palermo	2.90	2.90	123.8	−3.20	nd	3.43E+10	This work
11	Csiszárfürdő-Timsós pool	1st Campaign	Debrecen	2.46	3.09	0.95	−2.47	nd	2.33E+09	This work
12	Csiszárfürdő-Csokoládés pool	1st Campaign	Debrecen	2.44	2.90	1.21	−3.40	nd	2.37E+10	This work
12		2nd Campaign	Palermo	2.90	2.91	55.00	−2.60	nd	2.68E+10	This work
13	Mikesfürdő-Vallató pool	1st Campaign	Debrecen	2.72	2.73	52.98	−2.28	−6.87	2.42E+10	This work
13		2nd Campaign	Palermo	2.55	2.57	31.4	−2.30	nd	6.18E+10	This work
14	Mikesfürdő-Vallató mofetta	1st Campaign	Debrecen	2.21	2.25	7.43	−2.45	−6.37	9.87E+10	This work
15	Mikesfürdő-Hammas pool	1st Campaign	Debrecen	2.74	2.74	266.70	−3.35	−7.09	3.19E+10	This work
15	l	2nd Campaign	Palermo	3.02	3.03	74.0	−2.90	nd	3.85E+10	This work
16	Mikesfürdő-Bükkös pool	1st Campaign	Debrecen	2.46	2.93	1.19	−2.65	nd	2.52E+10	This work
16		2nd Campaign	Palermo	1.98	2.16	2.0	−3.20	nd	3.64E+10	This work
17	Apor lányok feredeje-Small pool	1st Campaign	Debrecen	1.99	1.99	233.48	−3.09	−5.13	1.81E+10	This work
17		2nd Campaign	Palermo	2.81	2.86	12.8	nd	nd	2.95E+10	This work
18	Apor lányok feredeje-spring on fault 2	1st Campaign	Debrecen	3.10	3.15	11.80	−3.85	nd	2.87E+10	This work
18		2nd Campaign	Palermo	2.90	2.90	836.3	−4.00	nd	3.68E+10	This work
19	Apor lányok feredeje-Szemvíz 4	1st Campaign	Debrecen	1.85	1.85	425.84	−3.52	−2.79	1.20E+10	This work
19		2nd Campaign	Palermo	1.34	1.50	1.00	−2.60	nd	nd	This work
20	Gyógyvizek	1st Campaign	Debrecen	2.73	2.73	497.01	−3.42	−4.58	3.17E+10	This work
20		2nd Campaign	Palermo	1.46	1.73	0.9	−3.30	nd	4.37E+10	This work
21	Bálványos Sósmező drilling 1	1st Campaign	Debrecen	0.78	0.27	0.41	−4.61	−5.44	8.13E+11	This work
22	Bálványos Sósmező drilling 2	1st Campaign	Debrecen	0.82	0.72	0.82	−4.37	−5.30	1.82E+11	This work
23	Bálványos Sósmező drilling 3	1st Campaign	Debrecen	2.43	2.83	1.32	−3.92	nd	nd	This work
24	St Anna crater rim	1st Campaign	Debrecen	1.99	2.58	0.78	−2.80	−9.05	7.78E+09	This work
25	Jajdon pool	1st Campaign	Debrecen	2.30	2.83	0.99	−3.41	nd	5.02E+09	This work
26	Jajdon mofetta	1st Campaign	Debrecen	1.45	3.25	0.36	−3.96	nd	4.51E+09	This work
27	Băile Tuşnad mofetta	1st Campaign	Debrecen	2.02	2.32	1.28	−1.50	nd	7.48E+10	This work
28	Lăzăreşti Nyírfürdő mofetta	1st Campaign	Debrecen	1.43	1.45	6.50	−2.08	nd	3.84E+11	This work
29	Lăzăreşti Nyírfürdő pool	1st Campaign	Debrecen	1.11	1.46	0.38	−1.40	nd	1.24E+11	This work
29		2nd Campaign	Palermo	1.01	1.01	40.2	−1.50	nd	6.45E+11	This work
30	Lăzăreşti Nyírfürdő pool 2	1st Campaign	Debrecen	1.30	1.32	4.69	−1.91	nd	4.13E+11	This work
31	Ciucsângeorgiu mofetta	1st Campaign	Debrecen	0.77	0.14	0.39	−2.95	nd	5.50E+10	This work
32	Csiszárfürdő Băile Reci			0.796	0.796	0.99	nd	nd	3.89E+10	Frunzeti, 2013
33	Gyógyvizek Izvoarele Tămăduitoare			2.302	2.302	766.09	−3.25	−7.43	8.62E+09	Frunzeti, 2013
34	Apor lányok feredeje			2.438	2.438	2686.92	−3.72	−4.92	8.17E+09	Frunzeti, 2013
35	Torjai Büdös Cave (Stinky Cave)			2.199	2.199	583.84	−3.15	−7.48	1.17E+10	Frunzeti, 2013
36	Mikesfürdő–Hammas			2.242	2.242	656.89	−3.16	−9.87	9.47E+09	Frunzeti, 2013
37	Buffogó peat bog			2.274	2.274	2711.03	−2.77	−9.21	8.31E+09	Frunzeti, 2013
38	Tusnad			0.724	0.724	9.79	−4.7	−8.2	1.79E+12	Frunzeti, 2013

Table 3 *(continued)*

No.	Site	Campaign	Laboratory	R/Ra measured	R/Ra corrected	4He/ 20Ne	δ^{13} C–CO_2	δ18 O–CO_2	CO_2/3He	Source
39	Tusnad Nadas			1.66	1.66	1.28	−4.42	nd	7.19E+12	Vaselli et al., 2002
40	Lăzărești Nyir			2.95	2.95	7.7	nd	nd	2.79E+10	Vaselli et al., 2002
41	Sf Anna			3.18	3.18	25	nd	nd	3.20E+10	Vaselli et al., 2002
42	Puturosul			2.29	2.29	10.11	nd	nd	7.53E+10	Vaselli et al., 2002
43	Puturosul Sud			nd	nd	nd	−4.7	nd	nd	Vaselli et al., 2002
44	Bálványos			4.48	4.48	163	nd	nd	2.52E+10	Vaselli et al., 2002
45	Torjai Büdös Cave (Stinky Cave)			3.1	3.100	47.3	nd	nd	2.07E+10	Althaus et al., 2000
46	Apor lányok feredeje-Upper pool			3.12	3.120	151	nd	nd	1.72E+10	Althaus et al., 2000
47	Apor lányok feredeje-Lower pool			3.19	3.190	712	nd	nd	1.70E+10	Althaus et al., 2000
48	Bixad			1.47	1.470	0.67	nd	nd	nd	Althaus et al., 2000
49	Bixad			0.8	0.8	1.3	nd	nd	nd	Althaus et al., 2000
50	Tusnad Nagy			1.2	1.2	6.44	nd	nd	nd	Althaus et al., 2000
51	Balvanyos Carpatii			3.04	3.04	1.06	nd	nd	nd	Althaus et al., 2000

Note. $^3He/^4He$ ratios are normalized to the atmosphere and listed as R/R_a values corrected for the atmospheric He contamination (R/R_{ac}) considering the $^4He/^{20}Ne$ ratio; $\delta^{13}C–CO_2$ and $\delta^{18}O–CO_2$ are expressed in permil versus Vienna Pee Dee Belemnite. nd = not determined.

In constrast, crustal assimilation furnishes ^4He by interaction between magma and the whole rock. First, we investigated the likelihood that the magma aging model can interpret the low He isotopic signature in the fluids that outgas at Ciomadul volcano.

The $^3He/^4He$ ratio of the fluid inclusions of the Persani clinoproxene (5.95 $R_a \pm 0.01$) can be assumed to represent the mantle end member value beneath of the region. Thus, the primary magmas of Ciomadul could be also characterized by such isotope ratio. The Ciomadul dacites have U and Th concentrations of 3 and 15 ppm, respectively (Molnár et al., 2018, 2019; Vinkler et al., 2007). Using these data, the magma-aging model calculation yield $^3He/^4He$ ratio around 4.65 R_a after 30 kyr (Figure 6). Thus, this process alone cannot be responsible for the low He (approximately 3.1 R_a) isotopic signature of the Ciomadul fluids. Furthermore, if we assume the U (1.5 ppm) and Th (5.5 ppm) contents of the Persani basalts (Harangi et al., 2013), the magma-aging model is still not a viable process to provide the required ^4He addition and generate the low $^3He/^4He$ for Ciomadul gases.

The relatively low He isotopic ratio can also be explained by high-level crustal assimilation (e.g., van Soest et al., 2002), which has to also be evaluated. Assuming the U and Th amount of the typical upper crust, 2.7 and 10.5 ppm, respectively (Rudnick & Gao, 2003), and an age of 5 Ma, 3% of crustal assimilation could be sufficient to achieve the observed low He isotopic ratios. The Sr–Nd–O isotope compositions of the erupted magmas sensitively reflect such a process. Mason et al. (1996) published isotopic data for three samples of the Ciomadul volcanic system. They have distinct isotopic features compared to the calc-alkaline volcanic suite of the Calimani-Gurghiu-Harghita chain. Although the Sr–Nd isotopic data could suggest an assimilation and fractional crystallization process with 10–35% assimilation of flysch sediment, such a high crustal contamination is not feasible, based on the fairly low $\delta^{18}O$ values (6.3–7.1‰) of the phenocrysts from the dacites (Mason et al., 1996). Instead, they suggested that these isotopic characteristics could also be explained by source contamination from subduction-related fluids. In fact, the bulk-rock composition of the Ciomadul dacites has unique characteristics with high Sr, Ba (both showing typically >1,000 ppm),

Table 4
Isotopic Composition of Persani Clinopyroxene

Sample	He (mol/g)	Ne (mol/g)	He/Ar	$^4He/^{20}Ne$	R/R_a	R/R_{ac}
Cpx xenolith	4.06E-12	2.00E-15	0.92	2030.46	5.96	5.96
Cpx xenolith 2	3.81E-12	2.74E-15	0.91	1389.41	5.94	5.94

Note. $^3He/^4He$ ratios are normalized to the atmosphere and listed as R/R_a values ($R = {}^3He/{}^4He$ isotopic ratio of the sample, R_a = atmospheric $^3He/^4He = 1.382 \times 10^{-6}$) and corrected for the atmospheric helium contamination (R/R_{ac}) considering the $^4He/^{20}Ne$ ratio.

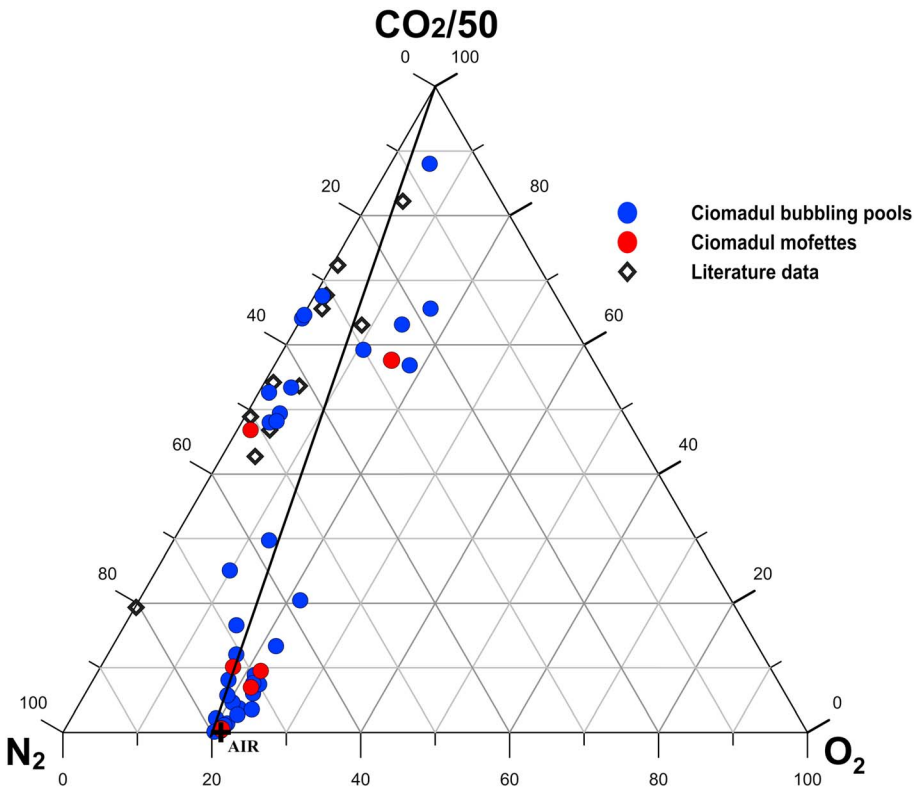

Figure 3. $CO_2/50–O_2–N_2$ triangular diagram showing the relative contents of components. The samples distribution highlights mixing between CO_2 and atmospheric gas species. Literature data from Ciomadul area are represented by data from Althaus et al., 2000, Frunzeti, 2013, and Vaselli et al., 2002).

and high K compositions and low concentrations of heavy rare Earth elements (Molnár et al., 2018, 2019; Seghedi et al., 1987; Vinkler et al., 2007). Furthermore, the high-Mg pargasitic amphiboles thought to have derived from the less differentiated magmas have also relatively high Ba content (Kiss et al., 2014). Thus, these peculiar compositional characters can be due to the nature of the magma source rather than magma differentiation processes. The elevated K, Sr, and Ba contents of the assumed mantle source of the Ciomadul primary magmas can be due to metasomatism, and this is in contrast what the peridotite xenoliths from the Persani volcanic field show (Vaselli et al., 1995). In fact, the He signature of the outgassed volatiles at Ciomadul resembles the values in fluids from other subduction-related volcanic systems (i.e., Italy, and Indonesia; Hilton et al., 1992; Martelli et al., 2004), where the mantle source regions seem to be contaminated by crustal material that added radiogenic ^{4}He and decreased the pristine He isotopic signature (Hilton et al., 2002).

Such a small-scale spatial heterogenity of the lithospheric mantle beneath this area can be explained by the closer location of Ciomadul to the collision front, where subduction is expected to have occurred during the Miocene up to around 11 Ma (Cloetingh et al., 2004; Mațenco et al., 2007; Royden et al., 1982; Seghedi et al., 2011). Such a scenario is not unique; Martelli et al. (2004) suggested that the relatively low He isotopic ratio in the volcanic rocks of Central Italy can be explained by magma source features (i.e., contribution of radiogenic He from metasomatic, subduction-related fluids and ingrowth of ^{4}He in the lithospheric mantle). We note that the $^{87}Sr/^{86}Sr$ isotopic ratio of the Ciomadul dacites and the highest $^3He/^4He$ isotopic values of the emitted gases plot into the same trend (Figure 5 in Martelli et al., 2004) what the Central Italian volcanic areas form.

In summary, considering the petrology of the Ciomadul volcanic products, the relatively low He isotope magmatic end member of the Ciomadul gases can be interpreted as due to magma-source characteristics, where the radiogenic He was added via subduction-related fluids and increased radioactive ingrowth following the metasomatism. However, a mixing between mantle-derived fluids with and SCLM He isotopic

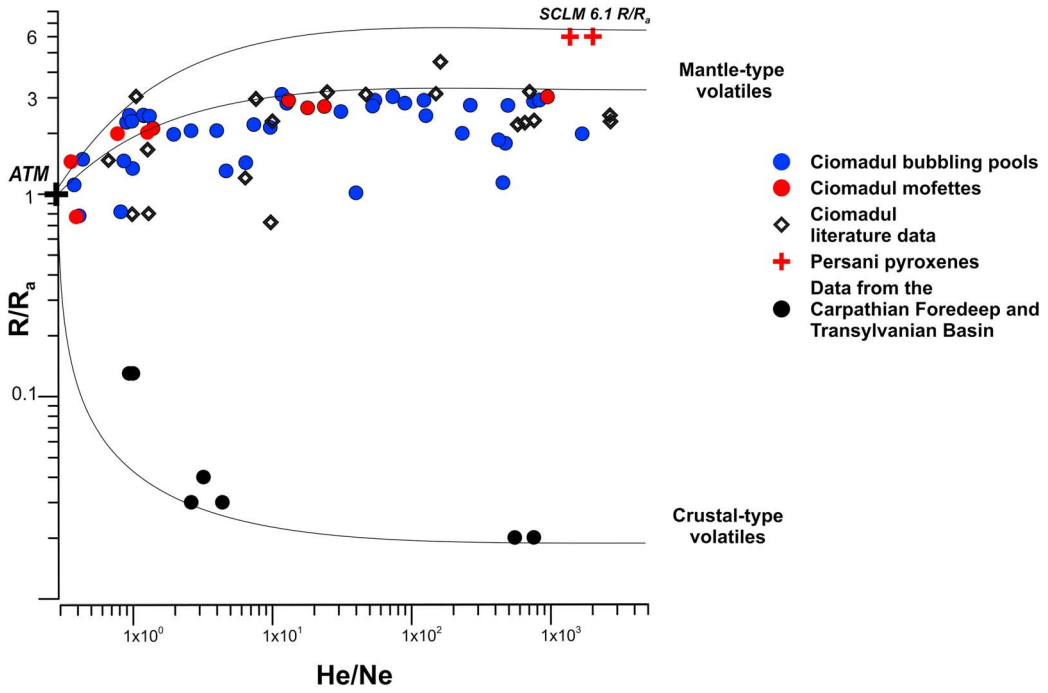

Figure 4. Helium isotopic ratios (R/R_a values) and $^4He/^{20}Ne$ relationships. The theoretical lines represent binary mixings of atmospheric He with mantle-originated and crustal He (Pik & Marty, 2008). The assumed end members for He-isotopic ratios and $^4He/^{20}Ne$ ratios are ATM (1 R_a, He/Ne = 0.318, Sano & Wakita, 1985); subcontinental European mantle is 6.1 ± 0.9 R_a and $^4He/^{20}Ne$ ratio = 1,000 (Gautheron & Moreira, 2002); typical crustal end member is 0.02 R_a and $^4He/^{20}Ne$ ratio = 1,000 (Sano & Marty, 1995). Literature data for comparison: data after Althaus et al. (2000), Baciu et al. (2007, 2017), Frunzeti (2013), and Vaselli et al. (2002). SCLM = subcontinental lithospheric mantle.

signature and ^{4}He-rich crustal fluids coming from shallow crustal layers should still be further explored as a possible process responsible of the low He isotopic ratios in the Ciomadul fluids. This likelihood will be discussed in the next section.

5.2. Sources and Origin of Carbon Dioxide

The carbon isotopic composition of CO_2 ($\delta^{13}C_{CO2}$) from the studied fluids range between −1.40‰ and −4.61‰ versus VPDB, consistent with previous measurements in the area (−2.77‰ to −4.70‰; Frunzeti, 2013; Sarbu et al., 2018; Vaselli et al., 2002). In the Pannonian Basin (Central Europe), the carbon isotopic composition of CO_2 gases shows values in a narrow range between −3‰ and −7‰ with an average value of −5‰ VPDB based on hundreds of measurements (Bräuer et al., 2016; Cornides, 1993; Palcsu et al., 2014; Sherwood-Lollar et al., 1997). These values are consistent with a mantle origin. In contrast, crustal-derived CO_2 is characterized by a $\delta^{13}C$ of about −25‰ in case of biogenic sedimentary source and around 0‰ considering thermometamorphism of limestone (Sano & Marty, 1995 and references therein). The Ciomadul gases overlap the range of mantle composition, even if some samples have more positive values that cannot be explained by the addition of a crustal biogenic component (Table 3 and Figures 7 and 8). To constrain the origin of CO_2 in the fluids emitted by the Ciomadul volcano, we used the relationship between the elemental ratio $CO_2/^3He$ and the isotopic signature $\delta^{13}C_{CO2}$ (Sano & Marty, 1995; Figure 7).

The $CO_2/^3He$ ratios of the Ciomadul gases are higher than 2×10^9, the expected mantle ratio (Marty & Jambon, 1987) and which suggests an addition of a crustal component. It is interesting that these ratios fall into the same trend as shown by volcanic and fumarolic gases measured at volcanic arcs, worldwide (Mason et al., 2017; Figures 8a and 8b). Almost all the Ciomadul samples fall close the mixing line between a mantle component and a limestone end member suggesting that mixing of the two sources could be the main process that controls the CO_2–^3He systematics in these fluids. In contrast, CO_2 fluids in the Transylvanian Basin, (Baciu et al., 2007, 2017) west of the volcano have distinct character and fall closer to the mantle-organic sediment mixing line. Rayleigh-type fractionation due to gas exsolution from water is not a

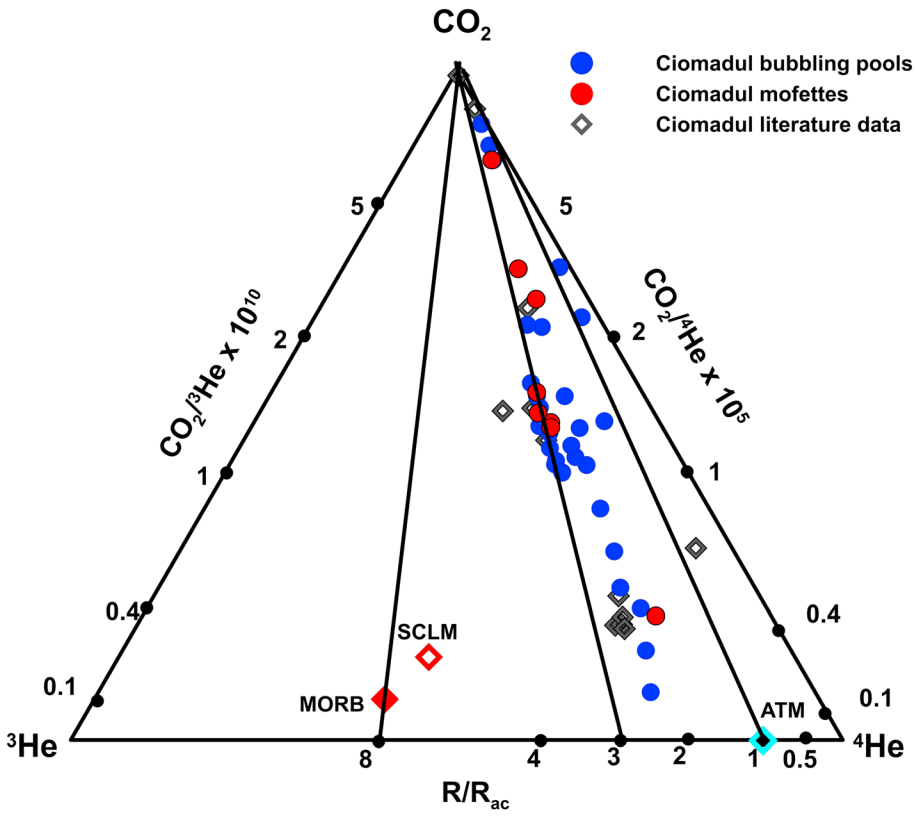

Figure 5. Ternary CO_2–^{3}He–^{4}He diagram of Ciomadul gas samples. Ciomadul literature data after Althaus et al. (2000), Frunzeti (2013) and Vaselli et al. (2002). For reference, we have plotted the MORB (Marty & Jambon, 1987) and SCLM values (Gautheron & Moreira, 2002). SCLM = subcontinental lithospheric mantle.

plausible process to produce the carbon isotopic signature and the $CO_2/^3$He of the studied fluids (Figure 7; Holland & Gilfillan, 2013; Roulleau et al., 2015). However, the $^{13}C_{CO2}$ values of most of the samples fall in the narrow range of −2‰ and −5‰, which is a typical signature for mantle-derived carbon. We obtain the same trend in the He isotopic ratios (R/R_a) versus $^{13}C_{CO2}$ (VPDB) plot (Figures 8a and 8b), where the Ciomadul samples clearly approach the mantle end member and overlap the isotopic values of many other volcanic systems related to subduction areas. Remarkably the Ciomadul samples show similarities in He–C isotopic composition with active and dormant volcanic regions (e.g., Italy and Indonesia).

The involvement of carbonatic component can be explained by mixing with fluids derived from thermometamorphic decomposition of carbonates in the flysch sedimentary pile or by mantle source contamination via subducted carbonatic material. The mantle source of the Ciomadul magmas is considered to be a metasomatic lithospheric mantle based on the compositional features of the dacitic rocks. The relatively low He isotopic ratio can be due to these source characteristics, whereas metasomatism was the result of slab-derived fluids during the Miocene subduction along the Eastern Carpathians followed by ingrowth of radiogenic He by radioactive decay. The Sr–Nd–O isotope data of the volcanic rocks do not support significant upper-level crustal contamination but rather crustal component addition to the source region via slab-derived fluid metasomatism (Mason et al., 1996). The combination of He and C isotopic data suggests that this crustal component consisted of decomposed subducted carbonate material as suggested also for the volcanic rocks in Italy, although addition of fluids from carbonate decomposition at shallow crustal level cannot be unambiguously excluded.

5.3. Relationship With the Deep Magmatic System

Dormant volcanoes pose a particular hazard to society since there is much less awareness about a possible eruption event. However, the scientific community is giving increased attention to these volcanoes and

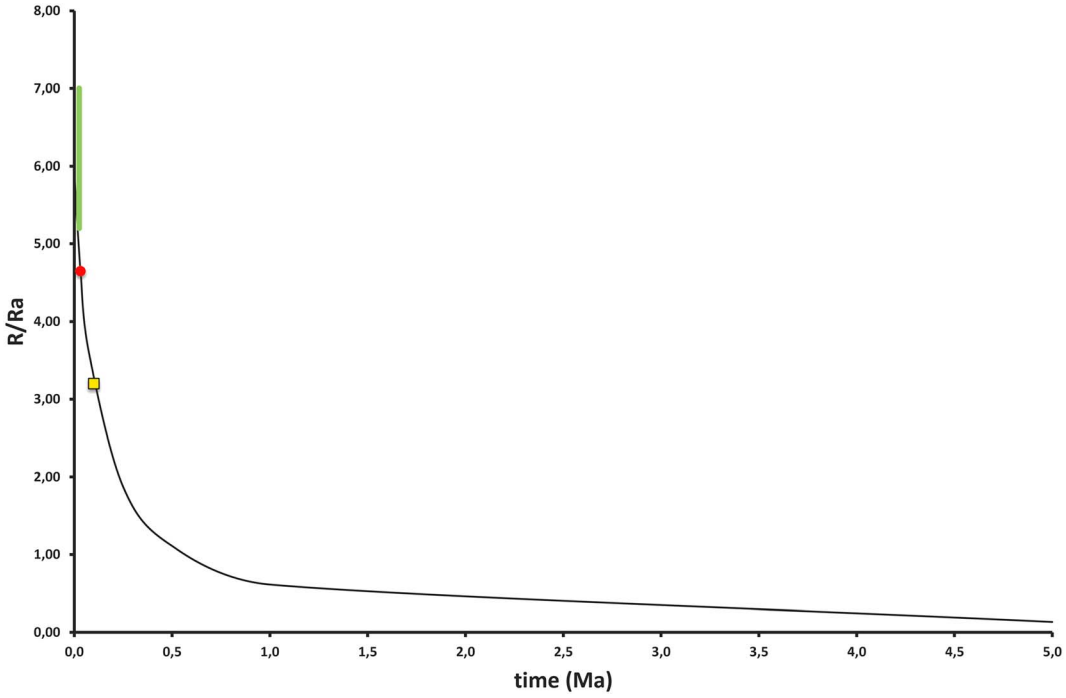

Figure 6. Magma aging evolution over time of the He isotopic signature (as R/R_a). The green bar is the range of the subcontinental lithospheric mantle He isotopic ratio (6.1 ± 0.9; Gautheron & Moreira, 2002). The red circle is the value or the $^3He/^4He$ (4.65 R_a) at 30 ka for the magma aging evolution. $^3He/^4He = 3.2$ is at 100 ka (yellow square).

the surrounding areas that are generally characterized by intense gas emissions (Burton et al., 2013, and references therein). Recent investigations highlighted the presence of an active plumbing system even below volcanoes which last erupted >10 kyr (e.g., Colli Albani, Italy; Trasatti et al., 2018; Uturuncu, Bolivia; Sparks et al., 2008; Comeau et al., 2015; Tatun, Taiwan; Konstantinou et al., 2007; Lin & Pu, 2016). Harangi, Novák, et al. (2015) suggested the term PAMS volcano, that is, volcano with potentially active magma storage for these long-dormant volcanoes, which have clear implication for a subvolcanic melt-bearing magma plumbing system. Ciomadul belongs to this category, since there are a number of observations suggesting that a melt-bearing magma body could still exist beneath it (Harangi, Novák, et al., 2015; Popa et al., 2012; Szakács & Seghedi, 2013). The isotopic composition of the emitted gases coupled to the high localized heat flow in the area of the Ciomadul vocano gives additional support to this interpretation.

This involves the similarities in the isotope composition of CO_2 and He of the gases emitted at the Ciomadul with those found in other active and dormant volcanic arc systems worldwide and their proposed high magmatic component. Furthermore, the Ciomadul volcanic system is characterized by relatively high CO_2 gas fluxes (Kis et al., 2017). This is consistent with the presence of a still-degassing magma below the Ciomadul system as inferred by geophysical investigations that recognized a low-resistivity and low-velocity anomaly in the crust, below the volcano (Harangi, Novák, et al., 2015; Popa et al., 2012) as well as petrologic observations suggesting the involvement of a mafic magma in the petrogenesis of the erupted dacite (Kiss et al., 2014). The measurements of U–Th and U–Pb spot ages on zircons suggest a long-standing magma storage that could go back as far as about 350 ka (Harangi, Lukács, et al., 2015; Lukács et al., 2018). Molnár et al. (2018, 2019) presented a detailed eruption chronology for the Ciomadul lava dome field involving the Ciomadul volcanic complex and emphasized that volcanic activity could be renewed even after long (>100 kyr) repose times. Several tens-of-kiloyears quiescence periods between the active phases have also been pointed out also during the evolution of the Ciomadul volcanic complex (Harangi, Lukács, et al., 2015; Molnár et al., 2019). However, the zircon U–Th and U–Pb ages suggest that crystallization was ongoing also during the long quiescence periods, that is, there was an active magma storage beneath the apparently inactive volcano This suggests a long-standing felsic upper-crustal crystal mush system underlain by a mafic

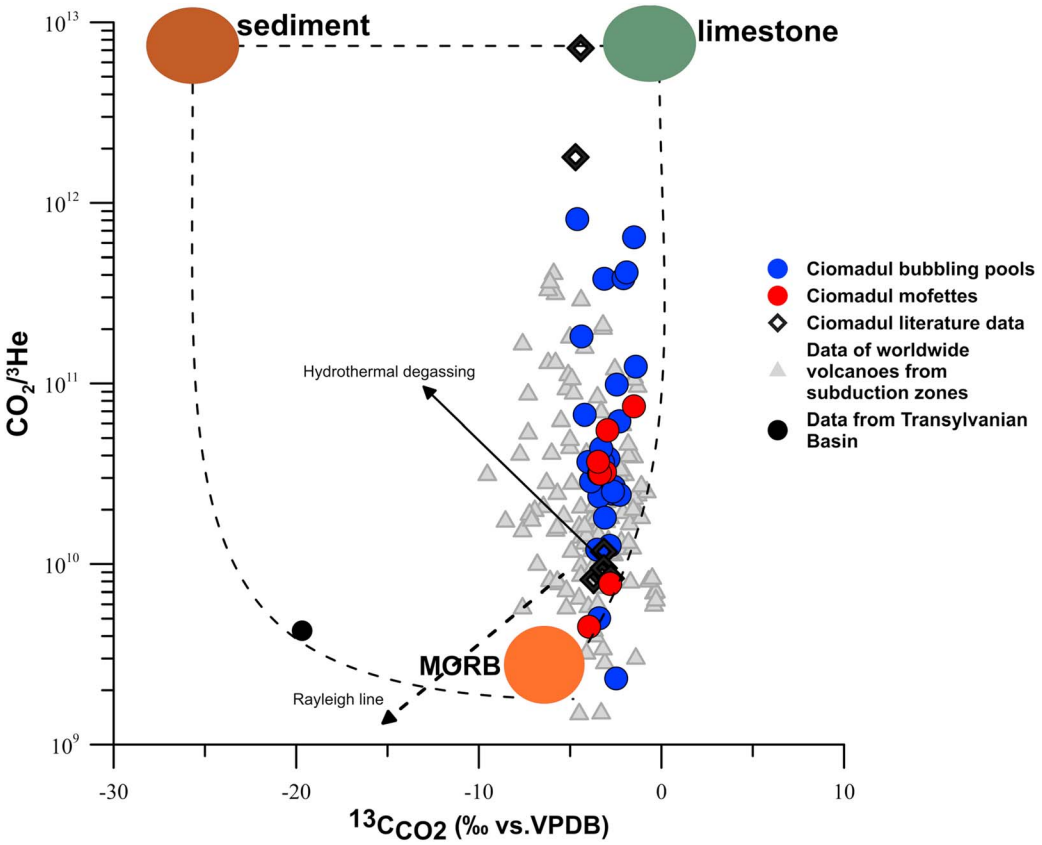

Figure 7. Correlation diagram of Sano & Marty (1995) plotting $CO_2/^3He$ versus $^{13}C_{CO2}$ (VPDB) of Ciomadul gas emissions. Lines show the theoretical mixing between a mantle end member and a crustal end member represented by marine limestone and organic sediment carbon. Ciomadul samples are showing a trend of mixing between fluids of mantle origin and fluids originating from limestone. Literature data for comparison: data after Althaus et al. (2000), Baciu et al. (2007, 2017), and Frunzeti et al. (2013) and Vaselli et al. (2002). Data on individual volcanoes worldwide are based on the compilation of Mason et al. (2017), by Allard (1983), Marty and Giggenbach (1990), Poorter et al. (1991), Varekamp et al. (1992), Sturchio et al. (1993), Sano et al. (1994), Sano and Marty (1995), Tedesco et al. (1995), Hilton (1996), Sano and Williams (1996), Allard et al. (1997), Fischer et al. (1998), van Soest et al. (1998), Pedroni et al. (1999), Lewicki et al. (2000), Parello et al. (2000), Favara et al. (2001), Snyder et al. (2001), Shaw et al. (2003), Symonds et al. (2003), Jaffe et al. (2004), Capasso et al. (2005), Carapezza et al. (2007), de Leeuw et al. (2007), Werner et al. (2009), Capaccioni et al. (2011), Tassi et al. (2011), Aguilera et al. (2012), Melián et al. (2012), and Caracausi et al. (2013).

hot zone in the lower crust, as has already been suggested by petrologic interpretations (Kiss et al., 2014). The diverse amphibole compositions in the dacites are consistent with a polybaric magma evolution, that is, with transcrustal magma storage (Cashman et al., 2017; Sparks & Cashman, 2017) comprising ephemeral melt-dominated bodies, that is, magma chambers at various depths. In addition, fluid-gas accumulation zones can also have developed within this magma storage (Christopher et al., 2015; Sparks & Cashman, 2017). Thus, a possible source of the CO_2 gases could be these fluid entrapment zones within the crystal mush during quiescent period. However, gas emission is more common around the Ciomadul volcanic complex and significantly lower within the volcano itself (Kis et al., 2017). Allard et al. (1991), and Edmonds (2008) pointed out that stronger degassing around the volcanic edifice is not uncommon in volcanic regions. An alternative source of the CO_2 gases could be mafic magma residing at deeper level, possibly at the lower crust. Indeed, the occurrence of high-Mg minerals, such as olivine, clinopyroxene, and orthopyroxene in the dacites (Kiss et al., 2014; Vinkler et al., 2007) suggests that mafic magma also played an important role in the magma evolution. Harangi, Novák, et al. (2015) detected a lower crustal low resistivity anomaly, which might represent the mafic magma accumulation. Thus, we propose that most of the CO_2 gases could come directly from the presumed mafic-magma accumulation zone at the lower crust through fractures (Kis et al., 2017), whereas only limited amount of gases is derived from the mushy magma storage.

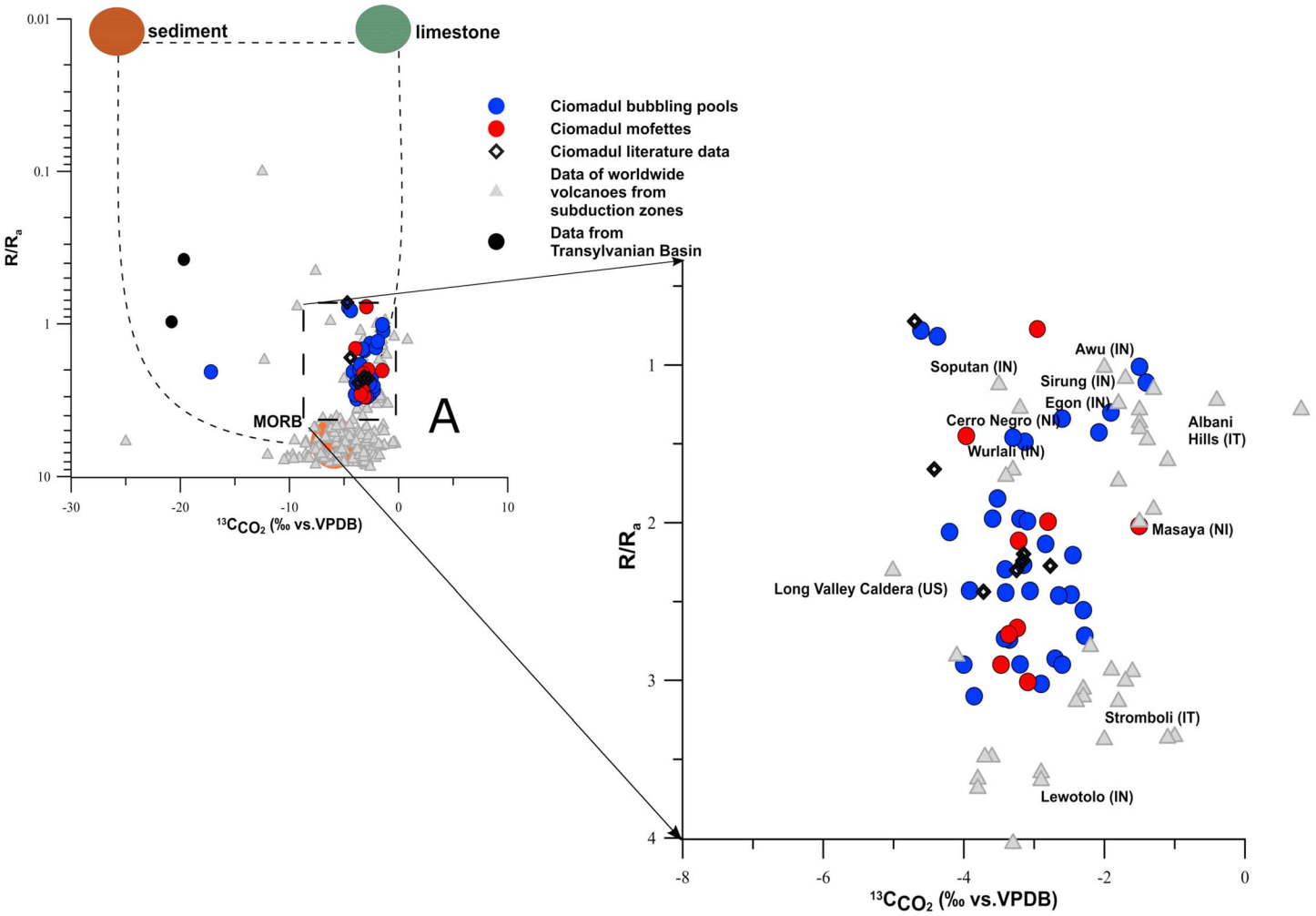

Figure 8. (a, b) Correlation diagram (Ciotoli et al., 2013) plotting He isotopic ratios (R/R_a) versus $^{13}C_{CO2}$ (VPDB) of Ciomadul gas emissions. Lines show the theoretical mixing between a mantle end member (MORB) and a crustal end member represented by marine limestone and organic sediment carbon (Sano & Marty, 1995, Sherwood-Lollar et al., 1997). Literature data for comparison: data after Althaus et al. (2000), Vaselli et al. (2002), Baciu et al. (2007, 2017), Frunzeti et al. (2013). Data on individual volcanoes worldwide are based on the compilation of Mason et al. (2017) from the data presented by Allard (1983), Marty and Giggenbach (1990), Poorter et al. (1991), Varekamp et al. (1992), Sturchio et al. (1993), Sano et al. (1994), Sano and Marty (1995), Tedesco et al. (1995), Hilton (1996), Sano and Williams (1996), Allard et al. (1997), Fischer et al. (1998), van Soest et al. (1998), Pedroni et al. (1999), Lewicki et al. (2000), Parello et al. (2000), Favara et al. (2001), Snyder et al. (2001), Shaw et al. (2003), Symonds et al. (2003), Jaffe et al. (2004), Capasso et al. (2005), Carapezza et al. (2007), de Leeuw et al. (2007), Werner et al. (2009), Capaccioni et al. (2011), Tassi et al. (2011), Aguilera et al. (2012), Melián et al. (2012), and Caracausi et al., 2013.

Vaselli et al. (2002) already suggested that the emitted gases in Southern Harghita could have a magmatic component. Based on our new measurements, we support this interpretation, particularly in the area of Ciomadul volcano. Assuming that a deep-seated mafic magma body can be the main source of the CO_2 gases and considering that it is characterized by relatively low $^3He/^4He$ isotope signature (3.1 R_a) inherited by the mantle source region, we can use this value to calculate the relative magmatic component of the emitted gases (Sano & Wakita, 1985). If no interaction with crustal fluids occurred, the magmatic component in the gases could exceed even the 80%. Remarkably, we obtained such high values for the areas having a larger diffusive CO_2 flux. This high magmatic He content of the gases is not unique and resembles what Trasatti et al. (2018) proposed for Colli Albani volcanic complex, another long-dormant volcanic field, where they assumed more than 80% mantle-derived component in the emitted CO_2 gases. However, the magmatic component can be lower, if interaction between the ascending gases with crustal gases occurred at shallow crustal depth, a possibility what we cannot test at this stage but requires further studies.

6. Conclusions

We investigated 31 gas emissions at the Ciomadul volcano, a long-dormant PAMS volcano in Eastern-Central Europe, to constrain the origin of the emitted volatiles and the possible processes that modify their chemistry during the transfer of these fluids toward the surface. The carbon and helium isotopic compositions provide evidence for a significant magmatic component. Our study shows a clear magmatic component in the emitted fluids and the highest values correspond to the area characterized by the highest CO_2 flux from soil, so the high fluxes can be associated with the highest contribution of volatiles derived from a magma body.

The relatively large CO_2 gas emission and significant magmatic component of the gases are consistent with geophysical and petrologic models (Harangi, Lukács, et al., 2015; Harangi, Novák, et al., 2015; Popa et al., 2012), that a degassing magmatic intrusion could still exist beneath Ciomadul. A long-standing silicic crystal mush body should be developed in the shallow crust, while a mafic magma accumulation zone is inferred at the lower crustal level. The magmatic gases could be derived either from a deep mafic magma and/or from the volatile accumulation zones developed in the shallow crustal felsic-crystal mush body. Petrology and geochemistry of the erupted dacitic magma imply that upper crustal contamination played no or subordinate role and the primary magmas could have derived from a mantle source contaminated by subduction-related fluids that is consistent with the He and C isotope composition of the gases emitted at Ciomadul volcano. Thus, a magma source with relatively low He isotope value (3.10 R_a), similar to what was proposed for volcanic systems in central Italy seems to be viable beneath Ciomadul. This differs from the SCLM value detected at the nearby Persani volcanic field (Althaust et al., 1998; this study) and also in the Pannonian basin (Bräuer et al., 2016; Cornides, 1993; Palcsu et al., 2014) and requires a spatially variable modified lithospheric mantle even a small scale. The isotopic composition (He and CO_2) of the emitted volatiles implies interaction of crustal gases to varying degrees, although some of them could reach the surface without major modification.

Acknowledgments
Information regarding the support of the conclusions of this work can be found in the tables and within the text. This research on the Ciomadul volcano was initiated during the MTA Postdoctoral Fellowship of Boglárka-Mercedesz Kis and belongs to the scientific project supported by the OTKA (Hungarian National Research Fund) K116528. The research was also supported by the European Union and the State of Hungary, cofinanced by the European Regional Development Fund in the project of GINOP-2.3.2-15-2016-00009 "ICER," and we acknowledge the support of the Deep Energy Community and Reservoirs and Fluxes Community of the Deep Carbon Observatory. Thorough reviews and constructive comments provided by Emilie Roulleau and Daniele Pinti helped considerably to clarify the ideas described in the paper. We thank Timothy Jull who provided a final polishing of the English of the manuscript.

References

Aguilera, F., Tassi, F., Darrah, T., Moune, S., & Vaselli, O. (2012). Geochemical model of magmatic-hydrothermal system at the Lastarria volcano, Northern Chile. *Bulletin of Volcanology*, *74*(1), 119–134. https://doi.org/10.1007/s00445-011-0489-5

Agusto, M., Tassi, F., Caselli, A. T., Vaselli, O., Rouwet, D., Capaccioni, B., et al. (2013). Gas geochemistry of the magmatic-hydrothermal fluid reservoir in the Copahue-Cavihue Volcanic Complex (Argentina). *Journal of Volcanology and Geothermal Research*, *257*, 44–56. https://doi.org/10.1016/j.jvolgeores.2013.03.003

Aiuppa, A., Moretti, R., Federico, C., Giudice, G., Gurrieri, S., Liuzzo, M., et al. (2007). Forecasting Etna eruptions by real-time observation of volcanic gas composition. *Geology*, *35*(12), 1115–1118. https://doi.org/10.1130/G24149A.1

Allard, P. (1983). The origin of hydrogen, carbon, suplhur, nitrogen and rare gases in volcanic exhalations: Evidence from isotope geochemisty. In H. Tazieff, & J. C. Sabroux (Eds.), *Forecasting Volcanic Events*, (pp. 337–386). Elsevier: Amsterdam.

Allard, P., Carbonelle, J., Dajlevic, D., Le Bronec, J., Morel, P., Robe, M. C., et al. (1991). Eruptive and diffuse emissions of CO_2 from Mount Etna. *Nature*, *351*(6325), 387–391. https://doi.org/10.1038/351387a0

Allard, P., Jean-Baptiste, P., D'Alessandro, W., Parello, F., Parisi, B., & Flehoc, C. (1997). Mantle-derived helium and carbon in groundwaters and gases of Mount Etna, Italy. *Earth and Planetary Science Letters*, *148*(3-4), 501–516. https://doi.org/10.1016/S0012-821X(97)00052-6

Althaus, T., Niedermann, S., & Erzinger, J. (2000). Noble gas studies of fluids and gas exhalations in the East Carpathians, Romania. *Chemie der Erde*, *60*, 189–207.

Althaust, A., Niedermann, S., & Erzinger, J. (1998). Noble gas in ultramafic mantle xenoliths in the Persani Mountains, Transylvanian Basin, Romania. *Mineralogical Magazine*, *62A*(1), 43–44. https://doi.org/10.1180/minmag.1998.62A.1.23

Baciu, C., Caracausi, A., Etiope, G., & Italiano, F. (2007). Mud volcanoes and methane seeps in Romania: Main features and flux. *Annals of Geophysics*, *50*, 4. https://doi.org/10.4401/ag-4435

Baciu, C., Ionescu, A., & Etiope, G. (2017). Hydrocarbon seeps in Romania: Gas origin and release to the atmosphere. *Marine and Petroleum Geology*, *89*(1), 130–143. https://doi.org/10.1016/j.marpetgeo.2017.06.015

Bănciă, I. (1958). *Geology of the Eastern Carpathians*. Editura Stiintifica: Bucharest.

Barry, P. H., Hilton, D. R., Fischer, T. P., de Moor, J. M., Mangasini, F., & Ramirez, C. (2013). Helium and carbon isotope systematic of cold "mazucu" CO_2 vents and hydrothermal gases and fluid from Rungwe Volcanic Province, southern Tanzania. *Chemical Geology*, *339*, 141–156. https://doi.org/10.1016/j.chemgeo.2012.07.003

Barry, P. H., Hilton, D. R., Füri, E., Halldórsson, S. A., & Grönvold, K. (2014). Carbon isotope and abundance systematics of Icelandic geothermal gases, fluids and subglatial basalts with implications from mantle plume-related CO_2 fluxes. *Geochimica et Cosmochimica Acta*, *134*, 74–99. https://doi.org/10.1016/j.gca.2014.02.038

Berszán, J., Cs, J., Jánosi, K., Kristály, F., Péter, É., Szakáll, S., & Ütő, G. (2009). *The mineral waters of Szeklerland*. Tipographic: Miercurea Ciuc. (In Hungarian)

Bräuer, K., Geissler, W. H., Kämpf, H., Niedermann, S., & Rman, N. (2016). Helium and carbon isotope signatures of gas exhalations in the westernmost part of the Pannonian Basin (SE Austria/NE Slovenia): Evidence for active litospheric mantle degassing. *Chemical Geology*, *422*, 60–70. https://doi.org/10.1016/j.chemgeo.2015.12.016

Bräuer, K., Kämpf, H., Niedermann, S., & Strauch, G. (2018). Monitoring of helium and carbon isotopes in the western Eger Rift area (Czech Republic): Relationships with the 2014 seismic activity and indications for recent (2000-2016) magmatic unrest. *Chemical Geology*, *482*, 131–145. https://doi.org/10.1016/j.chemgeo.2018.02.017

Bräuer, K., Kämpf, H., Niedermann, S., Strauch, G., & Tesar, J. (2008). Natural laboratory NW Bohemia: Comprehensive fluid studies between 1992 and 2005 used to trace geodynamic processes. *Geochemistry, Geophysics, Geosystems*, *9*, Q04018. https://doi.org/10.1029/2007GC001921

Burton, M. R., Sawyer, G. M., & Granieri, D. (2013). Deep carbon emissions from volcanoes. *Reviews in Mineralogy and Geochemistry*, *75*(1), 323–354. https://doi.org/10.2138/rmg.2013.75.11

Caliro, S., Viveiros, F., Chiodini, G., & Ferreira, T. (2015). Gas geochemistry of hydrothermal fluids of the S. Miguel and Terceira Islands, Azores. *Geochimica et Cosmochimica Acta*, *168*, 43–57. https://doi.org/10.1016/j.gca.2015.07.009

Capaccioni, B., Aguilera, F., Tassi, F., Darrah, T., Poreda, R., & Vaselli, O. (2011). Geochemical and isotopic evidences of magmatic inputs in the hydrothermal reservoirs feeding the fumarolic discharges on Tacora volcano (Northern Chile). *Journal of Volcanology and Geothermal Research*, *208*(3-4), 77–85. https://doi.org/10.1016/j.jvolgeores.2011.09.015

Capasso, G., Carapezza, M., Federico, C., Inguaggiato, S., & Rizzo, A. (2005). Geochemical monitoring of the helium isotopic composition of fumarole gases and thermal waters. *Bulletin of Volcanology*, *68*(2), 118–134. https://doi.org/10.1007/s00445-005-0427-5

Capasso, G., Favara, R., Grassa, F., Inguaggiato, S., & Longo, M. (2005). On-line technique for preparation and measuring stable carbon isotope of total dissolved inorganic carbon in water samples ($\delta^{13}C_{TDIC}$). *Annals of Geophysics*, *48*(1), 159–166.

Caracausi, A., Favara, R., Giammanco, S., Italiano, F., Paonita, A., Pecoraino, G., & Rizzo, A. (2003). Mount Etna: Geochemical signals of magma ascentand unusually extensive plumbing system. *Geophysical Research Letters*, *30*(2), 1057. https://doi.org/10.1029/2002GL015463

Caracausi, A., Martelli, M., Nuccio, P. M., Paternoster, M., & Stuart, F. M. (2013). Active degassing of mantle-derived fluid: A geochemical study along the Vulture line, southern Apenninnes (Italy). *Journal of Volcanology and Geothermal Research*, *253*, 65–74. https://doi.org/10.1016/j.jvolgeores.2012.12.005

Caracausi, A., Nuccio, P. M., Favara, R., Nicolosi, M., & Paternoster, M. (2009). Gas hazard assessment at the Monticchio crater lakes of Mt. Vulture, a volcano in southern Italy. *Terra Nova*, *21*, 83–87. https://doi.org/10.11111/1365-3121.200800858

Caracausi, A., Paternoster, M., & Nuccio, P. M. (2015). Mantle CO_2 degassing at Mt. Vulture volcano (Italy): Relationship between CO_2 outgassing of volcanoes and the time of their last eruption. *Earth and Planetary Science Letters*, *411*, 268–280. https://doi.org/10.1016/j.epsl.2014.11.049

Carapezza, M. L., Badalamenti, B., Cavarra, L., & Scalzo, A. (2003). Gas hazard assessment in a densely inhabited area of Colli Albani Volcano (Cava dei Selci, Roma). *Journal of Volcanology and Geothermal Research*, *123*(1-2), 81–94. https://doi.org/10.1016/S0377-0273(03)00029-5

Carapezza, M. L., Barbieri, F., Ranaldi, M., Ricci, T., Tarchini, L., Barrancos, J., et al. (2012). Hazardous gas emissions from the flanks of the quiescent Colli Albani volcano (Rome, Italy). *Applied Geochemistry*, *27*(9), 1767–1782. https://doi.org/10.1016/j.apgeochem.2012.02.012

Carapezza, M. L., & Tarchini, L. (2007). Accidental gas emission from shallow pressurized aquifers at Alban Hills volcano (Rome, Italy): Geochemical evidence of magmatic degassing? *Journal of Volcanology and Geothermal Research*, *165*(1-2), 5–16. https://doi.org/10.1016/j.jvolgeores.2007.04.008

Cardellini, C., Chiodini, G., Frondini, F., Avino, R., Bagnato, E., Caliro, S., et al. (2017). Monitoring diffuse volcanic degassing during volcanic inrest: The case of Campi Flegrei (Italy). *Scientific Reports*, *7*(1), 6757. https://doi.org/10.1038/s41598-017-06941-2

Cashman, K. V., Sparks, S., & Blundy, J. D. (2017). Vertically extensive and unstable magmatic systems: An unified view of igneous processes. *Science*, *355*, 6331. https://doi.org/10.1126/eaay3055

Chiodini, G., Cardellini, C., Amato, A., Boschi, E., Caliro, S., Frondini, F., & Ventura, G.(2004). Carbon dioxide earth degassing and seismogenesis in central and southern Italy. *Geophysical Research Letters*, *31*, L07615. https://doi.org/10.1029/2004gl019480

Christopher, T., Edmonds, M., Humphreys, M. C. S., & Herd, R. A. (2010). Volcanic gas emissions from Soufriere Hills Volcano, Montserrat 1995-2009, with implications for mafic magma supply and degassing. *Geophysical Research Letters*, *37*, L00E04. https://doi.org/10.1029/2009GL041325

Christopher, T. E., Blundy, J., Cashman, K., Cole, P., Edmonds, M., Smith, P. J., et al. (2015). Crustal-scale degassing due to magma system destabilization and magma-gas decoupling at Soufriere Hills Volcano, Montserrat. *Geohemistry, Geophysics, Geosystems*, *16*, 2797–2811. https://doi.org/10.1002/2015GC005791

Ciotoli, G., Etiope, G., Florindo, F., Marra, F., Ruggiero, L., & Sauer, P. E. (2013). Sudden deep gas eruption nearby Rome's airport of Fiumicino. *Geophysical Research Letters*, *40*, 5632–5636. https://doi.org/10.1002/2013GL058132

Cloetingh, S. A. P. L., Burov, E., Matenco, L., Toussaint, G., Bertotti, G., Andriessen, P. A. M., et al. (2004). Thermo-mechanical controls on the mode of continental collision in the SE Carpathians (Romania). *Earth and Planetary Science Letters.*, *218*(1–2), 57–76. https://doi.org/10.1016/S0012-821X(03)00645-9

Comeau, J. M., Unsworth, M. J., & Cordell, D. (2016). New constraints on the magma distribution and composition beneath Volcan Uturuncu and the southern Bolivian Altiplano from magnetotelluric data. *Geosphere*, *12*(5), 1391–1421. https://doi.org/10.1130/GES01277.1

Comeau, M. J., Unsworth, M. J., Ticona, F., & Sunagua, M. (2015). Magnetotelluric images of magma distribution beneath Volcano Uturuncu, Bolivia: Implications for magma dynamics. *Geology*, *43*(3), 243–246. https://doi.org/10.1130/G36258.1

Condomines, M., Gronvold, K., Hooker, P. J., Muehlenbachs, K., O'Nions, R. K., Oskarsson, N., & Oxburgh, E. R. (1983). Helium, oxygen, strontium and neodymium isotopic relationships in Iceland volcanics. *Earth and Planetary Science Letters*, *66*, 125–136. https://doi.org/10.1016/0012-821X(83)90131-0

Cornides, I. (1993). Magmatic carbon dioxide at the crust's surface in the Carpathian Basin. *Geochemical Journal*, *27*(4/5), 241–249. https://doi.org/10.2343/geochemj.27.241

Correale, A., Martelli, M., Paonita, A., Rizzo, A., Brusca, L., & Scribano, V. (2012). New evidence of mantle heterogeneity beneath the Hyblean Plateau (southeast Sicily, Italy) as inferred from noble gases and geochemistry of ultramafic xenoliths. *Lithos*, *132-133*, 70–81. https://doi.org/10.1016/j.lithos.2011.11.007

Csontos, L., Nagymarosy, A., Horváth, D., & Kovác, M. (1992). Tertiary evolution of the intra Carpathian area: A model. *Tectonophysics*, *208*(1-3), 221–241. https://doi.org/10.1016/0040-1951(92)90346-8

de Leeuw, G., Hilton, D., Fischer, T. P., & Walker, J. (2007). The He-CO_2 isotope and relative abundance characteristics of geothermal fluids in El Salvador and Honduras: New constraints on volatile mass balance of the Central American Volcanic Arc. *Earth and Planetary Science Letters*, *258*(1-2), 132–146. https://doi.org/10.1016/j.epsl.2007.03.028

Demetrescu, C., & Andreescu, M. (1994). On the thermal regime of some tectonic units in a continental collision environment in Romania. *Tectonophysics*, *230*(3-4), 265–276. https://doi.org/10.1016/0040-1951(94)90140-6

Downes, H., Seghedi, I., Szakács, A., Dobosi, G., James, D. E., Vaselli, O., et al. (1995). Petrology and geochemistry of late Tertiary/Quaternarymafic alkaline volcanism in Romania. *Lithos*, *35*(1-2), 65–81. https://doi.org/10.1016/0024-4937(95)91152-Y

Edmonds, M. (2008). New geochemical insights into volcanic degassing. *Philosophical Transactions of the Royal Society A*, *366*, 4559–4579. https://doi.org/10.1098/stra.2008.0185

Falus, G., Tommasi, A., Ingrin, J., & Cs, S. (2008). Deformation and seismic anisotropy of the lithospheric mantle in the southeastern Carpathians inferred from the study of mantle xenoliths. *Earth and Planetary Science Letters*, *272*(1-2), 50–64. https://doi.org/10.1016/j.epsl.2008.04.035

Farrar, C. D., Sorey, M. L., Evans, W. C., Howle, J. F., Kerr, B. D., Kennedy, B. M., et al. (1995). Forest-killing diffuse CO_2 emission at Mammoth Mountain as a sign of magmatic unrest. *Nature*, *376*(6542), 675–678. https://doi.org/10.1038/376675a0

Favara, R., Giammanco, S., Inguaggiato, S., & Pecoraino, G. (2001). Preliminary estimate of CO_2 output from Pantelleria Island volcano (Sicily, Italy): Evidence for active mantle degassing. *Applied Geochemistry*, *16*(7-8), 883–894. https://doi.org/10.1016/S0883-2927(00)00055-X

Fischer, T., Horalek, J., Hrubcova, P., Vavrycuk, V., Bräuer, K., & Kämpf, H. (2014). Intra-continental earthquake swarms in West-Bohemia and Vogtland: A review. *Tectonophysics*, *611*, 1–27. https://doi.org/10.1016/j.tecto.2013.11.001

Fischer, T. P. (2008). Fluxes of volatiles (H_2O, CO_2, N_2, Cl, F) from arc volcanoes. *Geochemical Journal*, *42*(1), 21–38. https://doi.org/10.2343/geochemj.42.21

Fischer, T. P., Giggenbach, W. F., Sano, Y., & Williams, S. N. (1998). Fluxes and sources of volatiles discharged from Kudryavy, a subduction zone volcano, Kurile Islands. *Earth and Planetary Science Letters*, *160*(1-2), 81–96. https://doi.org/10.1016/S0012-821X(98)00086-7

Frunzeti, N. (2013). *Geogenic emissions of greenhouse gases in the Southern part of the Eastern Carpathians, (Doctoral dissertation)*, Retrieved from Faculty of Environmental Science and Engineering. Cluj-Napoca: Babes-Bolyai University. (In Romanian)

Gautheron, C., & Moreira, M. (2002). Helium signature of the subcontinental lithospheric mantle. *Earth and Planetary Science Letters*, *199*(1-2), 39–47. https://doi.org/10.1016/S0012-821X(02)00563-0

Grasu, C., Catana, C., & Bobos, I. (1996). *Petrology of the flysch formations in the inner Carpathians*. Editura Tehnica: Bucharest.

Harangi, S., Sági, T., Seghedi, I., & Ntaflos, T. (2013). Origin of basaltic magmas of Perşani volcanic field, Romania: A combined whole rock and mineral scale investigation. *Lithos*, *180-181*, 43–57. https://doi.org/10.1016/j.lithos.2013.08.025

Harangi, S., Lukács, R., Schmitt, A. K., Dunkl, I., Molnár, K., Kiss, B., et al. (2015). Constraints on the timing of Quaternary volcanism and duration of magma residence at Ciomadul volcano, east-central Europe, from combined U-Th/He and U-Th zircon geochronology. *Journal of Volcanology and Geothermal Research*, *301*, 66–80. https://doi.org/10.1016/j.jvolgeores.2015.05.002

Harangi, S., Molnár, M., Vinkler, A. P., Kiss, B., Jull, A. J. T., & Leonard, A. E. (2010). Radiocarbon dating of the last volcanic eruptions of Ciomadul volcano, Southeast Carpathians, eastern-central Europe. *Radiocarbon*, *52*(3), 1498–1507. https://doi.org/10.1017/S0033822200046580

Harangi, S., Novák, A., Kiss, B., Seghedi, I., Lukács, R., Szarka, L., et al. (2015). Combined magnetotelluric and petrologic constrains for the nature of the magma storage system beneath the Late Pleistocene Ciomadul volcano (SE Carpathians). *Journal of Volcanology and Geothermal Research*, *290*, 82–96. https://doi.org/10.1016/j.jvolgeores.2014.12.006

Hilton, D. (1996). The helium and carbon isotope systematics of a continental geothermal system: Results from monitoring studies at Long Valley caldera (California, U.S.A.). *Chemical Geology*, *127*(4), 269–295. https://doi.org/10.1016/0009-2541(95)00134-4

Hilton, D. R., Fischer, T. P., & Marty, B. (2002). Noble gases and volatile recycling at subduction zones. *Review in Mineralogy and Geochemistry*, *47*(1), 319–370. https://doi.org/10.2138/rmg.2002.47.9

Hilton, D. R., Hoogewerff, J. A., Van Bergen, M. J., & Hammerschmidt, K. (1992). Mapping magma sources in the east Sunda-Banda arcs, Indonesia: Constraints from helium isotopes. *Geochimica et Cosmochimica Acta*, *56*(2), 851–859. https://doi.org/10.1016/0016-7037(92)90105-R

Holland, G., & Gilfillan, S. (2013). Application of the noble gases to the variability of CO2 storage. In P. Burnad (Ed.), *The noble gases as geochemical tracers*, (pp. 177–223). Springer, Berlin-Heidelberg.

Horváth, F., Bada, G., Windhoffer, G., Csontos, L., Dombradi, E., Dövényi, P., et al. (2006). The geodynamic atlas of the Pannonian Basin: Euro-conform maps and explanations. *Magyar Geofizika*, *47*(4), 133–137. (In Hungarian)

Ianovici, V., & Rădulescu, D. (1968). *Geological map 1:200000 L-35-XIV, 20th Sheet-Odorhei*. Bucharest: Geological Institute of Romania. (In Romanian)

Ismail-Zadeh, A., Matenco, L., Radulian, M., Cloetingh, S., & Panza, S. (2012). Geodynamics and intermediate-depth seismicity in Vrancea (the south-eastern Carpathians): Current state-of-the art. *Tectonophysics*, *530-531*, 50–79. https://doi.org/10.1016/j.tecto.2012.01.016

Italiano, F., Kis, B. M., Baciu, C., Ionescu, A., Harangi, S., & Palcsu, L. (2017). Geochemistry of dissolved gases from the Eastern Carpathians-Transylvanian Basin boundary. *Chemical Geology*, *469*, 117–128. https://doi.org/10.1016/j.chemgeo.2016.12.019

Jaffe, L. A., Hilton, D. R., Fischer, T. P., & Hartono, U. (2004). Tracing magma sources in an arc-arc collision zone: Helium and carbon isotope and relative abundance systematics of theSanhihe Arc, Indonesia. *Geochemistry, Geophysics, Geosystems*, *5*, Q04J10. https://doi.org/10.1029/2003GC000660

Jánosi, C. (1980). *The hydrogeology of the inferior part of the Ciuc Basin, with focus on the mineral water springs*. (Doctoral dissertation). Retrieved from Faculty of Biology and Geology. Cluj-Napoca: Babes-Bolyai University. (In Romanian)

Jánosi Cs., Berszán J. & Péter É. (2011). The mineral baths of Ciomadul Mountains, Acta Siculica 2011, Miercurea Ciuc, (pp.41-56) In Hungarian.

Karátson, D., & Timár, G. (2005). Comparative volumetric calculations of two segments of the Carpathian Neogene/Quaternary volcanic chain using SRTM elevation data: Implications for erosion and magma output rates. *Zeitschrift fur Geomorphologie*, *140*, 19–35. Supplementary Issues

Karátson, D., Wulf, S., Veres, D., Magyari, E., Gertisser, R., Timár-Gabor, A., et al. (2016). The latest explosive eruptions of Ciomadul (Csomád) volcano, East Carpathians—A tephrostratigrapic approach for the 51-29 ka BP time interval. *Journal of Volcanology and Geothermal Research*, *319*, 29–51. https://doi.org/10.1016/j.jvolgeores.2016.03.005

Kato, A., Terakawa, T., Yamanaka, Y., Maeda, Y., Horikawa, S., Matsushiro, K., & Okuda, T. (2015). Preparatory and precursory processes leading up to the 2014 phreatic eruption of Mount Ontake. Japan. *Earth, Planets and Space*, *67*(1), 111. https://doi.org/10.1186/s40623-015-0288-x

Kennedy, B. M., & van Soest, M. C. (2006). A helium isotope perspective on the Dixie Valley, Nevada, hydrothermal system. *Geothermics*, *35*(1), 26–43. https://doi.org/10.1016/j.geothermics.2005.09.004

Kis, B. M., Ionescu, A., Cardellini, C., Harangi, S., Baciu, C., Caracausi, C., & Viveiros, F. (2017). Quantification of carbon dioxide emissions of Ciomadul, the youngest volcano of the Carpathian-Pannonian Region (Eastern-Central Europe, Romania). *Journal of Volcanology and Geothermal Research*, *341*, 119–130. https://doi.org/10.1016/j.jvolgeores.2017.05.025

Kiss, B., Harangi, S., Ntaflos, T., Mason, P., & Pál-Molnár, E. (2014). Amphibole perspective to unravel pre-eruptive processes and conditions in volcanic plumbing systems beneath intermediate arc volcanoes: A case study from Ciomadul volcano (SE Carpathians). *Contributions to Mineralogy and Petrology*, *167*(3). https://doi.org/10.1007/s00410-014-0986-6

Konstantinou, K. I., Lin, C.-H., & Liang, W.-T. (2007). Seismicity characteristics of a potentially active Quaternary volcano: The Tatun Volcano Group, northern Taiwan. *Journal of Volcanology and Geothermal Research*, *160*(3-4), 300–318. https://doi.org/10.1016/j.volgeores.2006.09.009

Lee, H., Muirhead, J., Fischer, T. P., Ebinger, C. J., Kattenhorn, S. A., Sharp, Z. D., & Kianji, G. (2016). Massive and prolonged deep carbon emissions associated with continental rifting. *Nature Geoscience*, *9*(2), 145–149. https://doi.org/10.1038/ngeo2622

Lewicki, J. L., Fischer, T., & Williams, S. N. (2000). Chemical and isotopic compositions of fluid at Cumbal Volcani, Colombia: Evidence for magmatic contribution. *Bulletin of Volcanology*, *62*(4-5), 347–361. https://doi.org/10.1007/s004450000100

Lin, C. H., & Pu, H. C. (2016). Very-long-period seismic signals at the Tatun Volcano Group, northern Taiwan. *Journal of Volcanology and Geothermal Research*, *328*, 230–236. https://doi.org/10.1016/j.volgeores.2016.11.007

Liotta, M., & Martelli, M. (2012). Dissolved gases in brackish thermal waters: An improved analytical method. *Geofluids*, *12*(3), 236–244. https://doi.org/10.1111/j.1468-8123.2012.00365.x

Lukács, R., Guillong, M., Schmitt, A. K., Molnár, K., Bachman, O., & Harangi, S. (2018). La-ICP-MS and SIMS U-Pb and U-Th zircon geochronological data of Late Pleistocene lava domes of the Ciomadul Volcanic Dome Complex (Eastern Carpathians). *Data in Brief*, *18*, 808–813. https://doi.org/10.1016/j.dib.2018.03.100

Mandarano, M., Paonita, A., Martelli, M., Viccaro, M., Nicotra, E., & Millar, I. L. (2016). Revealing magma degassing below closed-conduit active volcanoes: Geochemical features of volcanic rocks versus fumarolic fluids at Vulcano (Aeolian Islands, Italy). *Lithos*, *248-251*, 272–287. https://doi.org/10.1016/j.lithos.2016.01.026

Martelli, M., Nuccio, P. M., Stuart, F. M., Burgessd, R., Ellamc, R. M., & Italiano, F. (2004). Helium–strontium isotope constraints on mantle evolution beneath the Roman Comagmatic Province, Italy. *Earth and Planetary Science Letters*, *224*(3-4), 295–308. https://doi.org/10.1016/j.epsl.2004.05.025

Marty, B., & Giggenbach, W. F. (1990). Major and rare gases at White Island volcano, New Zealand: Origin and flux of volatiles. *Geophysical Research Letters*, *17*(3), 247–250. https://doi.org/10.1029/GL017i003p00247

Marty, B., & Jambon, A. (1987). C/3He in volatile fluxes from the solid Earth: Implications for carbon geodynamics. *Earth and Planetary Science Letters*, *83*(1-4), 16–26. https://doi.org/10.1016/0012-821X(87)90047-1

Mason, E., Edmonds, M., & Turchyn, A. (2017). Remobilization of crustal carbon may dominate volcanic arc emissions. *Science*, *357*, 290–294. https://doi.org/10.1126/science.aan5049

Mason, P., Downes, H., Thirlwall, M.F., Seghedi, I., Szakács, A., Lowry, D., Mattey, D., (1996). Crustal assimilation as a major petrogenetic process in the East Carpathian Neogene and Quaternary Continental Margin Arc, Romania

Mațenco, L., & Bertotti, G. (2000). Tertiary tectonic evolution of the external East Carpthians (Romania). *Tectonophysics*, *316*(3-4), 255–286. https://doi.org/10.1016/S0040-1951(99)00261-9

Mațenco, L., Bertotti, G., Leever, K., Cloething, S., Schmidt, S. M., Tărăpoancă, M., & Dinu, C. (2007). Large-scale deformation in a locked collisional boundary: Interplay between subsidence and uplift, intraphase stress, and inherited litospheric structure in the large stage of the SE Carpathian evolution. *Tectonics*, *26*, TC4011. https://doi.org/10.1029/2006TC001951

Mazot, A., Rouwet, D., Taran, Y., Inguaggiato, S., & Varley, N. (2011). CO_2 and He degassing at El Chicón volcano, Chiapas, Mexico: Gas flux, origin and relationship with local and regional tectonics. *Bulletin of Volcanology*, *73*, 423–441. https://doi.org/10.1007/s00445-010-0443-y

Melián, G., Tassi, F., Pérez, N., Hernández, P., Sortino, F., Vaselli, O., et al. (2012). A magmatic source for fumaroles and diffuse degassing from the summit crater of Teide Volcano (Tenerife, Canary Islands): A geochemical evidence for the 2004-2005 seismic-volcanic crisis. *Bulletin of Volcanology*, *74*(6), 1465–1483. https://doi.org/10.1007/s00445-012-0613-1

Molnár, K., Harangi, S., Lukács, R., Dunkl, I., Schmitt, A. K., Kiss, B., et al. (2018). The onset of the volcanism in the Ciomadul Volcanic Dome Complex (Eastern Carpathians): Eruption chronology and magma type variation. *Journal of Volcanology and Geothermal Research*, *354*, 39–56. https://doi.org/10.1016/j.jvolgeores.2018.01.025

Molnár, K., Lukács, R., Dunkl, I., Schmitt, A. K., Kiss, B., Seghedi, I., et al. (2019). Episodes of dormancy and eruption of the Late Pleistocene Ciomadul volcanic complex (Eastern Carpathians, Romania) constrained by zircon geochronology. *Journal of Volcanology and Geothermal Research*, *373*, 133–147. https://doi.org/10.1016/j.jvolgeores.2019.01.025

Moriya, I., Okuno, M., Nakamura, E., Szakács, A., & Seghedi, I. (1995). Last eruption and its ^{14}C age of Ciomadul Volcano, Romania. *Summaries of Researches Using AMS at Nagoya University*, *6*, 82–91.

Moriya, I., Okuno, M., Nakamura, T., Ono, K., & Seghedi, I. (1996). Radiocarbon ages of charcoal fragments from the pumice flow deposits of the last eruption of Ciomadul Volcano, Romania. *Summaries of Researches Using AMS at Nagoya University*, *3*, 252–255.

Moussallam, Y., Bani, P., Schipper, C. I., Cardona, C., Franco, L., Barnie, T., et al. (2018). Unrest and the Nevados de Chillan volcanic complex: A failed or yet to unfold magmatic eruption. *Volcanica*, *1*(1), 19–32. https://doi.org/10.30909/vol.01.01.1932

Nicolaescu, V. (1973). Contributions to the knowledge on the Cretaceous flysch of the western part of Bodoc Mts. *Studii şi cercetări Geologie Geofizica,Geografie*, *18*(2), 479–488. (In Romanian)

O'Nions, R. K., & Oxburgh, E. R. (1988). Helium, volatile fluxes and the development of the continental crust. *Earth and Planetary Science Letters*, *90*(3), 331–347. https://doi.org/10.1016/0012-821X(88)90134-3

Oppenheimer, C., Fischer, T. P., & Scaillet, B. (2014). Volcanic degassing: Process and impact. In H. D. Holland, & K. K. Turekian (Eds.), *Treatise on Geochemistry*, (2nd ed.pp. 111–179). Oxford: Elsevier. https://doi.org/10.1016/B978-0-08-095975-7.00304-1

Ozima, M., & Podosek, F. A. (2002). *Noble gas geochemistry*. Cambridge: Cambridge University Press.

Palcsu, L., Vető, I., Futó, I., Vodila, G., Papp, L., & Major, Z. (2014). In-reservoir mixing of mantle-derived CO_2 and metasedimentary CH_4-N_2 fluids. Noble gas and stable isotope study of two multistached fields (Pannonian Basin System, W-Hungary). *Marine and Petroleum Geology*, *54*, 216–227. https://doi.org/10.1016/j.marpetgeo.2014.03.013

Panaiotu, C. G., Jicha, B. R., Singer, B. S., Tugui, A., Seghedi, I., Panaiotu, A. G., & Necula, C. (2013). $^{40}Ar/^{39}Ar$ chronology and paleomagnetism of Quaternary basaltic lavas from the Perşani Mountains (East Carpathians). *Physics of the Earth and Planetary Interiors*, *221*, 1–24. https://doi.org/10.1016/j.pepi.2013.06.007

Panaiotu, C. G., Pécskay, Z., Hambach, U., Seghedi, I., Panaiotu, C. E., Tetsumaru, I., et al. (2004). Short-lived Quaternary volcanism in the Persani Mountains (Romania) revealed by combined K–Ar and paleomagnetic data. *Geologica Carpathica*, *55*(4), 333–339.

Paonita, A., Caracausi, A., Iacono-Marziano, G., Martelli, M., & Rizzo, A. (2012). Geochemical evidence for mixing between fluids exsolved at different depths in the magmatic system of Mt. Etna (Italy). *Geochimica et Cosmochimica Acta*, *84*, 380–394. https://doi.org/10.1016/j.gca.2012.01.028

Paonita, A., Longo, M., Bellomo, S., D'Alessandro, W., & Brusca, L. (2016). Dissolved inert gases (He, Ne and N_2) as markers of groundwater flow and degassing areas at Mt. Etna volcano (Italy). *Chemical Geology*, *443*, 10–21. https://doi.org/10.1016/j.chemgeo.2016.09.018

Parello, F., Allard, P., D'Alessandro, W., Federico, C., Jean-Baptiste, P., & Catani, O. (2000). Isotope geochemistry of Pantelleria volcanic fluids, Sicily Channel rift: A mantle volatile end-member for volcanism in southern Europe. *Earth and Planetary Science Letters*, *180*(3–4), 325–339. https://doi.org/10.1016/S0012-821X(00)00183-7

Pécskay, Z., Lexa, J., Szakács, A., Seghedi, I., Balogh, K., Konecny, V., et al. (2006). Geochronology of Neogene magmatism in the Carpathian arc and intra-Carpathian area. *Geologica Carpathica*, *57*(6), 511–530.

Pedroni, A., Hammerschidt, K., & Friedrichsen, H. (1999). He, Ne, Ar and C isotope systematics of geothermal emanations in the Lesser Antilles Islands Arc. *Geochimicaet Cosmochimica Acta*, *63*(3-4), 515–532. https://doi.org/10.1016/S0016-7037(99)00018-6

Pik, R., & Marty, B. (2008). Helium isotopic signature of modern and fossil fluids associated with the Corinth rift fault zone (Greece): Implication for fault connectivity in the lower crust. *Chemical Geology*, *266*(1-2), 67–75. https://doi.org/10.1016/j.chemgeo.2008.09.024

Pizzino, L., Galli, G., Mancini, C., Quattrocchi, F., & Scarlato, P. (2002). Natural gas hazard (CO_2 and ^{222}Rn) within a quiescent volcanic region and its relations with tectonics: The case of Ciampino-Marino Area, Albani Hills Volcano, Italy. *Natural Hazards*, *27*(3), 257–287. https://doi.org/10.1023/A:1020398128649

Poorter, R., Varekamp, J., Poreda, R., Van Bergen, M., & Kreuen, R. (1991). Chemical and isotopic compositions of volcanic gases from the east Sunda and Banda arcs, Indonesia. *Geochimica et Cosmochimica Acta*, *55*(12), 3798–3807. https://doi.org/10.1016/0016-7073(91)90075-G

Popa, M., Radulian, M., Szakács, A., Seghedi, I., & Zaharia, B. (2012). New seismic and tomography data inthe southern part of the Harghita Mountains (Romania, Southeastern Carpathians): Connection with recent volcanic activity. *Pure Applied Geophysics*, *169*(9), 1557–1573. https://doi.org/10.1007/s00024-011-0428-6

Rădulescu, D., Peter, E., Stanciu, C., Stefanescu, M., & Veliciu, S. (1981). Discussion on the geothermal anomalies within South Harghita Mountains. *Studii si Cercetari Geologie, Geografie, Geofizica, Seria Geologie*, *26*(2), 169–184. In Romanian

Rizzo, A. L., Barbieri, F., Carapezza, M. L., Di Piazza, A., Francalanci, L., Sortino, F., & D'Alessandro, W. (2015). New mafic magma refilling a quiescent volcano: Evidence from He-Ne-Ar isotopes during the 2011–2012 unrest at Santorini, Greece. *Geochemistry, Geophysics, Geosystems*, *16*, 798–814. https://doi.org/10.1002/2014GC005653

Roulleau, E., Sano, Y., Takahata, N., Yang, F. T., & Takahashi, H. A. (2015). He, Ar, N and C isotope compositions in Tatun Volcanic Group (TVG), Taiwan: Evidence for an important contribution of pelagic carbonates in the magmatic source. *Journal of Volcanology and Geothermal Research*, *303*, 7–15. https://doi.org/10.1016/j.volgeores.2015.07.017

Roulleau, E., Tardani, D., Sano, Y., Takahata, N., Vinet, N., Bravo, F., et al. (2016). New insight from noble gas and stable isotopes of geothermal/hydrothermal fluids at Caviahue-Copahue Volcanic Complex: Boiling steam separation and water-rock interaction at shallow depth. *Journal of Volcanology and Geothermal Research*, *328*, 70–83. https://doi.org/10.1016/j.jvolgeores.2016.10.007

Rouwet, D., Hidalgo, S., Joseph, E. P., & González-Ilama, G. (2017). Fluid geochemistry and volcanic unrest: Dissolving the haze in time and space. In *Advances in Volcanology*, (pp. 221–239). Berlin, Heidelberg: Springer. https://doi.org/10.1007/11157_2017_12

Rouwet, D., Sandri, L., Marzocchi, W., Gottsmann, J., Selva, J., Tonini, R., & Papale, P. (2014). Recognizing and tracking volcanic hazards related to non-magmatic unrest: A review. *Journal of Applied Volcanology*, *3*(1), 1–17. https://doi.org/10.1186/s13617-014-0017-3

Royden, L. H., Horváth, F., & Burchfiel, B. C. (1982). Transform faulting, extension and subduction in the Carpathian Pannonian Region. *GSA Bulletin*, *93*(8), 717–725. https://doi.org/10.1130/0016-7606(1982)93

Rudnick, R. L., & Gao, S. (2003). Composition of the continental crust. *Treatise in Geochemistry*, *3*, 1–64. https://doi.org/10.1016/B0-08-043751-6/03016-4

Ruzié, L., Moreira, M., & Crispi, O. (2012). Noble gas isotopes in hydrothermal volcanic fluids of La Soufriére volcano, Guadeloupe, Lesser Antilles arc. *Chemical Geology*, *304-305*, 158–165. https://doi.org/10.1016/j.chemgeo.2012.02.012

Sano, Y., Hirabayashi, J.-I., Oba, T., & Gamo, T. (1994). Carbon and helium isotopic ratios at Kusatsu-Shirane volcano, Japan. *Applied Geochemistry*, *9*(4), 371–377. https://doi.org/10.1016/0883-29274)90059-0

Sano, Y., Kagoshima, T., Takahata, N., Nishio, Y., Roulleau, E., Pinti, D. L., & Fischer, T. P. (2015). Ten-year helium anomaly prior to the 2014 Mt. Ontake eruption. *Scientific Reports*, *5*(1), 13069. https://doi.org/10.1038/srep13069

Sano, Y., & Marty, B. (1995). Origin of carbon in fumarolic gas from island arcs. *Chemical Geology*, *119*(1-4), 265–274. https://doi.org/10.1016/0009-2541(94)00097-R

Sano, Y., & Wakita, H. (1985). Geographical distribution of $^3He/^4He$ ratios in Japan: Implications for arc tectonics and incipient magmatism. *Journal of Geophysical Research*, *90*(B10), 8729–8741. https://doi.org/10.1029/JB090iB10p08729F

Sano, Y., & Williams, S. N. (1996). Fluxes of mantle and subducted carbon along convergent plate boundaries. *Geophysical Research Letters*, *23*(20), 2749–2752. https://doi.org/10.1029/96GL02260

Sarbu, S., Aerts, J. W., Flot, J. F., Van Spanning, R. J. M., Baciu, C., Ionescu, A., et al. (2018). Sulfur Cave (Romania), an extreme environment with microbial mats in a CO_2-H_2S/O gas chemocline dominated by mycobacteria. *International Journal of Speleology*, *47*(2), 173–187. https://doi.org/10.5038/1827-806X.47.2.2164

Seghedi, I., Downes, H., Harangi, S., Mason, P. R. D., & Pécskay, Z. (2005). Geochemical response of magmas to Neogene–Quaternary continental collision in the Carpathian–Pannonian region: A review. *Tectonophysics*, *410*(1-4), 485–499. https://doi.org/10.1016/j.tecto.2004.09.015

Seghedi, I., Downes, H., Szakács, A., Mason, P. R. D., Thirlwall, M. F., Rosu, E., et al. (2004). Neogene-Quaternary magmatism and geodinamics in the Carpathian-Pannonian region: A synthesis. *Lithos*, *72*(3-4), 117–146. https://doi.org/10.1016/j.lithos.2003.08.006

Seghedi, I., Maţenco, L., Downes, H., Mason, P. R. D., Szakács, A., & Pécskay, Z. (2011). Tectonic significance of changes in post-subduction Pliocene-Quaternary magmatism in the south east part of the Carpathian-Pannonian Region. *Tectonophysics*, *502*(1-2), 146–157. https://doi.org/10.1016/j.tecto.2009.12.003

Seghedi, I., Popa, R. G., Panaiotu, C. G., Szakács, A., & Pécskay, Z. (2016). Short-lived eruptive episodes during the construction of a Na-alkalic basaltic field (Perşani Mountains, SE Transylvania, Romania). *Bulletin of Volcanology*, *78*(10), 69. https://doi.org/10.1007/s00445-016-1063-y

Seghedi, I., & Szakács, A. (1994). The Upper Pliocene–Pleistocene effusive and explosive basalticvolcanism from the Perşani Mountains. *Romanian Journal of Petrology*, *76*, 101–107.

Seghedi, I., Szakács, A., Udrescu, C., Stoian, M., & Graban, G. (1987). Trace element geochemistry of the South Harghita volcanic (East Carpathians). Calc-alkaline and shoshinitic associations. *Dari de Seama a Sedintelor Institutului Geologic si Geofizic*, *72*(73), 1.

Shaw, A. M., Hilton, D. R., Fischer, T. P., Walker, J. A., & Alvarado, G. E. (2003). Contrasting He-C relationships in Nicaragua and Costa Rica: Insights into C cycling through subduction zones. *Earth and Planetary Science Letters*, *214*(3-4), 499–513. https://doi.org/10.1016/S0012-821X(03)00401-1

Sherwood-Lollar, B., Ballentine, C. J., & Onions, R. K. (1997). The fate of mantle-derived carbon in a continental sedimentary basin: Intergration of C He relationships and isotope signatures. *Geochimica et Cosmochimica Acta*, *61*(11), 2295–2307. https://doi.org/10.1016/S0016-7037(97)00083-5

Snyder, G., Poreda, R., Hunt, A., & Fehn, U. (2001). Regional variations in volatile composition: Isotopic evidence for carbonate recycling in the Central American volcanic arc. *Geochemistry, Geophysics, Geosystems*, *2*(10), 1057. https://doi.org/10.1029/2001GC000163

Sorey, M. L., Evans, W. C., Kennedy, B. M., Farrar, C. D., Hainsworth, L. J., & Hausback, B. (1998). Carbon dioxide and helium emission from a reservoir of magmatic gas beneath Mammoth Mountain, California. *Journal of Geophysical Research*, *103*(B7), 15,303–15,323. https://doi.org/10.1029/98JB01389

Sparks, R. S. J., Folkes, C. B., Humphreys, M. C. S., Barfod, D. N., Clavero, J., Sunagua, M. C., et al. (2008). Uturuncu volcano, Bolivia: Volcanic unrest due to mid-crustal magma intrusion. *American Journal of Science*, *308*(6), 727–769. https://doi.org/10.2475/06.2008.01

Sparks, S., & Cashman, K. (2017). Dynamic magma systems: Implications for forecasting volcanic activity. *Elements*, *13*(1), 35–40. https://doi.org/10.2113/gselements.13.1.35

Sturchio, N. C., Williams, S. N., & Sano, Y. (1993). The hydrothermal system of Volcan Purace, Colombia. *Bulletin of Volcanology*, *55*(4), 289–296. https://doi.org/10.1007/BF00624356

Symonds, R.B., Poreda, R.J., Evans, W.C., Janik, C.J. & Ritchie, B.E. (2003). Mantle and crustal sources of carbon, nitrogen and noble gases in Cascade-Range and Aleutian-Arc volcanic gases.*US Geological Survey Open-File Report*, 03–436

Szakács, A., & Seghedi, I. (1987). Base surge deposits in the Ciomadul Massif (South Harghita Mountains). *Dari de Seama ale sedintelor Institutului Geologic Geofizic*, *74*(1), 175–180.

Szakács, A., & Seghedi, I. (1995). The Călimani-Gurghiu-Harghita volcanic chain, East Carpathians, Romania: Volcanological features. *Acta Volcanologica*, *7*, 145–153.

Szakács, A., & Seghedi, I. (2013). The relevance of volcanic hazard in Romania: Is there any? *Environmental Engineering and Management Journal*, *12*, 125–135. https://doi.org/10.30638/eemj.2013.015

Szakács, A., Seghedi, I., & Pécskay, Z. (1993). Pecularities of South Harghita Mts. as terminal segment of the Carpathian Neogene to Quaternary volcanic chain. *Revue Roumaine de Geophysique*, *37*, 21–36.

Szakács, A., Seghedi, I., Pécskay, Z., & Mirea, V. (2015). Eruptive history of a low-frequency and low-output rate Pleistocene volcano, Ciomadul, South Harghita Mts., Romania. *Bulletin of Volcanology*, *77*(2). https://doi.org/10.1007/s00445-014-0894-7

Tassi, F., Aguilera, F., Benavente, O., Paonita, A., Chiodini, G., Caliro, S., et al. (2016). Geochemistry of fluid discharges from Peteroa volcano (Argentina-Chile) in 2010-2015: Insights into compositional changes related to the fluid source region(s). *Chemical Geology*, *432*, 41–53. https://doi.org/10.1016/j.chemgeo.2016.04.007

Tassi, F., Aguilera, F., Darrah, T., Vaselli, O., Capaccioni, B., Poreda, R. J., & Delgado Huertas, A. (2010). Fluid geochemistry of hydrothermal systems in the Arica-Parinacota, Taracapa and Antofagasta regions (northern Chile). *Journal of Volcanology and Geothermal Research*, *192*(1-2), 1–15. https://doi.org/10.1016/j.jvolgeores.2010.02.006

Tassi, F., Aguilera, F., Vaselli, O., Darrah, T., & Medina, E. (2011). Gas discharges from four remote volcanoes in Chile (Putana, Olca, Irruputuncu and Alitar): A geochemical survey. *Annals of Geophysics*, *54*. https://doi.org/10.4401/ag-5173

Tassi, F., Nisi, B., Cardellini, C., Capecchiacci, F., Donnini, M., Vaselli, O., et al. (2013). Diffuse soil emission of hydrothermal gases (CO_2, CH_4, C_6H_6) at Solfatara crater (Campi Flegrei, Southern Italy). *Applied Geochemistry*, *35*, 142–153. https://doi.org/10.1016/j.apgeochem.2013.03.020

Tedesco, D., Miele, G., Sano, Y., & Tardani, J. P. (1995). Helium isotopic ratio in Vulcano island fumaroles: Temporal variations in shallow level mixing and deep magmatic supply. *Journal of Volcanology and Geothermal Research*, *64*(1-2), 117–128. https://doi.org/10.1016/0377-0273(94)00045-I

Torgersen, T., Drenkard, S., Stute, M., Schlosser, P., & Shapiro, A. (1995). Mantle helium in-ground waters of eastern North-America—Time and space constraints on sources. *Geology*, *23*(8), 675–678. https://doi.org/10.1130/0091-7613(1995)023<0675:MHIGWO>2.3.CO;2

Trasatti, E., Marra, F., Polcari, M., Etiope, G., Ciotoli, G., Darrah, T. H., et al. (2018). Coeval uplift and subsidence reveal magma recharging near Rome (Italy). *Geochemistry, Geophysics, Geosystems*, *19*, 1484–1498. https://doi.org/10.1029/2017GC007303

Túri, M., Palcsu, L., Papp, L., Horváth, A., Futó, I., Molnár, M., et al. (2016). Isotope characterization of the water and sediment in volcanic lake Saint Ana, East-Carpathians, Romania. *Carpathian Journal of Earth and Environmental Sciences*, *11*(2), 475–484.

van Soest, M., Hilton, D., & Kreulen, R. (1998). Tracing crustal and slab contributions to arc magmatism in the Lesser Antilles island arc using helium and carbon relationships in geothermal fluids. *Geochimica et Cosmochimica Acta*, *62*(19-20), 3323–3335. https://doi.org/10.1016/S0016-7037(98)00241-5

van Soest, M. C., Hilton, D. R., Macpherson, C. G., & Mattey, D. P. (2002). Resolving sediment subduction and crustal contamination in the Lesser Antilles Island arc: A combined he–O–Sr isotope approach. *Journal of Petrology*, *43*(1), 143–170. https://doi.org/10.1093/petrology/43.1.143

Varekamp, J., Kreulen, R., Poorter, R., & Bergen, M. (1992). Carbon sources in arc volcanism, with implications for the carbon cycle. *Terra nova*, *4*(3), 363–373. https://doi.org/10.1111/j.1365-3121.1992.tb00825.x

Vaselli, O., Downes, H., Thirlwall, M. F., Dobosi, G., Coradossi, N., Seghedi, I., et al. (1995). Ultramafic xenoliths in Plio-Pleistocene alkali basalts from theEastern Transylvanian Basin: Depleted mantle enriched by vein metasomatism. *Journalof Petrology*, *36*(1), 23–53. https://doi.org/10.1093/petrology/36.1.23

Vaselli, O., Minissale, A., Tassi, F., Magro, G., Seghedi, I., Ioane, D., & Szakács, A. (2002). Ageochemical traverse across the Eastern Carpathians (Romania): Constraints on the origin andevolution of the mineral waters and gas discharge. *Chemical Geology*, *182*(2-4), 637–654. https://doi.org/10.1016/S0009-2541(01)00348-5

Vinkler, A. P., Sz, H., Ntaflos, T., & Szakács, A. (2007). Petrology and geochemistry of pumices from the Ciomadul volcano (Eastern Carpathians)—implications for petrogenetic processes. *Földtani Közlöny*, *137*(1), 103–128. In Hungarian

Wei, F., Xu, J., Shangguan, Z., Pan, S., Yu, H., Wei, W., et al. (2016). Helium and carbon isotopes in the hot spring of Changbaishan Volcano, northeastern China: A material connection between Changbaishan Volcano and the west Pacific plate. *Journal of Volcanology and Geothermal Research*, *327*, 398–406. https://doi.org/10.1016/j.jvolgeores.2016.09.005

Wenzel, F., Lorenz, F. P., Sperner, B., & Oncescu, M. C. (1999). Seismotectonics of the Romanian Vrancea Area. In F. Wenzel, D. Lungu, & O. Novak (Eds.), *Vrancea earthquakes: Tectonics, hazard and risk mitigation*, (pp. 15–25). Netherlands: Springer.

Werner, C., Evans, W. C., Poland, M., Tucker, D., & Doukas, M. (2009). Long-term changes in quiescent degassing at Mount Baker Volcano, Washington, USA: Evidence for a staller intrusion in 1975 and connection to a deep magma source. *Journal of Volcanology and Geothermal Research*, *186*(3-4), 379–386. https://doi.org/10.1016/j.jvolgeores.2009.07.006

Wortel, M. J. R., & Spakman, W. (2000). Subduction and slab detachment in the Mediterranean-Carpathian Region. *Science*, *290*(5498), 1910–1917. https://doi.org/10.1126/science.290.5498.1910

3) Mantle-Derived Fluids in the East Java Sedimentary Basin, Indonesia

La présence des éléments volatils dérivés du manteau est généralement associée au dégazage de panaches volcaniques, d'émissions diffuses autour d'édifices volcaniques, de dorsales océaniques, de rifts continentaux modernes ou de systèmes de failles actives profondes (par exemple, Caracausi et al., 2015; Caracausi & Sulli, 2015, 2019; Halldórsson et al., 2013; Lee et al., 2016; Sano et Fischer, 2013). Ces systèmes sont généralement dominés par l'eau et le CO_2 et contiennent des traces de gaz rares avec des compositions isotopiques spécifiques qui indiquent une origine dérivée du manteau (Moreira & Kurz, 2013). Il a été démontré que certains bassins sédimentaires abritent des réservoirs d'hydrocarbures (HC) contenant des éléments volatils dérivées du manteau, par exemple, le bassin de Tuff Vert au Japon, le dépression d'Okinawa dans la mer de Chine orientale, le bassin de Sacramento et la dépression d'Escanaba en Californie, et plusieurs bassins distribués en Nouvelle-Zélande, Thaïlande, Indonésie, Philippines, Taiwan et la péninsule du Kamchatka (Ishibashi et al., 2002; Jenden et al., 1993; Kamenskiy et al., 1971; Poreda et al., 1986; Sakata et al., 1997; Xu et al., 1995). Le gaz thermogénique produit à ces endroits ($\delta^{13}C_{CH4}$ entre -30 et -60‰) est principalement généré par le craquage thermique de la matière organique. La composition isotopique de l'hélium (ci-après He) dans ces réservoirs indique la présence d'éléments volatils dérives du manteau (R = 0,2–7,7 Ra, où R = $^3He/^4He$ de l'échantillon, Ra = $^3He/^4He$ d'air ($1,4 \times 10^{-6}$)).
Un cadre similaire à ceux décrits ci-dessus se retrouve dans le bassin sédimentaire de Java oriental, au nord de l'arc volcanique de la Sunda, formé par la subduction de la plaque indo-australienne sous la plaque continentale eurasienne (Hall, 2002; figure 1a). Le bassin est caractérisé par des taux de sédimentation élevés, des dépôts de sédiments riches en matières organiques et des pièges volcanoclastiques et carbonatés, ce qui a entraîné la formation d'une province de HC comprenant de nombreux champs de pétrole et de gaz et des structures de perforation diffuses en surface et sous la surface (Istadi et al., 2012). ; Mazzini et al., 2018; Mazzini et al., 2007; Moscariello et al., 2018; Satyana et Purwaningsih, 2003a, 2003b). Le bassin bordé au sud par les volcans Penanggungan, Arjuno - Welirang et Bromo constitue une configuration idéale pour étudier la relation entre les éléments volatils dérivés du manteau et les fluides de HC dans les gisements de pétrole et de gaz.
Cette région présente également un intérêt particulier en raison du percement de Lusi, la plus grande éruption de boue active au monde adjacente aux volcans Holocene Penanggungan et Arjuno - Welirang, situés respectivement à 10 et 25 km au sud-ouest (Figures 1b et 2). Lusi (du nom de Lumpur, qui signifie boue en indonésien, et SIdoarjo, la régence locale) a commencé son activité éruptive le 29 mai 2006 et continue depuis à faire éclater de l'eau bouillante, du gaz, de la boue, du pétrole et des roches (Van Noorden, 2006). Un ensemble de campagnes de terrain ciblées a été achevé depuis le début de l'éruption pour rechercher l'origine des fluides en éruption et le système de plomberie sous la surface (Miller & Mazzini, 2018, et références y figurant). Les résultats ont révélé que les fluides en ébullition dégagés à la surface de Lusi contiennent des traces d'eaux hydrothermales et un mélange de gaz inorganiques et organiques, notamment des gaz géothermiques (thermométamétamorphiques et dérivés du manteau) et biotiques (méthane thermogénique) (Mazzini et al., 2012; Mazzini et al., 2018). La tomographie de bruit ambiant a révélé une connexion entre la chambre magmatique Arjuno-Welirang et le conduit de Lusi à une profondeur d'environ 4,5 km, indiquant la migration des fluides magmatiques et hydrothermaux vers le bassin sédimentaire.
(Fallahi et al., 2017). Ces résultats ont confirmé que Lusi n'était en effet pas un volcan de boue, mais plutôt un système géothermique encaissé dans les sédiments (Mazzini & Etiope, 2017; Procesi et al., 2019). Les échantillons prélevés dans les fumerolles du complexe volcanique Arjuno-Welirang ont fourni une preuve supplémentaire de la connexion entre ces

deux systèmes éruptifs (Inguaggiato et al., 2018). Les auteurs ont révélé que les fumerolles d'Arjuno-Welirang et le gaz du site de Lusi contiennent des éléments volatils magmatiques très abondantes en ^{3}He (R = 7,3 et 6,5Ra, respectivement). En outre, le système de faille de Watukosek (WFS), qui s'étend du complexe volcanique Arjuno-Welirang vers le nord-est de l'île (Figure 2), héberge Lusi et plusieurs volcans de boue (Fallahi et al., 2017; Mazzini et al., 2009; Mazzini et al., 2012; Moscariello et al., 2018; Obermann et al., 2018; Sciarra et al., 2018). Les auteurs indiquent que ce système de glissade secondaire offre une voie idéale pour la propagation des fluides hydrothermaux surpressés en profondeur vers le bassin sédimentaire et plus loin vers la surface.

Ce système de plomberie complexe et ces structures tectoniques contrôlent en grande partie la migration passée et présente des fluides. Lusi est entourée de trois champs de pétrole et de gaz peu profonds (figures 1b et 2) qui reflètent la paléo-migration des HC dans le bassin. Malgré la proximité évidente entre Lusi et ces réservoirs de HC, aucune étude spécifique n'a encore été menée pour déterminer (1) si le gaz de HC présent à Lusi est identique à celui stocké dans les réservoirs, (2) si une corrélation représente une potentielle connexion entre ces deux systèmes, et (3) si le WFS pourrait également fournir une voie de migration des fluides dérivés du manteau aux réservoirs peu profonds. Cette étude a pour objectif de caractériser la composition et l'origine du gaz piégé dans le sous-sol et de résoudre les questions ci-dessus en analysant des échantillons ciblés.
Nous rapportons les résultats d'un levé géochimique des gaz réalisé dans la partie sud du bassin sédimentaire de Java Est. Ici, plusieurs champs de HC et des sites d'infiltration de surface adjacents sont situés près du complexe volcanique Arjuno-Welirang et autour du site de l'éruption de Lusi. Les échantillons prélevés dans les champs de HC peu profonds (200 à 1 000 m) (groupe 1) révèlent la présence de gaz thermogénique principalement sec ($-58,3$ ‰$<\delta^{13}C_{CH4}<-40,7$‰). Les processus de biodégradation en cours sont confirmés par la signature CO2 avec $+18,9 <\delta^{13}C_{CO2} <+22,8$‰. Les suintements superficiels (groupe 2) situés au-dessus des réservoirs révèlent une signature géochimique remarquablement différente, dans laquelle le gaz thermogénique moins fractionné au niveau moléculaire et isotopique et généré récemment sont mélangés avec du CO_2 avec $+1,2$ ‰$<\delta^{13}C_{CO2} <+2,7$‰. Tous les échantillons analysés révèlent la présence de gaz nobles avec une signature claire de l'He dérivé du manteau comparable à celle des fluides émis aux fumerolles de Lusi et d'Arjuno-Welirang. On n'observe qu'une diminution modérée du rapport $^{3}He/^{4}He$ le long d'un transect orienté NE des fouillards d'Arjuno-Welirang (R = 7,3 Ra), à travers le réservoir voisin de HC Carat (R = 6,7 Ra), Lusi (R jusqu'à 6,5 Ra) et les champs HC environnants qui affichent toujours des valeurs remarquablement élevées (R jusqu'à 6,3 Ra).
La zone d'étude est coupée par le WFS provenant du complexe volcanique Arjuno-Welirang, qui abrite les champs Lusi et HC échantillonnés. Des études antérieures ont révélé que ce système de failles fournissait la voie d'accès aux fluides magmatiques alimentant l'éruption de Lusi. Nos nouveaux résultats montrent que ce système de failles permet également la migration continue de fluides dérivés du manteau sur une plus grande région du bassin sédimentaire abritant les champs de HC. Une migration potentielle des fluides de Lusi peu profonds vers les réservoirs, suivie de processus d'altération (c'est-à-dire de biodégradation), ne peut être totalement exclue. Cependant, la signature distincte de C (c'est-à-dire CO_2 et CH_4) observés sur le site de l'éruption de Lusi et dans les champs HC indique que cet apport devrait être limité.
Des fluides supplémentaires expulsés par des milliers de suintements autour du cratère de Lusi (y compris ceux du groupe 2) migrent du conduit de Lusi à travers un réseau de fractures antithétiques au système de faille à glissement de Watukosek et à travers la

fracture de la caldera, des fractures peu profondes s'étendant sur des kilomètres le principal évent de Lusi.
Cette étude souligne que la surveillance continue de la composition des gaz rares dans les champs de HC voisins des centres volcaniques pourrait représenter un outil efficace et simple sur le plan logistique pour distinguer les perturbations des complexes magmatiques adjacents.

JGR Solid Earth

RESEARCH ARTICLE
10.1029/2018JB017274

Mantle-Derived Fluids in the East Java Sedimentary Basin, Indonesia

Alexandra Zaputlyaeva[1], Adriano Mazzini[1], Antonio Caracausi[2], and Alessandra Sciarra[3,4]

[1]Centre for Earth Evolution and Dynamics (CEED), University of Oslo, Oslo, Norway, [2]Istituto Nazionale di Geofisica e Vulcanologia (INGV), Palermo, Italy, [3]Istituto Nazionale di Geofisica e Vulcanologia (INGV), Rome, Italy, [4]Consiglio Nazionale delle Ricerche—Istituto di Geologia Ambientale e Geoingegneria, Rome, Italy

Key Points:
- Advective migration of mantle-derived volatiles occurs through faults and fractures in the sedimentary basin
- Mantle-derived volatiles are trapped within shallow hydrocarbon accumulations
- Biodegradation processes in the hydrocarbon reservoirs and gas dissolution in the formation water mask the abiogenic carrier gas

Correspondence to:
A. Zaputlyaeva,
alexandra.zaputlyaeva@geo.uio.no

Citation:
Zaputlyaeva, A., Mazzini, A., Caracausi, A., & Sciarra, A. (2019). Mantle-derived fluids in the East Java sedimentary basin, Indonesia. *Journal of Geophysical Research: Solid Earth*, *124*. https://doi.org/10.1029/2018JB017274

Received 29 DEC 2018
Accepted 8 JUL 2019
Accepted article online 16 JUL 2019

Abstract The Tertiary back-arc sedimentary basin in East Java (Indonesia) hosts a large variety of piercement structures and hydrocarbon fields. Some of the latter (Wunut, Tanggulangin, Carat, Watudakon) are located a few kilometers away from the Arjuno-Welirang volcanic complex and neighboring Lusi, the largest active sediment-hosted hydrothermal system on Earth. In order to investigate interactions between volcanic and sedimentary settings, we performed gas sampling on these four shallow (200- to 1,000-m depth) petroleum fields. The fields around Lusi are dominated by thermogenic gas that was altered during biodegradation processes. The helium isotope ratios ($^3He/^4He$) are as high as 6.7 R_A, which is remarkably similar to those measured at the fumaroles of the adjacent volcanic complex (R = 7.3 R_A) and at the Lusi site (up to 6.5 R_A). This highlights the pervasive outgassing of mantle-derived fluids in the sedimentary basin. Despite these two systems sharing the same mantle-derived helium source, their hydrocarbons have two different genetic histories: Lusi hydrocarbon gas has been more recently generated and is less molecularly and isotopically fractionated, while the gas trapped in the reservoirs is older and more altered. Unlike Lusi, the hydrocarbon fields contain small amounts of CO_2 resulting from biodegradation processes. The Watukosek fault system, originating from the Arjuno-Welirang volcanic complex and extending toward the northeast of Java, intersects Lusi and the hydrocarbon fields. This network of faults controls the migration of mantle-derived fluids within the sedimentary basin, feeding the focused venting at the Lusi site and promoting the slower and pervasive migration in the reservoirs.

Plain Language Summary The East Java sedimentary basin is located to the north of the E-W trending chain of active volcanoes that transects the Java Island. The basin hosts numerous oil and gas fields, as well as buried diapirs and active mud eruption sites. This study focuses on gas geochemical analyses from the surface seeps and four shallow petroleum fields located around Lusi, the largest active mud eruption on Earth. Comparative results show that the biodegraded thermogenic gas in the reservoirs differs from the thermogenic gas vented at Lusi and its surrounding seeps. In contrast, helium gas analysis from the hydrocarbon reservoirs, the Lusi eruption and satellite seeps, and from the fumaroles at the neighboring Arjuno-Welirang volcanic complex share a common mantle-derived component. Available seismic data from the region confirm that a system of faults (Watukosek fault system), extending from the volcanic complex toward the sedimentary basin, promotes the migration of mantle-derived fluids through a broad area in the East Java sedimentary basin. These results confirm that the Lusi system is fueled by the lateral migration of mantle-derived fluids that trigger reactions within the organic rich formations in the sedimentary basin.

1. Introduction

The presence of mantle-derived volatiles is typically associated with degassing of volcanic plumes, diffuse emissions around volcanic edifices, mid-ocean ridges, modern continental rifts, or deep active fault systems (e.g., Caracausi et al., 2015; Caracausi & Sulli, 2019; Halldórsson et al., 2013; Lee et al., 2016; Sano & Fischer, 2013). These systems are commonly dominated by water and CO_2 and contain trace amounts of noble gases with specific isotopic compositions that indicate a mantle-derived origin (Moreira & Kurz, 2013). Some sedimentary basins have been documented to host hydrocarbon (HC) reservoirs containing mantle-derived volatiles, for example, Green Tuff Basin in Japan, Okinawa Trough in East China Sea,

©2019. The Authors.
This is an open access article under the terms of the Creative Commons AttributionNonCommercialNoDerivs License, which permits use and distribution in any medium, provided the original work is properly cited, the use is noncommercial and no modifications or adaptations are made.

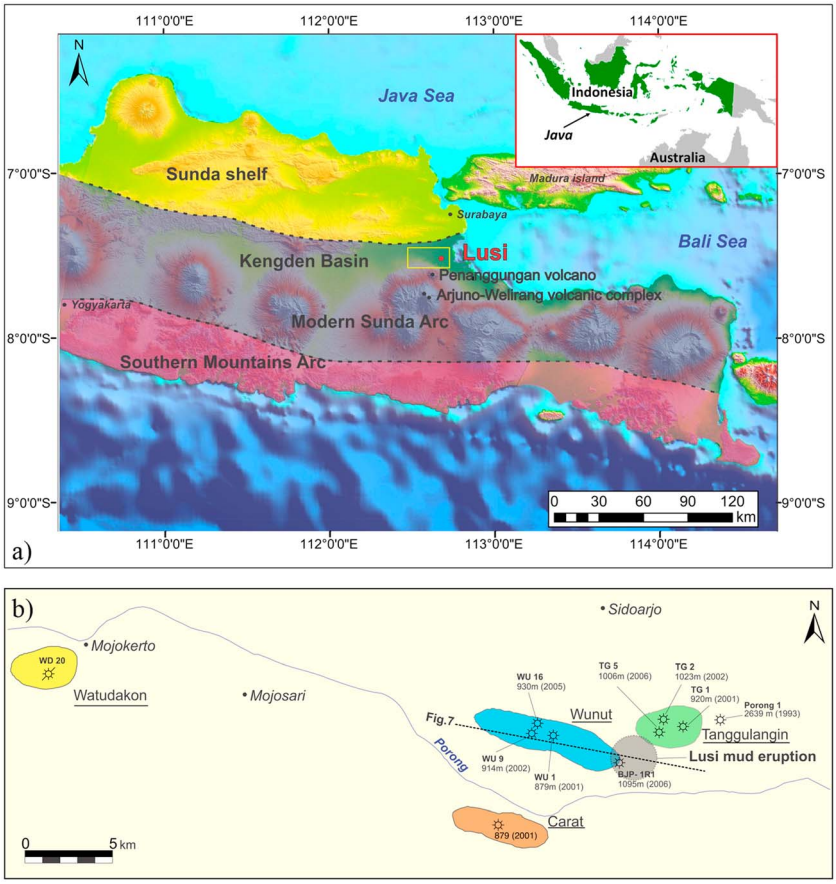

Figure 1. (a) Digital elevation model of the central and eastern Java with main tectonic zones (redrawn and modified after Istadi et al., 2009; Smyth et al., 2008); the yellow rectangle indicates the study area depicted at (b); inset map of Indonesia; (b) location of the sampled wells in the Wunut, Tanggulangin, Carat, Watudakon fields, bottom hole depth, and drilling year. Dashed line indicates the location of the seismic profile, shown at Figure 7.

Sacramento Basin and Escanaba Trough in California, and multiple basins distributed in New Zealand, Thailand, Indonesia, Philippines, Taiwan, and Kamchatka peninsula (Ishibashi et al., 2002; Jenden et al., 1993; Kamenskiy et al., 1971; Poreda et al., 1986; Sakata et al., 1997; Xu et al., 1995). Thermogenic gas produced at these localities ($\delta^{13}C_{CH4}$ between −30‰ and −60 ‰) was mainly generated by the thermal cracking of organic matter. Helium (hereafter He) isotope compositions at these reservoirs indicate the presence of mantle-derived volatiles (R = 0.2–7.7 R_A, where R = $^3He/^4He$ of the sample, R_A = $^3He/^4He$ of air (1.4×10^{-6})).

A setting similar to those described above is encountered in the Tertiary-aged East Java sedimentary basin, north of the volcanic Sunda Arc, formed by the subduction of the Indo-Australian plate beneath the Eurasian continental plate (Hall, 2002; Figure 1a). The basin is characterized by high sedimentation rates, deposition of organic-rich sediments, and volcaniclastic and carbonate traps, resulting in the formation of a HC province with numerous oil and gas fields and diffused surface and subsurface piercement structures (Istadi et al., 2012; Mazzini et al., 2018; Mazzini et al., 2007; Moscariello et al., 2018; Satyana & Purwaningsih, 2003a, 2003b). The basin bordered to the south by the Penanggungan, Arjuno-Welirang, and Bromo volcanoes and represents an ideal opportunity to investigate the relationship between mantle-derived volatiles and HC fluids in oil and gas reservoirs.

This region is also of particular interest because of the Lusi piercement, the world's largest active mud eruption neighboring the Holocene Penanggungan and Arjuno-Welirang volcanoes, situated, respectively, at 10 and 25 km to the southwest (Figures 1b and 2). Lusi (named after LUmpur, meaning mud in Indonesian, and SIdoarjo, the Local Regency) started its eruptive activity on the 29 May 2006 and has since been continuously

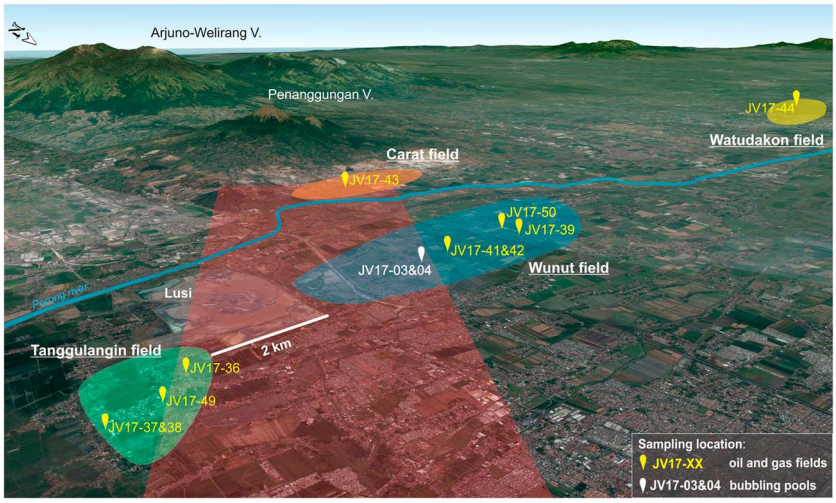

Figure 2. 3-D Google Earth view of the study area with indicated location of the oil and gas fields (color shaded areas), the sampling stations, and the Watukosek fault system (red shaded area).

bursting boiling water, gas, mud, oil, and rock clasts (Van Noorden, 2006). A set of targeted field campaigns has been completed since the beginning of the eruption to investigate the origin of the erupted fluids and the subsurface plumbing system (Miller & Mazzini, 2018, and references therein). Results revealed that outgassing boiling fluids at the Lusi surface contain evidence of hydrothermal waters and a mix of inorganic and organic gases, including geothermal (thermo-metamorphic and mantle-derived) and biotic (i.e., thermogenic methane) gases (Mazzini et al., 2012; Mazzini et al., 2018). Ambient noise tomography revealed a connection between the Arjuno-Welirang magma chamber and the Lusi conduit at around 4.5-km depth, indicating the migration of magmatic and hydrothermal fluids toward the sedimentary basin (Fallahi et al., 2017). These results confirmed that Lusi is indeed not a mud volcano but rather a sediment-hosted geothermal system (Mazzini & Etiope, 2017; Procesi et al., 2019). Sampling from the fumaroles of the Arjuno-Welirang volcanic complex provided further evidence of the connection between these two eruptive systems (Inguaggiato et al., 2018). The authors revealed that both the fumaroles of the Arjuno-Welirang and gas at the Lusi site contain magmatic volatiles with high ^{3}He abundance ($R = 7.3$ and 6.5 R_A, respectively). Furthermore, the Watukosek fault system (WFS), extending toward the northeast of the island from the Arjuno-Welirang volcanic complex (Figure 2), hosts Lusi and several mud volcanoes (Fallahi et al., 2017; Mazzini et al., 2009; Mazzini et al., 2012; Moscariello et al., 2018; Obermann et al., 2018; Sciarra et al., 2018). The authors indicate that this sinistral strike-slip system provides an ideal pathway for the propagation of the deep overpressured hydrothermal fluids toward the sedimentary basin and further to the surface.

This complex plumbing system and tectonic structures are largely controlling the past and present migration of fluids. Lusi is surrounded by three shallow oil and gas fields (Figures 1b and 2) that reflect the paleo-migration of HCs in the basin. Despite the obvious proximity between Lusi and these HC reservoirs, no dedicated studies have yet been conducted to investigate (1) if the HC gas currently erupted at Lusi is the same as that stored in the reservoirs, (2) if any correlation represents a potential connection between these two systems, and (3) whether the WFS could also provide a migration pathway for the mantle-derived fluids to the shallow reservoirs. This study aims to characterize the composition and origin of the gas trapped in the subsurface and to unravel the above questions by analyzing targeted samples.

2. Geological Setting

The East Java Basin is located on the southeastern margin of the Sunda plate, bounded to the south by the northward subduction of the Indian-Australian Plate. The subduction initiated in the Middle Eocene and resulted in the formation of two volcanic arcs: the Southern Mountain Arc (active between ca. 45 and

20 Ma) and Sunda Arc (active since ca. 12–10 Ma; Hall, 2013; Smyth et al., 2008). The axis of the Sunda Arc is located 50 km to the north from the older Southern Mountain Arc. The Arjuno-Welirang volcanic complex consists of Holocene stratovolcanoes, located in the eastern part of the Sunda Arc. Penanggungan is the northeasternmost volcano of this complex and is in the vicinity (~10 km) of the Lusi mud eruption and the studied oil and gas fields. The most recent recorded eruptive activity occurred at the Welirang volcano in 1952 (Global Volcanism Program, 2013). Currently, the crater is characterized by solfataric fields, with several hydrothermal seeps distributed on the flanks (Inguaggiato et al., 2018; Mazzini et al., 2012; Mazzini et al., 2018).

The East Java Basin comprises a complex of northeast to southwest trending troughs, developed during Late Eocene to Early Miocene due to the extensional regime of the Sunda plate (Doust & Noble, 2008). The sedimentary section contains more than 5 km of deposits, spanning in age from Eocene to recent, overlying the pre-Tertiary basement, with the maximum sediment thickness of 8–10 km in the Kengden graben (Hall et al., 2011; Kusumastuti et al., 1999; Martha et al., 2017). In the study area, the lithostratigraphic section is constrained by drilled boreholes, analyzed clasts erupted at the Lusi site, and by seismic surveys from the 1990s–2000s (Istadi et al., 2009; Malvoisin et al., 2018; Mazzini et al., 2018; Mazzini et al., 2007; Moscariello et al., 2018; Samankassou et al., 2018; Satyana & Purwaningsih, 2003b; Sharaf et al., 2005; Tingay, 2015). The sedimentary section constrained in the deepest well (BJP1, TVD 2,833 m) consists of (from top to down) the following:

1. recent alluvial sediments (intercalated sands, shales, and volcaniclastic sands and clays), 0–290 m;
2. volcaniclastic shales and sands of the Pucangan Formation, Pleistocene, 290–900 m;
3. bluish gray shales of the upper part of the Upper Kalibeng Formation, Pleistocene, 900–1,871 m; and
4. tight volcanic and volcaniclastic units of the lower part of the Upper Kalibeng Formation, Upper Pliocene-Pleistocene, 1,871 to at least ~2,833 m.

Lithostratigraphy below 2,833 m is based on regional studies, Lusi mud breccia analyses, and seismic data

1. marls and shales of the Tuban Formation, Lower-Upper Miocene, from >2,833 to ~3,250 m;
2. reefal and platform carbonates of the Kujung Formation, Upper Oligocene-Lower Miocene, from ~3,250 to ~3,800 m; and
3. organic-rich black shales of the Ngimbang Formation, Middle Eocene-Lower Oligocene, >3,800 m.

The basin is characterized by high sedimentation rates (0.7 km/Ma) since Late Pliocene, which resulted in fast burial and preservation of the semilithified deposits.

3. Petroleum System of the East Java Basin

The East Java Basin is a petroleum province with a total reserve volume of 1,830 Million Barrels of Oil Equivalent (Doust & Noble, 2008). The HC accumulations in the basin are confined to shallow volcaniclastic Pleistocene reservoirs (Pucangan Fm.), Miocene sands of the Ngrayong and Woncolo Formations, Upper Oligocene-Lower Miocene reefal carbonates of the Kujung Fm., and carbonates and sands of the Ngimbang Formation (Doust & Noble, 2008; Satyana & Purwaningsih, 2003b).

The main HC source rock is suggested to be the Middle Eocene-Lower Oligocene organic-rich shales, coals, and coaly shales of the Ngimbang Fm. (Devi et al., 2018; Satyana & Purwaningsih, 2003a). These sediments were deposited in a fluvio-deltaic to near-shore marine environment. Organic-rich shales of the Ngimbang Fm. contain up to 5.7 wt.% Total Organic Carbon (TOC) and coal bearing interval with TOC up to 67 wt.% (Satyana & Purwaningsih, 2003a).

The study area is located in the southern part of the East Java Basin, to the north of the Arjuno-Welirang volcanic complex and in the neighborhood of the Lusi eruption site. Three production HC fields, Wunut, Tanggulangin, and Carat, surrounding Lusi site were targeted for investigation. Here producing reservoir intervals are confined to the Pucangan Fm., 200- to 1,000-m depth, that was deposited as a northeastward prograding, volcaniclastic sedimentary wedge (Istadi et al., 2009; Kusumastuti et al., 1999). The Pucangan Fm. consists of predominantly fine-grained material (up to 80% of net shales) and layers of sandstones, 3–47 m thick (Kusumastuti et al., 1999). The intercalating shales seal the HC accumulations. The traps

are four-way dip closures with multiple reservoir layers. The lower intervals of the Pucangan Fm. contain oil, while the shallower units are gas prone. The measured thermal gradient in the wells varies from 2.8 to 4.9 °C/100 m.

4. Sampling and Analytical Procedures

During spring 2017, a gas sampling campaign was conducted in northeast Java with the aim to obtain surface and subsurface gas samples of the southern part of the East Java Basin. Two main settings and localities have been targeted (Figures 1b and 2). The first set of samples (Group 1) was collected from several production wells of targeted gas fields (Wunut, Tanggulangin, and Carat). Surface seeping gas was collected from bubbling pools, located above the Wunut field (Group 2). In addition, the Watudakon gas field (~36 km west of the Lusi on the outskirts of the Arjuno-Welirang volcanic complex) was sampled (Group 3). Formation waters from the Wunut and Watudakon fields were also sampled to conduct dissolved gas analyses (Group 4). Finally, selected rock cuttings from the BJP1-R1 well, originally drilled in the outskirts of the Lusi eruption site (Sutrisna, 2009), were analyzed for the TOC content through the interval 543–884 m of the Pucangan Fm. and 900–993 m of the Up. Kalibeng Fm.

Gas samples were collected in two valve steel and glass samplers. Prior to sampling, the head well was routinely flushed for 20 min to reduce potential contamination of the sample. Bubbling seeps were sampled using a plastic funnel positioned upside-down and connected by silicone tubes to glass or steel tanks. Water was collected in crimped 245-ml glass water flasks.

The analyses of chemical composition of fluids were completed at the Istituto Nazionale di Geofisica e Vulcanologia (INGV-Palermo, Italy). Gas chromatography (GC) was performed using a gas chromatograph (Perkin Elmer Clarus 500) equipped with a double detector (thermal conductivity detector and a flame ionization detector with a methanizer) using Ar as the carrier gas and a 3-m packed column (Restek Shincarbon ST), with analytical errors of <3%.

Dissolved gas samples were extracted by the collected waters and analyzed by using the methodology proposed by Capasso and Inguaggiato (1998).

The carbon isotopic composition of CO_2 ($\delta^{13}C_{CO2}$) was determined using a Thermo Delta XP Isotope Ratio Mass Spectrometer coupled with a Thermo Scientific™ TRACE™ Ultra Gas Chromatograph. Separation prior to analysis was done through a 30-m Q-plot column (i.e., of 0.32 mm). The resulting $\delta^{13}C_{CO2}$ values are expressed in per mil notation with respect to the international Vienna Pee Dee Belemnite (VPDB) standard and analytical uncertainties of ±0.15‰.

The carbon and deuterium isotopic composition of CH_4 ($\delta^{13}C_{CH4}$ and δD_{CH4}) was determined using a Thermo TRACE GC interfaced to a Delta Plus XP gas source mass spectrometer and equipped with a Thermo GC/C III (for Carbon) and with GC/TC peripherals (for Hydrogen). The $^{13}C/^{12}C$ ratios are reported as $\delta^{13}C_{CH4}$ values with respect to the VPDB standard, and $^{2}H/^{1}H$ ratios are reported here as δD_{CH4} values with respect to the Vienna Standard Mean Ocean Water (VSMOW) standard. The analytical uncertainty of the measurements was 0.1‰.

Carbon isotopes of the methane homologs were measured in the Isotech Labs Inc. (Illinois, USA) using three IRMS instruments: Delta Plus, Delta Plus XL, and Delta V Plus.

^{3}He, ^{4}He and ^{20}Ne, and the $^{4}He/^{20}Ne$ ratios were determined by separately injecting He and Ne into a split flight tube mass spectrometer (GVI-Helix SFT, for He analysis) and then into a multicollector mass spectrometer (Thermo-Helix MC plus, for Ne analysis), after standard purification procedures (Correale et al., 2012). The analytical error was generally less than 1%. The R/R_A values were corrected for atmospheric contamination based on the $^{4}He/^{20}Ne$ ratio (Sano & Wakita, 1985). The Ar-isotope composition was measured in a multicollector mass spectrometer (GVI Argus), for which the analytical uncertainty was 0.5%.

Measured He isotopes values are reported as R/R_A, where $R = {}^{3}He/{}^{4}He$, measured in the sample, and $R_A = {}^{3}He/{}^{4}He$ of air (1.4×10^{-6}). Helium concentrations in the analyzed samples range from 5 to 140 ppm. $^{4}He/^{20}Ne$ ratio is 120–1,690 times higher than that measured in air ($^{4}He/^{20}Ne = 0.318$), confirming very low air contamination and validating the accuracy of the results.

Table 1
Major Gas Components of the Sampled Free Gas (Group1-3, in vol.%) and Dissolved Gas (Group 4, in cm3 per Liter at Standard Temperature and Pressure)

Sample ID	Group	Field	Well, sampling depth interval (m)	He	H_2	O_2	N_2	CH_4	CO	H_2S	CO_2	C_2H_6	C_3H_8	$C_1/(C_2+C_3)$
JV17-36	1	Tanggulangin	Well TG5, 742–966	0.0008	nd	0.01	0.7	91.6	nd	nd	4.58	2.66	0.66	28
JV17-37			Well TG1, 468–471	0.0013	nd	0.20	2.1	97.7	nd	nd	0.22	0.14	nd	698
JV17-38			Well TG1SS, 417–425	0.0023	nd	0.11	2.6	96.9	nd	nd	0.06	0.05	nd	1,978
JV17-49			Well TG2, 435–460	0.0026	0.0043	0.16	3.3	96.1	nd	nd	0.08	0.05	nd	2,056
JV17-41		Wunut	Well WU-1ST, 218–246	0.0050	0.0005	1.13	6.9	91.0	nd	nd	0.05	0.03	nd	2,757
JV17-42			Well WU 1A-LS, 341–347	0.0046	0.0002	0.06	2.7	97.2	nd	nd	0.10	0.04	nd	2,745
JV17-50			Well WU9LS, 790–885	0.0005	0.0007	0.25	1.2	96.5	nd	nd	0.37	0.61	nd	158
JV17-39			Well WU16, 627–807 (?573?)	0.0015	0.0008	0.07	1.3	96.3	nd	nd	0.02	1.72	0.42	45
JV17-43		Carat	Well CA-1, 494–500	0.0012	0.0002	0.004	1.2	98.7	nd	nd	0.06	0.06	nd	1,646
JV17-03	2	Surface seep	Bubbling pool	0.0141	0.0043	0.33	7.0	85.2	nd	nd	1.10	3.88	1.60	16
JV17-04			Bubbling pool	0.0139	0.0040	0.28	6.9	83.4	nd	nd	1.18	3.86	1.68	15
JV17-44	3	Watudakon	well WD20, ~350 m	0.0006	0.0011	0.04	0.5	100.0	nd	nd	0.04	0.09	nd	1,118
JV17-46	4	Watudakon	well WD17, ~600 m	0.000426	0.024	0.17	2.33	20.8	0.00204	b.d.l.	8.28	b.d.l.	b.d.l.	
JV18-08		Wunut	well WU15, ~900 m	0.0002	0.00004	3.26	10.5	14.0	b.d.l.	b.d.l.	28.15	b.d.l.	b.d.l.	

Note. nd = not defined, b.d.l. = below detection limit.

TOC measurements were performed on the LECO CS-230, in the Federal Institute for Geosciences and Natural Resources (BGR), Germany. The method is described in Blumenberg et al. (2016).

5. Results

Gas geochemistry results obtained from the sampled localities are summarized in Tables 1 and 2. All sampled gases are methane-dominated (CH_4 > 91.6 vol.%). N_2 is present in variable concentrations (from 0.5 to 7.5 vol.%), and O_2 concentrations are up to 1.13 vol.%. The O_2/N_2 ratio in the collected gases is lower than 0.1 (except the sample JV17-50, 0.21), that is, lower than the same ratio in air (0.27) and in the air saturated water (0.53) showing that these fluids were not affected by strong air contamination.

More specifically, gas samples from the oil and gas production wells around Lusi (Group 1) contain methane ranging from 91 to 99 vol.% and higher methane homologs (ethane < 2.7 vol.% and propane < 0.7 vol.%). The gas dryness ratio $C_1/(C_2+C_3)$ varies from 28 to 2,757 and follows a general trend decreasing with the reservoir depth (Figure 3a). CO_2 concentrations are very low (average value 0.1 vol.%), except for the deepest producing units of TG5 well of Tanggulangin field (4.6 vol.%). The $\delta^{13}C_{CH4}$ varies from −40.7‰ to −58.3‰ and δD_{CH4} from −201‰ to −177‰. The low CO_2 content present in the samples allowed the isotopic measurements to be performed in only two samples from Tanggulangin and Carat fields (18.9‰ and 22.8‰, respectively). He isotopes have a R/R_A ranging between 5.1 and 6.7, with the lowest values recorded in the deepest samples. Ar isotope composition ($^{40/36}$Ar) ranges between 303 and 435, higher than the same ratio in atmosphere (298.6; Ozima & Podosek, 2002).

Two gas samples from the bubbling pools above the Wunut field (Group 2, named surface seep in the Tables 1 and 2) revealed almost identical composition. Together with methane (average 84.3 vol.%) and CO_2 (average 1.14 vol.%), ethane and propane were also detected (3.9 and 1.6 vol.%, respectively). The average gas dryness ratio is 15.3, which is significantly lower than that measured for the Group 1 samples (Figure 3a). The isotopic analyses reveal $\delta^{13}C_{CH4} = -42.5$‰ and ranges of δD_{CH4} from −170‰ to −173‰, $\delta^{13}C_{CO2}$ from 1.2‰ to 2.7‰, and $R/R_A = 6.1$ and $^{40/36}$Ar from 330 to 357.

The gas sampled at the Watudakon gas field (Group 3) is also CH_4-dominated, with ethane abundance <0.09 vol.%. Isotopic analyses revealed $\delta^{13}C_{CH4} = -62.4$‰ and $\delta D_{CH4} = -190$‰, while $\delta^{13}C_{CO2}$ was not measured due to low CO_2 concentration (599 ppm).

Table 2
Isotopic Composition of the Sampled Free Gas

Sample ID	Group	Field	$\delta^{13}C_{C1}$	$\delta^{13}C_{C2}$	$\delta^{13}C_{C3}$	$\delta^{13}Ci_{C4}$	$\delta^{13}Cn_{C4}$	$\delta^{13}Ci_{C5}$	$\delta^{13}Cn_{C5}$	$\delta^{13}C_{CO2}$	δD_{CH4}	R/ R_A	He	Ne	$^4He/^{20}Ne$	R/Ra $_c$	$^{40}Ar/^{36}Ar$	^{40}Ar
JV17-36	1	Tanggulangin	−40.7	−25.7	−16.6	−22.6	−19.3	−21.8	−18.4	18.9	−181.5	5.9	7.3	0.04	194.3	5.9	435.0	18.7
JV17-37			−50.7								−200.9	5.9	13.8	0.09	147.6	5.9	323.2	83.8
JV17-38			−57.1								−196.9	6.6	22.7	0.17	130.1	6.6	308.9	181.1
JV17-49			−58.3								−198.4	6.2	25.4	0.66	38.4	6.2	303.4	288.9
JV17-41		Wunut	−48.5								−197.3	6.3	50.3	0.09	537.4	6.3	345.2	142.6
JV17-42			−47.8								−195.1	6.3	45.2	0.09	492.0	6.3	368.6	99.1
JV17-50			−57.7								−190.6	5.1	4.6	0.09	51.6	5.1	307.0	36.5
JV17-39			−41.8	−23.4	−16.1	−21.8	−18.1	−20.8			−176.8	5.9	14.9	0.18	81.6	5.9	357.0	40.6
JV17-43		Carat	−41.4							22.8	−195.6	6.7	11.2	0.03	371.4	6.7	313.8	84.3
JV17-03	2	Surface seep	−42.6	−27.1	−24.5	−25.7	−23.2	−23.8	−21.6	2.7	−170.4	6.1	143.1	0.46	313.5	6.2	357.3	326.3
JV17-04			−42.5							1.2	−173.3	6.1	142.7	0.92	155.5	6.1	329.5	563.5
JV17-44	3	Watudakon	−62.4	−30.8							−190.1	2.1	5.8	0.10	56.5	2.1	300.5	83.1

Note. Isotopic data: $\delta^{13}C$ (‰VPDB); δD (‰VSMOW); $R/R_A = (^3He/^4He)$ sample/$(^3He/^4He)$ atmosphere. He, Ne, and ^{40}Ar concentrations in parts per million.

The measurements of water-dissolved gases of the Watudakon gas field (Group 4) are CH_4-dominated (20.8-cm^3/l Standard Temperature and Pressure (STP); Table 1) but with also high content of CO_2 (up to 8.28 cm^3/l STP). This last value is 27 times higher than that measured in the Air Saturated Waters values (ASW = 0.31 cm^3/l STP). Helium isotope composition revealed R/R_A = 2.14 and $^{40/36}Ar$ equals to 300.5‰. Water-dissolved gases at the Wunut field (Group 4) are CO_2-dominated (28.15 cm^3/l STP, Table 1) with CH_4 content of 13.97 cm^3/l STP.

Measured TOC in the cuttings of the Pucangan and Upper Kalibeng Formations from the BJP-R1 well resulted in 0.5 to 1.75 wt.% (average 0.9 wt.%).

6. Discussion

The acquired geochemical data set allowed to identify the origin of the gases that are trapped in the shallow HC reservoirs produced in the northeast Java. Furthermore, we combined the data in order to investigate if a possible connection exists between the neighboring Arjuno-Welirang volcanic complex and the reservoirs. This is described in detail in the following sections.

6.1. HC Origin and Alteration Processes in the Reservoirs

The origin of natural gases, trapped in the porous media, is commonly characterized using binary genetic diagrams of $\delta^{13}C_{CH4}$ versus δD_{CH4}, $\delta^{13}C_{CH4}$ versus $C_1/(C_2 + C_3)$, and $\delta^{13}C_{CH4}$ versus $\delta^{13}C_{CO2}$. These empirical diagrams were first proposed in 1970s–1980s (Bernard et al., 1977; Gutsalo & Plotnikov, 1981; Schoell, 1983; Whiticar et al., 1986) and have been more recently revised based on >690,000 data entries (Milkov & Etiope, 2018). This recent study highlights that the original molecular and isotopic composition of CH_4, its homologs, and CO_2 could be affected by several post-generation processes, including mixing, migration, biodegradation, thermochemical sulfate reduction, and oxidation. Therefore, a combined use of these plots is required to obtain distinctive conclusions in order to classify gases in natural systems.

Methane isotope composition of the gas from Group 1 ($\delta^{13}C_{CH4}$ range from −58.3‰ to −40.7‰ and δD_{CH4} from −201‰ to −170‰) coupled to the ratio $C_1/(C_2 + C_3)$ indicates that the studied natural gases have mainly thermogenic origin (i.e., generated within organic-rich sediments due to thermal cracking of the kerogen), even if CH_4 from different reservoirs of the Group 1 shows a large variability of its isotopic composition (Figures 3b and 3c). These results are consistent with the migration of HCs from the organic-rich deep sited (>4 km) Middle Eocene-Lower Oligocene Ngimbang source rock (Kusumastuti et al., 1999). The HCs were presumably initially trapped in the Miocene reef carbonates of the Porong structure (located few kilometers to the east from the studied HC fields; see Figure 1b for location). After the collapse of the seal above this carbonate reservoir, HCs migrated through a system of faults to the shallow porous units of the Pucangan Fm during the Late Pleistocene-Holocene and migrated toward the west in the targeted reservoirs (Kusumastuti et al., 1999).

The positive carbon isotope ratio of the CO_2 ($\delta^{13}C_{CO2}$ +18.9‰ and +22.8‰) indicates that the HC reservoirs are affected by biodegradation processes (Figure 3d). Biodegradation is commonly taking place in

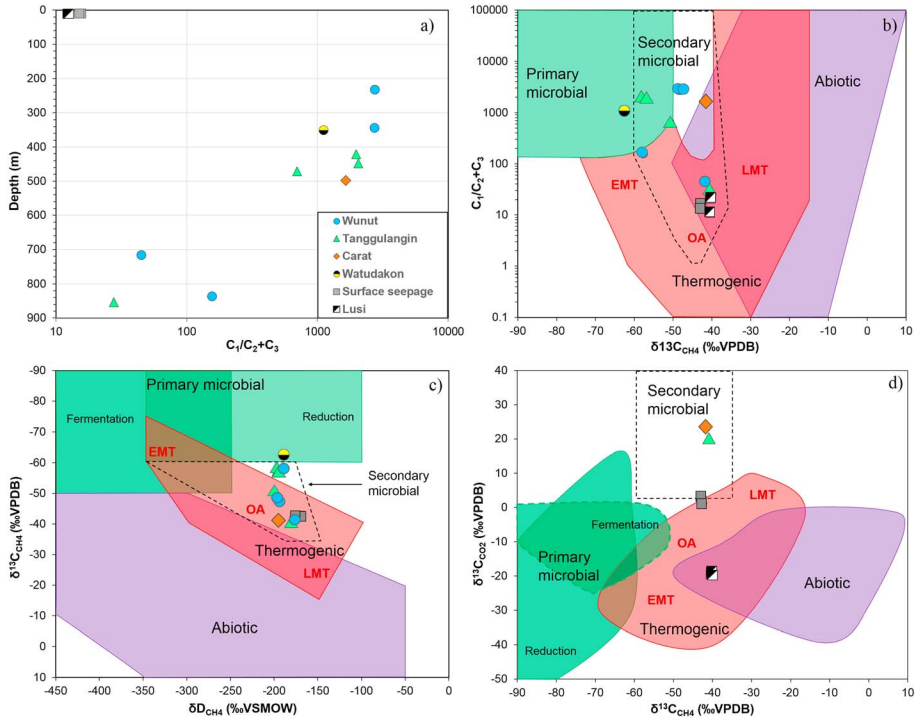

Figure 3. (a) The dryness plot of the sampled HC gases versus the reservoir depth reveals decreasing values at higher depths. The gas erupted at the Lusi surface, and adjacent seepages is wet. Gas genetic diagrams of (b) $C_1/(C_2 + C_3)$ versus $\delta^{13}C_{CH4}$; (c) $\delta^{13}C_{CH4}$ versus δD_{CH4}; (d) $\delta^{13}C_{CO2}$ versus $\delta^{13}C_{CH4}$; after Milkov and Etiope (2018). The genetic diagrams reveal the thermogenic origin of the gas sampled from the shallow HC reservoirs at Wunut, Tanggulangin, and Carat fields (Group 1) and the surface seepages (Group 2). The gas composition is altered by biodegradation processes, therefore mixed with secondary microbial gas. The gas sampled from the Watudakon field is of primary microbial origin. The majority of the sampled HC gas from the reservoirs is dry. HC gas from the Lusi crater (Mazzini et al., 2012), surface seepages, and two HC reservoirs (this study) is wet. EMT = Early Mature Thermogenic gas; LMT = Late Mature Thermogenic gas; OA = oil-associated gas; HC = hydrocarbon.

shallow HC reservoirs at temperatures below 80–90 °C (Head et al., 2003; Milkov, 2010, and references therein) and can be simplified in two main steps: 1) anaerobic oxidation of the thermogenic HCs followed by microbial CO_2 production, combined with (2) microbial (operated by methanogens) CH_4 generation via CO_2 reduction (Etiope et al., 2009; Milkov, 2018). Due to preferential selection by the methanogens of the ^{13}C-depleted CO_2, the residue CO_2 is enriched in ^{13}C carbon isotope (Head et al., 2003; Milkov, 2011). Occurrence of biodegradation process in the reservoirs is also supported by the available carbon isotope analyses of the methane homologs (C_nH_{2n+2}) in the studied samples. The $\delta^{13}C$ measured on gaseous HCs formed due to thermocracking processes of, typically follows a regression trend (i.e., $\delta^{13}C_{CH4} < \delta^{13}C_{C2H6} < \delta^{13}C_{C3H8} < \delta^{13}C_{C4H10}$, Chung et al., 1988; Schoell, 1983). An irregular trend is instead present in reservoirs with T < 80–90 °C affected by the HC biodegradation processes. This process occurs because of the selective preference of bacteria to use some homologs over others, that is propane and n-butane over ethane and isobutane (Wenger et al., 2002). Similarly to CO_2 microbial consumption, the bacteria favor the ^{13}C-depleted C_nH_{2n+2}, that is controlled by the bacterial enzymatic processes and C-C bond energies (Peters et al., 2005). As a result, the remaining C_nH_{2n+2} molecules are enriched in ^{13}C carbon. Our analyses, and the one described in Mazzini et al. (2012), reveal that the observed carbon isotope ratios trend (Figure 4) are consistent with the biodegradation processes described above.

A potential contribution of methane generated within the shales of the Pucangan and/or Kalibeng Formations cannot be excluded; however, this should be a limited amount given the relatively low TOC in this formation (TOC from 0.5 to 1.75 wt.%, average 0.9 wt.%).

The natural gas sampled at the Watudakon field is essentially methane-dominated with a clear microbial isotopic signature ($\delta^{13}C_{CH4}$ and δD_{CH4} are −62.4‰ and −190.1‰, respectively; Figures 3b and 3c). This

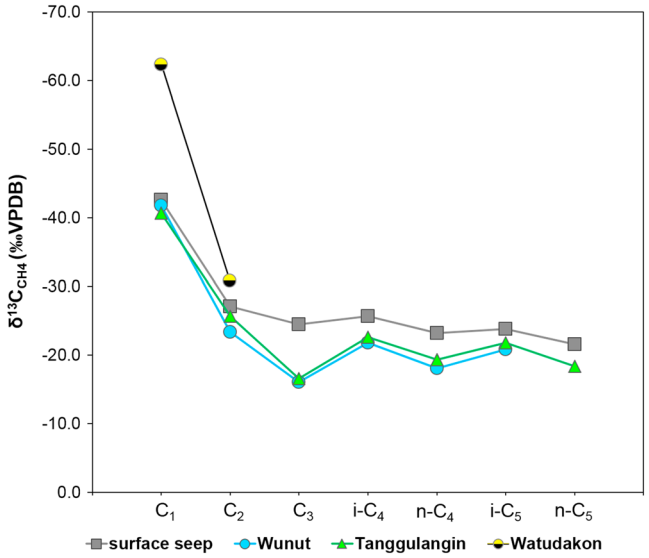

Figure 4. Carbon isotope distribution of the methane homologues in the samples from the Tanggulangin, Wunut, and Watudakon fields and surface seep. The plot indicates the occurrence of the hydrocarbon biodegradation processes in the Tanggulangin and Wunut reservoirs. Gas sampled at the surface seep above the Wunut field does not show the evidence of significant biodegradation.

indicates either (1) biodegradation processes of thermogenic HCs (gaseous and liquid), earlier generated by thermocracking process, or (2) ongoing microbial methanogenesis in the shallow organic-rich clays that interbed the porous media hosting the gas. According to the well log data from the Watudakon 20 well, there is no record of oil shows or other oil traces in the well. The trace amount of C_{2+} gases (lower than 0.1%) also supports a primary microbial origin of the methane. These data may suggest that the migration of HCs from the Ngimbang source rock did not occur in this peripheral part of the basin and that more recent microbial processes are currently very active.

6.2. Migration of the Mantle-Derived Fluids in the Sedimentary Basin

He isotopes represent a powerful tool for recognizing the occurrence of mantle-derived fluids in sedimentary HC reservoirs and in continental region away from volcanism (e.g., O'Nions & Oxburgh, 1988; Prinzhofer, 2013). He is an inert gas, highly mobile, physically stable, it has two stable isotopes (^{3}He and ^{4}He), and their isotopic signatures in the pristine reservoirs (atmosphere, crust and mantle) are strongly different: ^{3}He has a primordial origin and is usually degassed from the mantle (Ozima & Podosek, 2002); ^{4}He is produced by U and Th decay. Three major He reservoirs have distinct ^{3}He/^{4}He isotope ratios: (1) crust 0.01 R_A ($R_A = {}^3\text{He}/{}^4\text{He}$ of air, 1.4×10^{-6}); (2) atmosphere 1 R_A; and (3) mantle from ~8 ± 1 R_A (Mid-Ocean Ridge Basalts mantle reservoir; Ozima & Podosek, 2002).

Our results (Table 2) reveal that all the samples from the HC reservoirs have a high ^{3}He/^{4}He isotope ratios (R/R_A as high as 6.7). Argon isotope composition ($^{40/36}$Ar) in the collected fluids shows that these fluids have low air contamination. This is confirmed by the values of the ^{4}He/^{20}Ne ratios that are higher than the same ratio in the atmosphere ($^4\text{He}/^{20}\text{Ne}_{AIR} = 0.318$, Table 2).

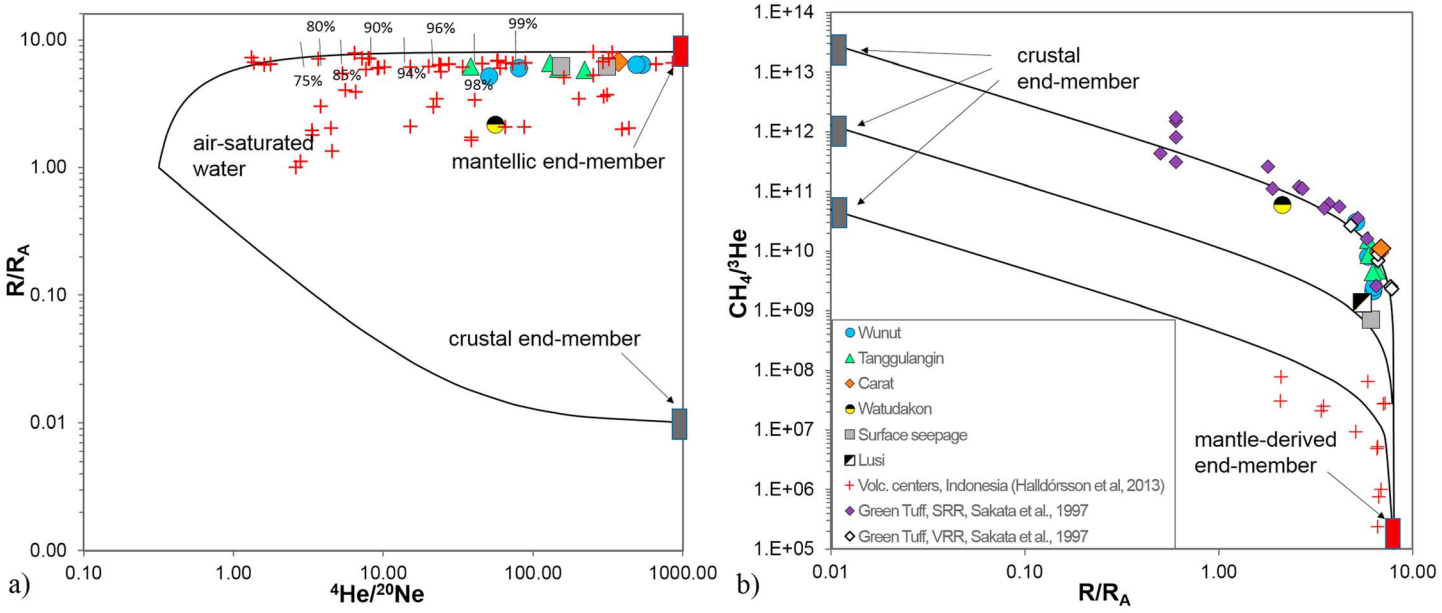

Figure 5. (a) Plot of the measured He isotopes versus ^{4}He/^{20}Ne ratio showing the integrity of the He isotope results. The curves represent mixing between air-saturated water (1 R_A), Mid-Ocean Ridge Basalts (8 R_A), and crust (0.01 R_A); (b) plot of the $CH_4/^3$He ratio versus He isotopes (R/R_A). Black lines indicate two-component mixing of the mantle-derived end-member ($CH_4/^3\text{He} = 1.0 \times 10^5$ and ^{3}He/^{4}He = 8 R_A) and crustal end-member with three possible compositions ($CH_4/^3\text{He} = 5.0 \times 10^{10}$, 1.3×10^{12}, and 3.0×10^{13} with a common ^{3}He/^{4}He = 0.01 R_A), adopted after Halldórsson et al. (2013) and Jenden et al. (1993). The plot demonstrates that even in the systems with high CH_4 abundance, He could have low crustal contamination.

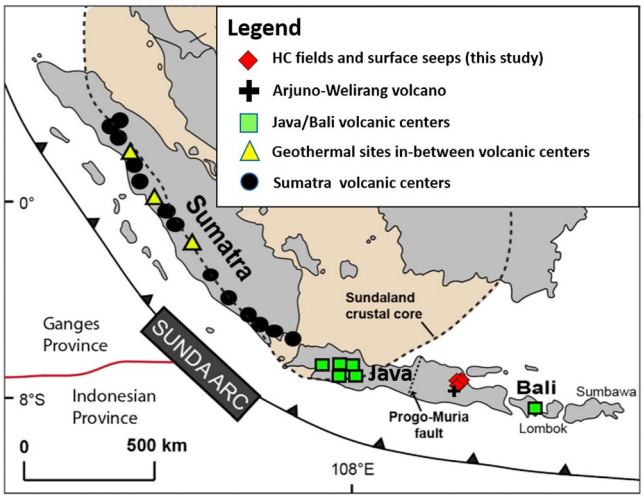

Figure 6. Map of Indonesia, modified after Halldórsson et al. (2013), showing measured He isotopes distribution through the Sunda arc (Halldórsson et al., 2013), at the Arjuno-Welirang volcano (Inguaggiato et al., 2018), and in the southern part of the East Java sedimentary basin (this study, red diamonds). HC = hydrocarbon.

The ranges of the measured He-isotope compositions and $^4He/^{20}Ne$ ratios in the collected gases can be explained in terms of mixing between three sources of He (Sano et al., 1997): atmosphere, mantle, and crust (Figure 5a). Since the investigated systems are located in a continental region, we assumed a Mid-Ocean Ridge Basalts mantle source in the area with a He-isotope ratio of 8 ± 1 Ra, as suggested by Halldórsson et al. (2013). We then computed the contributions of atmospheric, radiogenic, and mantle-derived He on the basis of the analytical $^3He/^4He$ and $^4He/^{20}Ne$ ratios (Sano et al., 1997). The fluids associated with the investigated HCs contain mantle He contributions from ~98% to ~99.9% (Figure 5a).

In order to constrain the possible origin of CH_4 in the HC reservoirs, we used the approach proposed by Poreda et al. (1988) that is based on a two component crust-mantle mixing model, $CH_4/^3He$ ratios versus He isotopes (Figure 5b). We used three possible crustal end-members with $CH_4/^3He = 5.0 \times 10^{10}$, 1.3×10^{12}, and 3.0×10^{13}, with common $^3He/^4He = 0.01\ R_A$, and a mantle-derived end-member with $CH_4/^3He = 1 \times 10^5$ and $^3He/^4He = 8\ R_A$ (Halldórsson et al., 2013). The proposed mixing model reveals that crustal end-member with $CH_4/^3He = 3.0 \times 10^{13}$ is the most suitable for our data set. Although the investigated reservoirs are methane-dominated, the measured $CH_4/^3He$ ratios are similar to those in the geothermal systems of subduction zones (Snyder et al., 2003, and references therein) and those measured in the volcanic rock reservoirs of natural gas fields in the Green Tuff basin, Japan (Sakata et al., 1997; Figure 5b). However, $CH_4/^3He$ ratio in the HC reservoirs is 2 to 3 orders of magnitude higher than in the volcanic centers along the western Sunda Arc (Halldórsson et al., 2013). These findings confirm the presence of a specific setting where methane-dominated reservoirs are heavily affected by the migration of mantle-derived He. This situation presents new questions and scenarios regarding the migration of magmatic fluids that are typically CO_2-dominated.

6.3. Noble Gas Distribution Through the Sunda Arc

Our data fit well with those from previous investigations in natural fluids emitted in volcanic and hydrothermal systems in the western and central Sunda Arc (Halldórsson et al., 2013), where the outgassing volatiles are dominated by CO_2. Here the majority of the He isotopes ratios range from 5.3 to 8.1 R_A (Figure 6). Hence, at regional scale, the mantle wedge is considered to be the principal source of He at volcanic centers. However, a minor radiogenic contamination from the subducted crust can also be inferred, particularly in the western part of the Sunda Arc, where thicker and older crust is present, decreasing the typical mantle-derived He signature in the emitted volatiles. However, the large database described by Halldórsson et al. (2013) contains a gap in the central and eastern part of Java. Our novel data together with the He data from the Arjuno-Welirang volcanic system (Inguaggiato et al., 2018) and those from the Lusi crater (Mazzini et al., 2012) contribute to the filling of this gap and to the reconstruction of the general distribution of the magmatic volatile sources along the eastern Sunda Arc. Furthermore, our results demonstrate a propagation of the mantle-derived volatiles from the volcanic complex to the sedimentary basin around the Lusi system.

6.4. The Fate of Magmatic CO_2

CO_2, CH_4, and H_2O are considered as the main He carriers for migration through the crust in sedimentary and volcanic settings. Previous results and modeling indicate that CO_2 is the major magmatic volatile migrating through the East Java Basin, particularly at and around the Lusi eruption site (Mazzini et al., 2012; Sciarra et al., 2018; Svensen et al., 2018; Vanderkluysen et al., 2014). Therefore, in our study case, CO_2 is assumed to be the carrier for the migration of the mantle-derived He in the sedimentary basin and the HC reservoirs. Nevertheless, the gas sampled in the HC reservoirs (Group 1) reveals very low CO_2 concentrations, varying from 0.02 to 0.37 vol.% (except for the well TG5), and concurrently high R/R_A values (Tables 1 and 2). Furthermore, the carbon isotopic composition of CO_2 is extremely positive (from +18.9‰ to +22.8‰) and significantly different from the typical composition of the mantle-derived CO_2

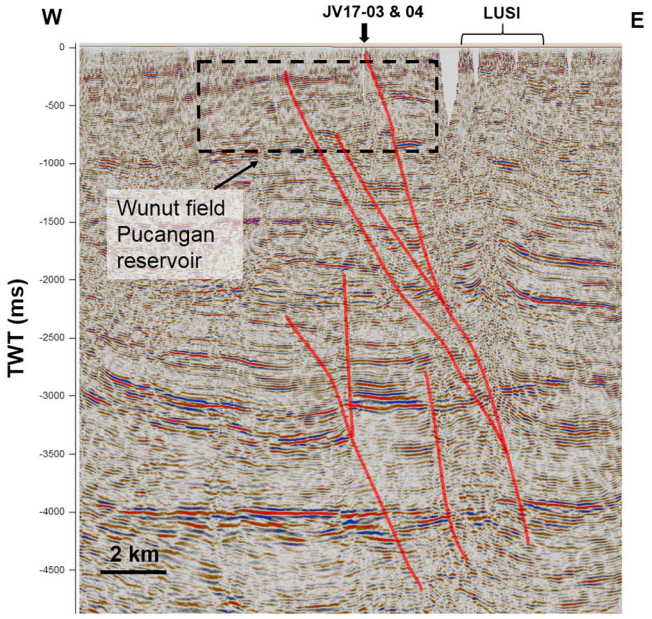

Figure 7. W-E-oriented seismic profile from 2003, with indicated location of the sampled surface seepage site, Lusi, the conditional location of the shallow hydrocarbon reservoirs of the Wunut field and several faults as part of the Watukosek Fault System (highlighted in red). Faults act as migration pathway for the fluids. Profile location indicated in Figure 1b. TWT represents two-way travel time.

($-8‰ < \delta^{13}C_{CO2} < -4‰$; Clark & Fritz, 1997; Deines, 2002). Hence, mantle-derived CO_2 seems to be decoupled from the mantle-derived He. There are two potential mechanisms able to mask the CO_2 as carrier gas: (1) CO_2 transformation to CH_4 by microbial activity and (2) CO_2 dissolution in the water. The first hypothesis is that large part of the CO_2 is transformed by microbial activity operated by methanogens (as described in the section 6.1). An additional hypothesis is that during the migration of mantle-derived He and CO_2, the latter gets mainly dissolved in formation water. This process is able to reduce the amount of CO_2 in the gas phase and preserve the pristine isotopic ratio of He that does not dissolve into water (Caracausi et al., 2003). This mechanism is not applicable for ongoing focused and vigorous seepage. For example, deep and hot CO_2-rich fluids at Lusi are flushed rapidly toward the surface without cooling. When instead diffused fluids migration occurs at slower rates through gradually colder sedimentary rock formations, the dissolution of CO_2 takes place. Furthermore, it is recognized that the transport of He could be decoupled from that of carbon gases in the areas away from the active volcanism (Giggenbach et al., 1993). The depicted scenario is further supported by the significant concentration of dissolved CO_2 in the water (8.28 and 28.15 cm^3/l STP at the Watudakon and Wunut fields, respectively, Group 4). Here the amount of the dissolved CO_2 is higher than in the water in equilibrium with the atmosphere (0.31 cm^3 SPT/l; Capasso & Inguaggiato, 1998), indicating that part of CO_2 can be dissolved in the shallow formation waters.

6.5. The Subsurface Plumbing System

To investigate potential fluid migration pathways, we compared the fluid geochemistry at different sites and complemented these data with available subsurface geophysical data. Gas compositions of the fluids emitted at the surface seepage sites above the Wunut reservoir (Group 2) are distinctively different from those recorded at the adjacent WU1 well (Tables 1 and 2). However, the origin of the HC gases is always thermogenic ($\delta^{13}C_{CH4}$ as high as $-42.5‰$ and δD_{CH4} as high as 170.4‰ $C_1/(C_2 - C_3) = 15$; Table 2 and Figures 3b and 3c). Furthermore, these seeps contain 5–10 times more CO_2 than samples of Group 1 (where CO_2 is almost absent) with a different isotopic signature (i.e., $\delta^{13}C_{CO2}$ between 1.2‰ and 2.7‰). These marked differences suggest that a diverse source of fluids is present at this locality or that some processes (i.e., mixing) may occur during the transfer of the fluids toward the surface.

Insights about the subsurface plumbing system are provided by seismic profiles acquired during the 1990–2000s in this part of the basin. Geophysical data highlight the occurrence of the WFS that extends from the Arjuno-Welirang volcanic complex, intersects Lusi, and progresses toward the northeast Java (Moscariello et al., 2018). The authors describe the presence of this deep-rooted fault system that splits laterally at shallower depths and creates a network of fractures. These faults either stop within the topmost kilometer of sediments or can be traced all the way to the surface. This type of features can also be observed on the seismic lines crossing the Wunut field, sampled seepage zone (Group 2), and Lusi (Figure 7). Here one of these faults reaches the surface exactly at the Group 2 seepages locality. Additional faults can also be observed ending below, and sometimes within, the Wunut field. Therefore, these fractured zones represent ideal pathways for the transfer of fluids due to their high permeability within the reservoir and at the surface.

An additional fluids source that is feeding the surface seeps at the Wunut locality (Group 2) is potentially provided through broad caldera collapse and diffused fracturing ongoing around the neighboring Lusi crater, located 3.5 km to the east (Mauri et al., 2018; Panzera et al., 2018). These newborn fractures represent additional active pathways for radial transfer of the Lusi fluids in the shallow surface. Here thousands of active seeps are scattered around the Lusi vent and have CO_2 and CH_4 signatures similar to those measured for Group 2 (Tables 1 and 2; Mazzini et al., 2012; Sciarra et al., 2018). Further, the authors also describe the presence of ~W-E-oriented systems of newborn antithetic fractures that are interpreted to result from the sinistral strike-slip activity of the WFS. These fractures, similarly to the NE-SW-oriented WFS, are proven

to be an active advective pathway for the migration of fluids (Sciarra et al., 2018). Gravimetry data (Mauri et al., 2018) also confirm the presence of these structures that are likely recycled by the radial fluids expulsion from the over pressured Lusi conduit.

6.6. HC Reservoirs, Lusi, and the Volcanic System

Our results indicate that mantle-derived fluids not only migrate from the volcanic complex at focused localities such as the Lusi site (Inguaggiato et al., 2018; Mazzini et al., 2012) but also disperse over a broader area within the sedimentary basin through which the WFS extends. The highest He isotope signature was measured in the fluids trapped in the Carat field (6.7 R_A), the closest field to the volcanic complex. (Figures 1b and 2). In contrast, the lowest He isotope ratio was distinguished in the Watudakon field (2.1 R_A), located on the outskirts of the magmatic complex (Figures 1b and 2) but in a part of the basin that is not intersected by the WFS (i.e. ~36 km west of Lusi). This lower He isotope signature indicates that here the crustal He component (^{4}He due to U and Th decay in the crust) is higher (Figures 5a and 5b). The migration pathway of the mantle-derived volatiles toward the Watudakon field is less developed than the one existing for the fields located along the WFS. It is worth noting that the Watudakon field also has a different CH_4 signature indicated as primary microbial origin (Figures 3b and 3c). Hence, this reservoir contains volatiles that are very distinct with respect to those in the Wunut, Tanggulangin, and Carat reservoirs. This observation strengthens the hypothesis that the migration of mantle-derived fluids mainly occurs in the region around the volcanoes but that enhanced migration is promoted in the NE-SW-oriented corridor crossed by the WFS. This observation is also consistent with the thermal gradient measured from these fields based on the available shallow boreholes. The data indicate a gradient of 2.8–4.8 °C/100 m from Wunut field, 3.8–4.8 °C/100 m from Tanggulangin, and 4.9 °C/100 m from Carat. These values are remarkably similar to the gradient measured at the BJP-1 well (4.2 °C/100 m; Mazzini et al., 2007) drilled prior to the occurrence of the Lusi eruption. The evidence of a widespread high thermal gradient is in agreement with the broadly diffused migration of mantle-derived fluids.

Our new data also help to refine the fluids migration imaged by the ambient noise tomography acquired in the region that indicates the migration of hydrothermal fluids from the volcanic arc toward the sedimentary basin (Fallahi et al., 2017). The major migration pathway is linked to the WFS as well as W-E-oriented systems of antithetic fractures present around Lusi. Considering the remarkable variation of the geochemical composition of the C-rich gases (i.e., CO_2 and CH_4) sampled from the HC fields (this study) and the Lusi system (Mazzini et al., 2012), we can conclude that these two systems are essentially compartmentalized and input of fluids from the Lusi system to reservoirs is limited. The slow migration of mantle-derived He in the HC reservoirs occurs independently from the focused one occurring at the Lusi crater. We cannot rule out the possibility that fluids (i.e., CO_2 and CH_4) outgassing from the Lusi system may also move laterally toward the HC reservoirs (Wunut, Carat, and Tanggulangin) and are later modified by secondary processes (i.e., biodegradation). However, the collected data do not support this scenario.

6.7. Basinal Fluids Migration

Based on the findings and observations reported herein, merged with the known regional studies, we have developed a schematic model describing the fluids migration in the studied petroleum system (Figure 8).

1. *Deposition of petroleum system elements:* (a) Ngimbang Fm. HC source rock; (b) reservoir (volcaniclastic sands and sandstones); and (c) seals (intercalating shales) both within the Pucangan Fm. HC generation within the Ngimbang Fm., offshore northeast Java.
2. Late Pleistocene-Holocene HC fluid *migration to shallow reservoirs* of the Pucangan Fm., following the collapse of the Porong trap (7 km to the east).
3. *Alteration* of the gas and oil via HC biodegradation process.
4. *Magmatic and hydrothermal fluids migration* toward the organic-rich shales of the deep-seated Ngimbang Fm. (>3,800-m depth) generated additional HCs and CO_2, creating overpressure within the Ngimbang Fm., enriching the gas with mantle-derived trace noble gases (^{3}He and ^{36}Ar).
5. These fluids migrated toward the surface through fractured and weak zones and are present today in the producing HC reservoirs and at the Lusi eruption site.

The gas geochemistry survey described herein corroborates all the previously collected geophysical, petrographic, geochemical, and modeling evidences (Collignon et al., 2018; Fallahi et al., 2017; Malvoisin et al.,

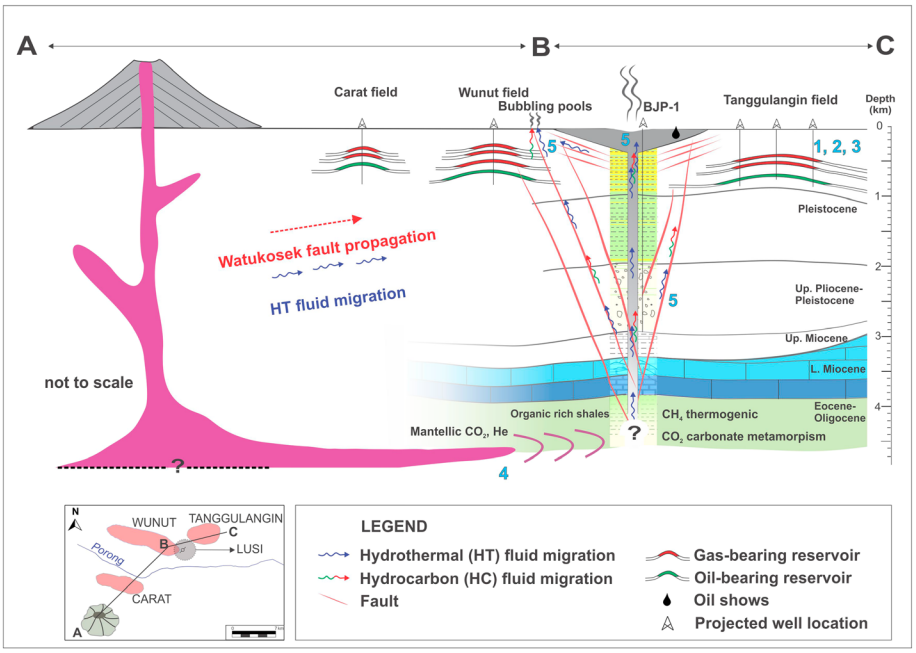

Figure 8. Conceptual geological model depicting the development of the petroleum system and the migration pathways of the mantle-derived and HC fluids in the study area. The major events are marked with Numbers 1–5, described in the section 6.7.

2018; Mazzini et al., 2012; Mazzini et al., 2018; Samankassou et al., 2018; Svensen et al., 2018). These converging data indicate that prior to the Lusi eruption and prior to the drilling of the BJP-1 well, an overpressured zone in the deeply buried Ngimbang Fm. (>4 km) already existed. Here the migration of magma and hydrothermal fluids from the neighboring volcanic arc generated significant overpressure confined in this proliferous source rock buried more than 1 km below the bottom of the BJP-1 well. Therefore, the presence of this naturally overpressured system and its final manifestation at the surface appear to be unrelated to the drilling of the BJP-1 well.

7. Conclusions

We report the results of a gas geochemistry survey conducted in the southern part of the East Java sedimentary basin. Here several HC fields and adjacent surface seepage sites are located near the Arjuno-Welirang volcanic complex and around the Lusi eruption site. The samples collected from the shallow (200–1,000 m) HC fields (Group 1) reveal the presence of predominantly dry thermogenic gas ($-58.3 < \delta^{13}C_{CH4} < -40.7$). Ongoing biodegradation processes are confirmed by the CO_2 signature with $+18.9 < \delta^{13}C_{CO2} < +22.8$. The surface seepages (Group 2) located above the reservoirs reveal a remarkably different geochemical signature where less molecularly and isotopically fractionated and recently generated thermogenic gas is mixed with CO_2 with $+1.2 < \delta^{13}C_{CO2} < +2.7$. All the analyzed samples reveal the presence of noble gases with a clear mantle-derived He signature that is comparable to that in the fluids emitted at the Lusi and Arjuno-Welirang fumaroles. Only a moderate decrease in $^3He/^4He$ ratio is observed along a NE-oriented transect from the Arjuno-Welirang fumaroles ($R = 7.3\ R_A$), through the neighboring Carat HC reservoir ($R = 6.7\ R_A$), Lusi (R up to $6.5\ R_A$), and the surrounding HC fields that still display remarkably high values (R up to $6.3\ R_A$).

The study region is intersected by the WFS that originates from the Arjuno-Welirang volcanic complex, hosting Lusi and the sampled HC fields. Previous studies revealed that this fault system provided the pathway for the magmatic fluids fueling the Lusi eruption. Our new results show that this system of faults also allows the ongoing migration of mantle-derived fluids over a larger region of the sedimentary basin hosting the HC fields. Potential migration of the shallow Lusi fluids to the reservoirs followed by alteration processes (i.e., biodegradation) cannot be totally excluded. However, the distinct signature of the C gases (i.e., CO_2 and

CH_4) observed at the Lusi eruption site and in the HC fields indicates that this input should be limited. Additional fluids expelled at the thousands of seeps around the Lusi crater (including those from Group 2) are migrating from the Lusi conduit through a network of fractures antithetic to the Watukosek strike slip fault system and through the caldera collapse shallow fractures that extend over kilometers around the main Lusi vent.

This study highlights that continuous monitoring of noble gas composition in HC fields neighboring volcanic centers could represent an efficient and logistically simple tool to distinguish perturbations of adjacent magmatic complexes.

Acknowledgments
The work was funded by the European Research Council under the European Union's Seventh Framework Programme Grant agreement 308126 (LUSI LAB project, A. Mazzini). We acknowledge the support from the Research Council of Norway through its Centres of Excellence funding scheme, Project 223272 (CEED). The authors would like to thank the management of Lapindo Brantas Indonesia and PT. Kimia Farma for providing access to the subsurface data and for the authorization to publish the results of this study. BPLS is thanked for their support during the field operations. Federal Institute for Geosciences and Natural Resources (BGR) is thanked for helping with TOC measurements. The interpretation and model presented in this paper reflect solely the view of the authors at the stage of the manuscript preparation. We are grateful to the Editor and two Reviewers who made insightful comments and contributed to improve the quality of the manuscript. The data supporting the paper is represented in the Tables 1 and stored at the NIRD database (https://archive.sigma2.no/pages/public/datasetDetail.jsf?id=C9898994-C249-4190-84B4-13334E9E7B59).

References

Bernard, B., J. M. Brooks, and W. M. Sackett (1977), A geochemical model for characterization of hydrocarbon gas sources in marine sediments, paper presented at 9th Annual OTC Conference.

Blumenberg, M., Lutz, R., Schlömer, S., Krüger, M., Scheeder, G., Berglar, K., et al. (2016). Hydrocarbons from near-surface sediments of the Barents Sea north of Svalbard—Indication of subsurface hydrocarbon generation? *Marine and Petroleum Geology*, *76*, 432–443. https://doi.org/10.1016/j.marpetgeo.2016.05.031

Capasso, G., & Inguaggiato, S. (1998). A simple method for the determination of dissolved gases in natural waters. An application to thermal waters from Vulcano Island. *Applied Geochemistry*, *13*(5), 631–642. https://doi.org/10.1016/S0883-2927(97)00109-1

Caracausi, A., Italiano, F., Paonita, A., Rizzo, A., & Nuccio, P. M. (2003). Evidence of deep magma degassing and ascent by geochemistry of peripheral gas emissions at Mount Etna (Italy): Assessment of the magmatic reservoir pressure. *Journal of Geophysical Research*, *108*(B10), 2463. https://doi.org/10.1029/2002JB002095

Caracausi, A., Paternoster, M., & Nuccio, P. M. (2015). Mantle CO_2 degassing at Mt. Vulture volcano (Italy): Relationship between CO_2 outgassing of volcanoes and the time of their last eruption. *Earth and Planetary Science Letters*, *411*, 268–280. https://doi.org/10.1016/j.epsl.2014.11.049

Caracausi, A., & Sulli, A. (2019). Outgassing of mantle volatiles in compressional tectonic regime away from volcanism: The role of continental delamination. *Geochemistry, Geophysics, Geosystems*, *20*, 2007–2020. https://doi.org/10.1029/2018GC008046

Chung, H. M., Gormly, J. R., & Squires, R. M. (1988). Origin of gaseous hydrocarbons in subsurface environments: Theoretical considerations of carbon isotope distribution. *Chemical Geology*, *71*(1-3), 97–104. https://doi.org/10.1016/0009-2541(88)90108-8

Clark, I., & Fritz, P. (1997). *Environmental isotopes in hydrogeology*. Boca Raton, FL: CRC Press/Lewis Publishers.

Collignon, M., Mazzini, A., Schmid, D. W., & Lupi, M. (2018). Modelling fluid flow in active clastic piercements: Challenges and approaches. *Marine and Petroleum Geology*, *90*, 157–172. https://doi.org/10.1016/j.marpetgeo.2017.09.033

Correale, A., Martelli, M., Paonita, A., Rizzo, A., Brusca, L., & Scribano, V. (2012). New evidence of mantle heterogeneity beneath the Hyblean Plateau (southeast Sicily, Italy) as inferred from noble gases and geochemistry of ultramafic xenoliths. *Lithos*, *132-133*, 70–81. https://doi.org/10.1016/j.lithos.2011.11.007

Deines, P. (2002). The carbon isotope geochemistry of mantle xenoliths. *Earth-Science Reviews*, *58*(3-4), 247–278. https://doi.org/10.1016/S0012-8252(02)00064-8

Devi, E. A., Rachman, F., Satyana, A. H., Fahrudin, F., & Setyawan, R. (2018). Paleofacies of Eocene Lower Ngimbang source rocks in Cepu Area, East Java Basin based on biomarkers and carbon-13 isotopes. *IOP Conference Series: Earth and Environmental Science*, *118*, 012009. https://doi.org/10.1088/1755-1315/118/1/012009

Doust, H., & Noble, R. A. (2008). Petroleum systems of Indonesia. *Marine and Petroleum Geology*, *25*, 103–129. https://doi.org/10.1016/j.marpetgeo.2007.05.007

Etiope, G., Feyzullayev, A., Milkov, A. V., Waseda, A., Mizobe, K., & Sun, C. H. (2009). Evidence of subsurface anaerobic biodegradation of hydrocarbons and potential secondary methanogenesis in terrestrial mud volcanoes. *Marine and Petroleum Geology*, *26*, 1692–1703. https://doi.org/10.1016/j.marpetgeo.2008.12.002

Fallahi, M. J., Obermann, A., Lupi, M., Karyono, K., & Mazzini, A. (2017). The plumbing system feeding the Lusi eruption revealed by ambient noise tomography. *Journal of Geophysical Research: Solid Earth*, *122*, 8200–8213. https://doi.org/doi:10.1002/2017JB014592

Giggenbach, W. F., Sano, Y., & Wakita, H. (1993). Isotopic composition of helium, and CO_2 and CH_4 contents in gases produced along the New Zealand part of a convergent plate boundary. *Geochimica et Cosmochimica Acta*, *57*(14), 3427–3455. https://doi.org/10.1016/0016-7037(93)90549-C

Global Volcanism Program (2013). In E. Venzke (Ed.), *Volcanoes of the World*, v. 4.8.1. Smithsonian Institution. https://doi.org/10.5479/si.GVP.VOTW4-2013

Gutsalo, L. K., and A. M. Plotnikov (1981), Carbon isotopic composition in the CH_4-CO_2 system as a criterion for the origin of methane and carbon dioxide in Earth natural gases (in Russian), paper presented at Doklady Akademii Nauk SSSR (Proceedings of the USSR Academy of Science).

Hall, R. (2002). Cenozoic geological and plate tectonic evolution of SE Asia and the SW Pacific: Computer-based reconstructions, model and animations. *Journal of Asian Earth Sciences*, *20*(4), 353–431. https://doi.org/10.1016/S1367-9120(01)00069-4

Hall, R. (2013). The palaeogeography of Sundaland and Wallacea since the Late Jurassic. *Journal of Limnology*, *72*, –1, 17. https://doi.org/10.4081/jlimnol.2013.s2.e1

Hall, R., Cottam, M. A., & Wilson, M. E. J. (2011). Australia–SE Asia collision: Plate tectonics and crustal flow. In M. A. C. R. Hall, & M. E. J. Wilson (Eds.), *The SE Asian gateway: history and tectonics of Australia-Asia collision*, edited by, *Special Publications*, (Vol. 355, pp. 75–109). London: Geological Society. https://doi.org/10.1144/SP355.5

Halldórsson, S. A., Hilton, D. R., Troll, V. R., & Fischer, T. P. (2013). Resolving volatile sources along the western Sunda arc, Indonesia. *Chemical Geology*, *339*, 263–282. https://doi.org/10.1016/j.chemgeo.2012.09.042

Head, I. M., Jones, D. M., & Larter, S. R. (2003). Biological activity in the deep subsurface and the origin of heavy oil. *Nature*, *426*(6964), 344–352. https://doi.org/10.1038/nature02134

Inguaggiato, S., Mazzini, A., Vita, F., & Sciarra, A. (2018). The Arjuno-Welirang volcanic complex and the connected Lusi system: Geochemical evidences. *Marine and Petroleum Geology*, *90*, 67–76. https://doi.org/10.1016/j.marpetgeo.2017.10.015

Ishibashi, J.-I., Sato, M., Sano, Y., Wakita, H., Gamo, T., & Shanks, W. C. (2002). Helium and carbon gas geochemistry of pore fluids from the sediment-rich hydrothermal system in Escanaba Trough. *Applied Geochemistry*, *17*(11), 1457–1466. https://doi.org/10.1016/S0883-2927(02)00112-9

Istadi, B., Wibowo, H. T., Sunardi, E., Hadi, S., & Sawolo, N. (2012). Mud volcano and its evolution. *Earth Sciences, Imran Ahmad Dar, IntechOpen*, *375-434*, 861–888. https://doi.org/10.5772/24944

Istadi, B. P., Pramono, G. H., Sumintadireja, P., & Alam, S. (2009). Modeling study of growth and potential geohazard for LUSI mud volcano: East Java, Indonesia. *Marine and Petroleum Geology*, *26*, 1724–1739. https://doi.org/10.1016/j.marpetgeo.2009.03.006

Jenden, P. D., Hilton, D. R., Kaplan, I. R., & Craig, H. (Eds.) (1993). *Abiogenic hydrocarbons and mantle helium in oil and gas fields*, *United States Geological Survey, Professional Paper* (Vol. 1570, pp. 31–56).

Kamenskiy, I. L., Yakutseni, V. P., Mamyrin, B. A., Anufriyev, S. G., & Tolstikhin, I. N. (1971). Helium isotopes in nature. *Geochemistry International*, *8*, 575–589.

Kusumastuti, A., Darmoyo, A.B., Suwarlan, W., Sosromihardjo, S.P.C. (1999), The Wunut field: Pleistocene volcaniclastic gas sands in East Java, *Proceedings, Indonesian Petroleum Association, Twenty Seventh Annual Convention & Exhibition, October 1999*.

Lee, H., Muirhead, J. D., Fischer, T. P., Ebinger, C. J., Kattenhorn, S. A., Sharp, Z. D., & Kianji, G. (2016). Massive and prolonged deep carbon emissions associated with continental rifting. *Nature Geoscience*, *9*, 145–149. https://doi.org/10.1038/ngeo2622

Malvoisin, B., Mazzini, A., & Miller, S. A. (2018). Deep hydrothermal activity driving the Lusi mud eruption. *Earth and Planetary Science Letters*, *497*, 42–49. https://doi.org/10.1016/j.epsl.2018.06.006

Martha, A. A., Cummins, P., Saygin, E., Sri, W., & Masturyono (2017). Imaging of upper crustal structure beneath East Java–Bali, Indonesia with ambient noise tomography. *Geoscience Letters*, *4*(1), 14. https://doi.org/10.1186/s40562-017-0080-9

Mauri, G., Husein, A., Mazzini, A., Irawan, D., Sohrabi, R., Hadi, S., et al. (2018). Insights on the structure of Lusi mud edifice from land gravity data. *Marine and Petroleum Geology*, *90*, 104–115. https://doi.org/10.1016/j.marpetgeo.2017.05.041

Mazzini, A., & Etiope, G. (2017). Mud volcanism: An updated review. *Earth-Science Reviews*, *168*, 81–112. https://doi.org/10.1016/j.earscirev.2017.03.001

Mazzini, A., Etiope, G., & Svensen, H. (2012). A new hydrothermal scenario for the 2006 Lusi eruption, Indonesia, Insights from gas geochemistry. *Earth and Planetary Science Letters*, *317-318*, 305–318. https://doi.org/10.1016/j.epsl.2011.11.016

Mazzini, A., Nermoen, A., Krotkiewski, M., Podladchikov, Y., Planke, S., & Svensen, H. (2009). Strike-slip faulting as a trigger mechanism for overpressure release through piercement structures. Implications for the Lusi mud volcano, Indonesia. *Marine and Petroleum Geology*, *26*(9), 1751–1765. https://doi.org/10.1016/j.marpetgeo.2009.03.001

Mazzini, A., Scholz, F., Svensen, H. H., Hensen, C., & Hadi, S. (2018). The geochemistry and origin of the hydrothermal water erupted at Lusi, Indonesia. *Marine and Petroleum Geology*, *90*, 52–66. https://doi.org/10.1016/j.marpetgeo.2017.06.018

Mazzini, A., Svensen, H., Akhmanov, G. G., Aloisi, G., Planke, S., Malthe-Sørenssen, A., & Istadi, B. (2007). Triggering and dynamic evolution of the LUSI mud volcano, Indonesia. *Earth and Planetary Science Letters*, *261*(3-4), 375–388. https://doi.org/10.1016/j.epsl.2007.07.001

Milkov, A. V. (2010). Methanogenic biodegradation of petroleum in the West Siberian Basin (Russia): Significance for formation of giant Cenomanian gas pools. *AAPG Bulletin*, *94*(10), 1485–1541. https://doi.org/10.1306/01051009122

Milkov, A. V. (2011). Worldwide distribution and significance of secondary microbial methane formed during petroleum biodegradation in conventional reservoirs. *Organic Geochemistry*, *42*(2), 184–207. https://doi.org/10.1016/j.orggeochem.2010.12.003

Milkov, A. V. (2018). Secondary microbial gas. In H. Wilkes (Ed.), *Hydrocarbons, oils and lipids: Diversity, origin, chemistry and fate*, edited by, (pp. 1–10). Cham: Springer International Publishing. https://doi.org/10.1007/978-3-319-54529-5_22-1

Milkov, A. V., & Etiope, G. (2018). Revised genetic diagrams for natural gases based on a global dataset of >20,000 samples. *Organic Geochemistry*, *125*, 109–120. https://doi.org/10.1016/j.orggeochem.2018.09.002

Miller, S. A., & Mazzini, A. (2018). More than ten years of Lusi: A review of facts, coincidences, and past and future studies. *Marine and Petroleum Geology*, *90*, 10–25. https://doi.org/10.1016/j.marpetgeo.2017.06.019

Moreira, M. A., & Kurz, M. D. (2013). Noble gases as tracers of mantle processes and magmatic degassing. In P. Burnard (Ed.), *The Noble Gases as Geochemical Tracers* (pp. 371–391). Berlin, Heidelberg: Springer-Verlag.

Moscariello, A., Do Couto, D., Mondino, F., Booth, J., Lupi, M., & Mazzini, A. (2018). Genesis and evolution of the Watukosek fault system in the Lusi area (East Java). *Marine and Petroleum Geology*, *90*, 125–137. https://doi.org/10.1016/j.marpetgeo.2017.09.032

Obermann, A., Karyono, K., Diehl, T., Lupi, M., & Mazzini, A. (2018). Seismicity at Lusi and the adjacent volcanic complex, Java, Indonesia. *Marine and Petroleum Geology*, *90*, 149–156. https://doi.org/10.1016/j.marpetgeo.2017.07.033

O'Nions, R. K., & Oxburgh, E. R. (1988). Helium, volatile fluxes and the development of continental crust. *Earth and Planetary Science Letters*, *90*(3), 331–347. https://doi.org/10.1016/0012-821X(88)90134-3

Ozima, M., & Podosek, F. A. (2002). *Noble gas ceochemistry*. Cambridge: Cambridge University Press.

Panzera, F., D'Amico, S., Lupi, M., Mauri, G., Karyono, K., & Mazzini, A. (2018). Lusi hydrothermal structure inferred through ambient vibration measurements. *Marine and Petroleum Geology*, *90*, 116–124. https://doi.org/10.1016/j.marpetgeo.2017.06.017

Peters, K. E., Walters, C. C., & Moldowan, J. M. (2005). *The biomarker guide*. Cambridge: Cambridge University Press.

Poreda, R. J., Jeffrey, A. W. A., Kaplan, I. R., & Craig, H. (1988). Magmatic helium in subduction-zone natural gases. *Chemical Geology*, *71*(1-3), 199–210. https://doi.org/10.1016/0009-2541(88)90115-5

Poreda, R. J., Jenden, P. D., Kaplan, I. R., & Craig, H. (1986). Mantle helium in Sacramento basin natural gas wells. *Geochimica et Cosmochimica Acta*, *50*(12), 2847–2853. https://doi.org/10.1016/0016-7037(86)90231-0

Prinzhofer, A. (2013). Noble gases in oil and gas accumulations. In P. Burnard (Ed.), *The noble gases as geochemical tracers* (pp. 225–248). Berlin, Heidelberg: Springer.

Procesi, M., Ciotoli, G., Mazzini, A., & Etiope, G. (2019). Sediment-hosted geothermal systems: Review and first global mapping. *Earth-Science Reviews*, *192*, 529–544. https://doi.org/10.1016/j.earscirev.2019.03.020

Sakata, S., Sano, Y., Maekawa, T., & Igari, S.-I. (1997). Hydrogen and carbon isotopic composition of methane as evidence for biogenic origin of natural gases from the Green Tuff Basin, Japan. *Organic Geochemistry*, *26*(5-6), 399–407. https://doi.org/10.1016/S0146-6380(97)00005-3

Samankassou, E., Mazzini, A., Chiaradia, M., Spezzaferri, S., Moscariello, A., & Do Couto, D. (2018). Origin and age of carbonate clasts from the Lusi eruption, Java, Indonesia. *Marine and Petroleum Geology*, *90*, 138–148. https://doi.org/10.1016/j.marpetgeo.2017.11.012

Sano, Y., & Fischer, T. P. (2013). The analysis and interpretation of noble gases in modern hydrothermal systems. In P. Burnard (Ed.), *The noble gases as geochemical tracers*, edited by, (pp. 249–317). Berlin, Heidelberg: Springer Berlin Heidelberg. https://doi.org/10.1007/978-3-642-28836-4_10

Sano, Y., Gamo, T., & Williams, S. N. (1997). Secular variations of helium and carbon isotopes at Galeras volcano, Colombia. *Journal of Volcanology and Geothermal Research*, *77*(1-4), 255–265. https://doi.org/10.1016/S0377-0273(96)00098-4

Sano, Y., & Wakita, H. (1985). Geographical distribution of $^{3}He/^{4}He$ ratios in Japan: Implications for arc tectonics and incipient magmatism. *Journal of Geophysical Research*, *90*(B10), 8729–8741. https://doi.org/10.1029/JB090iB10p08729

Satyana, A. H., & Purwaningsih, M. E. M (2003a), Geochemistry of the East Java Basin: New observations on oil grouping, genetic gas types and trends of hydrocarbon habitats, *Proceedings of the 29th IAGI Annual Convention and Exhibition*.

Satyana, A. H., Purwaningsih, M. E. M. (2003b), Oligo-Miocene carbonates of Java: Tectonic setting and effects of volcanism, *Proceedings of the 32nd IAGI and 28th HAGI Annual Convention and Exhibition*.

Schoell, M. (1983), Genetic characterization of natural gases. American Association of Petroleum Geologists Bulletin paper presented at American Association of Petroleum Geologists Bulletin.

Sciarra, A., Mazzini, A., Inguaggiato, S., Vita, F., Lupi, M., & Hadi, S. (2018). Radon and carbon gas anomalies along the Watukosek Fault System and Lusi mud eruption, Indonesia. *Marine and Petroleum Geology*, *90*, 77–90. https://doi.org/10.1016/j.marpetgeo.2017.09.031

Sharaf, E., Simo, J. A., Carroll, A. R., & Shields, M. (2005). Stratigraphic evolution of Oligocene–Miocene carbonates and siliciclastics, East Java basin, Indonesia. *AAPG Bulletin*, *89*(6), 799–819. https://doi.org/10.1306/01040504054

Smyth, H. R., Hall, R., & Nichols, G. J. (2008). Cenozoic volcanic arc history of East Java, Indonesia: The stratigraphic record of eruptions on an active continental margin. In A. E. Draut, P. D. Clift, & D. W. Scholl (Eds.), *Formation and Applications of the Sedimentary Record in Arc Collision Zones* (pp. 199–222).Boulder, CO: Geological Society of America.

Snyder, G., Poreda, R., Fehn, U., & Hunt, A. (2003). Sources of nitrogen and methane in Central American geothermal settings: Noble gas and 129I evidence for crustal and magmatic volatile components. *Geochemistry, Geophysics, Geosystems*, *4*(1), 9001. https://doi.org/10.1029/2002GC000363

Sutrisna, E. (2009), "Can LUSI be stopped?—A case study and lessons learned from the relief wells", *Eos Transactions American Geophysical Union*, *90*(52), Fall Meet. Suppl., Abstract NH51A-1053. https://doi.org/10.1029/eost2009eo52

Svensen, H. H., Iyer, K., Schmid, D. W., & Mazzini, A. (2018). Modelling of gas generation following emplacement of an igneous sill below Lusi, East Java, Indonesia. *Marine and Petroleum Geology*, *90*, 201–208. https://doi.org/10.1016/j.marpetgeo.2017.07.007

Tingay, M. (2015). Initial pore pressures under the Lusi mud volcano, Indonesia. *Interpretation*, *3*(1), SE33–SE49. https://doi.org/10.1190/int-2014-0092.1

Van Noorden, R. (2006). Mud volcano floods Java. In *Nature News*. Italy:University of Padua. https://doi.org/10.1038/news060828-1

Vanderkluysen, L., Burton, M. R., Clarke, A. B., Hartnett, H. E., & Smekens, J.-F. (2014). Composition and flux of explosive gas release at LUSI mud volcano (East Java, Indonesia). *Geochemistry, Geophysics, Geosystems*, *15*, 2932–2946. https://doi.org/10.1002/2014gc005275

Wenger, L. M., Davis, C. L., & Isaksen, G. H. (2002). Multiple controls on petroleum biodegradation and impact on oil quality. *SPE Reservoir Evaluation and Engineering*, *5*(05), 375–383. https://doi.org/10.2118/80168-PA

Whiticar, M. J., Faber, E., & Schoell, M. (1986). Biogenic methane formation in marine and freshwater environments: CO_2 reduction vs. acetate fermentation—Isotope evidence. *Geochimica et Cosmochimica Acta*, *50*(5), 693–709. https://doi.org/10.1016/0016-7037(86)90346-7

Xu, S., Nakai, S. I., Wakita, H., Xu, Y., & Wang, X. (1995). Helium isotope compositions in sedimentary basins in China. *Applied Geochemistry*, *10*(6), 643–656. https://doi.org/10.1016/0883-2927(95)00033-X

4) *Outgassing of Mantle Volatils in Compressional Tectonic Regime Away From Volcanism : The Role of Continental Delamination*

L'identification du transfert de chaleur et de fluides provenant du manteau (CO_2, H_2O et He, par exemple) dans les régions continentales est essentielle pour développer des stratégies d'exploration et pour identifier et quantifier la distribution des ressources économiques (Ballentine et al., 2001; Holland & Gilfillan, 2013; Prinzhofer, 2013). En outre, les évaluations quantitatives des flux de chaleur et des éléments volatils provenant du manteau fournissent de nouvelles informations sur la tectonique de la croûte et du manteau et sur la relation possible entre magmatisme et géodynamique (par exemple, Caracausi et al., 2005; Caracausi et al., 2013; Chiarabba & Chiodini, 2013; Kennedy et Van Soest, 2007; O'Nions et Oxburgh, 1988; Torgersen, 1993). Récemment, il a également été démontré que l'intrusion magmatique de corps ressemblant à des dykes dans les chaînes de montagnes pouvait déclencher des séismes d'une magnitude pouvant être utile à l'évaluation des risques sismiques (Di Luccio et al., 2018). Par conséquent, le dégazage d'éléments volatils dérivés du manteau (par exemple, CO_2 et He) dans une région sismique offre une nouvelle perspective pour interpréter la sismicité dans les chaînes de montagne et fournit éventuellement de nouveaux outils pour la surveillance des régions sismiques actives.
L'hélium (He) est un bon traceur pour reconnaître le dégazage des fluides dérivés du manteau dans les régions continentales, y compris celles où l'évidence de l'activité volcanique fait défaut (Burnard et al., 2012; Caracausi et al., 2005; Caracausi et al., 2013; Italiano et al., 2000; O'Nions et Oxburgh, 1988). Le manteau terrestre a conservé une fraction importante de l'He primordial au moment de sa formation. En revanche, la croûte continentale a été considérablement retravaillée au cours des temps géologiques, ce qui a entraîné la perte de la majeure partie de son He primordial, et son inventaire est principalement radiogénique, produit par la désintégration de l'U et du Th de la croûte. Par conséquent, un rapport $^3He/^4He$ relativement élevé (R; 8 ± 1 fois la valeur dans l'atmosphère, Ra) caractérise le dégazage de He dans les régions de fusion du manteau, telles que les rides mi-océaniques (par exemple, O'Nions et Oxburgh, 1988). Les fluides dérivés du manteau injectés dans la croûte sont progressivement dilués par l'He radiogénique produit dans la croûte, où le rapport $^3He/^4He$ est ~ 0,02Ra. Par conséquent, les rapports $^3He/^4He$ supérieurs à 0,1 Ra dans les fluides naturels fournissent une preuve solide de la présence de fluides dérivés du manteau (Ballentine et Burnard, 2002).
La plupart des questions durables sur le dégazage de l'He primordial dans les régions continentales loin du volcanisme découlent de la localisation de sa source et des mécanismes de transfert de l'He à travers la croûte terrestre. La survenue d'un dégazage de fluides dérivés du manteau dans les régions continentales indique fortement la génération et le dégazage de corps magmatique en profondeur (c.-à-d. O'Nions et Oxburgh, 1988). En fait, sans la génération de magma et sa migration successive, il serait difficile pour le manteau de perdre ses volatils (O'Nions et Oxburgh, 1988; Oxburgh et al., 1986; Watson et Brenan, 1987). Les volatils dérivés du manteau sont transférés à travers toute la croûte lorsque ceux-ci sont capables de traverser la croûte inférieure ductile, ce qui constitue une barrière au transfert advectif des fluides en raison de sa faible perméabilité sur des échelles de temps longues (Kennedy et Van Soest, 2007 et références y figurant). En fait, s'il est vrai que les défauts conduisent à une plus grande perméabilité des discontinuités tectoniques dans la région, la zone ductile peut néanmoins servir de frontière imperméable car les fractures de la croûte ne peuvent y rester ouvertes sur le long terme (Byerle, 1993; Sleep & Blampied, 1992). Les concepts classiques ne permettent toutefois pas d'expliquer la migration des fluides dans la croûte moyenne. Des études récentes ont montré que la cavitation par fluage peut créer une pompe à fluide granulaire dynamique dans les zones de cisaillement ductile (Fusseis et al., 2009), ouvrant ainsi de nouvelles

frontières sur le transfert de fluides dans la croûte ductile et les processus associés (par exemple, le dégazage du manteau).
Même s'il est bien admis (par exemple, O'Nions et Oxburgh, 1988) que les éléments volatils peuvent signaler la présence d'intrusions magmatiques en profondeur et la règle des défauts dans le transfert des fluides, il est difficile de reconnaître la position de la source pour les éléments volatils dérivés du manteau en profondeur et le réseau de voies par lesquelles ils atteignent l'atmosphère. Récemment, la tomographie sismique a contribuée à combler cette lacune. Par exemple, dans les Apennins, une forte émission de CO_2, la sismicité et la topographie de la ceinture, en corrélation avec une anomalie thermique / fluide dans le manteau, ont été associés à une faille en extension et au remplacement du manteau sublithosphérique après délamination de la lithosphère (Chiarabba & Chiodini, 2013).
Dans la région centrale de la Méditerranée, le cadre tectonique actif résulte de la lente convergence des plaques africaine et européenne. Dans la marge continentale nord de la Sicile, elle a donné naissance au complexe collisionnel sicilien Fold and Thrust Belt à côté du système de subduction ionien-tyrrhénien, dont l'interaction complexe est responsable de la coexistence de déformations en compression, en extension et transformant, accompagnées d'anomalies de flux de chaleur et émission de fluide en l'absence d'évidences volcaniques.
Nous présentons ici des nouvelles données chimiques et isotopiques de He provenant de systèmes hydrothermaux du centre de la Sicile et étudions les relations entre He et la chaleur afin de limiter l'origine des fluides émis. Nous discutons également des données géochimiques ainsi que des résultats du profil sismique profond SiRiPro qui permet d'étudier les caractéristiques tectoniques de la croûte et du manteau de la région (Catalano et al., 2013) et les principales discontinuités tectoniques à l'échelle régionale. Cette étude multidisciplinaire vise à localiser la source des fluides mantellqiues (c'est-à-dire, He et CO_2) dégazés loin du volcanisme et des discontinuités tectoniques à travers lesquelles les fluides se déplacent vers la surface. Ce travail apporte une nouvelle contribution à la compréhension de la tectonique de la croûte terrestre dans le centre-ouest de la Méditerranée, qui constitue un domaine clé de l'évolution géodynamique de la Méditerranée. Enfin, nous fournissons également des données préliminaires sur les émissions de CO_2 dérivées du manteau dans un régime tectonique par compression.
Ce travail démontre que le dégazage des éléments volatils du manteau peut également se produire dans un régime géodynamique de compression. Nous avons souligné ici que les isotopes de l'He sont de puissants outils pour résoudre la tectonique de la croûte et du manteau impliquant l'apparition de magma sans aucune trace de volcanisme à la surface. Le dégazage de He issu du manteau implique le fait que la région étudiée soit également affectée par le dégazage de CO2 mantellique, car il s'agit d'un composant majeur volatil pouvant être le support de l'He mantellique à travers la croûte. Sur la base du rapport $CO_2/^3He$ et des flux de ^3He, nous avons calculé ici le flux de CO2 mantellique dans ce secteur de la Méditerranée (de $1,8 \times 10^3$ à $8,2 \times 10^3$ mol • km $^{-2}$ • année $^{-1}$). Ces valeurs de flux de CO_2 sont inférieures à celles des systèmes volcaniques actifs et au repos (par exemple, Caracausi et al., 2015, et leurs références), et elles sont comparables à celles d'autres régions sismiques (par exemple, San Andrea Faults, USA) où un dégazage actif de éléments volatils dérivées du manteau est bien reconnu. Cependant, nos données proviennent d'une région continentale appartenant à un système de subduction de type A affecté tectoniquement par un régime de compression. Les résultats de cette étude montrent qu'un flux de chaleur et d'éléments volatils dans le manteau (à savoir CO_2 et He) sont dues à des intrusions magmatiques en profondeur, impliquant que celles-ci puissent également se produire sous une chaîne tectonique. En fait, les données géologiques et géophysiques confirment la présence d'un coin de manteau chaud au-dessous de la zone caractérisée par le dégazage des éléments volatils du manteau. La présence de ce coin de manteau situé

entre deux couches de la croûte, l’Africain au-dessus et l’Europe au-dessous, est la conséquence de processus de délamination bien connus pour produire du magmatisme à grande échelle.
De plus, nos données géochimiques confirment que le transfert d’éléments volatils dérivées du manteau à travers la croûte est dû à des processus advectifs par le biais de discontinuités tectoniques en extension, orientées WNW-ESE, toujours actives dans le centre et le nord de la Sicile. Enfin, nous discutons d’une coupe géologique qui met en évidence la présence d’un système de failles profondes traversant la croûte continentale et reliant le coin du manteau à la surface en correspondance du NCStb. Ces discontinuités tectoniques représentent les chemins structurels possibles à travers lesquels les volatils se déplacent à travers toute la croûte et atteignent la surface.

Geochemistry, Geophysics, Geosystems

RESEARCH ARTICLE
10.1029/2018GC008046

Special Section:
Carbon degassing through volcanoes and active tectonic regions

Outgassing of Mantle Volatiles in Compressional Tectonic Regime Away From Volcanism: The Role of Continental Delamination

Antonio Caracausi[1] **and Attilio Sulli**[2]

[1]Istituto Nazionale di Geofisica e Vulcanologia, Palermo, Italy, [2]Dipartimento di Scienze della Terra e del Mare, Università di Palermo, Palermo, Italy

Key Points:
- Mantle-derived volatiles outgas in the continental convergent region without any evidences of volcanism at the surface
- Heat-helium relationship highlights the occurrence of magmatic intrusion at depth in convergent region
- Delamination processes in continental convergent margin can produce magmatism at depth

Correspondence to:
A. Caracausi,
antonio.caracausi@ingv.it

Citation:
Caracausi, A., & Sulli, A. (2019). Outgassing of mantle volatiles in compressional tectonic regime away from volcanism: The role of continental delamination. *Geochemistry, Geophysics, Geosystems*, *20*. https://doi.org/10.1029/2018GC008046

Received 29 OCT 2018
Accepted 23 FEB 2019
Accepted article online 13 MAR 2019

Abstract In this study we discuss the occurrence of mantle-derived heat and volatiles (i.e., helium and CO_2) feeding hydrothermal systems in a seismically active margin between two convergent plates (African and European) without any signals of volcanism. The helium (He) isotopes clearly indicate a mantle-derived component in the outgassing volatiles. The estimated mantle-derived He fluxes are up to two to three orders of magnitude greater than those in a stable continental area. Such high He fluxes cannot be provided by a long-lasting diffusion, thereby implying a more efficient transport (i.e., advective transport through faults). He data coupled to heat-He relationship suggest the occurrence of active degassing of magmatic intrusions in this area of continental collisional. Geophysical data indicate the presence of a hot mantle wedge below the outgassing of mantle volatiles and a system of faults cutting the continental crust down to the hot mantle wedge. Here we discuss the hot mantle wedge and possible associated magmatic intrusions as the source of the mantle-derived volatiles outgassing in the region. We also assessed the output of mantle-derived CO_2 from the investigated hydrothermal basins. The possible occurrence of magma at depth as well as the geometry of the thick-skinned deformed wedge unambiguously indicates delamination processes that are related to continental subduction. Hence, we show that delamination processes can really produce magma at depth without evidences of volcanism at the surface. Finally, we have also provided the fault systems that work as a network of pathways and actively sustain the advective transfer of the mantle fluids toward the surface.

Plain Language Summary Volatiles from the Earth's mantle escape into the atmosphere mainly in volcanic districts and in submarine regions where new magma reaches the oceanic bottom. A lesser extent occurs in continental regions undergoing active tectonics. How mantle volatiles degas in continental regions and where evidences of volcanic activity are lacking remain a key challenge, given that in absence of magma the mantle would not lose its volatiles. Here we use the He-heat systematics and recognize the presence of mantle volatiles in a continental region where there is no evidence of volcanism on the surface. This is a rare case of active outgassing of fluids coming from the mantle in a region that is characterized by continental collision. These geochemical evidences support the occurrence of magmatic bodies at depth and an advective flow of volatiles and heat through the crust. Geophysical data corroborate the geochemical evidences demonstrating the occurrence of a portion of hot mantle in between two crustal layers in correspondence of the mantle volatiles at the surface. Geology coupled to geophysics shows the presence of tectonic discontinuities cutting the crust down to the mantle working as a network of pathways through which mantle fluids move to the surface.

1. Introduction

Identification of the transfer of mantle-derived heat and fluids (e.g., CO_2, H_2O, and He) in continental regions is critical for developing exploration strategies and for identifying and quantifying the distribution of economic resources (i.e., Ballentine et al., 2001; Holland & Gilfillan, 2013; Prinzhofer, 2013). Furthermore, quantitative evaluations of fluxes of both mantle-derived heat and volatiles provide new insights into mantle-crust tectonic and on the possible relation between magmatism and geodynamics (i.e., Caracausi et al., 2005; Caracausi et al., 2013; Chiarabba & Chiodini, 2013; Kennedy & Van Soest, 2007; O'Nions & Oxburgh, 1988; Torgersen, 1993). Recently, it has also been shown that magmatic intrusion of dike-like bodies in mountain chains may trigger earthquakes with magnitudes that could be relevant to

©2019. The Authors.
This is an open access article under the terms of the Creative Commons Attribution-NonCommercial-NoDerivs License, which permits use and distribution in any medium, provided the original work is properly cited, the use is non-commercial and no modifications or adaptations are made.

seismic hazard assessment (Di Luccio et al., 2018). Hence, the outgassing of mantle-derived volatiles (e.g., CO_2 and He) in seismic region provides a new perspective for interpreting the seismicity in mountain chains and possibly furnishes new tools for the monitoring of active seismic regions.

Helium (He) is a good tracer for recognizing the outgassing of mantle-derived fluids in continental regions, including where evidences of volcanic activity are lacking (i.e., Burnard et al., 2012; Caracausi et al., 2005; Caracausi et al., 2013; Italiano et al., 2000; O'Nions & Oxburgh, 1988). The Earth's mantle has retained a significant fraction of the primordial He at the time of its formation. In contrast, the continental crust has been extensively reworked over geological time, which has resulted in losing most of its primordial He, and its inventory is predominantly radiogenic, produced by the decay of U and Th content in the crust. Consequently, a relatively high $^3He/^4He$ ratio (R; 8 ± 1 times higher the value in atmosphere, R_a) characterizes He degassing in regions of mantle melting, such as at midoceanic ridges (e.g., O'Nions & Oxburgh, 1988). Mantle-derived fluids injected into the crust became progressively diluted by radiogenic He produced in the crust, where the $^3He/^4He$ ratio is ~$0.02R_a$. Hence, $^3He/^4He$ ratios higher than $0.1R_a$ in natural fluids provide strong evidence for the presence of mantle-derived fluids (Ballentine & Burnard, 2002).

Most durable questions about the outgassing of primordial He in continental regions away from volcanism arise from the localization of its source and from the mechanisms of He transfer through the crust. The occurrence of an outgassing of mantle-derived fluids in continental regions strongly indicates the generation and degassing of magma bodies at depth (i.e., O'Nions & Oxburgh, 1988). In fact, without magma generation and its successive migrations, it would be difficult for the mantle to lose its volatiles (O'Nions & Oxburgh, 1988; Oxburgh et al., 1986; Watson & Brenan, 1987). Mantle-derived volatiles are transferred through the entire crust when the volatiles are able to cross the ductile lower crust, which represents a barrier to the advective transfer of fluids because of its low permeability on long timescales (i.e., Kennedy & Van Soest, 2007, and references therein). In fact, if it is true that faults lead to greater permeability in the region of the tectonic discontinuities, nevertheless, the ductile zone can work as an impermeable boundary because crustal fractures are unable to remain open over long timescales (i.e., Byerle, 1993; Sleep & Blampied, 1992). However, fluid migration in the middle crust cannot be explained in terms of classical concepts, and recent studies highlight that creep cavitation can establish a dynamic granular fluid pump in ductile shear zones (i.e., Fusseis et al., 2009), opening new frontiers in the transfer of fluids in the ductile crust and associated processes (e.g., mantle degassing).

Even if it is well accepted (e.g., O'Nions & Oxburgh, 1988) that volatiles can report the occurrence of magmatic intrusions at depth and the rule of faults in the transfer of fluids, it is difficult to recognize the position of the source of mantle-derived volatiles at depth and the network of pathways through which they reach the atmosphere. Recently, seismic tomography is contributing to fill this gap. For instance, in the Apennines, strong CO_2 emission, seismicity, and belt topography, correlated with thermal/fluid anomaly in the mantle, have been associated with extensional faulting and sublithospheric mantle replacement after delamination of the lithosphere (Chiarabba & Chiodini, 2013).

In the Central Mediterranean region, the active tectonic setting is the result of the slow convergence between African and European plates. In the northern Sicily continental margin, it gave rise to the Sicilian Fold and Thrust Belt collisional complex beside the Ionian-Tyrrhenian subduction system, whose complex interaction is responsible for coexisting compressional, extensional, and strike-slip deformation, accompanied by heat flow anomalies and fluid emission in the absence of volcanic evidences.

Here we present new chemical and He isotope data from hydrothermal systems of central Sicily and investigate the relationships between He and heat in order to constrain the origin of the emitted fluids. We also discuss the geochemical data together with the results of the deep seismic profile SiRiPro that arrive to investigate the mantle-crust tectonic features of the region (Catalano et al., 2013) and the main tectonic discontinuities at a regional scale. This multidisciplinary study points to localize the source of the mantle fluids (i.e., He and CO_2) degassing away from volcanism and the tectonic discontinuities through which the fluids move toward the surface. This work gives a new contribution to figure out the crust-mantle tectonic in the central-western Mediterranean that is a key area in the geodynamic evolution of the Mediterranean. Finally, we also furnish a preliminary data of mantle-derived CO_2 output in a compressional tectonic regime.

2. Geological Framework

The central Mediterranean is a complex area constituted by a puzzle of different lithospheric segments, whose geological evolution is constrained by the continuing northward advance of the African plate (Doglioni et al., 2012; Goes et al., 2004) toward Europe. In this geological domain, the northern Sicily continental margin represents a link between the Sicilian-Maghrebian chain and the Tyrrhenian extensional (backarc) area in the north-south direction, while in the east-west direction the collisional complex is replaced by a subduction system (Figures 1 and 2; Catalano et al., 1996; Catalano & Sulli, 2006; Cernobori et al., 1996; Lentini et al., 1994; Roure et al., 1990).

In this area the structure of the lithosphere is strongly a matter of debate (Chiarabba et al., 2008; Doglioni et al., 2007; Faccenna et al., 2005). A high-penetration seismic reflection profile along the central Sicily (SiRiPro) has evidenced the deep structure of the A-subduction system, showing a basement-involved collisional belt (Catalano et al., 2013). The deformed wedge rises from the folding, detachment, and thrusting of sedimentary rocks deposited on both the Mesozoic-Paleogene rifted-passive African continental margin and the Neogene-Quaternary convergent margin. The collisional complex of Sicily, pertaining to the Apenninic-Maghrebian chain, is formed by the following (Figures 1 and 2): (1) the E-to-SE vergent fold and thrust belt. The tectonic history of the Sicily Fold and Thrust Belt (hereafter FTB), started from the early Miocene collision with the Sardinia Block, was a combination of progressive frontal accretion of shallow seated thrust sheets and duplex and underthrusting of deep-seated units (Figure 3), combined with backthrusting and clockwise rotation of the allochthons. Accordingly, two main noncoaxial compressional events, generated and developed at different structural levels (shallow- and deep-seated thrusts) and at different time intervals, formed the present-day tectonic assemblage.

Eastward, along a region developing from southern Tyrrhenian (Marsili basin), through Aeolian Islands and Calabrian Arc (including northeastern Sicily), to the Ionian sea, a B-subduction complex occurs (Figure 2). The forward migration of the accretionary wedge-volcanic arc system was accompanied by rifting episodes. As a consequence, Plio-Pleistocene high-angle extensional to transtensional faults are widespread in northern Sicily continental margin, which dissected also the internal part of the Sicilian collisional system (Bello et al., 2000; Catalano et al., 2000b, 2013; Roure et al., 1990) affecting up to the middle-upper Pleistocene marine and continental deposits. Conversely, some authors (e.g., Giunta et al., 2009) postulated the existence in this area of an E-W trending right-lateral wrenching connected to a crustal discontinuity inherited from the African margin dissection.

The behavior of the subduction beneath Apennines and Maghrebides is explained by different geodynamic models schematized by two endmembers: (1) a continuous laterally bent slab underlying the whole Apenninic-Maghrebian salient (Doglioni et al., 1999); and (2) a seismically active Calabrian slab solely driving the subduction processes being the Southern Apennines and Sicily only lateral rootless belts (Faccenna et al., 2005). Seismic tomography evidenced a continuous 25-km-deep low *P* velocity feature beneath Southern Apennines-Calabria-Sicilian Maghrebides (Chiarabba et al., 2008). Different geometries and shortening between the Apennine-Maghrebide and Calabrian wedges could be explained by tears separating different sectors of a composite continental-oceanic subduction system, producing variable shortening in the upper plate and variable subduction angle in the lower plate.

2.1. Geophysical Constraints

Geophysical data reveal different types of crust (from thin anomalous Tyrrhenian to normal African) across the northern Sicily continental margin. The Moho depth increases southward from 10 km in the Tyrrhenian abyssal plain to about 25 km near the Sicily margin reaching about 37–40 km under the Sicilian FTB (Cassinis et al., 2003; Scarascia et al., 1994); from here it decreases southward until about 27 km beneath the Iblean platform (Chironi et al., 2000) and from 20 to 16 km along the Ionian margin and the abyssal plain, respectively (Catalano et al., 2000a; De Voogd et al., 1992). *S* wave tomography indicates a shallow upper mantle source for the Apennines-Tyrrhenian igneous system, while the asthenosphere is postulated to be very shallow, as deep as 30–40 km (Panza et al., 2007). The map of the magnetic basement (Morelli, 2003) shows depth values of 8–10 km beneath the Iblean domain, 10–12 km in western Sicily, more than 14 km in the Caltanissetta trough, and about 13 km along the northern margin (Bello et al., 2000; Catalano et al., 2000b; Finetti, 2005).

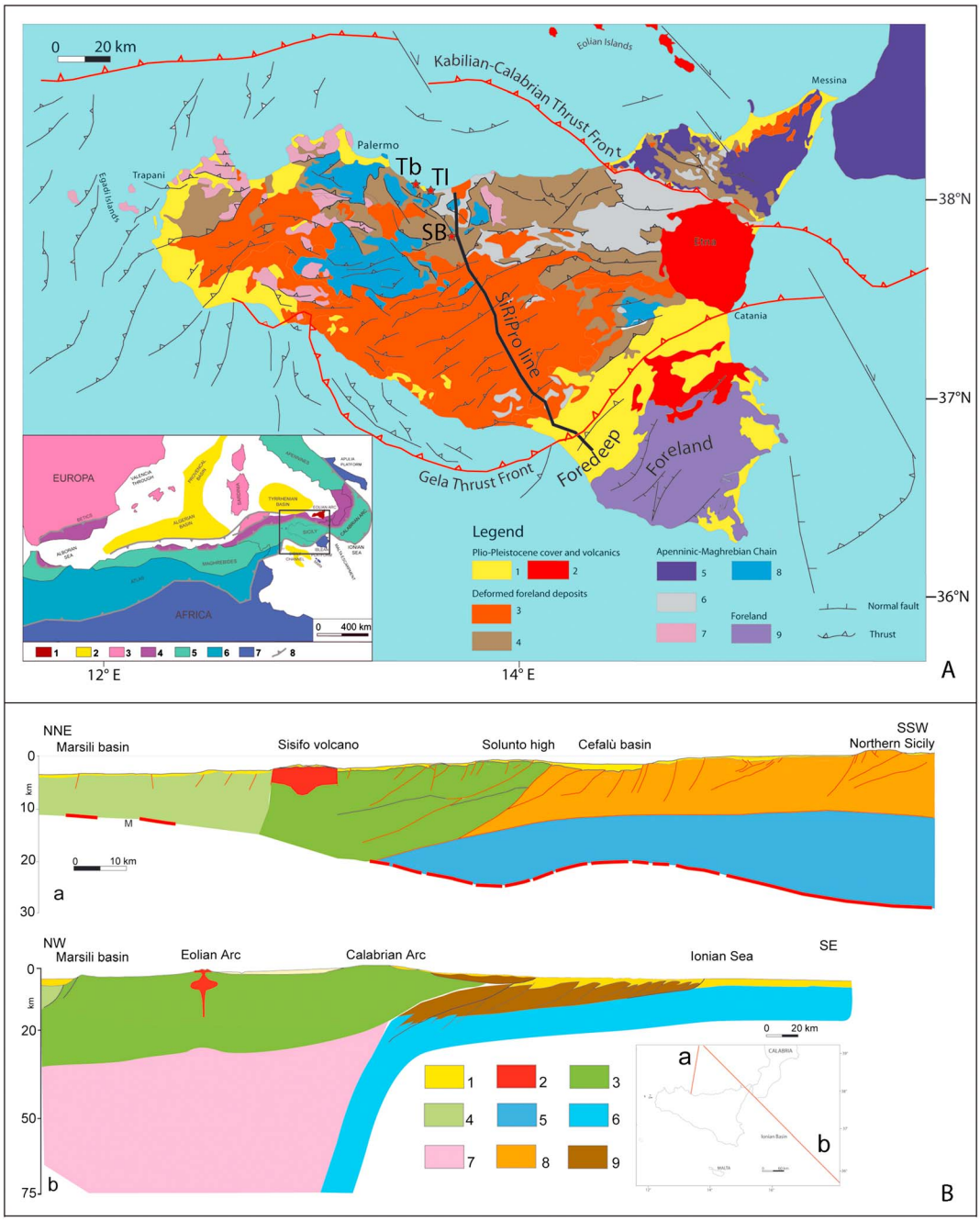

Figure 1. (A) Structural map of Sicily (modified from Catalano et al., 2013). (1) Plio-Pleistocene cover, (2) volcanics, (3) upper Miocene-lower Pliocene deformed foreland deposits, (4) upper Oligocene-lower Miocene deformed foreland deposits, (5) Kabilian-Calabrian crystalline units, (6) Sicilide units, (7) Meso-Cenozoic carbonate platform deformed units (Sicilian-Maghrebian shallow-water units), (8) Meso-Cenozoic slope-to-deep-basin deformed units (Sicilian-Maghrebian deep-water units), and (9) Meso-Cenozoic carbonate platform not-deformed units (Sicilian-Maghrebian foreland). Red stars indicate the sampling points (i.e., TI, Tb, and SB). Inset map shows the main physiographic regions of the central western Mediterranean. (1) Volcanics, (2) extensional basins, (3) European units, (4) Kabilian-Calabrian units, (5) Apenninic-Maghrebian units, (6) Atlas units, (7) African foreland, (8) main thrust fronts (modified from Roure et al., 2012; Catalano et al., 2013). (B) Geological sections showing the Sicilian collisional system in the southern Tyrrhenian Sea (a) and the B-subduction complex, from the Ionian Sea to the southern Tyrrhenian Sea (b). (1) Plio-Pleistocene cover, (2) volcanics, (3) Kabylian-Calabrian (European) units, (4) thinned to oceanic Tyrrhenian crust, (5) African crust, (6) Ionian crust, (7) mantle, (8) Sicilian-Maghrebian units, and (9) Ionian accretionary wedge. The geological sections were obtained from the interpretation of the crustal seismic profile CROPM6 (a) and M2 (b), respectively, calibrated by refraction data, well logs, and field geology.

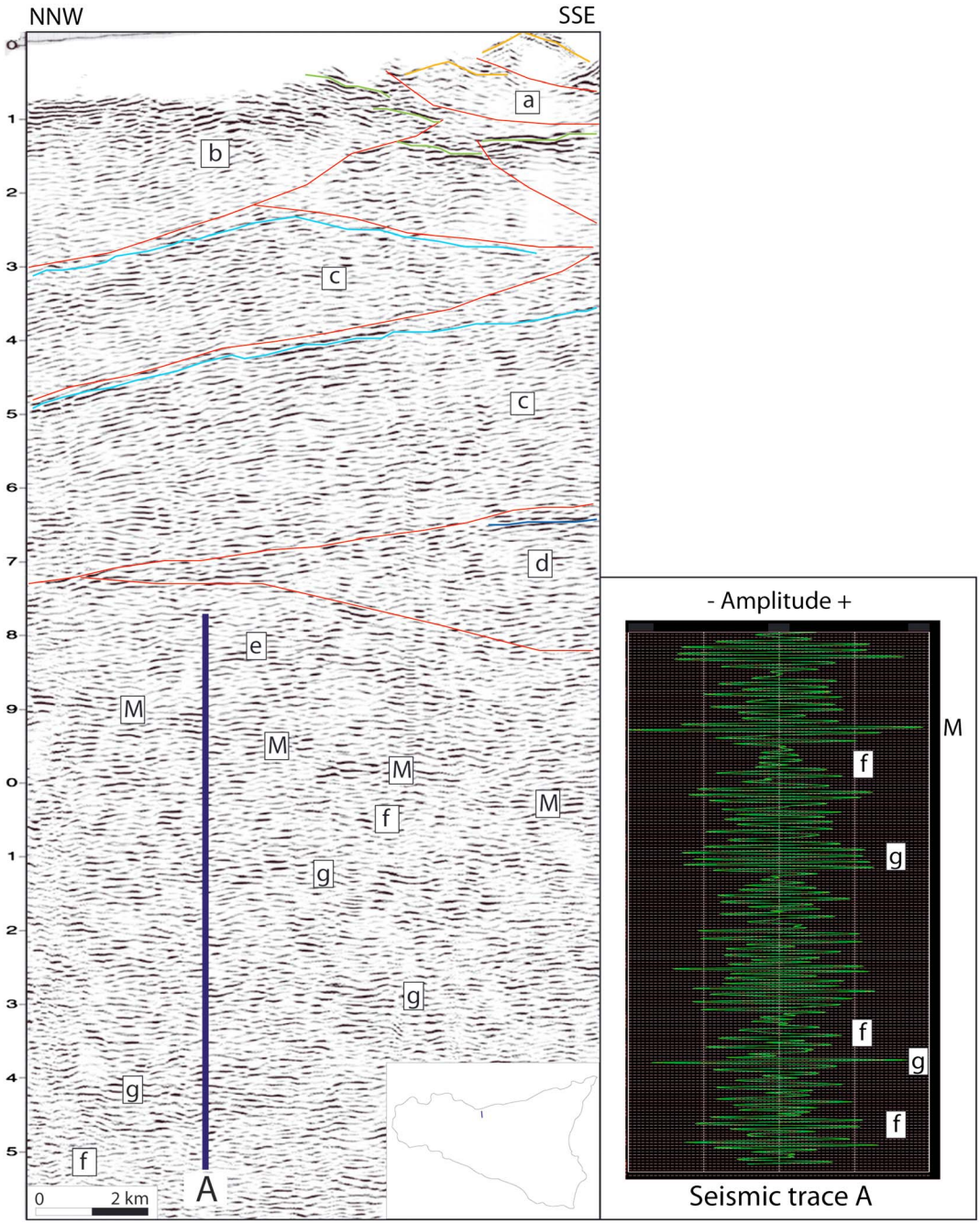

Figure 2. Detail of the northernmost sector of the SiRiPro line (see Figure 1). Seismic units: (a) high-frequency to reflection-free bodies, assembled as tightly deformed thin slices, interpreted as a stack of both detached terrigenous Tertiary cover and Upper Mesozoic-lower Tertiary Sicilide units; (b) high frequency deformed slices, interpreted as Permian-Cenozoic deep water carbonate units; (c) low-to-high frequency deformed bodies, interpreted as pertaining to the Meso-Cenozoic shallow-water carbonate units; (d) low-to-high frequency shallow-water Meso-Cenozoic carbonate unit, derived from the deformed northward prolongation of the Iblean foreland; (e) transparent-to-reflective body, topped by a high-amplitude reflector, interpreted as the continental crust, with a steep ascent in a northward direction. The lower part has an anomalously high reflectivity, which could be linked to stretching extensional processes; (f) transparent layer, interpreted as mantle due to its position below the Moho and its correlation with seismic refraction data; (g) lens/wedge-shaped reflective bodies, which could correspond to delaminated fragments of the lower crust (and possibly part of the lithospheric mantle) inside the mantle. Brown line, top of Numidian Flysch and Sicilide units; green line, top of Meso-Cenozoic Sicilian-Maghrebian deep-water units; light-blue line, top of Meso-Cenozoic Sicilian-Maghrebian shallow-water units; blue line, top of Meso-Cenozoic deformed foreland; M, Moho discontinuity; red lines, faults. On the right, the lower part (from 8 to 15 s/TWT) of the seismic trace is shown.

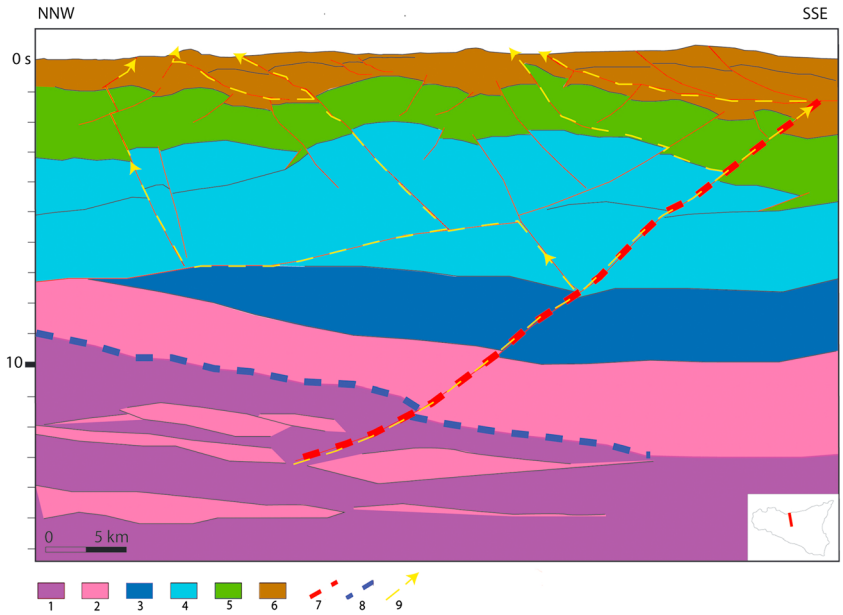

Figure 3. Geoseismic section showing the tectonic stack forming the Sicilian FTB and relationships with the crust-mantle layers. The complex network of faults is shown by red lines. (1) Mantle, (2) African continental crust and delaminated layers, (3) deformed and undeformed Iblean carbonate units, (4) deep-seated, shallow-water Meso-Cenozoic carbonate tectonic units, (5) shallow-seated, deep-water Meso-Cenozoic carbonate tectonic units, (6) shallow-seated, terrigenous Tertiary detached cover, (7) basement-involved main thrust, crossing the crust and penetrating the mantle, (8) delamination surface, and (9) pathways for ascending fluids.

In Sicily, heat flow values vary generally from 40 to 50 mW/m^2 (Della Vedova et al., 2001). Localized areas of higher values are present in the Iblean foreland (up 80 mW/m^2), in westernmost Sicily (up to 80 mW/m^2), in northern Sicily (up to 70 mW/m^2), and in the Tyrrhenian Sea (more than 100 mW/m^2). The high heat flow in the westernmost sector can be linked to an excess of heat due to accumulations of mantle-derived melts into the crust or at the crust-mantle boundary (Caracausi et al., 2005). The high heat flow of the Tyrrhenian Sea is linked to the Eolian volcanism (Della Vedova et al., 2001), while no detailed studies have been still carried out to investigate the origin of the high heat flow in northern Sicily and in the Iblean foreland.

Sicily and the surrounding areas are characterized by intense recent tectonic activity, testified by a strong seismicity, individuating main seismotectonic zones. In particular, excluding areas located far away from the study area, major earthquakes are concentrated in the following (Billi et al., 2010; Pondrelli et al., 2006): (1) a contractional-transpressional belt in southern Tyrrhenian and western Sicily, passing eastward and southward to (2) an extensional-transtensional belt in the Madonie-Peloritani mountains (e.g., Pollina cluster) and Caltanissetta trough; (3) a transtensional belt in the Iblean foreland, parallel to the Malta Escarpment, separating the Sicily from the Ionian abyssal plain (Catalano et al., 2000a).

In northern central Sicily, clusters of deep earthquakes, concentrated mainly along N-S to NNW-SSE trends, point out an anomalous lithosphere depth that encourages the hypothesis of subduction processes beneath central Sicily (Billi et al., 2010; Chiarabba et al., 2008).

3. Fluids Geochemistry

3.1. Sampling and Analytical Methods

Three hydrothermal systems are localized in the northernmost Sicily (TI, Tb, and SB; Figure 1), just in correspondence of the SiRiPro profile (Catalano et al., 2013). A total of 12 waters were sampled from springs and wells localized in TI, Tb, and SB between 2002 and 2013. The water samples for the analysis of the chemistry of the dissolved gases and the He-isotope ratio were collected in glass bottles according to protocols described by Capasso and Inguaggiato (1998) and analyzed in a few days from their collection in order to prevent any contamination and/or loss of volatiles.

Table 1
Chemical Data

Site	Data	T (°C)	He	N_2	CH_4	CO_2	$^4He/^{20}Ne$	$^3He/^4He$
TI 1	Sep 2002	43.4	1.3E−03	1.1E+01	9.4E−03	3.2E+01	9.55	1.33
TI 2	Sep 2002	42.6	1.3E−03	1.2E+01	3.6E−03	2.9E+01	8.83	1.32
TI 3	Apr 2001	41.4	1.1E−03	1.6E+01	3.1E−03	4.8E+01	6.97	1.31
TI 1	Jun 2012	43.1	1.7E−03	1.4E+01	1.6E−02	3.1E+01	6.19	1.31
TI 2	Apr 2012	42.2	2.0E−03	1.3E+01	1.4E−02	3.4E+01	18.15	1.29
TI 1	Feb 2013	42.9	1.7E−03	1.2E+01	1.3E−02	3.1E+01	6.81	1.30
Tb	Sep 2004	27.8	1.2E−03	2.0E+01	1.4E−02	8.5E+00	4.09	0.36
Tb	Dec 2004	27.5	1.2E−03	1.4E+01	3.4E−02	8.5E+00	4.52	0.39
Tb	May 2013	27.5	1.1E−03	1.7E+01	1.2E−02	1.0E+01	3.88	0.36
SB	Dec 2004	33.2	4.4E−04	3.1E+00	1.9E+01	1.9E+01	7.88	0.77
SB	Nov 2004	32.3	6.6E−04	1.9E+00	2,1E+01	3.6E+01	3.78	0.77
SB	May 2013	32.8	6.1E−04	n.a.	n.a.	n.a.	12.1	0.74

Note. Total dissolved inorganic carbon is expressed in mmol/L; He concentrations are in ccSTP/L; $^3He/^4He$ are expressed as R/R_a values; $\delta^{13}C$ values are in ‰. n.a. not available data.

The chemical compositions of the dissolved gases were determined with a gas chromatograph (Perkin Elmer 8500) with Ar carrier gas on a 4-m column (Carbosieve SII) and double detector (TCD and FID). The analytical error was about ±3% for all species. The concentrations of the dissolved gases in the waters have been computed on the basis of the solubility data of the gaseous species in water (Capasso & Inguaggiato, 1998).

He isotopes were analyzed using a static vacuum mass spectrometer (GVI Helix SFT) with a double collector in order to detect ^3He and ^4He ion beams simultaneously (isotopic ratio precision within ±0.5%); this method ensured very low errors for the $^3He/^4He$ measurements. The $^3He/^4He$ ratio was determined by measuring ^3He in an electron multiplier detector and ^4He in an axial Faraday detector. $^4He/^{20}Ne$ ratios were measured with a quadrupole mass spectrometer.

He isotopic ratios are reported as R/R_a values, where R_a is the He-isotope ratio in atmosphere (1.39×10^{-6}; Ozima & Podosek, 2002). All sampling and analytical devices were provided by the Istituto Nazionale di Geofisica e Vulcanologia, Sezione di Palermo.

3.1.1. Geochemical Data

The chemical and isotopic data of the collected samples are reported in Table 1. The temperature of the emerging waters ranges from 27.5 to 43.4 °C for Tb and TI waters, respectively (Table 1). The temperature of the SB waters is from 32.3 °C to 33.2 °C. Previous investigations (Carapezza et al., 1987; Grassa et al., 2006) highlighted the following: (1) TI and SB waters are chloride-sulfate-alkaline waters, in contrast to the bicarbonate-alkaline-terrigenous waters of Tb; and (2) a meteoric recharge of the hydrological basins with a large contribution from seawater in the TI basin.

Gases dissolved in TI waters are CO_2 dominated (from 29 to 48 ccSTP/L), with an amount higher than in water in equilibrium with the atmosphere (air saturated water). In contrast, N_2 (14–20 ccSTP/L) is the main dissolved gas in Tb waters. SB waters are CH_4- and CO_2-rich, from 19 to 21 ccSTP/L and 19 to 36 ccSTP/L, respectively. He is always in trace and its abundance is up to two orders of magnitude higher than the air saturated water (4.41×10^{-8} ccSTP/g at 25 °C; Ozima & Podosek, 2002).

He-isotope composition in the collected fluids is from $0.36R_a$ (Tb) to $1.33R_a$ (TI). He isotope signature at SB site is $0.74–0.77R_a$. All of the $^4He/^{20}Ne$ ratios are at least one order of magnitude higher than the value for the atmosphere (0.318; Ozima & Podosek, 2002), indicating that air contamination was negligible in all of the investigated fluids (Table 1).

3.1.2. Mantle-Derived He Degassing

In large crustal fluid systems, reasonable sampling "average" crust $^3He/^4He$ ratios in excess of $1–3 \times 10^{-8}$ (i.e., more than three times the upper crust value; Ballentine & Burnard, 2002) are due to a ^3He excess from sources external to the crust (Marty et al., 1993). $^3He/^4He$ ratios in the study area are from 5.0×10^{-7} ($0.4R_a$) to 1.8×10^{-6} ($1.3R_a$), at least one order of magnitude higher than the upper crust value ($0.01–0.03R_a$), so considering that the He atmospheric contribution is negligible in the North-Central Sicily thermal basins (NCStb), there is a clear contribution of mantle-derived He.

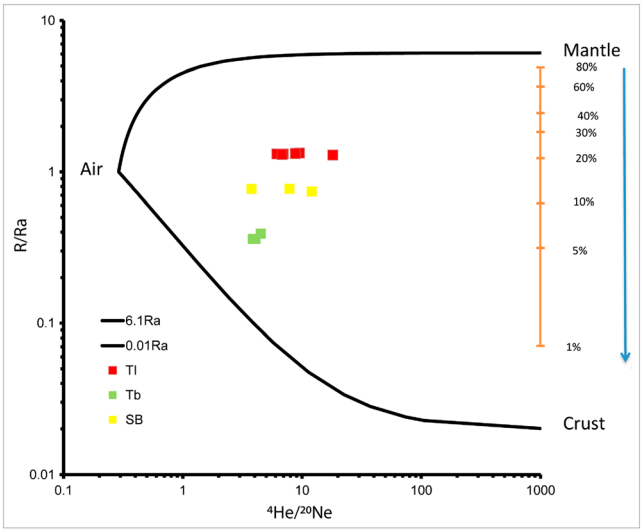

Figure 4. $^{3}He/^{4}He$ ratios (as R/R_a) plotted against the $^{4}He/^{20}Ne$ ratios. The line shows the mixing between the three possible end-members: air, crust, and mantle.

On the basis of the approach proposed by Sano et al. (1997), it is possible to solve the percentage of mantle-derived He and crustal He (U and Th decay in the crust) in the studied gases by using mixing equations and both the He isotopic ratio and the $^{4}He/^{20}Ne$ ratio of the three possible source of He: atmosphere, mantle, and crust (Figure 4). The typical crustal He endmember, dominated by ^{4}He production due to U and Th decay in the crust, is 0.01–0.02R_a (Ozima & Podosek, 2002). Because the investigated thermal systems are in a continental region, we made calculations assuming a subcontinental lithospheric mantle, with a He-isotope ratio of 6.1 ± 0.9R_a (Gautheron & Moreira, 2002), as mantle source in the area. Fluids associated with NCStb are characterized by a very low atmospheric contribution and contain mantle helium contributions from ~5% to ~20% (Figure 4).

Considering that the tectonics in NCStb acts upon the hydrology of the thermal systems (Carapezza et al., 1987), according to Kennedy et al. (1997), we computed the ^{3}He flux (Φ_{3He}) based on the upward fluid flow rates through faults and the production of radiogenic He in the crust. Mantle He moving through the crust across faults is diluted by radiogenic ^{4}He produced by the decay of U and Th in the crust. The result is a vertical gradient of He isotopic ratio as a function of the radiogenic He production rate and of the vertical rate of fluid flow (Kennedy et al., 1997). The upward flow rate (q) is as follows:

$$q = \frac{H_c \rho_s P(\mathrm{He})}{\rho_f [\mathrm{He}]_{F,m}} \times \left[\frac{R_s - R_c}{R_m - R_c}\right] \quad (1)$$

where H_c is the crustal thickness, ρ_f and ρ_s are the density of fluids and rocks, respectively, P(He) is the radiogenic He production rate (Ozima & Podosek, 2002), which is computed by using the U and Th contents of the rocks, $[He]_{F,m}$ is the initial concentration in the mantle fluid and is calculated from the measured ^{4}He concentration and He isotopic composition of the sampled fluid, R is the $^{3}He/^{4}He$ of sample (s), mantle (m), and crust (c). Based on crustal thickness below the investigated region (40 km: 3 km shales, 12 km limestone, and 25 km crystalline basement plus mantle wedge; Figures 2 and 3) and computing the ^{4}He production rate by assuming the U and Th contents in the different lithology of the CWS crust (shale U = 4 ppm and Th = 12 ppm; limestone U = 1.3 ppm and Th =0.2 ppm; crystalline basement U = 1.4 ppm and Th = 5.6 ppm; data in Rudnick & Fountain, 1995; Schön, 1996; Caracausi et al., 2005), the calculated upward fluids flow rates range from about 30 to ~110 mm/year.

On the basis of the upward flow rate of fluids, it is possible to calculate the ^{3}He flux (Kulongosky et al., 2013):

$$\Phi_{3He} = q \times \rho_f \times [\mathrm{He}] \times R \quad (2)$$

where [He] and R are the concentrations of ^{4}He and $^{3}He/^{4}He$ ratio in the sample, respectively. The computed Φ_{3He} in the NCStb ranges from 1.8×10^{4} to 7.7×10^{4} atoms·m^{-2}·s^{-1} (at Tb and TI, respectively; at SB is 4.3×10^{4} atoms·m^{-2}·s^{-1}); these values are much higher than the ^{3}He flux from stable continental crust (less than 10^{2} atoms·m^{-2}·s^{-1}; Ozima & Podosek, 2002) and are comparable with flux from continental areas undergoing extensive tectonics (up to 10^{5} atoms·m^{-2}·s^{-1}; Ozima & Podosek, 2002). Furthermore, according to equations (1) and (2), if the radiogenic He production rate is higher than the computed values (U-rick crust: contents of U up to 4 ppm vol. and Th up to 12 ppm vol.; Rudnick & Fountain, 1995), the Φ_{3He} will be higher than 1.5×10^{5} atoms·m^{-2}·s^{-1}. This still supports that the Φ_{3He} are in the range of the values from continental areas undergoing extensive tectonics. Such high He fluxes cannot be sustained by a long-lasting diffusion (Ballentine & Burnard, 2002), thereby implying an efficient He transport (i.e., advective transport through faults). In fact, high mantle He fluxes are typical of continental regions affected by extensional tectonics (e.g., Caracausi et al., 2005; Italiano et al., 2000; O'Nions & Oxburgh, 1988; Ozima & Podosek, 2002), where magmatic intrusions in the crust were inferred (Ballentine & Burnard, 2002).

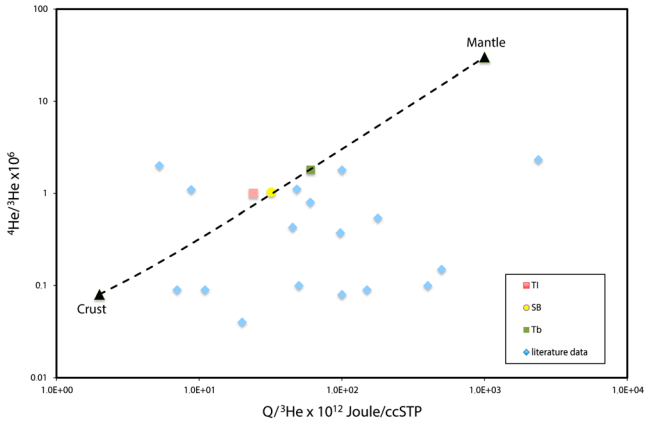

Figure 5. Heat versus He relationship in continental-hosted geothermal systems. Mantle-derived He is associated with heat coming from the mantle in the investigated hydrothermal basins. Heat and He in these basins have not experienced significant $Q/^3$He fractionation (e.g., magma aging or adiabatic cooling). Data on the crust and mantle endmembers and literature data characteristics are available in Kennedy et al. (2000) and Mutlu et al. (2008).

Furthermore, assuming that the mantle $CO_2/^3$He is 2×10^9 (Marty & Jambon, 1995), we also compute the flux of mantle-derived CO_2, by using the computed ^{3}He flux, and it is from 1.8×10^3 to 8.2×10^3 mol·km^{-2}·year^{-1}. These values are at least three orders of magnitude lower than the CO_2 flux in active and quiescent worldwide volcanic systems (Caracausi et al., 2015, and reference therein) and one to two orders of magnitude lower than the flux of mantle-derived CO_2 along the African rift system (up to 2.5×10^5 mol·km^{-2}·year^{-1}; Foley & Fischer, 2017). However, the computed mantle-CO_2 flux in the NCStb is comparable with that from the San Andreas Fault (4.0×10^4 mol·km^{-2}·year; Kulongosky et al., 2013), and these are rare data from a continental region away from volcanism in a compressional tectonic regime.

The three investigated hydrothermal systems fall in a E-W elongated region of high heat flow, up to 70 mW/m^2, so from 20 to 30 mW/m^2 higher than the heat flow in the surrounding area at regional scale (Cataldi et al., 1995). This evidence supports that in the NCStb the outgassing of mantle-derived He is associated to high heat flux. Hence, in order to investigate a possible relation between heat and mantle-derived volatiles, we computed the heat/^{3}He ratios, by dividing the heat flux in the region of the investigated hydrothermal systems (70 mW/m^2; Cataldi et al., 1995) and the computed ^{3}He flux, from 1.8×10^4 to 7.7×10^4 atoms·m^{-2}·s^{-1} (Tb and TI, respectively). In geothermal system associated to midoceanic ridge, the He isotopic compositions of plume fluids are indistinguishable from the mantle, and the Q/^{3}He ratios vary from ~1–10 $\times 10^{12}$ J/ccSTP (Baker & Lupton, 1990). Moreover, the measured heat/He ratios are remarkably similar to the theoretically predicted value, providing a measure of validity to the theory of heat-He coherence in geothermal systems. In a stable continental crust, He is dominated by radiogenic He production and the Q/^{3}He ratio is ~1×10^{15} J/ccSTP, up to three orders of magnitude larger than the expected mantle value (Kennedy et al., 2000). Because of the large difference between the ratio in volcanic and nonvolcanic systems, the heat/^{3}He ratio can allow discriminating possible contributions of mantle heat feeding continental geothermal system. The computed heat/^{3}He ratios for the NCStb (TI, SB, and Tb) fall in a narrow range of values, from 25 to 60×10^{12} J/ccSTP, which are lower than the typical values of geothermal systems in continental crust far from volcanoes. Furthermore, the NCStb values are comparable with the same ratio in geothermal systems (Figure 5), which are characterized by deep permeability and fluid circulation along an elevated geothermal gradient partially driven by mantle melting (Kennedy et al., 2000; Kennedy & Van Soest, 2007; Mutlu et al., 2008). This evidence, coupled with (1) structural conditions (active extension in central northern Sicily), (2) localized high heat flow, (3) evidences of a hot mantle wedge embedded into crust (sections 2 and 4), and (4) high ^{3}He flux that are typical of continental region affected by crustal extensional tectonics, strongly supports that the release of mantle-derived He in the NCStb is related to magmatism at depth. In actual fact, mantle volatiles are more efficiently transferred by mantle-derived melt intrusion into the crust (Ballentine & Burnard, 2002), thus showing evidence of a subsurface magmatism when other possible indicators are lacking (i.e., Italiano et al., 2000; O'Nions & Oxburgh, 1988). Release of mantle He is often associated with magmatism, and it seems logical that the mantle must melt in order to liberate He: in fact diffusion through solid mantle would be too slow to account for the observed fluxes (Burnard et al., 2012).

4. Gravity Modeling, Seismic Reflection, and Geological Features

Starting from the hypothesis of magmatic intrusion as source of degassing of mantle-derived fluids, we used geological and geophysical constraints to identify the geodynamic mechanism responsible for the crust-mantle features and behavior.

It is generally agreed that processes as post-orogenic extensional collapse, regional uplift, deep-seated magmatism, elevated heat flow, and subcrustal seismicity could be the tectonic and geodynamic consequences of lithospheric delamination (Bird, 1979; Knapp et al., 2005; Meissner & Mooney, 1998).

The geometry of the lithosphere down to the mantle-crust interface along the Sicily FTB can be drawn by the high-penetration seismic reflection profile (SiRiPro) that crosses Sicily for more than 100 km from the Tyrrhenian Sea to the Sicily Channel (Catalano et al., 2013). Data related to gravity modeling, seismic refractions, shallower reflections, field geology, and borehole stratigraphy are widely available for the studied region (Gasparo Morticelli et al., 2015; Giustiniani et al., 2018), and they support the interpretation of the seismic data. Just below the area of the outgassing of mantle-derived volatiles degassing coupled to heat flow anomalies in the NCStb, the seismic line provides evidence that the crystalline basement is involved in thrusting and appears to be in a stacked arrangement down to the mantle-crust interface (Figure 2). The sedimentary portion is detached from the basement and more tightly deformed and accreted to form a tectonic edifice with thickness more than 15 km. Still in this region, at a depth of 30–40 km, a wedge-shaped body is interbedded between two crustal segments, the uppermost resting above the wedge, and climbing up toward the north, where it links with the thinned continental crust beneath the Tyrrhenian sea, and the lowermost deepening abruptly beneath it (Figure 3). The resulting feature is a trough-shaped geometry of the deep crust and a dome-shaped geometry of the overlying tectonic edifice. In correspondence of this wedge-shaped body, gravity modeling has provided an anomalous high density of 3.1 g/cm^3 at the base of the crust (supported by a positive Bouguer anomaly of +40 mGal), compared with the mean value of 2.9 g/cm^3 along the profile. This anomalously high density cannot be explained by the typical density of crust, instead of being more similar to the mantle density. Distribution of the refraction seismic velocities (Scarascia et al., 1994) indicates the presence of velocity inversion, which was attributed to a doubling of the crust and a northward subduction of the African plate. If we analyze the geophysical evidences considering the outgassing of mantle-derived volatiles fed by magmatic intrusions at depth, this high-density, wedge-shaped body must be interpreted as a mantle wedge composed of asthenospheric and/or lithospheric mantle, located between two different crustal bodies (Figures 2 and 3).

Wedging generally develops in B-subduction systems, and its high temperatures produce melting and feeding the volcanism of arcs. The peculiarity of the present case is that wedging develops in a collisional system produced by A-subduction.

In the southern Tyrrhenian Sea, a transition zone in the northern Sicilian belt separates the collisional from the subduction system (Figure 1). This area experienced faulting and stretching related to the Tyrrhenian backarc rifting (Malinverno & Ryan, 1986) and consequently is characterized by lithospheric thinning, which could be responsible for the passive up-doming of the asthenosphere in a context of passive rifting, in relation to the role of mantle.

Westward, a cold and dense lithospheric root of the orogen slips into the hotter asthenosphere, creating lateral temperature instability. This drives convective flow that can delaminate the lower portions of the thickened lithosphere. Therefore, a mantle wedge separating two crustal bodies should be the consequence of delamination processes of the continental crust, already invoked as being necessary to explain the continental subduction of the African plate in the framework of southern Apennines orogenesis.

The recent tectonics along the central northern Sicily is well documented by structural and seismological data (Billi et al., 2010), demonstrating that the network of a mainly compressional-transpressional fault system could be negatively inverted in still-active WNW striking extensional-transtensional faults, descending to the deep crust. These observations support the existence of the structural condition necessary for delamination processes, as well as the generation and transfer of hot melt material among the upper and lower crust, whose surface evidence is the active degassing of mantle-derived volatiles coupled to a high heat flow.

Examples from the Alps have demonstrated that their late-stage widespread uplift, as in the northern Sicily belt, could be explained by delamination and/or convective removal of a thickened lithosphere and mechanical decoupling between the mantle and crust of the subducted lithosphere, enhanced by erosional unloading (Genser et al., 2007). Beneath the Apennines and Calabria, along the western margin of Adria, as well as in the Aegean Arc and other segments of the Eastern Mediterranean, delamination processes between the Apulian crust and its mantle lithosphere, linked to the back-arc extension and related asthenospheric upwelling, in addition to slab pull, were considered responsible for the progressive retreat of the mantellic slab, giving rise to downflexing and accelerated subsidence of the foreland crust besides areas of rapid uplift (Roure et al., 2012).

5. Delamination and Mantle-Derived Volatiles Degassing

Recognition of delamination-related magma is a key tool to constrain the occurrence of delamination events at depth (Anderson, 2005; Kay & Kay, 1993). Hence, the occurrence of magmatic intrusions at depth in the central part of the Mediterranean—as inferred from geochemical data of mantle-derived fluid outgassing coupled to heat-flow anomalies—together with the geological and geophysical data strongly supports the possible occurrence of delamination processes that are related to the continental subduction as a consequence of the convergence between the European and African plates (e.g., Chiarabba & Chiodini, 2013).

Above the mantle wedge, the SiRiPro data highlight a very complex pattern of faults that are Mesozoic to Tertiary-Quaternary in age and represented by two different systems (Avellone et al., 2010; Bello et al., 2000): (1) the older is quasihorizontal, separating the different structural layers constituting the Sicily Chain, and (2) the younger has a high angle and is from transpressional to transtensional, crossing the whole tectonic edifice and reaching depths from the crust down to the mantle-crust interface (Figure 3). Since it is linked directly to the anomalous wedge, it acts as the escape route for the transfer of mantle volatiles across the entire crust (Figure 3).

Degassing of mantle-derived fluids coupled to active tectonics and seismicity points to a deformation-enhanced permeability in the deep crust. Moreover, the present-day seismicity indicates that the prevailing focal mechanisms are extensional, and the hypocenters of the earthquakes are mainly concentrated at locations deeper than 30 km and shallower than 10 km (Doglioni et al., 2012), supporting that the tectonic is active and the faults are able to transfer fluids through the deep crust toward the surface.

6. Conclusions

Our work demonstrates that outgassing of mantle volatiles can also occur in a compressional geodynamic regime. Here we highlighted that He isotopes are powerful tools to solve the mantle-crust tectonics involving the occurrence of magma without any evidences of volcanism on the surface. The outgassing of mantle-derived He constrains that the investigated region is also affected by mantle CO_2 degassing because it is a major magmatic volatile component and it can be the carrier of mantle He through the crust. On the basis of the $CO_2/^3He$ ratio and the ^3He fluxes, here we computed the mantle CO_2 flux in this sector of the Mediterranean (from 1.8×10^3 to 8.2×10^3 mol·km^{-2}·year^{-1}). These values of CO_2 flux are lower than those from active and quiescent volcanic systems (e.g., Caracausi et al., 2015, and references therein), and they are comparable with those from other seismic regions (e.g., San Andrea Faults, USA) through which an active degassing of mantle-derived volatiles is well recognized. However, our data are from a continental region in a type A subduction system that is tectonically affected by a compressional regime. Results of this study show that a flux of heat and mantle volatiles (i.e., CO_2 and He) are due to magmatic intrusions at depth, highlighting that these can also occur below a tectonic chain. In fact, the geological and geophysical data support the presence of a hot mantle wedge below the area characterized by the outgassing of mantle volatiles. The presence of this mantle wedge that is in between two layers of crust, the African above and the European below, respectively, is the consequence of delamination processes that is well recognized to produce magmatism at a large scale.

Furthermore, our geochemical data support that the transfer of mantle-derived volatiles through the crust is due to advective processes through WNW-ESE trending extensional tectonic discontinuities, still active in central northern Sicily. Finally, we discuss a geological section that highlights the occurrence of a system of deep faults crossing the continental crust and connecting the mantle wedge to the surface in correspondence of the NCStb. These tectonic discontinuities represent the possible structural paths through which volatiles move across the entire crust and reach the surface.

Acknowledgments
All the geochemical data of the NCStb that we discussed in this paper are unpublished and are in Table 1. Seismic data were acquired in the frame of the SiRiPro Italian project, funded by MIUR Italian Research Ministry, and are stored at the Department of Earth and Marine Science of the University of Palermo; the data are available at www.siripro.it or by contacting the authors (e.g., attilio.sulli@unipa.it). The geological data discussed in this manuscript are literature data, and all the references are cited in our manuscript.

References

Anderson, D. L. (2005). Large igneous provinces: Origin and environmental consequences: Large igneous provinces, delamination, and fertile mantle. *Elements*, *1*(5), 271–275. https://doi.org/10.2113/gselements.1.5.271

Avellone, G., Barchi, M. R., Catalano, R., Gasparo Morticelli, M., & Sulli, A. (2010). Interference between shallow and deep-seated structures in the Sicilian fold and thrust belt, Italy. *Journal of the Geological Society*, *167*(1), 109–126. https://doi.org/10.1144/0016-76492008-163

Baker, E. T., & Lupton, J. (1990). Changes in submarine hydrothermal ^3He/heat ratios as an indicator of magmatic/tectonic activity. *Nature*, *346*(6284), 556–558. https://doi.org/10.1038/346556a0

Ballentine, C. J., & Burnard, P. (2002). Production, release and transport of noble gases in the continental crust. *Reviews in Mineralogy and Geochemistry*, *47*(1), 481–538 Mineralogical Society of America 2002. https://doi.org/10.2138/rmg.2002.47.12

Ballentine, C. J., Schoell, M., Coleman, D., & Cain, B. A. (2001). 300-Myr-old magmatic CO_2 in natural gas reservoir of the west Texas Permian basin. *Nature*, *409*(6818), 327–331. https://doi.org/10.1038/35053046

Bello, M., Franchino, A., & Merlini, S. (2000). Structural model of eastern Sicily. *Memorie della Società Geologica Italiana*, *55*, 61–70.

Billi, A., Presti, D., Orecchio, B., Faccenna, C., & Neri, G. (2010). Incipient extension along the active convergent margin of Nubia in Sicily, Italy: Cefalù-Etna seismic zone. *Tectonics*, *29*, TC4026. https://doi.org/10.1029/2009TC002559

Bird, P. (1979). Continental delamination and the Colorado Plateau. *Journal of Geophysical Research*, *84*(B13), 7561–7571. https://doi.org/10.1029/JB084iB13p07561

Burnard, P., Bourlange, S., Blard, P. H., Geli, L., Tryon, M. D., Natal'in, B., et al. (2012). Constraints on fluid origins and migration velocities along the Marmara Main Fault (Sea of Marmara, Turkey) using helium isotopes. *Earth Planetary Science Letters*, *341-344*, 68–78. https://doi.org/10.1016/j.epsl.2012.05.042

Byerle, J. D. (1993). Model for episodic flow of high-pressure water in fault zones before earthquakes. *Geology*, *21*(4), 303–306. https://doi.org/10.1130/0091-7613(1993)021<0303:MFEFOH>2.3.CO;2

Capasso, G., & Inguaggiato, S. (1998). A simple method for the determination of dissolved gases in natural waters. An application to thermal waters from Vulcano Island. *Applied Geochemistry*, *13*(5), 631–642. https://doi.org/10.1016/S0883-2927(97)00109-1

Caracausi, A., Favara, R., Italiano, F., Nuccio, P. M., Paonita, A., & Rizzo, A. (2005). Active geodynamics of the central mediterranean sea: Tensional tectonic evidences in western Sicily from mantle-derived helium. *Geophysical Research Letter*, *32*, L04312. https://doi.org/10.1029/2004GL021608

Caracausi, A., Martelli, M., Nuccio, M., & Paternoster, M. (2013). Active degassing of mantle-derived fluids; a geochemical study along the Vulture Line, Southern Appennines. *Journal of Volcanology and Geothermal Research*, *253*, 65–74. https://doi.org/10.1016/j.jvolgeores.2012.12.005

Caracausi, A., Paternoster, M., & Nuccio, P. M. (2015). Mantle CO_2 degassing at Mt. Vulture volcano (Italy): Relationship between CO_2 outgassing of a volcano and the time since its last eruption. *Earth Planetary Science Letters*, *411*, 268–280. https://doi.org/10.1016/j.epsl.2014.11.049

Carapezza, M., Cusumano, G., Liguori, V., Alaimo, R., Dongarrà, G., & Hauser, S. (1987). Nota Introduttiva allo studio delle sorgenti termali della Sicilia e delle Isole minori. *Bollettino della Società Geologica Italiana*, *96*, 813–836.

Cassinis, R., Scarascia, S., & Lozej, A. (2003). The deep crustal structure of Italy and surrounding areas from seismic refraction data. A new synthesis. *Bollettino della Società Geologica Italiana*, *122*, 365–376.

Catalano, R., Di Stefano, P., Sulli, A., & Vitale, F. P. (1996). Paleogeography and structure of the central Mediterranean: Sicily and its offshore area. *Tectonophysics*, *260*(4), 291–323. https://doi.org/10.1016/0040-1951(95)00196-4

Catalano, R., Franchino, A., Merlini, S., & Sulli, A. (2000a). A crustal section from North Algerian to the Ionian ocean (central Mediterranean). *Memorie della Società Geologica Italiana*, *55*, 71–85.

Catalano, R., Franchino, A., Merlini, S., & Sulli, A. (2000b). Central Western Sicily structural setting interpreted from seismic reflection profiles. *Memorie della Società Geologica Italiana*, *55*, 5–16.

Catalano, R., & Sulli, A. (2006). Crustal image of the Ionian basin and accretionary wedge. *Bollettino di Geofisica Teorica e Applicata*, *47*(3), 343–374.

Catalano, R., Valenti, V., Albanese, C., Accaino, F., Sulli, A., Tinivella, U., et al. (2013). Sicily's fold/thrust belt and slab roll-back: The SI.RI.PRO. seismic crustal transect. *Journal of the Geological Society of London*, *170*(3), 451–464. https://doi.org/10.1144/jgs2012-099

Cataldi, R., Mongelli, F., Squarci, P., Taffi, L., Zito, G., & Calore, C. (1995). Geothermal ranking of Italian territory. *Geothermics*, *24*(1), 115–129. https://doi.org/10.1016/0375-6505(94)00026-9

Cernobori, L., Hirn, A., McBride, J. H., Nicolich, R., Petronio, L., Romanelli, M., & STREAMERS/PROFILES Working Groups (1996). Crustal image of the Ionian basin and its Calabrian margins. *Tectonophysics*, *264*(1-4), 175–189. https://doi.org/10.1016/S0040-1951(96)00125-4

Chiarabba, C., & Chiodini, G. (2013). Continental delamination and mantle dynamics drive topography, extension and fluid discharge in the Apennines. *Geology*, *41*(6), 715–718. https://doi.org/10.1130/G33992.1

Chiarabba, C., De Gori, P., & Speranza, F. (2008). The southern Tyrrhenian subduction zone: Deep geometry, magmatism and Plio-Pleistocene evolution. *Earth Planetary Science Letters*, *268*(3-4), 408–423. https://doi.org/10.1016/j.epsl.2008.01.036

Chironi, C., De Luca, L., Guerra, I., Luzio, D., Moretti, A., Vitale, M., & Group, S.E.A.L.A.N.D. (2000). Crustal structures of the southern Tyrrhenian Sea and the Sicily Channel on the basis of the M25, M26, M28, M39WARR profiles. *Bolletttino della Società. Geologica Italiana*, *119*, 189–203.

De Voogd, B., Truffert, C., Chamot-Rooke, N., Huchon, P., Lallemant, S., & Le Pichon, X. (1992). Two-ship deep seismic soundings in the basins of the eastern Mediterranean Sea (Pasiphae cruise). *Geophysical Journal International*, *109*(3), 536–552. https://doi.org/10.1111/j.1365-246X.1992.tb00116.x

Della Vedova, B., Bellani, S., Pellis, G., & Squarci, P. (2001). Deep temperatures and surface heat-flow distribution. In G. B. Vai, & I. P. Martini (Eds.), *Anatomy of an orogen: The Apennines and adjacent Mediterranean basins* (pp. 65–76). Dordrecht, Netherlands: Kluwer Academic Publisher. https://doi.org/10.1007/978-94-015-9829-3_7

Di Luccio, F., Chiodini, G., Caliro, S., Cardellini, C., Convertito, V., Alessandro Pino, N., et al. (2018). Seismic signature of active intrusions in mountains chain. *Science Advances*, *4*(1), e1701825. https://doi.org/10.1126/SCIADV.1701825

Doglioni, C., Carminati, E., Cuffaro, M., & Scrocca, D. (2007). Subduction kinematics and dynamic constraints. *Earth Science Reviews*, *83*(3-4), 125–175. https://doi.org/10.1016/j.earscirev.2007.04.001

Doglioni, C., Harabaglia, P., Merlini, S., Mongelli, F., Peccerillo, A., & Piromallo, C. (1999). Orogens and slabs vs. their direction of subduction. *Earth Science Reviews*, *45*(3-4), 167–208. https://doi.org/10.1016/S0012-8252(98)00045-2

Doglioni, C., Ligi, M., Scrocca, D., Bigi, S., Bortoluzzi, G., Carminati, E., et al. (2012). The tectonic puzzle of the Messina area (southern Italy): Insights from new seismic reflection data. *Nature ScientificReports*, *2*(1), 970. https://doi.org/10.1038/srep00970

Faccenna, C., Civetta, L., D'Antonio, M., Funiciello, F., Margheriti, L., & Piromallo, C. (2005). Constraints on mantle circulation around the deforming Calabrian slab. *Geophysical Research Letters*, *32*, L06311. https://doi.org/10.1029/2004GL021874

Finetti, I. (2005). CROP project: Deep seismic exploration of the central Mediterranean and Italy. In I. R. Finetti (Ed.), *Atlases in geoscience 1* (pp. 1–779). Amsterdam: Elsevier.

Foley, S. F., & Fischer, T. P. (2017). An essential role for continental rifts and lithosphere in the deep carbon cycle. *Nature Geoscience*, *10*, 897–902. https://doi.org/10.1038/s41561-017-0002-7

Fusseis, F., Regenauer-Lieb, K., Liu, J., Hough, R. M., & De Carlo, F. (2009). Creep cavitation can establish a dynamic granular fluid pump in ductile shear zone. *Nature*, *459*(7249), 974–977. https://doi.org/10.1038/nature08051

Gasparo Morticelli, M., Valenti, V., Catalano, R., Sulli, A., Agate, M., Avellone, G., et al. (2015). Deep controls on foreland basin system evolution along the Sicilian fold and thrust belt. *Bulletin de la Societe Geologique de France*, *186*(4-5), 273–290. https://doi.org/10.2113/gssgfbull.186.4-5.273

Gautheron, C., & Moreira, M. (2002). Helium signature of the subcontinental lithospheric mantle. *Earth and Planetary Science Letters*, *199*(1-2), 39–47. https://doi.org/10.1016/S0012-821X(02)00563-0

Genser, J., Cloetingh, S. A. P. L., & Neubauer, F. (2007). Late orogenic rebound and oblique Alpine convergence: New constraints from subsidence analysis of the Austrian Molasse basin. *Global and Planetary Change*, *58*(1-4), 214–223. https://doi.org/10.1016/j.gloplacha.2007.03.010

Giunta, G., Luzio, D., Agosta, F., Calò, M., Di Trapani, F., Giorgianni, A., et al. (2009). An integrated approach to investigate the seismotectonics of northern Sicily and southern Tyrrhenian. *Tectonophysics*, *476*(1-2), 13–21. https://doi.org/10.1016/j.tecto.2008.09.031

Giustiniani, M., Tinivella, U., & Nicolich, R. (2018). Crustal structure of Central Sicily. *Tectonophysics*, *722*, 299–313. https://doi.org/10.1016/j.tecto.2017.08.034

Goes, S., Giardini, D., Jenny, S., Hollenstein, C., Kahle, H. G., & Geiger, A. (2004). A recent tectonic reorganization in the south–central Mediterranean. *Earth and Planetary Science Letters*, *266*, 335–345.

Grassa, F., Favara, R., Capasso, G., & Inguaggiato, S. (2006). Chemical and isotopic composition of waters and dissolved gases in some thermal springs of Sicily and adjacent Volcanic Islands, Italy. *Pure and Applied Geophysics*, *163*(4), 781–807. https://doi.org/10.1007/s00024-006-0043-0

Holland, G., & Gilfillan, S. (2013). Application of the noble gases to the viability of CO_2 storage. In P. Burnard (Ed.), *The noble gases as geochemical tracers* (pp. 177–223). Berlin, Heidelberg: Springer.

Italiano, F., Martelli, M., Martinelli, G., & Nuccio, P. M. (2000). Geochemical evidence of melt intrusions along lithospheric faults of the southern Apennines (Italy): Geodynamic and seismogenic implications. *Journal of Geophysical Research*, *106*, 13,569–13,578.

Kay, R. W., & Kay, S. M. (1993). Delamination and delamination magmatism. *Tectonophysics*, *219*(1–3), 177–189. https://doi.org/10.1016/0040-1951(93)90295-U

Kennedy, B. M., Fisher, T., & Shuster, D. L. (2000). Heat and helium in geothermal systems. PROCEEDINGS, Twenty-Fifth Workshop on Geothermal Reservoir Engineering Stanford University, Stanford, California, January 24–26.

Kennedy, B. M., Kharaka, Y. K., Evans, W. C., Ellwood, A., De Paolo, D. J., Thordsen, J., et al. (1997). Mantle fluids in the San Andreas fault system, California. *Science*, *278*(5341), 1278–1281. https://doi.org/10.1126/science.278.5341.1278

Kennedy, B. M., & Van Soest, M. C. (2007). Flow of mantle fluids through the ductile lower crust: Helium isotope trends. *Science*, *318*(5855), 1433–1436. https://doi.org/10.1126/science.1147537

Knapp, J. H., Knapp, C. C., Raileanu, V., Matenco, L., Mocanu, V., & Dinu, C. (2005). Crustal constraints on the origin of mantle seismicity in the Vrancea Zone, Romania: The case for active continental lithospheric delamination. *Tectonophysics*, *410*(1-4), 311–323. https://doi.org/10.1016/j.tecto.2005.02.020

Kulongosky, J. T., Hilton, D. R., Barry, P. H., Bradley, K. E., Darren, H., & Kenneth, B. (2013). Volatile fluxes through the Big Bend section of the San Andreas fault, California: Helium and carbon-dioxide systematics. *Chemical Geology*, *339*, 92–102. https://doi.org/10.1016/j.chemgeo.2012.09.007

Lentini, F., Carbone, S., & Catalano, S. (1994). Main structural domains of the central Mediterranean region and their tectonic evolution. *Bollettino di Geofisica Teorica e Applicata*, *36*(141–144), 103–125.

Malinverno, A., & Ryan, W. B. F. (1986). Extension in the Tyrrhenian Sea and shortening in the Apennines as a result of arc migration driven by sinking of the lithosphere. *Tectonics*, *5*(2), 227–245. https://doi.org/10.1029/TC005i002p00227

Marty, B., & Jambon, A. (1995). $C/^3He$ in volatile fluxes from the solid Earth: Implications for carbon geodynamics. *Earth Planetary Science Letters*, *83*, 16–26.

Marty, B., Torgersen, T., Meynier, V., O'Nions, R. K., & De Marsily, G. (1993). Helium isotope fluxes and groundwater ages in the Dogger aquifer, Paris Basin. *Water Resources Research*, *29*(4), 1025–1035. https://doi.org/10.1029/93WR00007

Meissner, R., & Mooney, W. (1998). Weakness of the lower continental crust: A condition for delamination, uplift, and escape. *Tectonophysics*, *296*(1-2), 47–60. https://doi.org/10.1016/S0040-1951(98)00136-X

Morelli, C. (2003). An historical perspective to the CROP Project. In D. Scrocca, C. Doglioni, F. Innocenti, P. Manetti, A. Mazzotti, L. Bertelli, et al. (Eds.), *CROP Atlas: Seismic reflection profiles of the Italian crust. Mem. Descr. Carta Geol. d'It* (Vol. 62, pp. 1–7). Roma: Istituto Poligrafico e Zecca dello Stato.

Mutlu, H., Gülec, N., & Hilton, D. R. (2008). Helium-carbon relationships in geothermal fluids of western Anatolia, Turkey. *Chemical Geology*, *247*(1-2), 305–321. https://doi.org/10.1016/j.chemgeo.2007.10.021

O'Nions, R. K., & Oxburgh, E. R. (1988). Helium, volatile fluxes and the development of continental crust. *Earth Planetary Science Letters*, *90*(3), 331–347. https://doi.org/10.1016/0012-821X(88)90134-3

Oxburgh, E. R., O'Nions, R. K., & Hill, R. I. (1986). Helium isotopes in sedimentary basins. *Nature*, *324*, 18–25.

Ozima, M., & Podosek, F. A. (2002). *Noble gas geochemistry* (p. 286). Cambridge, UK: Cambridge University Press.

Panza, G. F., Raykova, R. B., Carminati, E., & Doglioni, C. (2007). Upper mantle flow in the western Mediterranean. *Earth Planetary Science Letters*, *257*(1-2), 200–214. https://doi.org/10.1016/j.epsl.2007.02.032

Pondrelli, S., Salimbeni, S., Ekstrom, G., Morelli, A., Gasperini, P., & Vannucci, G. (2006). The Italian CMT dataset from 1977 to the present. *Physics of the Earth and Planetary Interiors*, *159*(3-4), 286–303. https://doi.org/10.1016/j.pepi.2006.07.008

Prinzhofer, A. (2013). Noble gas in oil and gas accumulations. In P. Burnard (Ed.), *The Noble gases as Geochemical Tracers* (pp. 225–247). Berlin, Heidelberg: Springer.

Roure, F., Casero, P., & Addoum, B. (2012). Alpine inversion of the North African margin and delamination of its continental lithosphere. *Tectonics*, *31*, TC3006. https://doi.org/10.1029/2011TC002989

Roure, F., Howell, D. G., Muller, C., & Moretti, I. (1990). Late Cenozoic subduction complex of Sicily. *Journal of Structural Geology*, *12*(2), 259–266. https://doi.org/10.1016/0191-8141(90)90009-N

Rudnick, R., & Fountain, D. M. (1995). Nature and composition of the continental crust: A lower crustal perspective. *Reviews of Geophysics*, *33*(3), 267–309. https://doi.org/10.1029/95RG01302

Sano, Y., Tominaga, T., & Williams, S. N. (1997). Secular variations of helium and carbon isotopes at Galeras volcano, Colombia. *Journal of Volcanology and Geothermal Research*, *77*(1-4), 255–265. https://doi.org/10.1016/S0377-0273(96)00098-4

Scarascia, S., Lozej, A., & Cassinis, R. (1994). Crustal structures of the Ligurian, Thyrrenian and Ionian seas and adjacent onshore areas interpreted from wide-angle seismic profiles. *Bollettino di Geofisica Teorica e Applicata*, *36*(141–144), 5–19.

Schön, J. H. (1996). *Physical properties of rocks: Fundamentals and principles of petrophysics*. Oxford, OX, UK; Tarrytown, N.Y., U.S.A.: Pergamon: Elsevier.

Sleep, N. H., & Blampied, M. L. (1992). Creep, compaction and the weak rheology of the major faults. *Nature*, *359*(6397), 687–692. https://doi.org/10.1038/359687a0

Torgersen, T. (1993). ^{3}He fluxes in extensional basins: Limits on the role of magmatism in extensional basins. *Journal Geophysical Research*, *98*(B9), 16,257–16,269. https://doi.org/10.1029/93JB00891

Watson, E. B., & Brenan, J. M. (1987). Fluids in the lithosphere 1: Experimentally-determined wetting characteristics of CO_2-H_2O fluids and their implications for fluids transport, host-rock physical properties, and fluid inclusion formation. *Earth Planetary Science Letters*, *85*(4), 497–515. https://doi.org/10.1016/0012-821X(87)90144-0

5) *Continental degassing of helium in an active tectonic setting (northern Italy): the role of seismicity*

Le transport vertical à grande échelle de fluides à travers la croûte continentale n'est pas toujours dominé par des processus de diffusion à l'équilibre, mais il peut être aussi advectif et épisodique (Torgersen, 2010; Shen et al., 2009; Torgersen and Clarke, 1992; Etheridge et al., 1984). Il a été reconnu que dans les régions continentales, le dégazage des volatils se produit principalement dans des zones en extension tectonique coïncidant souvent avec une activité sismique (Tamburello et al., 2018). Cette correspondance a été liée à la perméabilité accrue des discontinuités tectoniques en extension (Chiodini et al., 2004). Cependant, il a également été observé que les variations du taux de dégazage des volatils sont liées aux séismes, ces variations étant fréquemment post-sismiques (Girault et al., 2018; Manga et al., 2009; Maestrelli et al., 2017). Ainsi, la géochimie des fluides fournit des preuves du transport épisodique de volatils. Même si le flux des principaux gaz naturels (par example CO_2) vers l'atmosphère est mesuré à la surface de la Terre, il est difficile de contraindre les processus contrôlant sa variabilité car les fluides sont souvent réactifs (par exemple interaction eau-gaz-roche) et plusieurs processus fonctionnent simultanément pendant le transfert des fluides à travers la croute (Holland and Gilfillan, 2013). Par conséquent, afin de comprendre les relations entre les processus de génération de fluides et de séismes, base d'une possible approche moderne de prévision sismique, il est fondamental de démêler les processus qui causent et régulent le flux et la chimie des fluides.
En raison de leurs propriétés chimiques, les gaz rares contribuent à retracer l'histoire du dégazage de la Terre et des évolutions de l'atmosphère (Parai and Mukhopadhyay, 2018; Avice et al., 2017; Ballentine and Burnard, 2002; Ozima and Podosek, 2002; Mamyrin and Tolstikhin, 2002). En outre, pour étudier les mécanismes contrôlant le transport de fluides dans la région continentale, le gaz noble le plus léger, est largement utilisé car ses sources (air, croûte et manteau) sont facile à déconvoluer en utilisant le rapport isotopique ($^3He/^4He$). En fait, il est caractérisé par deux isotopes : ^3He, qui est un composant primordial et est principalement stocké dans le manteau terrestre, et ^4He qui est produit en permanence par les désintégrations de U et Th, de sorte que sa quantité stockée dans les minéraux et les roches augmente progressivement avec les temps géologiques.
La fusion et la libération de volatils via les magmas sont les processus principaux qui contrôlent le dégazage du manteau. A l'inverse, le dégazage d'He produit dans la croûte se produit dans des conditions différentes consistant principalement en deux étapes agissant à des degrés différents : (a) la libération des éléments volatils des minéraux / roches; (b) leur transport vers la surface (Ballentine and Burnard, 2002). Il en résulte que les fluides de la croûte sont dominés par ^4He; au contraire, les fluides dérivés du manteau présentent un excès de ^3He (MORB le manteau $^3He/^4He$ est égal à 8 ± 1 Ra, où Ra est le rapport isotopique dans l'atmosphère, $1{,}39 \times 10^6$) par rapport à la croute. Il se trouve également en quantités considérables dans certains gisements de gaz naturel, où il peut rester stocké pendant des millions d'années (Ballentine et al., 2001; O'Nions and Oxburgh, 1988).
Le dégazage continental de ^4He montre une variabilité spatiale et temporelle à l'échelle régionale, ce qui en fait un outil efficace pour évaluer le rôle de la tectonique dans l'amélioration du transport de masse à l'échelle crustale et déchiffrer les mécanismes de transfert de éléments volatils (Torgersen, 2010; Kulongosky et al., 2013; Caracausi and Paternoster, 2015; Kennedy et al., 1997; Kennedy and Van Soest, 2007). Les modifications des propriétés physiques des roches peuvent modifier le dégagement et le transfert de éléments volatils à travers la croûte (Ballentine et al., 2002). Par exemple, la déformation de la roche produit de nouvelles (micro) fractures améliorant la libération des éléments volatils piégés (par exemple, He) et, par conséquent, la fraction des éléments volatils libérées par les roches lors de la déformation, augmente avec les changements de volume

de la roche (processus de dilatance). Cependant, même si certaines études expérimentales montrent l'existence d'un lien direct entre la déformation/fracturation de la roche et la libération de He (Brauer et al., 2016; Torgersen and O'Donnel, 1991), il existe peu d'applications dans les systèmes naturels (Caracausi and Paternoster, 2015; Sano et al., 1998 and 2016).

Nos résultats montrent que le champ de stress associé à la sismicité a généré une libération de ^{4}He de la roche supportant la quantité de ^{4}He accumulée dans les réservoirs naturels depuis leur formation (1,8-4,5 Ma). Ces résultats démontrent que, dans les régions tectoniquement actives, le dégazage de ^{4}He peut se produire de manière épisodique par des processus sismo-génétiques advectifs. En fait, dans la zone étudiée, le flux de ^{4}He à travers la croûte vers l'atmosphère est plus élevée que celle due à un dégazage diffusif à l'état d'équilibre et cet excès peut être dû à la séismicité locale. Considérant le lien reconnu entre déformation / fracturation de la roche et dégazage de l'He, la surveillance du flux de He dans les régions sismiquement actives peut potentiellement apporter la preuve d'une modification du domaine de contrainte dû à la tectonique active, c'est donc un paramètre clé pour une meilleure connaissance du processus sismodénique à l'échelle régionale. Cependant, notre étude montre que les réservoirs naturels accumulent des éléments volatils provenant de sources profondes et les pièges naturels agissent comme une éponge dans le temps en absorbant le signal transféré vers la surface par les éléments volatils provenant des profondeurs des réservoirs, de sorte que ces éléments volatils n'atteignent pas rapidement la surface de la Terre.

Continental degassing of helium in an active tectonic setting (northern Italy): the role of seismicity

Dario Buttitta[1,*], Antonio Caracausi[1,*], Lauro Chiaraluce[1], Rocco Favara[1], Maurizio Gasparo Morticelli[2], and Attilio Sulli[2]

[1]Istituto Nazionale di Geofisica e Vulcanologia, Italy
[2]Dipartimento di Scienze della Terra e del Mare, Università di Palermo, Palermo, Italy
[*]buttittadario@gmail.com and antonio.caracausi@ingv.it

ABSTRACT

In order to investigate the variability of helium degassing in continental regions, its release from rocks and emission into the atmosphere, here we studied the degassing of volatiles in a seismically active region of central Italy (Mw_{MAX}=6) at the Nirano-Regnano mud volcanic system. The emitted gases in the study area are CH_4–dominated and it is the carrier for helium (He) transfer through the crust. Carbon and He isotopes unequivocally indicate that crustal-derived fluids dominate these systems. An high-resolution 3-dimensional reconstruction of the gas reservoirs feeding the observed gas emissions at the surface allow us to estimate the amount of He stored in the natural reservoirs. Our study demonstrated that the in-situ production of ^{4}He in the crust and a long-lasting diffusion through the crust are not the main processes that rule the He degassing in the region. Furthermore, we demonstrated that micro-fracturation due to the field of stress that generates the local seismicity increases the release of He from the rocks and can sustain the excess of He in the natural reservoirs respect to the steady-state diffusive degassing. These results prove that 1) the transport of volatiles through the crust can be episodic as function of rock deformation and seismicity and 2) He can be used to provide highlight changes in the stress field of stress that are earthquake-related.

Keywords: helium degassing, dilatancy, rock fracturation, earthquakes

Introduction

Large-scale vertical transport of fluids through the continental crust is not always dominated by steady-state diffusion processes but it can be also advective and episodic[1–4]. It has been recognized that in continental regions volatiles degassing mainly occurs in areas characterised by extensional tectonic and often coinciding with seismically active zones[5]. This correspondence has been related to the enhanced permeability of the extensional tectonic discontinuities[6]. However, it has been also observed that variations of the volatiles degassing rate are earthquake-related, being these variations frequently post-seismic[7–9]. Thus, fluids geochemistry provides evidences of the episodic large-scale transport of volatiles. Even if the flux of the major natural gases (i.e., CO_2) towards the atmosphere is measured at Earth surface it is difficult to constrain the processes controlling its variability because fluids are often reactive (e.g. water-gas-rock interaction) and several processes work concomitantly during the fluids transfer through the crust[10]. Therefore, in order to figure out the relationships between fluids and earthquakes generation processes, at the base of a possible modern earthquake forecast approach, it is fundamental to unravel the processes causing and regulating the fluids flux and chemistry.

Because of their chemical properties, noble gases contribute to retrace the degassing history of the Earth and the evolution of the atmosphere[11–15]. Furthermore, for investigating the mechanism controlling the transport of fluids in continental region, He, the lightest noble gas, is largely used because its sources (air, crust and mantle) are well resolvable by the use of the isotopic ratio (^{3}He/^{4}He)[14]. In fact, He is characterized by two isotopes: ^{3}He, which is a primordial component and it is mainly stored in Earth mantle, and ^{4}He that is continuously produced by the U and Th decay, so its amount stored into minerals and rocks progressively increases over geological time. Melting and volatiles release from magma are the main processes that control He outgassing from the mantle. Instead, degassing of He produced in the crust occurs under different conditions mainly consisting of two stages acting at different scales: (a) the release of the volatiles from the mineral/rocks; (b) their transport towards the surface[13]. It results that the crustal fluids are dominated by ^{4}He, on the contrary, mantle-derived fluids show an excess of ^{3}He (MORB mantel ^{3}He/^{4}He is 8 ± 1 Ra, were Ra is the isotopic ratio in atmosphere, 1.39×10^6) respect to the crustal. He is also found in considerable quantities in some natural-gas reservoirs, where it can remain stored for millions of years[16,17]. The continental ^{4}He degassing shows spatial and temporal variability at regional scale[1], so it is an efficient tool for

evaluating the role of tectonics in enhancing the crustal scale mass transport and decipherer the mechanisms of the transfer of volatiles[1,18–21]. Changes of physical properties of rocks can modify the release and transfer of volatiles through the crust[22]. For instance, rock deformation produces new (micro) fractures enhancing the release of the trapped volatiles (e.g., He) and as a consequence the fraction of volatiles released from the rocks during deformation, increase with the rock volume changes (dilatancy processes). However, even if some experimental studies show the existence of a direct link between rock deformation/fracturation and the release of He[23,24], there are a few of applications in natural systems[19,25,26]. In this study, we investigated the origin and processes controlling the transfer of He through the crust in a seismically active region of the Northern Apennines (Figure 1), to establish the possible contribution of the tectonic activity in enhancing the release of volatiles accumulated in the rock over time and more specifically, how earthquakes occurrence may contribute to the episodic volatiles degassing. To this end we collect fluids from mud volcanoes (Fig.1 a, b) and we analyse their chemical and isotopic composition (He, δ^{13}C-CO_2, δ^{13}C-CH_4, δ^{2}H-CH^4)to figure out the origin of the outgassing volatiles and the process controlling the crustal degassing. Once verified that the volatiles comes from deep natural reservoirs, we reconstructed the reservoirs volume to estimate the total amount of He stored in these natural traps. The balance between input and output of He in the reservoirs allow us to unravel the processes that control the crustal degassing from He production until its transfer towards the surface, giving also insights to the role and modality of tectonic and seismicity in the vertical transferring of fluids (diffusive vs. advective and episodic).

Results

In the Northern Apennine (Italy) the mud volcanoes are distributed along the external sector of the old-and-thrust belt (Figure 1). This region is considered a reference area to study fluid venting processes in an active fold-and-thrust belt[27] and the fluids geochemistry is used as a potential indicator of impending local earthquakes[28]. Here the seismicity is concentrated in the crust and at local scale the maximum magnitude is 6.0 (https://emidius.mi.ingv.it). Furthermore, it is recognized that the fluid output from the mud volcanoes increasead just after the earthquakes[9,29–31].

Previous investigations highlighted that the gases emitted from the mud volcanoes are CH_4-rich[32] and they are fed by two reservoirs that are strongly different in dimension and vertically separated[33]. At the regional scale, the studied mud volcanoes are localised at the top of the anticlines (Figure 1, a), particularly in joints perpendicular to the axis of the fold, where the impermeable cover allows pore fluid pressure build-up (close to lithostatic magnitudes)[33]. Mud volcanoes are placed along active normal faults (Figure 2, a), allowing a vertical migration of CH_4 coming from deep sources ($>$ 3–6 km)[34]. In this region mud volcanism can be potentially triggered by fault failure cycles and the overpressured fluids released during faulting[33]. Furthermore, the relatively quiescent but continuous activity of these mud volcanoes could instead reflect a short-lived leakage of overpressured fluids along permeable fractures/faults. We are therefore in the presence of a study-case site to investigate the mechanisms of fluid transfer through the crust and the possible relationships between degassing of crustal fluids and rocks deformation and seismicity.

Fluids geochemistry

We collected gas samples from four different mud volcanoes areas (Figure 1): Nirano, Montegibbio, Regnano and Casola. Nirano - Montegibbio sites are located 3.5 km apart, while Regnano - Casola only 2.0 km. Hereafter, we named Nirano-Montegibbio sites as the Nirano system and Regnano-Casola sites as the Regnano system. We analysed the fluids for defining the gas chemistry (He, H_2, O^2, N_2, CO, CH_4, CO_2 and C_2H_6) and the isotopic composition of He (^{3}He/^{4}He), ^{20}Ne, C of both CH_4 and CO_2 and H of CH_4 (table 1). According to previous investigations[34–36] the outgassing fluids from the Nirano and Regnano systems are CH_4 dominated (96.7-98.3%). CO_2 is up to 1.04%, O_2 and N_2 up to 0.09% and 1.27% respectively; He is in traces (up to 23 ppm vol.). The low concentrations of O_2 and N_2 indicate that the collected gases suffer low air contaminations (Figure 3a). The He isotopic ratios are 0.01-0.03 Ra, that is the typical range of the crustal radiogenic He (Figure 3b). The ^{4}He/^{20}Ne ratios in the collected fluids are from 59.4 to 636.5 and these values are more than 2 order of magnitude higher than the same ratio in air (^{4}He/^{20}NeAIR = 0.318) supporting the low atmospheric component in the gases from the Nirano and Regnano systems (figure 3, a and b). Hence, the outgassing He from the mud volcanoes systems is dominated by radiogenic ^{4}He that is produced by U and Th decay in the crust[14]. The C and H isotopic composition of CH_4 is in a good agreement with previous results highlighting the thermogenic nature of CH_4 (Figure 3c; table 1)[35–37]. Here we report the first data of C and H isotopes of CH_4 in gases from Casola and Montegibbio sites, indicating a unique origin of CH_4 emitted from these mud volcanoes systems (Figure 3c; Table 1). The carbon isotopic composition of CO_2 in all the studied fluids is from +13.8‰ to +18.6‰ and according to Milkov and Etiope (2018)[38] these values coupled to the isotopic composition of CH_4 indicate that CO_2 is of thermogenic origin

(Table 1; Fig. 3, c and d). These results are in a good agreement with those from previous investigations[34] that highlighted 1) the thermogenic nature of pristine methane in the deep reservoirs, 2) an origin of CH_4 in crustal layers deeper that the reservoirs (> 3-6 km) and 3) a vertical migration of CH_4 towards the surface. Considering the main component in the collected gases is CH_4 ($\sim 98\%$) and the average $CH_4/^4$He ratio in the emitted gases is ~ 46000 we computed the amount of ^{4}He in the two reservoirs by using the total amount of gases into the reservoirs, between 4.00×10^{11} and 4.50×10^{11} standard cubic meter (SCM) for the main reservoir, and 5.68×10^8 SCM for the shallow reservoir (supplementary information: gas reserves). So, the amount of ^{4}He into the shallower reservoir and deep reservoirs are 4.90×10^5 moles and 3.60×10^8- 4.20×10^8 moles respectively. The amount of ^{4}He in the shallow reservoir is three order of magnitude lower that the amount in the deep reservoir (lower than 1% of ^{4}He amount in the deep reservoir), so it can be considered negligible (table 2).

He degassing

There have been many consistent estimates of the flux of ^{4}He from the continental crust based on calculations of in situ production and steady-state release to the atmosphere by using the U and Th content in rocks, crustal thickness and total release of ^{4}He. These calculations yield a crustal degassing flux of ^{4}He of the order $3.3 \pm 0.5\times10^{10}$ (atoms$\times$m$^{-2}\times$s^{-1})[1,15,39]. However, experimental works highlighted that the release of volatiles increases in volume of rock in an active stress field supporting that the ^{4}He degassing through the crust can be episodic in active tectonic areas[24,40,41]. Mechanical deformation and rocks failure can break (or crack) mineral grains, causing pervasive micro-fracturing and dilation. Consequently, the rocks can increase porosities from 20% to as high as 400% prior to failure[42], open new micro-fracture surfaces, and eventually cause macroscopic failure and fracture of rocks[43]. These processes lead to a release of volatiles (e.g. He) previously trapped within mineral grains along fracture networks[44,45] and the pore fluids transport these volatiles through the crust. Here we firstly investigate if a steady state degassing is the main process that controlled the ^{4}He flux to the reservoirs below the Regnano and Nirano systems over time.

He degassing: Steady-State conditions

The local stratigraphy an tectonic evolution indicates that the age of formation of the anticlinal hosting the main gas reservoirs below the Regnano and Nirano systems goes from 1.8 to 4.5 Ma. Over a million-year the flux of ^{4}He through the Earth's crust to the atmosphere is comparable to the net in situ production (in steady state condition), in 30–40 km of crustal thickness[46]. In order to asses if the ^{4}He production in the crust and the successive migration to the natural reservoirs feeding the Nirano and Regnano systems can justify the amount of He that is stored in the reservoirs, we used a mass balance approach[47]:

$$^4He = {}^4He_{Initial} + {}^4He_{Insitu} + {}^4He_{Externalflux} - {}^4He_{Leak-d} - {}^4He_{leak-mv} \quad (1)$$

where ^4He represents the amount of radiogenic helium (moles) in the reservoir at time t. It includes three input and two outputs terms. Among the input terms, $^4He_{Initial}$ is the amount of ^4He that is in the reservoir at time t-zero, $^4He_{Insitu}$ the amount of radiogenic ^4He produced in the reservoir-rocks volume since its formation (from 1.8 to 4.5 Ma), $^4He_{Externalflux}$ is the flux from the crust below the reservoirs. $^4He_{Leak-d}$ and $^4He_{Leak-mv}$ are the two terms of outputs: $^4He_{Leak-d}$ is the He lost by diffusion from the main reservoir over time and it is from 4.37×10^5 mol to 1.09×10^6 for a t of 1.8 Ma and 4.5 Ma respectively (Methods; gas reserves). It is up to 0.36% of the total volume of He. The second one,$^4He_{Leak-mv}$, is the He leak due to advection, and we assume that is the He emitted from the mud volcanoes. We extrapolated the current He outgassing from mud volcanoes, to the past 10^4 years, ending up with about 9.46×10^5 mol (0.26% of the total He contained in the reservoir). Since these two outputs are less than 1% of the amount of He stored in the main reservoir, it is reasonable to neglect their contribution in eq. 1.

To compute $^4He_{Insitu}$ and $^4He_{Externalflux}$ we used literature data for the abundances of U and Th and for crust thickness. Hence, we based our calculations on the U and Th amounts for a Regional Refined Reference Model and the Global Refined Reference Model (table 3)[48]. The in-situ production of ^4He is computed on the basis of the approach proposed by Zhou and Ballentine (2006)[49]:

$$^4He_{Insitu} = \rho \times \wedge\alpha \times (1-\phi) \times V \times t \quad (2)$$

Where ρ is the rock density in g/cm^3 (2.21 g/cm^3), $\wedge$ a parameter defining the efficiency of the transfer from the rock matrix into the gas phase, ϕ is the porosity of reservoir (fraction), α the source function of radioactive production of ^{4}He in the rock matrix (mol ^{4}He/grock/year), V the volume of the gas reservoir (cm^3) and t the formation time of gas reservoirs (years). Since the process of ^{4}He released from a host mineral is short compared to the geologic age[13] $\wedge$ can be regarded as being equal to 1. α, according to the U and Th decay equations, can be calculated using the following equation[50]:

$$\alpha = 0.2355 \times 10^{-12} \times U \times [1 + 0.123 \times (Th/U - 4)] \quad (3)$$

where U and Th represent the concentrations of U and Th in rocks that hosting the reservoirs and are expressed in ppm. The accumulation rate of the in situ produced ^{4}He of gas reservoirs is expressed as (mol/y):

$$q^{in}_{^4He} = \rho \times \alpha \times (1 - \phi) \times V \quad (4)$$

The in-situ production of ^{4}He is 0.11±0.02 mol/y and 0.30±0.02 mol/yr (in Regional and Global model respectively).

The external flux of ^{4}He is computed by using the method in Zhou and Ballentine (2006)[49]:

$$^4He_{External flux} = q^c_{^4He}/S \times t \quad (5)$$

where S is the gas-bearing area of a reservoir (cm^2), t the gas reservoir formation time (years) and $q^{c}{}_{^4He}$ the average external crustal ^{4}He flux (mol ^{4}He/cm^2/year). $q^{c}{}_{^4He}$ can be calculated as:

$$q^c_{^4He} = \alpha \times \rho \times H \quad (6)$$

where ρ is the average crust density in g/cm^3 (2.80 g/cm^3)[51] and H is the crust thickness in cm (3.2×10^{6}cm, Lavecchia et al. 2003)[52].

The external flux of ^{4}He to the two reservoirs is 37.53±12.12 mol/y and 54.54±5.86 mol/y (in Regional and Global model respectively, Figure. 4). Considering these values of ^{4}He input in the reservoir, the total amount of ^{4}He that can be accumulated into the trap in a time going from 1.8 and 4.5 Myr, varies from 6.7×10^7 mol to 2.5×10^8 mol, respectively. These values are lower than the amount of He in the reservoir that we computed by using the volumetric method (from 3.64×10^8 mol to 4.12×10^8 mol, table 3). So, production of ^{4}He from the whole crust below the main reservoir and its successive transfer by diffusion processes, cannot support the amount of He stored into the reservoirs (Figure 5). If we consider a steady-state diffusion model to explain the excess of ^{4}He in the two reservoirs we need to invoke a volume of ^{4}He-productive crust from 1.5 to 6.2 times larger than that below the trap (∼1323 km3). Considering that previous investigations[36] highlighted that the source of CH_4 is in deep crustal layers (> 3-6 km) and CH_4 vertically migrated towards the natural reservoirs it is reasonable that processes of volatiles migration different from the steady-state diffusion occurred below the investigated mud volcanoes systems.

^{4}He flux: Episodic degassing and active tectonic

The release of volatiles from rocks increases as effect of dilatancy and in regions affected by active tectonic, the flux of ^{4}He through the crust should be higher than that in un-deforming areas where it is reasonable to assume that a diffusive steady-state transport system is acting. Our calculations show that ^{4}He in the natural reservoirs is in excess respect to a steady-state whole crust degassing. As a result, in the main reservoir, there are between 1.2×10^8 and 3.5×10^8 moles in excess of the ^{4}He produced in the crust below the main reservoir plus the $^4He_{Insitu}$.

Considering that the region is tectonically active and two main systems of active faults cross cut the deep reservoir (Figure 2 c and Methods: Geological setting), here we investigate if micro-fracturing can sustain the excess of ^{4}He in the reservoirs. The release of ^{4}He from rock, which are affected by dilatancy, is from 10 to 10^4 times higher than that in un-deformed rock[24], so the release of ^{4}He from a deforming fault damage zone is significative higher if compared to the one of a tectonically undisturbed rock volume (Figure 6 and S1). The volume of the damage zones of the reservoir-related faults (from 0.015 km^3 to 0.088 km^3; Figure 2) releases an amount of He that matches the excess of He in the reservoirs if the release of ^{4}He is 10^4 times higher than that produces by pure diffusion process occurring within an un-deformed rock volume (Figure 6 and S1). However, the high flux of volatiles from rocks as

effect of dilatancy is not constant over time and it decreases in a scale of ka[24]. It means that in order to produce a continuous flux of volatiles high enough to justify the amount of ^{4}He presumed to be into the reservoirs, the stress field has to be constantly active since the reservoir formation age. This result shows that the active regional tectonic could substantially contribute to enhance the ^{4}He flux within the reservoir and that it can be an additional process to sustain the amount of ^{4}He stored in the trap (Figure 7 and S2). This implies that also the seismic activity is occurring since the origin of the gas traps.

Seismicity and degassing

We explored the hypothesis that the excess of He in the reservoirs may be due the occurrence of local earthquakes producing micro-fractures in crustal layers. Following the approach used by Sano et al. (1998)[26]), which link the magnitude of an earthquake to the volume of rock affected by deformation and the related release of ^{4}He, we used the local (historical and instrumental) earthquakes activity as a proxy to calculate the amount of He released by the variation of the rock volume induced by each seismic event. We used the INGV database, covering the 1986-2018 time period (http://cnt.rm.ingv.it) for the instrumental earthquakes and the historical earthquakes catalogue (https://emidius.mi.ingv.it), covering the period 1501-1997, to compute the seismic energy released by the earthquakes located below the Nirano and Regnano systems. Moreover, we also extended the catalogue to the past (in terms of geological times), by assuming the same level of seismic energy release with time, from now up to the trap formation age. The considered events occurred at depths ranging between 5 km and 31 km and in 15 km wide sector along the axis of the anticline connecting Regnano to Nirano. We firstly converted the different types of magnitude reported in the catalogues (ML and Md) in moment magnitude (Mw). For the conversion from ML to Mw, we used the coefficients proposed by Castello et al., (2007)[53]. While we converted the Md to Mw by using the coefficients proposed by Selvaggi et al., (1997)[54]. We then computed the annual average of released energy (by using ZMAP computer code) for the analysis of seismic recurrences. The annual average of released energy is about 5.48×10^{16} ergs/y, which corresponds to one earthquake of magnitude equal to 3.3 per year. Thus, we computed the average volume of rock deformed by the earthquakes per year[26,55] by using the relationship:

$$LogV = 1.06M - 2.78 \quad (7)$$

where V and M are the volume of rock affected by seismicity (km^3) and the moment magnitude, respectively. These values correspond to a volume of deformed rock of 5.13 km^3 per year that is higher than the volume of the faults damage zones. The amount of He released from this volume are between 7.09×10^{-2} and 3.58×10^{-2} mol/y with a Regional or Global U and Th contents in the rock respectively. So, an increase of 3 orders of magnitude, which is due to dilatancy[24,41] of the He released by the volume of deformed rocks (5.13 km^3 per year) is still consistent to the amount of He estimated in the reservoirs demonstrating that the local earthquakes occurrence, may have a key role in ^{4}He degassing (Figure 7 and S2). This result clearly indicates that the volume of deformed rock by stress field of the seismicity must be larger that the volume of the damage zone of the reservoir-related faults.

Conclusion

Our results show that the field of stress associated to the seismicity generated a release of ^{4}He from rock supporting the amount of ^{4}He that accumulated in the natural reservoirs since their formation (1.8-4.5 Ma). These results demonstrate that in tectonically active regions, the crustal ^{4}He degassing can episodically occur and powered as an advective process by seismo-genetic processes. In fact, in the studied area the ^{4}He flux trough the crust towards the atmosphere is higher than that due to a steady-state diffusive degassing and this excess can be due to the local seismicity. Considering the recognized link between rock deformation/fracturation and He degassing, the monitoring of the He flux in seismically active regions can potentially provide evidences of a modification of the field of stress due to the active tectonics, so it a key a parameter for a better knowledge of the seismo-genetic processes at regional scale. However, our study shows that natural reservoirs accumulate deep sourced volatiles and the natural traps work as a sponge over time by absorbing the signal transferred towards the surface by the volatiles coming from deeper than the reservoirs, so these volatiles do not quickly reach Earth surface. These results well fit with the evidences that the increase of the activity from the mud volcanoes or vents because of earthquake is essentially post-seismic, so it occurs as a consequence of earthquakes[7,56] and no geochemical variations are generally recognized before and classified as precursors. Finally, mud volcanoes are surely preferential sites for studying the relationships between fluids and seismicity, however for using He and other volatiles to investigate the genesis of earthquakes it is fundamental to have a model of fluids circulation and its storage into the crust together with an

high frequency monitoring of the He that outgases at the surface. The seismogenesis is a dynamic process of ongoing rock deformation until to the fracturation, so even if fluids are directly involved in these processes nevertheless the effects of rock deformation can be also masked or reach the surface in delay.

Methods

0.1 Analytical procedures

Gas samples were collected in Pyrex bottles with vacuum valves at both ends, taking care to prevent air contamination, and these were analysed in 10 days from their sampling. Gas samples have been analysed in the laboratories of the Istituto Nazionale di Geofisica e Vulcanologia, sezione di Palermo. The chemical composition of He, H_2, O_2, N_2, CO, CH_4, CO_2 and C_2H_6 has been measured by a Perkin Elmer Clarus 500 gas chromatograph equipped with a 3.5-m Carboxen 1000 column and double detector (hot-wire detector and flame ionization detector), with analytical errors of $< 3\%$. Analytical precision for GC analyses is better than $\pm 5\%$ for trace gases and $\pm 10\%$ for alkanes. ^{3}He, ^{4}He and ^{20}Ne and the ^{4}He/^{20}Ne ratios were determined by separately admitting He and Ne into a split flight tube mass spectrometer (GVI-Helix SFT), after standard purification procedures[57]. ^{3}He/^{4}He ratio is expressed as R/Ra (being R the ^{3}He/^{4}He ratio of the sample, and Ra the ^{3}He/^{4}He ratio of air, 1.39×10^{-6}).

The analytical error is generally below 0.3%. The R/Ra values were corrected for the atmospheric contamination basing on the ^{4}He/^{20}Ne ratio[58] and reported as Rc/Ra (table 1)[59]. The C isotope composition of CO_2 (expressed as δ^{13}C‰ vs. V-PDB) was determined using a Thermo (Finningan) Delta Plus XP CF-IRMS, connected to a Trace GC gas chromatograph and a Thermo (Finningan) GC/C III interface[59,60]. The gas chromatograph, equipped with a Poraplot-Q column (length 30 m, i.d. 0.32 mm), kept at a constant temperature of 50 °C, uses He as the carrier gas. The analytical uncertainty was ± 0.1‰. Carbon and hydrogen isotopes of CH^4 were carried out on the same equipment. GC III combustion interface was used to produce carbon dioxide from CH_4[61]. GC-TC interface provides on-line high-temperature methane conversion into hydrogen suitable for isotope analyses. Typical reproducibility (1σ) for δ^{13}C-CH_4 and δD-CH_4 measurements is better than 0.2‰ and 2.5‰ respectively[62].

0.2 Gas reserves computations

The classic approach to estimate the gas reserves stored in a natural reservoir (Q) is based on a volumetric method[63] where the computed values of the gases volume are statistically considered the "best-estimate" value[64]. Here we applied this approach to compute the total amount of gas that is stored into the deep and shallow reservoirs (table 2).

The total gas amount in the reservoir is computed by using the equation[65]:

$$Q = \frac{G.B.V. \times Net/Gross \times \phi \times (1 - Sw - So)}{Bg} \tag{8}$$

where: G.B.V. = Gross Bulk Volume represents the gross volume of mineralized rock (inclusive of any clayey and / or compact horizons that do not contribute to production) (9.5×10^9 m^3 and 2.7×10^8 m^3 the deep and the shallow gas reservoirs); Net/Gross = Ratio between the rock thickness that actually contributes to the production and the gross thickness of rock (1 for this work); Ø = Average porosity of the reservoir (fraction, 15%); Sw = Average water saturation of the "reservoir" (fraction) o Volume fraction of porosity filled with interstitial water[66]; So = Oil saturation (between 0 and 10%); Bg = "Formation Volume Factor" that is used to express the volume of hydrocarbons originally in place at the "standard" surface conditions, i.e. at a pressure of 1 atm and at a temperature of 20 °C. The Sw it is equal to 15%, calculated with Timur 1968[67]. Where k is the permeability, equal to 80 mD.

$$Sw = \sqrt{\frac{10^4 \times \phi^{4.5}}{k}} \tag{9}$$

The Formation Volume Factor is given by the ratio of the volume of gas to the conditions of the reservoir and the volume of the gas to the standard conditions. Mathematically:

$$Bg = \frac{Vrc}{Vsc} = \frac{Psc \times Trc \times Zrc}{Prc \times Tsc \times Zsc} \tag{10}$$

Where, Psc, Tsc, Zsc, represent surface (pressure, temperature and compressibility factor) conditions while, Prc, Trc e Zsc, are the conditions (pressure, temperature and compressibility factor) in the reservoir. The compressibility

factor, Z, is calculated by using the approach in Piper and Corredor (1993)[68]. Therefore, the reverse of the Formation Volume Factor is equal to 1/Bg = 371.19 SCM/ResCM, i.e. 1 m^3 of pore volume under the reservoir conditions contains 1/Bg m^3 of gas under standard conditions. Table 2 shows the total gas amount in the two reservoirs, Q: 1) from 1.66×10^{13} moles to 1.87×10^{13} moles for the deep reservoir (depth 1850-2600 m) at P_{rc}^{Litho}=49 MPa, Trc = 327.15 °K and So from 0 to 10% and 2) 2.36×10^{10} moles for the shallow trap (depth 400-1000 m) at d Trc = 295.75 °K, P_{rc}^{Litho}= 4 MPa So = 0.0. The lithostatic pressure were calculated taking into account the mean thicknesses and densities of the crustal layers and the value of g.

0.3 Helium lost by diffusion

The helium lost by diffusion it was calculated by one-dimensional steady-state diffusion model was used to quantify He loss in gas reservoirs using the formula in Liu et al. 2017[47]:

$$\int_0^t \frac{D}{Z}\left(\frac{22.4\times Q\times C_{(t)}}{G.B.V.\times\phi\times K_{H_2O}}\times\frac{P_{NC}\times T_{RC}}{T_{NC}}-4.5\times10^{-8}\right)\times S\times dt \tag{11}$$

Where: D is the diffusion coefficient of He (2×10^{-6} cm^2/s)[47]; Z is the buried depth of reservoir, the middle point of deeper reservoir in this case (2225 m); Q is the total gas amount in the reservoir is computed by using the equation 8; $C_{(t)}$ is the 4He concentration at time t in %v; P_{NC} is the normal atmosphere (1 atm); T_{NC} is normal temperature (273 °K); T_{RC} is the reservoir condition temperature (327.15 °K); G.B.V is the gross bulk volume in (9.49×10^{11} cm^3); ϕ s the porosity (%); K_{H_2O} is the is Henry's constant calculated from the solubility model of noble gases in the water (approximately 2500)[22].

References

1. Torgersen, T. Continental degassing flux of 4He and its variability. *Geochem. Geophys. Geosystems* **11**, 1–15, DOI: 10.1029/2009GC002930 (2010).
2. Shen, B., Qin, J., Hu, W., Huang, Z. & Wang, J. Noble Gas Geochemistry of CO2 Gas Pool in Gaoqing-Pingnan Fault Zone,Jiyang Depression. *Geol. J. China Univ.* **2009**, 537–546 (2009).
3. Torgersen, T. & Clarke, W. B. Geochemical constraints on formation fluid ages, hydrothermal heat flux, and crustal mass transport mechanisms at Cajon Pass. *J. Geophys. Res.* **97**, 5031, DOI: 10.1029/91JB01505 (1992).
4. Etheridge, M. A., Wall, V. J., Cox, S. F. & Vernon, R. H. High fluid pressures during regional metamorphism and deformation: Implications for mass transport and deformation mechanisms. *J. Geophys. Res.* **89**, 4344–4358, DOI: 10.1029/JB089iB06p04344 (1984).
5. Tamburello, G., Pondrelli, S., Chiodini, G. & Rouwet, D. Global-scale control of extensional tectonics on CO 2 earth degassing. *Nat. Commun.* **9**, DOI: 10.1038/s41467-018-07087-z (2018).
6. Chiodini, G. *et al.* Carbon dioxide Earth degassing and seismogenesis in central and southern Italy. *Geophys. Res. Lett.* **31**, n/a–n/a, DOI: 10.1029/2004GL019480 (2004).
7. Girault, F. *et al.* Persistent CO2emissions and hydrothermal unrest following the 2015 earthquake in Nepal. *Nat. Commun.* **9**, 1–10, DOI: 10.1038/s41467-018-05138-z (2018).
8. Maestrelli, D. *et al.* Dynamic Triggering of Mud Volcano Eruptions During the 2016–2017 Central Italy Seismic Sequence. *J. Geophys. Res. Solid Earth* **122**, 9149–9165, DOI: doi:10.1002/2017JB014777 (2017).
9. Manga, M., Brumm, M. & Rudolph, M. L. Earthquake triggering of mud volcanoes. *Mar. Pet. Geol.* **26**, 1785–1798, DOI: 10.1016/j.marpetgeo.2009.01.019 (2009).
10. Holland, G. & Gilfillan, S. Application of Noble Gases to the Viability of CO2 Storage. *Noble Gases as Geochem. Tracers* 1–391, DOI: 10.1007/978-3-642-28836-4 (2013).
11. Parai, R. & Mukhopadhyay, S. Xenon isotopic constraints on the history of volatile recycling into the mantle, DOI: 10.1038/s41586-018-0388-4 (2018).
12. Avice, G., Marty, B. & Burgess, R. The origin and degassing history of the Earth's atmosphere revealed by Archean xenon. *Nat. Commun.* **8**, 1–9, DOI: 10.1038/ncomms15455 (2017). 1409.7398.
13. Ballentine, C. J. & Burnard, P. G. Production, Release and Transport of Noble Gases in the Continental Crust. *Rev. Miner. Geochem.* **47**, 481–538, DOI: 10.2138/rmg.2002.47.12 (2002).

14. Ozima, M. & Podosek, F. *Noble Gas Geochemistry: 2nd edition* (2002).

15. Mamyrin, B. A. & Tolstikhin, I. N. *Helium isotopes in nature DEVELOPMENTS IN GEOCHEMISTRY* (1984).

16. Ballentine, C. J., Schoell, M., Coleman, D. & Cain, B. A. 300-Myr-old magmatic CO2 in natural gas reservoirs of the west Texas Permian basin. *Nature* **409**, 327–331, DOI: 10.1038/35053046 (2001).

17. O'Nions, R. K. & Oxburgh, E. R. Helium, volatile fluxes and the development of continental crust. *Earth Planet. Sci. Lett.* **90**, 331–347, DOI: 10.1016/0012-821X(88)90134-3 (1988).

18. Kulongoski, J. T. *et al.* Volatile fluxes through the Big Bend section of the San Andreas Fault, California: Helium and carbon-dioxide systematics. *Chem. Geol.* **339**, 92–102, DOI: https://doi.org/10.1016/j.chemgeo.2012.09.007 (2013).

19. Caracausi, A. & Paternoster, M. Radiogenic helium degassing and rock fracturing: A case study of the southern Apennines active tectonic region. *J. Geophys. Res. Solid Earth* 1–12, DOI: 10.1002/2014JB011462.Received (2015).

20. Kennedy, B. M. *et al.* Mantle Fluids in the San Andreas Fault System, California. *Sci. (80-.).* **278**, 1278 LP – 1281, DOI: 10.1126/science.278.5341.1278 (1997).

21. Kennedy, B. M. & van Soest, M. C. Flow of Mantle Fluids Through the Ductile Lower Crust: Helium Isotope Trends. *Sci. (80-.).* **318**, 1433–1436, DOI: 10.1126/science.1147537 (2007).

22. Ballentine, C. J., Burgess, R. & Bernard, M. Tracing Fluid Origin, Transport and Interaction in the Crust. *Rev. Miner. Geochem.* **47**, 539–614, DOI: 10.2138/rmg.2002.47.13 (2002).

23. Bräuer, K., Geissler, W. H., Kämpf, H., Niedermannn, S. & Rman, N. Helium and carbon isotope signatures of gas exhalations in the westernmost part of the Pannonian Basin (SE Austria/NE Slovenia): Evidence for active lithospheric mantle degassing. *Chem. Geol.* **422**, 60–70, DOI: 10.1016/j.chemgeo.2015.12.016 (2016).

24. Torgersen, T. & O'Donnell, J. The degassing flux from the solid earth: Release by fracturing. *Geophys. Res. Lett.* **18**, 951–954, DOI: 10.1029/91GL00915 (1991).

25. Sano, Y. *et al.* Groundwater helium anomaly reflects strain change during the 2016 Kumamoto earthquake in Southwest Japan. *Sci. Rep.* **6**, DOI: 10.1038/srep37939 (2016).

26. Sano, Y., Takahata, N., Igarashi, G., Koizumi, N. & Sturchio, N. C. Helium degassing related to the Kobe earthquake. *Chem. Geol.* **150**, 171–179, DOI: 10.1016/S0009-2541(98)00055-2 (1998).

27. Martinelli, G. & Judd, A. Mud volcanoes of Italy. *Geol. J.* **39**, 49–61, DOI: 10.1002/gj.943 (2004).

28. Martinelli, G., Alberto, D. & Mucciarelli, M. Radon emissions from mud volcanoes in Northern Italy: possible connection with local seismicity. *Geophys. Res. Lett.* **22**, 1989–1992 (1995).

29. Rudolph, M. L. & Manga, M. Frequency dependence of mud volcano response to earthquakes. *Geophys. Res. Lett.* **39**, 1–5, DOI: 10.1029/2012GL052383 (2012).

30. Martinelli, G. & Panahi, B. *Mud Volcanoes, Geodynamics and Seismicity*, vol. 51 (2005).

31. Martinelli, G. & Dadomo, A. Mud Volcano Monitoring and Seismic Events. In Martinelli, G. & Panahi, B. (eds.) *Mud Volcanoes, Geodyn. Seism.*, 187–199 (Springer Netherlands, Dordrecht, 2005).

32. Etiope, G., Feyzullayev, A. & Baciu, C. L. Terrestrial methane seeps and mud volcanoes: A global perspective of gas origin. *Mar. Pet. Geol.* **26**, 333–344, DOI: 10.1016/j.marpetgeo.2008.03.001 (2009).

33. Bonini, M. Interrelations of mud volcanism, fluid venting, and thrust-anticline folding: Examples from the external northern Apennines (Emilia-Romagna, Italy). *J. Geophys. Res. Solid Earth* **112**, 1–21, DOI: 10.1029/2006JB004859 (2007).

34. Capozzi, R. & Picotti, V. Fluid migration and origin of a mud volcano in the Northern Apennines (Italy): The role of deeply rooted normal faults. *Terra Nov.* **14**, 363–370, DOI: 10.1046/j.1365-3121.2002.00430.x (2002).

35. Etiope, G., Martinelli, G., Caracausi, A. & Italiano, F. Methane seeps and mud volcanoes in Italy: Gas origin, fractionation and emission to the atmosphere. *Geophys. Res. Lett.* **34**, 1–5, DOI: 10.1029/2007GL030341 (2007).

36. Sciarra, A., Cantucci, B., Ricci, T., Tomonaga, Y. & Mazzini, A. Geochemical characterization of the Nirano mud volcano, Italy. *Appl. Geochem.* **102**, 77–87, DOI: 10.1016/j.apgeochem.2019.01.006 (2019).

37. Oppo, D., Capozzi, R. & Picotti, V. A new model of the petroleum system in the Northern Apennines, Italy. *Mar. Pet. Geol.* **48**, 57–76, DOI: 10.1016/j.marpetgeo.2013.06.005 (2013).

38. Milkov, A. V. & Etiope, G. Revised genetic diagrams for natural gases based on a global dataset of >20,000 samples. *Org. Geochem.* **125**, 109–120, DOI: 10.1016/j.orggeochem.2018.09.002 (2018).

39. Torgersen, T. & Clarke, W. B. Helium accumulation in groundwater, I: An evaluation of sources and the continental flux of crustal4He in the Great Artesian Basin, Australia. *Geochim. Cosmochim. Acta* **49**, 1211–1218, DOI: 10.1016/0016-7037(85)90011-0 (1985).

40. Scholz, C. H., Sykes, L. R. & Aggarwal, Y. P. Earthquake Prediction: A Physical Basis. *Sci. (80-.).* **181**, 803 LP – 810, DOI: 10.1126/science.181.4102.803 (1973).

41. Honda, M., Kurita, K., Hamano, Y. & Ozima, M. Experimental studies of He and Ar degassing during rock fracturing. *Earth Planet. Sci. Lett.* **59**, 429–436, DOI: 10.1016/0012-821X(82)90144-3 (1982).

42. Thomas, D. Geochemical precursors to seismic activity. *Pure Appl. Geophys. PAGEOPH* **126**, 241–266, DOI: 10.1007/BF00878998 (1988).

43. Tapponier, P. & Brace, W. F. Development of stress induced microcracks in {W}esterly granite. *Int. J. Mech. Min. Sci. Geomech. Abstr.* **13**, 103–112, DOI: 10.1016/0148-9062(76)91937-9 (1976).

44. Bauer. Real Time Degassing of Rock during Deformation. *No. SAND2016-1483C* (2016).

45. Bauer, S. J., Gardner, W. P. & Heath, J. E. Helium release during shale deformation: Experimental validation. *Geochem. Geophys. Geosystems* **17**, 2612–2622, DOI: 10.1002/2016GC006352 (2016).

46. Takahata, N. & Sano, Y. Helium flux from a sedimentary basin. *Appl. Radiat. Isot.* **52**, 985–992, DOI: 10.1016/S0969-8043(99)00159-1 (2000).

47. Liu, W. *et al.* Formation time of gas reservoir constrained by the time-accumulation effect of 4He: Case study of the Puguang gas reservoir. *Chem. Geol.* DOI: 10.1016/j.chemgeo.2017.05.025 (2017).

48. Coltorti, M. *et al.* U and Th content in the Central Apennines continental crust: A contribution to the determination of the geo-neutrinos flux at LNGS. *Geochim. Cosmochim. Acta* **75**, 2271–2294, DOI: 10.1016/j.gca.2011.01.024 (2011). 1102.1335.

49. Zhou, Z. & Ballentine, C. J. 4He dating of groundwater associated with hydrocarbon reservoirs. *Chem. Geol.* **226**, 309–327, DOI: 10.1016/j.chemgeo.2005.09.030 (2006).

50. Craig, H. & Lupton, J. E. Primordial neon, helium, and hydrogen in oceanic basalts. *Earth Planet. Sci. Lett.* **31**, 369–385, DOI: 10.1016/0012-821X(76)90118-7 (1976).

51. Rudnick, R. L. & Fountain, D. M. Nature and composition of the continental crust: A lower-crustal perspective. *Rev. Geophys.* **33**, 267–309, DOI: Doi10.1029/95rg01302 (1995).

52. Lavecchia, G., Boncio, P., Creati, N. & Brozzetti, F. Some aspects of the Italian geology not fitting with a subduction scenario. *J. Virtual Explor.* **10**, 1–14, DOI: 10.3809/jvirtex.2003.00064 (2003).

53. Castello, B., Olivieri, M. & Selvaggi, G. Local and duration magnitude determination for the Italian earthquake catalog, 1981-2002. *Bull. Seism. Soc. Am.* **97**, 128–139, DOI: 10.1785/0120050258 (2007).

54. Selvaggi, G., Castello, B. & Azzara, R. Spatial distribution of scalar seismic moment release in Italy (1983-1996): seismotectonics implications for the Apennines (1997).

55. Shimazu, Y. Physics of the Earth. *Shokabo Press.* (1971).

56. Manga, M. & Bonini, M. Large historical eruptions at subaerial mud volcanoes, Italy. *Nat. Hazards Earth Syst. Sci.* **12**, 3377–3386, DOI: 10.5194/nhess-12-3377-2012 (2012).

57. Rizzo, A. L. *et al.* New mafic magma refilling a quiescent volcano: Evidence from He-Ne-Ar isotopes during the 2011–2012 unrest at Santorini, Greece. *Geochem. Geophys. Geosystems* **16**, 798–814, DOI: 10.1002/2014GC005653 (2015).

58. Sano, Y. & Wakita, H. Geographical distribution of He3/He4 ratios in Japan: implications for arc tectonics and incipient magmatism. *J. Geophys. Res.* **90**, 8729–8741, DOI: 10.1029/JB090iB10p08729 (1985).

59. Battaglia, A. *et al.* The Magmatic Gas Signature of Pacaya Volcano, With Implications for the Volcanic CO 2 Flux From Guatemala. *Geochem. Geophys. Geosystems* **19**, 667–692, DOI: 10.1002/2017GC007238 (2018).

60. Gennaro, M. E., Grassa, F., Martelli, M., Renzulli, A. & Rizzo, A. L. Carbon isotope composition of CO2-rich inclusions in cumulate-forming mantle minerals from Stromboli volcano (Italy). *J. Volcanol. Geotherm. Res.* **346**, 95–103, DOI: 10.1016/j.jvolgeores.2017.04.001 (2017).

61. Nuccio, P. M., Caracausi, A. & Costa, M. Mantle-derived fluids discharged at the Bradanic foredeep/Apulian foreland boundary: The Maschito geothermal gas emissions (southern Italy). *Mar. Pet. Geol.* **55**, 309–314, DOI: 10.1016/j.marpetgeo.2014.02.009 (2014).

62. Carapezza, M. L. *et al.* Gas blowout from shallow boreholes near Fiumicino International Airport (Rome): Gas origin and hazard assessment. *Chem. Geol.* **407-408**, 54–65, DOI: 10.1016/j.chemgeo.2015.04.022 (2015).

63. Tobergte, D. R. & Curtis, S. ASSESSMENT OF UNCERTAINTIES IN OIL AND GAS RESERVES ESTIMATION BY VARIOUS EVALUATION METHODS. *J. Chem. Inf. Model.* **53**, 1689–1699, DOI: 10.1017/CBO9781107415324.004 (2013). arXiv:1011.1669v3.

64. Demirmen, F. Reserves Estimation: The Challenge for the Industry. *J. Pet. Technol.* **59**, 80–89, DOI: 10.2118/103434-MS (2007).

65. Mazzei, R. Calcolo volumetrico degli idrocarburi originariamente in posto. In *Elem. di Geol. e di Ing. dei giacimenti Pet.*, vol. FASCICOL07 (2001).

66. Mireault, R. & Dean, L. *RESERVOIR ENGINEERING for Geologists* (2012).

67. Timur, A. An Investigation Of Permeability, Porosity, & Residual Water Saturation Relationships For Sandstone Reservoirs. *Log Anal.* **9**, 10 (1968).

68. Piper, L. D., McCain, W. D. & Corredor, J. H. Compressibility factors for naturally occurring petroleum gases. *SPE Repr. Ser.* 23–33, DOI: 10.2118/26668-MS (1999).

69. Gautheron, C. & Moreira, M. Helium signature of the subcontinental lithospheric mantle. *Earth Planet. Sci. Lett.* **199**, 39–47, DOI: 10.1016/S0012-821X(02)00563-0 (2002).

Acknowledgements

This work was supported by Istituto Nazionale di Geofisica e Vulcanologia, Grant FSE (Fondi Sociali Europei) and FISR (Fondo Integrativo Speciale per la Ricerca).

Additional information

Supplementary information accompanies this paper at http://www.nature.com/srep.
Competing financial interests: Supplementary information Competing financial interests: The authors declare no competing financial interests.

Site	Sampling Date	Lat	Long	O_2 (%)	N_2 (%)	CH_4 (%)	CO_2 (%)	C_2H_6 (ppm)	He (ppm)	^{20}Ne (ppm)	$^4He/^{20}Ne$	(R/Ra)c	Err +/-	$\delta^{13}C\text{-}CO_2$	$\delta^{13}C\text{-}CH_4$	$\delta^{13}D\text{-}CH_4$	$C(tot)/^4He$
Nirano	29/09/2018	N 44° 30'49.57"	E 10° 49' 32.13"	0.01	0.34	98.26	0.54	381	18	0.029	636.47	0.01	1.27×10^{-4}	+18.61	-47.2	-173	5.4×10^4
Nirano 2	29/09/2018	N 44° 30' 46.14"	E 10° 49' 16.90"	0.05	0.55	98.18	0.53	374	18	0.098	187.02	0.01	1.06×10^{-4}	+13.77	-46.2	-179	5.4×10^4
Regnano	29/09/2018	N 44° 33' 28.75"	E 10° 34' 33.30"	0.09	0.62	97.74	1.04	1800	24	0.394	59.37	0.01	7.78×10^{-5}	+18.41	-46.7	-170	4.2×10^4
Casola	29/09/2018	N 44° 34' 26.56"	E 10° 33' 57.94"	0.02	0.56	96.74	0.97	587	20	0.070	354.35	0.01	1.00×10^{-4}	+16.08	-45.1	-176	4.8×10^4
Montegibbio	29/09/2018	N 44° 30' 58.13"	E 10° 46' 37.14"	bdl	01.27	97.08	0.27	135	37	0.171	215.32	0.01	9.67×10^{-5}	n.d.	-46.2	-178	7.9×10^4

Table 1. Chemical and isotopic composition of the venting gases from the mud volcanoes of Nirano and Regnano areas.

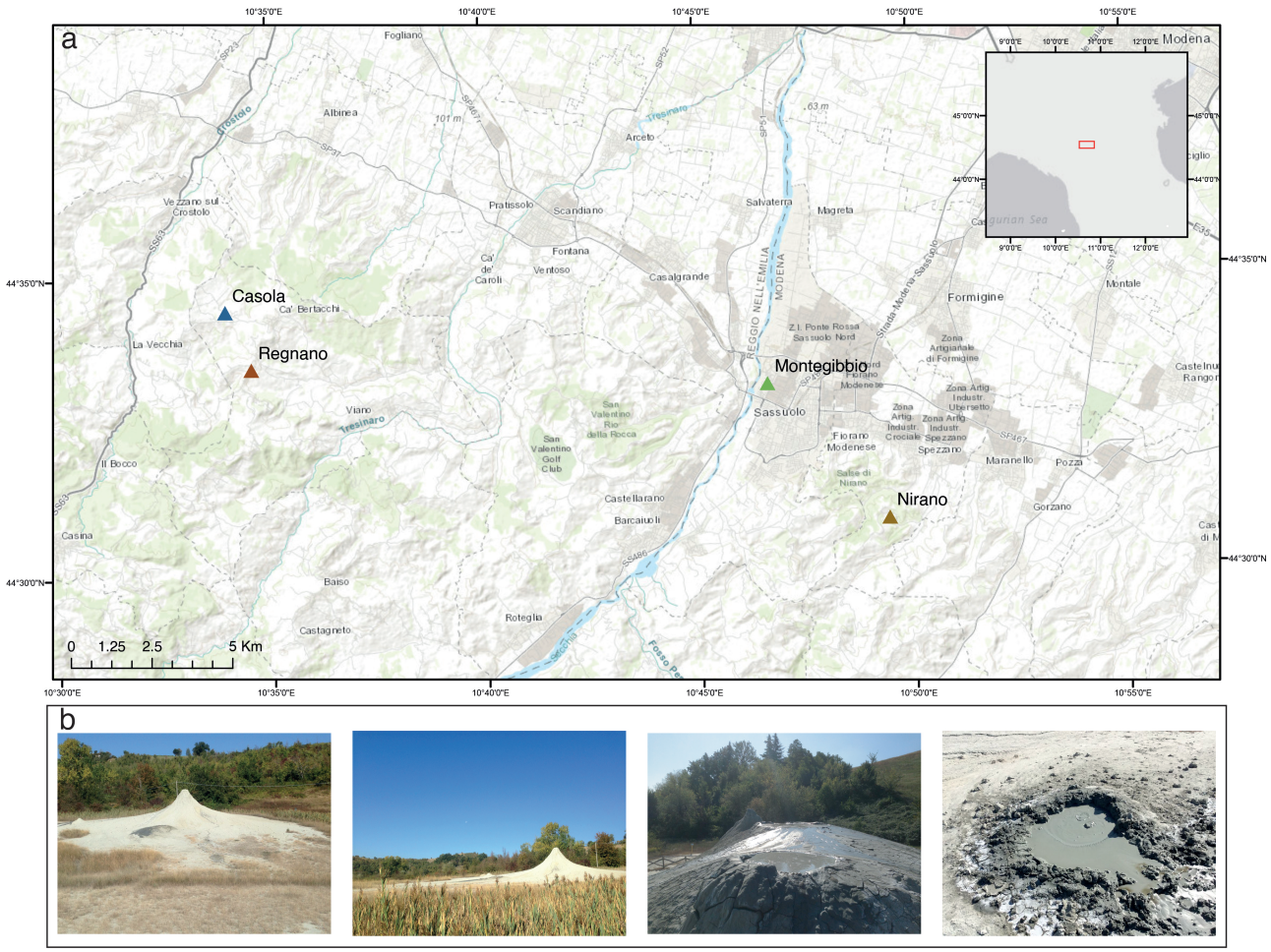

Figure 1. Study area. (a) geographical framework with sampled sites; (b) Some photos of the mud volcanoes of Nirano and Regnano during the 2018 sample campaign.

Table 2. Summary of reservoirs condition and initial gas in place into the traps calculated by volumetric method.

	Calculation of the initial gas in place		
	Main		Secondary
Reservoir Conditions	Trc = 327.15 °K P_{RC}^{Litho}= 48.98 MPa		Trc*= 295.75 °K P_{RC}^{Litho*}= 4 MPa
G.B.V. in m^3	9.49×10^9		2.69×10^8
ϕ	0.15		0.50*
(1-Sw-So)	0.75/0.85		0.10*
1/Bg in SCM/RCM	371.19		42.25
Z	1.1646		0.9244
	So=0.10	So=0	So=0
Q(SCM)	3.99×10^{11}	4.5×10^{11}	5.68×10^8
Q(mol)	1.66×10^{13}	1.87×10^{13}	2.35×10^{10}
$Q_{^4He}$(SCM)	8.78×10^6	9.94×10^6	1.19×10^4
$Q_{^4He}$(mol)	3.64×10^8	4.12×10^8	4.93×10^5

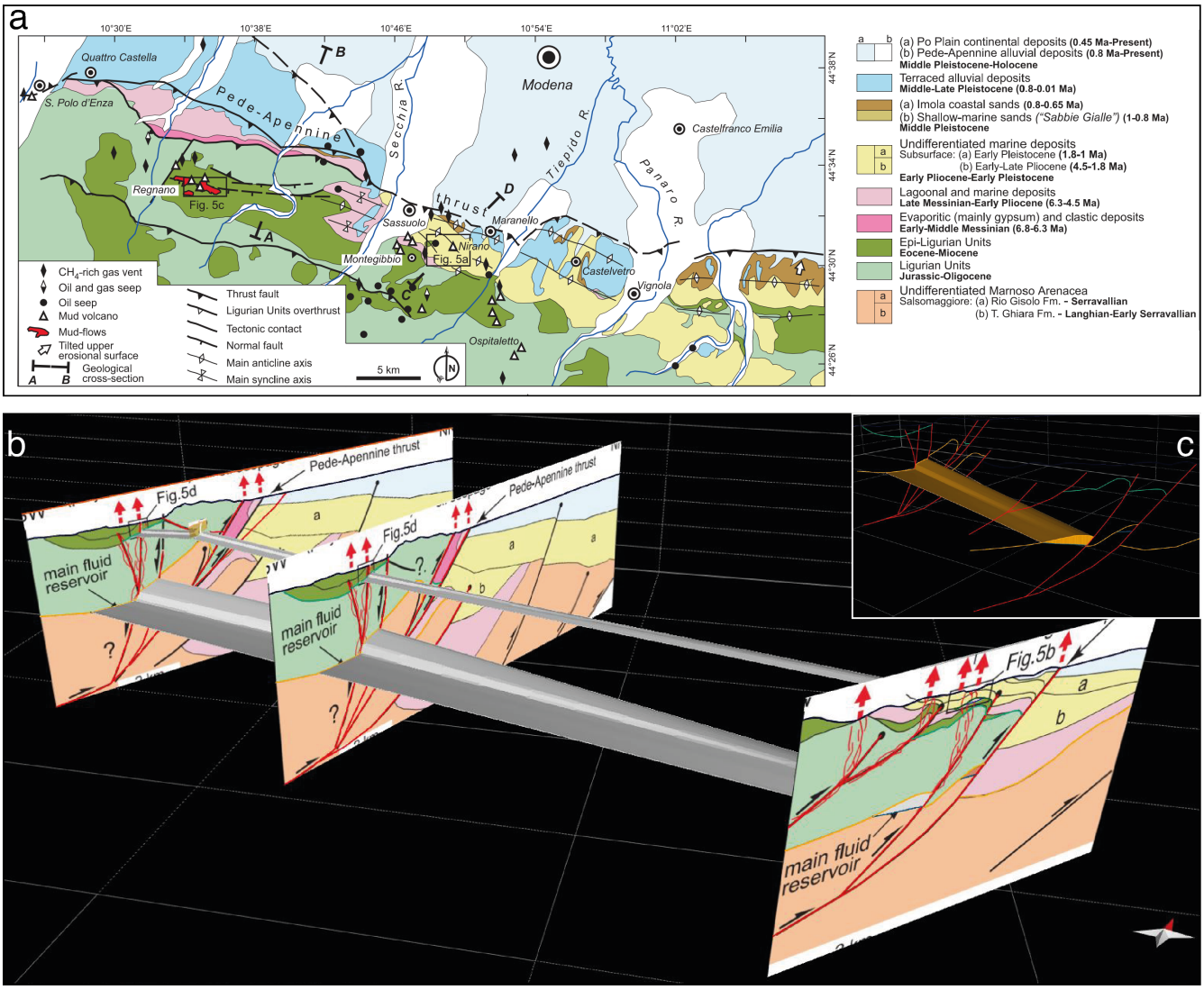

Figure 2. A general overview of the area with the geological units of the zone of interest from Bonini (2007)[33] (a); a view of the shallow and deep reservoirs by reconstruction carried out with Move 2015.1 software (b); deep reservoir and the system of faults that crosses it (c).

Table 3. Regional and Global suite of U and Th concentration distributed in the "Sediments", Upper Crust and Lower Crust. *data from Coltorti et al. (2011)[48].

	Thickness (km)	Density (g/cm3)	RRM-Regional*		RRM-Global*	
			U (ppm)	Th (ppm)	U (ppm)	Th (ppm)
Sediments	10	2.21	0.78±0.20	1.98±0.44	1.68±0.2	6.91±0.8
Upper Crust	10	2.80	2.20±1.20	8.30±4.90	2.70±0.6	10.50±1.0
Lower Crust	12	2.80	0.29±0.24	3.17±3.48	0.60±0.4	3.70±2.4

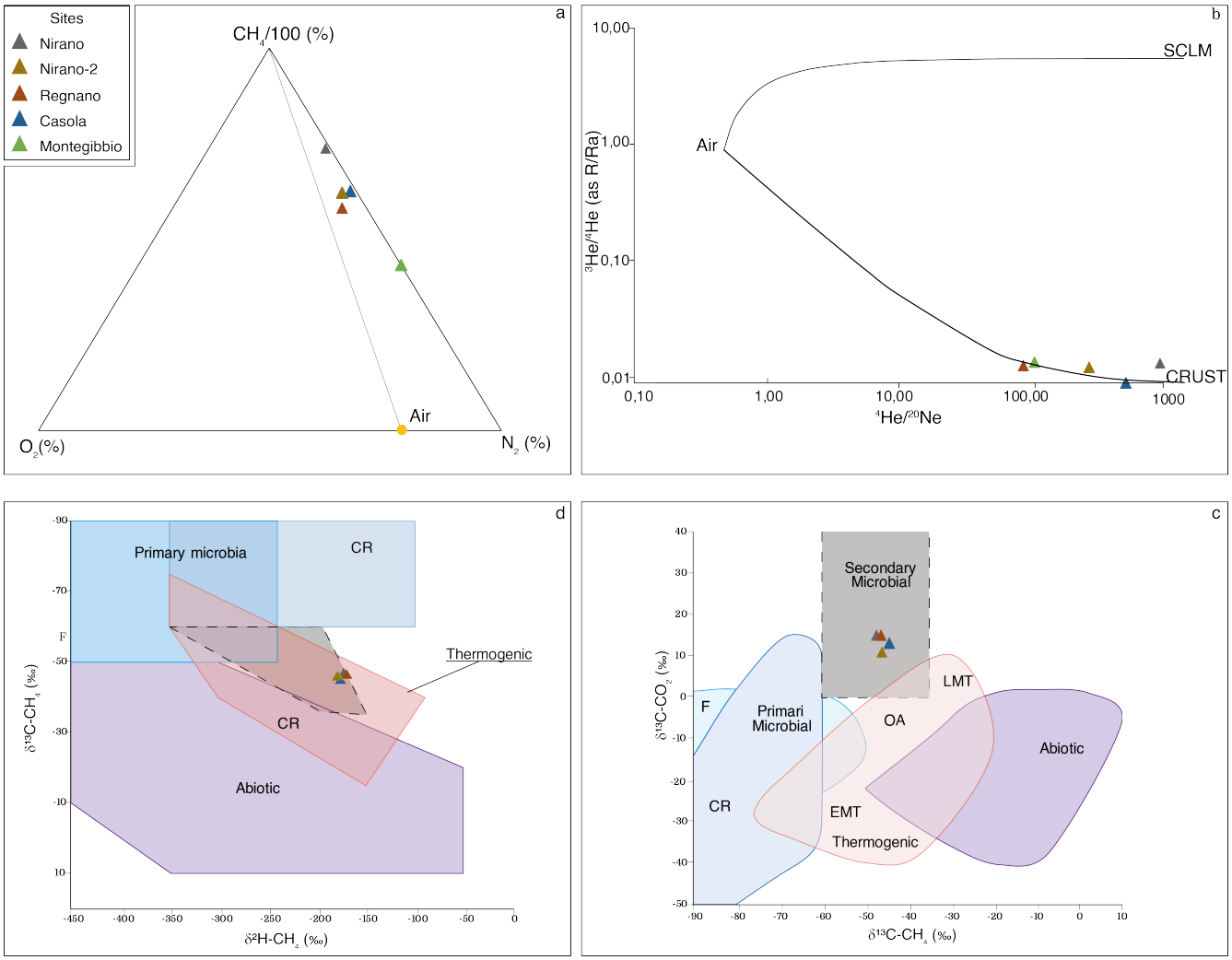

Figure 3. O_2–N_2–CH_4/100 ternary diagram for the gas samples investigated. All the gases are CH_4-dominated and are not along the mixing line between a pure CH_4 end-member and air showing that the sampled gases are not air-contaminated (a). A correlation diagram between the $^3He/^4He$ and $^4He/^{20}Ne$ ratios for the gas samples investigated. The whole black lines show the mixing lines between mantle-derived helium and between radiogenic helium with the Air. The mantle end-member is the Sub Continental Lithospheric Mantle (SCLM, 6.1±0.9 Ra)[69]. (b). Genetic diagrams of δ^{13}C-CH_4 versus δ^{13}C-CO_2 (c) and methane genetic diagrams based on δ^2H-CH_4 versus δ^{13}C-CH_4 (d). T – thermogenic, A – abiogenic, CR – CO_2 reduction, F – fermentation, MO – methane oxidation, OA – oil-associated thermogenic gas, LMT – late mature thermogenic gas, EMT – early mature thermogenic gas. All the genetic fields are from Milkov and Etiope (2018)[38]. The gaseous hydrocarbons are a mixture of secondary biogenic methane and primary and secondary thermogenic gases. The associated oils show both early and late maturities. These evidences account for different generation and migration steps, depending on burial conditions and deformation time[37].

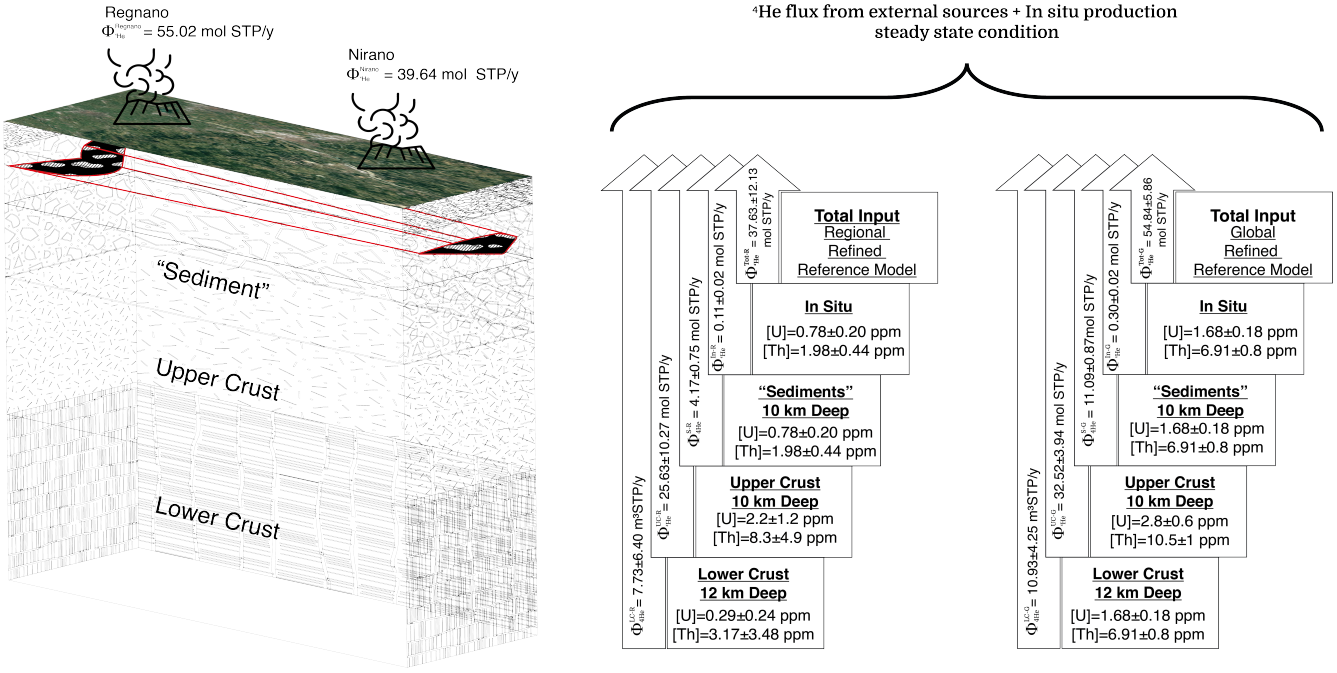

Figure 4. A simplified model of Nirano-Regnano mud volcanoes system. [U] and [Th] are the concentrations of Uranium and Thorium in "Sediment", upper and lower crust according to the Refined Reference Model global or Regional by Coltorti et al. (20011)[48]. $\Phi_{^4He}^{LC-G}$ and $\Phi_{^4He}^{LC-R}$ are the fluxes from the lower crust with [U] and [Th] relative to the Regional (R) and Global (G) models. $\Phi_{^4He}^{UC-G}$ and $\Phi_{^4He}^{UC-R}$ are the fluxes from the upper crust with [U] and [Th] relative to the Regional (R) and Global (G) models. $\Phi_{^4He}^{S-G}$ and $\Phi_{^4He}^{S-R}$ are the fluxes from the "Sediment" with [U] and [Th] relative to the Regional (R) and Global (G) models. $\Phi_{^4He}^{In-G}$ and $\Phi_{^4He}^{In-R}$ are the fluxes from in situ production with [U] and [Th] relative to the Regional (R) and Global (G) models. $\Phi_{^4He}^{Tot-G}$ and $\Phi_{^4He}^{Tot-R}$ are are the total input flow that feeds the reservoir with [U] and [Th] relative to the Regional (R) and Global (G) models. $\Phi_{^4He}^{Nirano}$ and $\Phi_{^4He}^{Regnano-R}$ are the total output flow from the mud volcanoes of Nirano and Regnano.

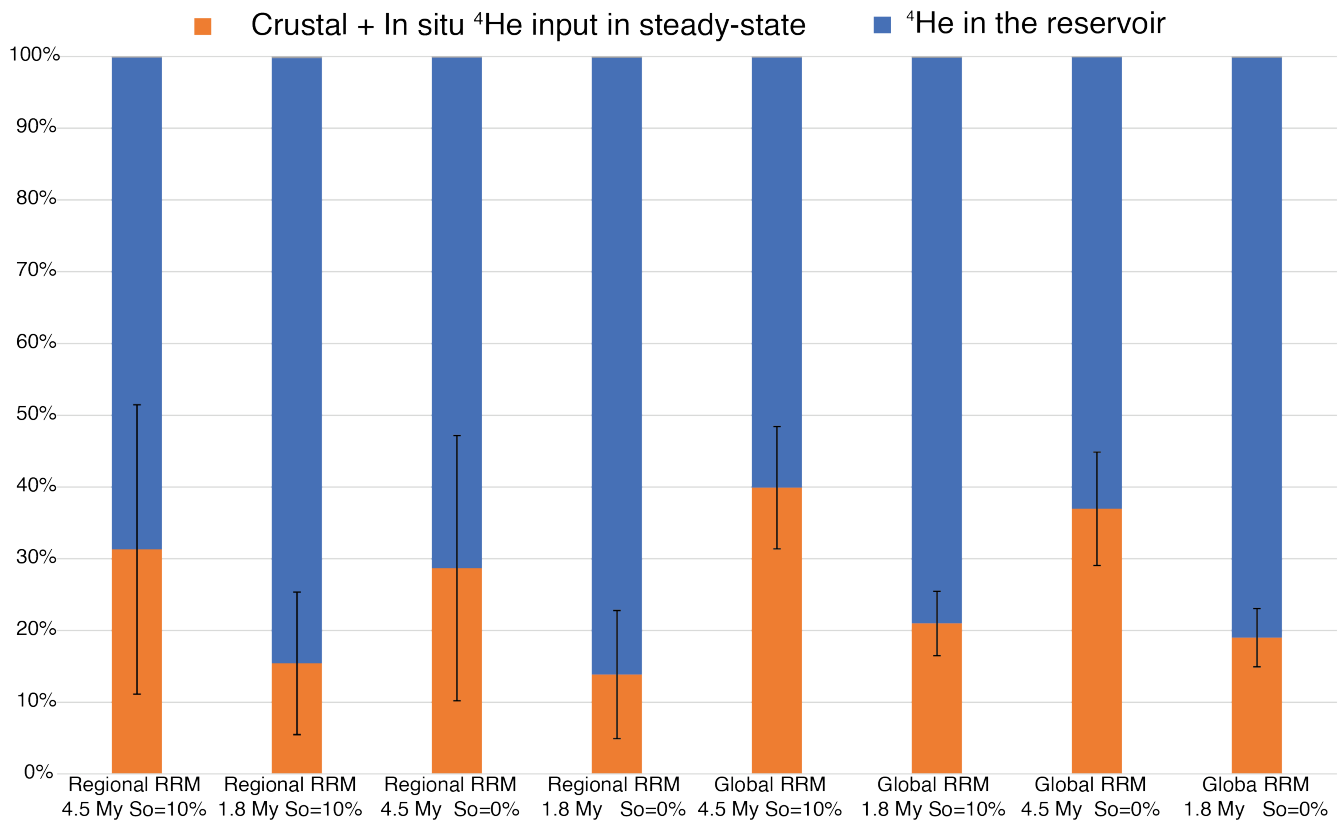

Figure 5. The production of radiogenic He and its release in stationary state, in the age of the trap (1.8 Ma or 4.5 Ma), represents from 15% to 40% of the helium present in the main reservoir. The error bars shown are 2σ.

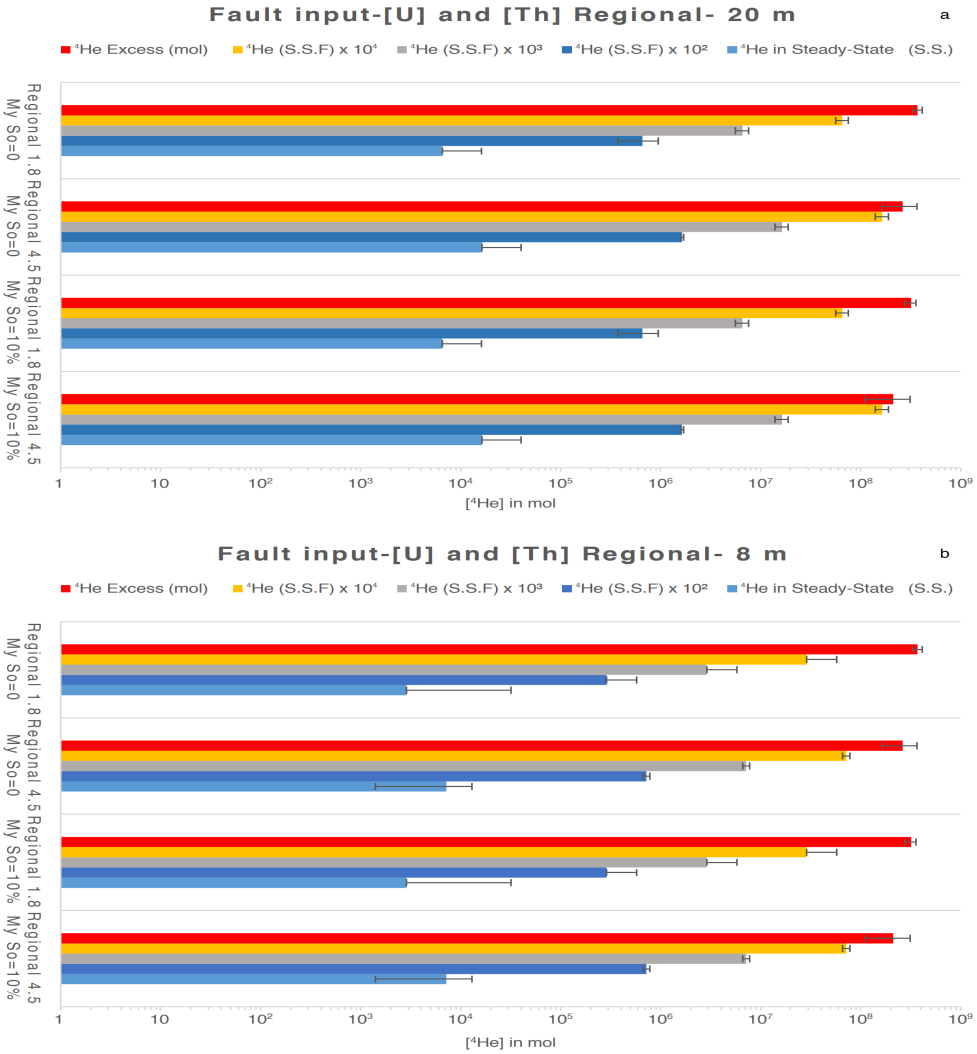

Figure 6. Fault contribution to the release of ^{4}He. Calculated ^{4}He released in Steady-state and S.S. $\times 10^3$-10^4 from faults system in Nirano (lateral extension 6250 m and length of the fault zone 300 m) and Regnano (lateral extension 8750 m and length of the fault zone 500 m) for a damage zone thickness of 20 m (a) and 8 m (b) with Regional U and Th contents.

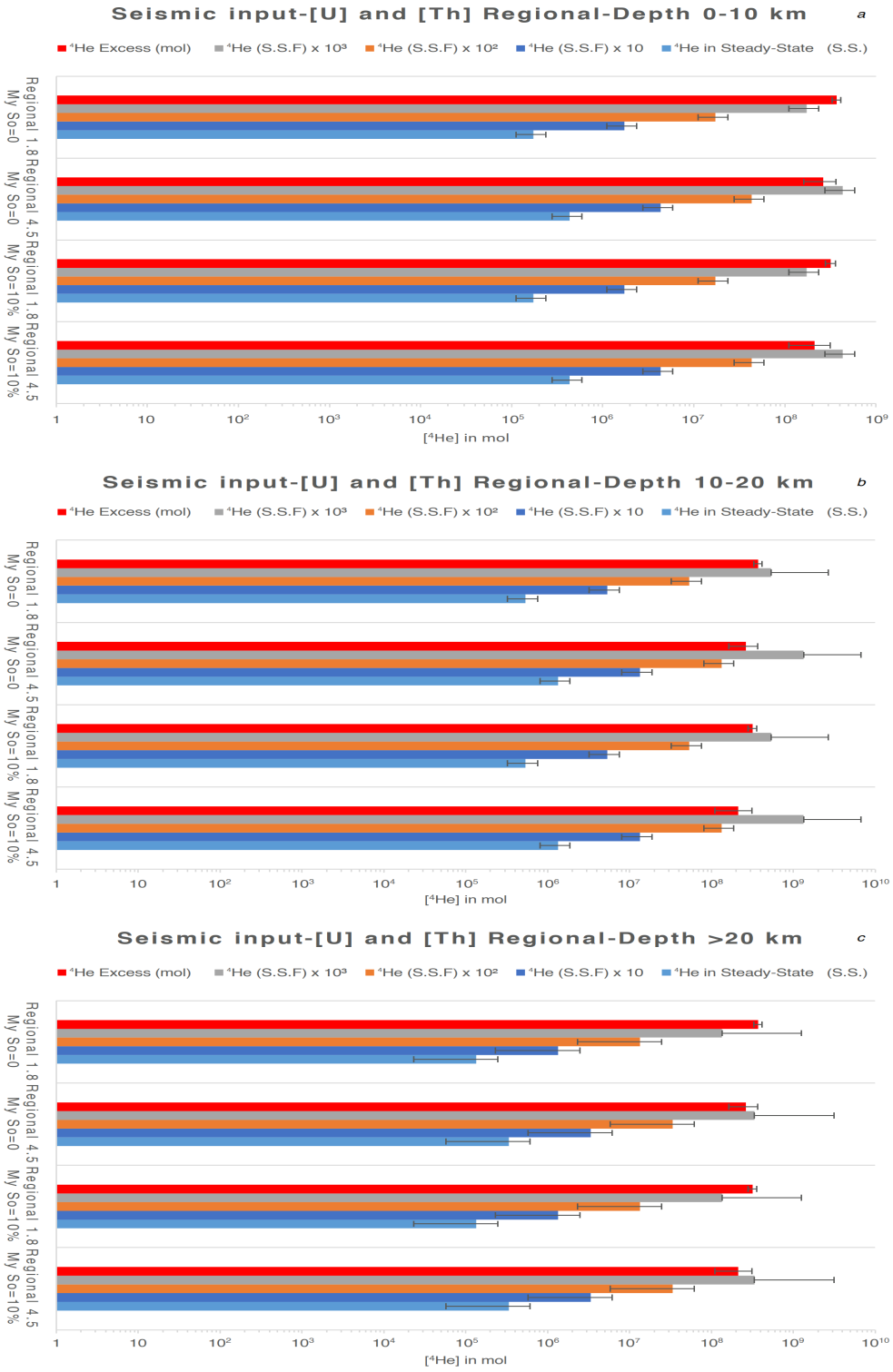

Figure 7. Seismic contribution to the release of ^{4}He. Calculated ^{4}He released in steady-state and S.S. $\times 10^3$-10^4 from deformed volume of rocks by earthquakes with average annual Mw calculated by means of estimated recurrence time after frequency-magnitude distribution by Zmap7 at 0-10 km depth (a), 10-20 km (b) 20-32 km (c) for the uranium and thorium contents of the Regional suite.

Continental degassing of helium in an active tectonic setting (northern Italy): the role of seismicity (supplementary informations)

Dario Buttitta[1,*], Antonio Caracausi[1,*], Lauro Chiaraluce[1], Rocco Favara[1], Maurizio Gasparo Morticelli[2], and Attilio Sulli[2]

[1]Istituto Nazionale di Geofisica e Vulcanologia, Italy
[2]Dipartimento di Scienze della Terra e del Mare, Università di Palermo, Palermo, Italy
[*]buttittadario@gmail.com and antonio.caracausi@ingv.it

ABSTRACT

In order to investigate the variability of helium degassing in continental regions, its release from rocks and emission into the atmosphere, here we studied the degassing of volatiles in a seismically active region of central Italy (Mw_{MAX}=6) at the Nirano-Regnano mud volcanic system. The emitted gases in the study area are CH_4–dominated and it is the carrier for helium (He) transfer through the crust. Carbon and He isotopes unequivocally indicate that crustal-derived fluids dominate these systems. An high-resolution 3-dimensional reconstruction of the gas reservoirs feeding the observed gas emissions at the surface allow us to estimate the amount of He stored in the natural reservoirs. Our study demonstrated that the in-situ production of ^{4}He in the crust and a long-lasting diffusion through the crust are not the main processes that rule the He degassing in the region. Furthermore, we demonstrated that micro-fracturation due to the field of stress that generates the local seismicity increases the release of He from the rocks and can sustain the excess of He in the natural reservoirs respect to the steady-state diffusive degassing. These results prove that 1) the transport of volatiles through the crust can be episodic as function of rock deformation and seismicity and 2) He can be used to provide highlight changes in the stress field of stress that are earthquake-related.

Geological setting

The study area is characterized by the presence of two main active mud volcanos systems (Nirano and Regnano, Figure 1 and 2 in the main text) that are located along the foothills of the Apennines on small anticlinal structures (22 km long). The presence of these structures at the top of anticlines is common because these are the structural conditions for the storage of fluids[1]. The study area develops in the external part of the NE verging Northern Apennines. It is bounded NE-wards by the Pede-Apennine thrust that separates the exposed Apennine foothills, to the southwest, from the buried chain, formed by SW dipping blind thrusts and folds, exhibiting an overall arcuate shape beneath the Po plain deposits, to the northeast. The Northern Apennines fold and thrust belt (NAFTB) formed by the deformation of the Adria continental margin since the Cretaceous. The early phase of convergence led to the subduction of the European plate below the Adria plate and the an accretionary prism resulted from the decollement of the Ligurian oceanic Units. From the Middle Eocene a change in the subduction polarity and vergence, with Adria becoming the lower plate, produced the tectonic overlapping of the accretionary prism above the Miocene siliciclastic foredeep successions (Marnoso Arenacea) deposited on the Adria plate. The thick syntectonic sedimentary wedges developed up to the Pliocene-Quaternary, showing a maximum thickness of 7–8 km. The retreating Adria subduction led to the opening of the Ligurian-Provençal and Tyrrhenian back-arc basins. The foredeep deposits were progressively incorporated into the orogenic belt, forming structural highs, which currently form the hydrocarbon traps in the subsurface of the Northern Apennines and Po Plain. Furthermore, satellite basins atop the Ligurian Units were filled during their emplacement by the Eocene-Pliocene Epiligurian successions. The Livorno-Sillaro Lineament separates the outcrop region of the Ligurian and Epiligurian units to the NW, from the Marnoso Arenacea area to the SE. The main orogenetic phase of this sector of the Northern Apennines took place between the Oligocene and early Miocene, but lasted until the Messinian. During the Quaternary, the reactivation of lateral ramps of the Miocene-Pliocene thrusts caused fluid migration and accumulation. Most of the Apennine foothills are affected by recent tectonic activity. Earthquake fault plane solutions coupled with analyses of geomorphic traces of recent faulting and deformation along the Pede-Apennine margin suggest that both frontal thrusts and lateral thrust ramps are potentially seismogenic. Along the mountain front, the activity of deep thrusts deforms the whole belt, and its

cover up to the Holocene continental deposits. Post-orogenic W-E high-angle normal faults, due to extensional stress field affecting shallow sequences, are the main pathways for the upward fluid migration and the formation of mud volcanoes at the surface, among which the Regnano and Nirano mud volcano fields, located meanly 5 km to the SW of the emergent NNE-verging Late Quaternary Pede-Apennine thrust (Fig. 1 in the main text). The Nirano mud volcano field develops in correspondence of a ramp anticline of Langhian to lower Pleistocene deposits. Geochemical analyses show that the greater fraction of the expelled fluids consists of formation water and methane generated in the Marnoso Arenacea sequence and are generally controlled by reverse faults, ramp anticline geometries, and associated fracture zones. Conversely, mud volcanism at Regnano can be related to SSW dipping normal faults developed on the hanging wall of the Pede-Apennine thrust, and rooted in the Marnoso Arenacea, which represent the main source layer of hydrocarbons. Fracture zone associated with the folding are expected to channel fluids to the Nirano field from a shallow mud reservoir located within the anticline core, below the lithological boundary between the impermeable clays (Argille Azzurre Formation) and the underlying more permeable sedimentary units, where the mud may fill the fracture network and achieve overpressuring. Instead, mud extrusion at Regnano field is directly controlled by a fault conduit funnelling the overpressured mud. Despite mud volcanism in Nirano and Regnano fields is controlled by different strain mechanisms, it can be considered as fed by a more or less continuous main reservoir settled in the anticline core developed in the hanging wall of the Pede-Apennine thrust (figure 1 in the main text). Here it is active the outgassing of volatiles methane-rich from pools and seepage in correspondence of the two mud volcanoes systems since historical times[2] 2. Several geological studies 1 recognized the presence of two-layered fluid reservoirs at depth feeding the gaseous emissions from the Nirano and Regnano systems and the role of the tectonic discontinuities that work as a network of pathway through which fluids mainly migrate vertically towards the surface[1].

Reservoirs and tectonic structures reconstruction

In order to evaluate the volume of the reservoirs feeding the mud volcanoes we reconstructed a 3D geological model of the area between the Regnano and Nirano mud volcanoes systems (Figure 2b in the main text), using 2D geological cross sections from previous investigations[1–3], and processed with the software Move 2015.1 (Figure 2 in the main text). After geo-referencing two NNE-SSW-oriented geological cross sections (Figure 2b) top and bottom lines of the reservoir and the faults bordering it haves been preliminarily depicted; afterwards we generated the surfaces using "create surface from line-Spline Curve method" tool. In the next step, we created the volume between the top and bottom surfaces using "Create TetraVolume Between Horizons" tool and then calculated the value. The reconstructed 3D geological model highlighted the existence of two main reservoirs (Figure 2b in the main text). A deepest one about 300-500 m thick that is located at depth-interval of 2000-2700 m of a ramp anticline with axis of 22 to 39 km, between the Regnano and Nirano areas, with a wavelength between 9 and 13 km. It is hosted into Miocene terrigenous rocks (Marnoso-Arenacea formation) characterized by 15% of porosity. The reconstructed volume is 9491469946 m^3. The geological setting of the shallow reservoir, placed in the Regnano area, is more heterogeneous. It is constituted by Jurassic-Paleogene limestones pertaining to the Liguridi unit sealed upwards and laterally by Paleogene marls (Ranzano formation) with stratigraphic and tectonic contact, respectively. The fault confining laterally the shallow reservoir is the same geological structure affecting the deeper reservoir (Fig. 2 in the main text). In the Nirano sector, the shallow reservoir is made up of Miocene sands of the Epi-Liguride units sealed upwards by Plio-Pleistocene blue clays. In this case, the geological trap is the culmination of a ramp-anticline in the Ligurian units. The reconstructed volume of the shallow reservoir is 268888456 m^3. The value of volume of the shallow reservoir is one order of magnitude smaller than the deeper one, allowing us to neglect its role in the model definition. These geological traps are laterally-bordered by tectonic discontinuities, which are well recognized at depth and mapped at the surface[1]. The reconstructed geological model highlights an extensional kinematic of the fault system in the Regnano sector, where it could be interpreted as a reactivated system, while it represents a compressional fault (thrust) in the Nirano sector (Figure 2c in the main text). Moreover, they permit the transfer of fluids from the reservoirs to the surface. Brittle faults are complex volumetric zones composed of a variety of internal structures, such as slip surfaces, fault rock assemblages, and subsidiary deformation structures. The damage zone of a fault, consisting of subsidiary structures through a relatively large volume of rock surrounding the fault core, is a key factor in controlling the rock permeability and fluids flow through the crust. To investigate the rule of the tectonic discontinuities to transfer volatiles trough the crust to the reservoirs and later to the surface we computed the damage zone dimension for the faults locally cutting the upper crust. It is fundamental to know the width of these zones to assess the fluid flow towards the surface. In the absence of field structural data for the main faults (such as orientation and spatial distribution of fractures in the different fault zones)[4], the evaluation of the thicknesses of the damage-zones of the faults at local scale is obtained by using the classical evolutionary models of

faulting[5–16] and the scale-relationship between width of the damage zone and displacement. Generally, it is difficult to find a linear relationship between the damage zone width and a single parameter, therefore several parameters, such as lithology and associated diagenesis, depth of faulting, tectonic environment, and deformation mechanism, have been taken into account to evaluate its volume. To limit the effects of the different factors, we analysed previous results relatively to normal faults; moreover, we considered only two types of deformation features in the analysed rocks: deformation bands in porous sandstones and fractures in brittle rocks. In summary, the system of faults that crosses the deep reservoir consists of two main fault systems (Figure 1 in the main text). The first system mainly involves the geological domains in the area of Nirano, whose length is 300 m at a depth between 2000 and 2300 m, with a lateral extension of about 6300 m, with a possible damage zone between 8 and 20 m (measured on rocks with similar lithology)[4,17]. The second one, which affects the sector of Regnano, is 500 m long and is located at a depth between 2200 and 2700, has a lateral extension of about 8800 m and a possible damage zone between 8 and 20 m (measured on rocks with similar lithology)[4,17]

References

1. Bonini, M. Interrelations of mud volcanism, fluid venting, and thrust-anticline folding: Examples from the external northern Apennines (Emilia-Romagna, Italy). *J. Geophys. Res. Solid Earth* **112**, 1–21, DOI: 10.1029/2006JB004859 (2007).

2. Etiope, G., Martinelli, G., Caracausi, A. & Italiano, F. Methane seeps and mud volcanoes in Italy: Gas origin, fractionation and emission to the atmosphere. *Geophys. Res. Lett.* **34**, 1–5, DOI: 10.1029/2007GL030341 (2007).

3. Oppo, D., Capozzi, R. & Picotti, V. A new model of the petroleum system in the Northern Apennines, Italy. *Mar. Pet. Geol.* **48**, 57–76, DOI: 10.1016/j.marpetgeo.2013.06.005 (2013).

4. Choi, J.-H., Edwards, P., Ko, K. & Kim, Y.-S. Definition and classification of fault damage zones: A review and a new methodological approach. *Earth-Science Rev.* **152**, 70–87, DOI: https://doi.org/10.1016/j.earscirev.2015.11.006 (2016).

5. Evans, J. P. Brevia SHORT NOTES Thickness–displacement relationships for fault zones. *J. Struct. Geol.* **12**, 1061–1065 (1990).

6. Scholz, C. H., Dawers, N. H., Yu, J.-Z., Anders, M. H. & Cowie, P. A. Fault growth and fault scaling laws: Preliminary results. *J. Geophys. Res. Solid Earth* **98**, 21951–21961, DOI: 10.1029/93JB01008 (1993).

7. Savage, H. M. & Brodsky, E. E. Collateral damage: Evolution with displacement of fracture distribution and secondary fault strands in fault damage zones. *J. Geophys. Res. Solid Earth* **116**, DOI: 10.1029/2010JB007665 (2011).

8. Torabi, A. & Berg, S. S. Scaling of fault attributes: A review. *Mar. Pet. Geol.* **28**, 1444–1460, DOI: https://doi.org/10.1016/j.marpetgeo.2011.04.003 (2011).

9. Childs, C., Nicol, A., Walsh, J. J. & Watterson, J. Growth of vertically segmented normal faults. *J. Struct. Geol.* **18**, 1389–1397, DOI: https://doi.org/10.1016/S0191-8141(96)00060-0 (1996).

10. Knott, S. D. *et al.* Spatial and mechanical controls on normal fault populations. *J. Struct. Geol.* **18**, 359–372, DOI: https://doi.org/10.1016/S0191-8141(96)80056-3 (1996).

11. Vermilye, J. M. & Scholz, C. H. The process zone: A microstructural view of fault growth. *J. Geophys. Res. Solid Earth* **103**, 12223–12237, DOI: 10.1029/98JB00957 (1998).

12. Beach, A., Welbon, A. I., Brockbank, P. J. & McCallum, J. E. Reservoir damage around faults; outcrop examples from the Suez Rift. *Pet. Geosci.* **5**, 109–116, DOI: 10.1144/petgeo.5.2.109 (1999).

13. Fossen, H. & Hesthammer, J. Possible absence of small faults in the Gullfaks Field, northern North Sea: implications for downscaling of faults in some porous sandstones. *J. Struct. Geol.* **22**, 851–863, DOI: https://doi.org/10.1016/S0191-8141(00)00013-4 (2000).

14. Shipton, Z. K., Soden, A. M., Kirkpatrick, J. D., Bright, A. M. & Lunn, R. J. *How Thick is a Fault? Fault Displacement-Thickness Scaling Revisited*, 193–198 (American Geophysical Union (AGU), 2006).

15. Mitchell, T. M. & Faulkner, D. R. The nature and origin of off-fault damage surrounding strike-slip fault zones with a wide range of displacements: A field study from the Atacama fault system, northern Chile. *J. Struct. Geol.* **31**, 802–816, DOI: https://doi.org/10.1016/j.jsg.2009.05.002 (2009).

16. Faulkner, D. R., Mitchell, T. M., Jensen, E. & Cembrano, J. Scaling of fault damage zones with displacement and the implications for fault growth processes. *J. Geophys. Res. Solid Earth* **116**, DOI: 10.1029/2010JB007788 (2011).

17. McGrath, A. G. & Davison, I. Damage zone geometry around fault tips. *J. Struct. Geol.* **17**, 1011–1024, DOI: https://doi.org/10.1016/0191-8141(94)00116-H (1995).

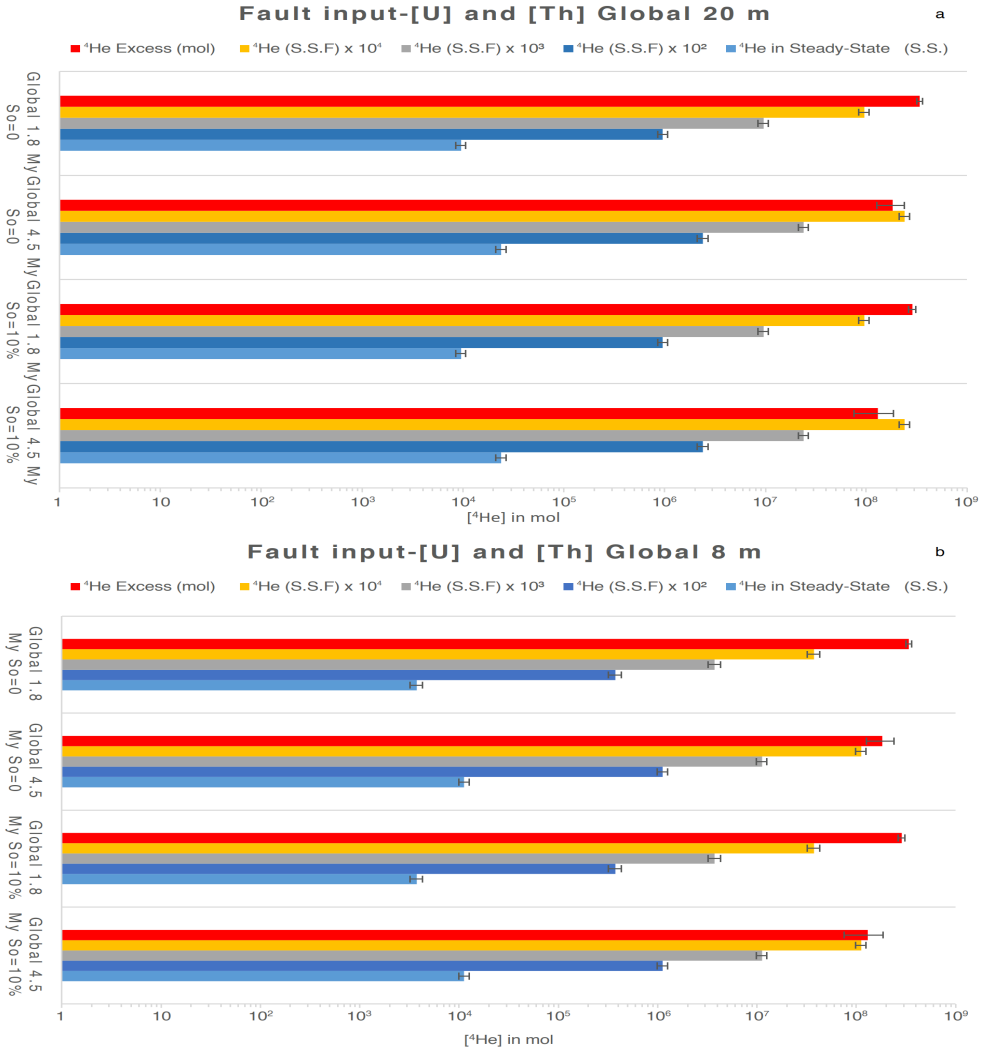

Figure S1. Fault contribution to the release of ^{4}He. Calculated 4He released in Steady-state and S.S. $\times$ 10^2-10^3 from faults system in Nirano (lateral extension 6250 m and length of the fault zone 300 m) and Regnano (lateral extension 8750 m and length of the fault zone 500 m) for a damage zone thickness of 20 m (a) and 8 m (b) with Global U and Th contents.

Figure S2. Seismic contribution to the release of ^{4}He. Calculated ^{4}He released in steady-state and S.S. $\times$ 10^2-10^3 from deformed volume of rocks by earthquakes with average annual Mw calculated by means of estimated recurrence time after frequency-magnitude distribution by Zmap7 at 0-10 km depth (a), 10-20 km (b) 20-32 km (c) for the uranium and thorium contents of the Global suite.